

**STRUCTURAL AND STRATIGRAPHIC EVOLUTION OF THE
CENTRAL MISSISSIPPI CANYON AREA:
INTERACTION OF SALT TECTONICS AND SLOPE PROCESSES IN THE
FORMATION OF ENGINEERING AND GEOLOGIC HAZARDS**

A Dissertation

by

JOHN RICHARD BRAND

Submitted to the Office of Graduate Studies of
Texas A&M University
in partial fulfillment of the requirements for the degree of

DOCTOR OF PHILOSOPHY

December 2004

Major Subject: Oceanography

**STRUCTURAL AND STRATIGRAPHIC EVOLUTION OF THE
CENTRAL MISSISSIPPI CANYON AREA:
INTERACTION OF SALT TECTONICS AND SLOPE PROCESSES IN THE
FORMATION OF ENGINEERING AND GEOLOGIC HAZARDS**

A Dissertation

by

JOHN RICHARD BRAND

Submitted to Texas A&M University
in partial fulfillment of the requirements
for the degree of

DOCTOR OF PHILOSOPHY

Approved as to style and content by:

William Bryant
(Chair of Committee)

David Prior
(Member)

William Sager
(Member)

Niall Slowey
(Member)

Wilford Gardner
(Head of Department)

December 2004

Major Subject: Oceanography

ABSTRACT

Structural and Stratigraphic Evolution of the Central Mississippi Canyon Area:
Interaction of Salt Tectonics and Slope Processes in the Formation of Engineering
and Geologic Hazards. (December 2004)

John Richard Brand, B. S., West Virginia University

Chair of Advisory Committee: Dr. William Bryant

Approximately 720 square miles of digital 3-dimensional seismic data covering the eastern Mississippi Canyon area, Gulf of Mexico, continental shelf was used to examine the structural and stratigraphic evolution of the geology in the study area. The analysis focused on salt tectonics and sequence stratigraphy to develop a geologic model for the study area and its potential impact on engineering and geologic hazards.

Salt in the study area was found to be established structural end-members derived from shallow-emplaced salt sheets. The transition from regional to local salt tectonics was identified through structural deformation of the stratigraphic section on the seismic data and occurred no later than ~450,000 years ago. From ~450,000 years to present, slope depositional processes have become the dominant geologic process in the study area.

Six stratigraphic sequences (I-VI) were identified in the study area and found to correlate with sequences previously defined for the Eastern Mississippi Fan. Condensed sections were the key to the correlation. The sequence stratigraphy for the Eastern

Mississippi Fan can be extended ~28 miles west, adding another ~720 square miles to the interpreted Fan.

A previously defined channel within the Eastern Fan was identified in the study area and extended the channel ~28 miles west. Previous work on the Eastern Fan identified the source of the Fan to be the Mobile River; however, extending the channel west suggests the sediment source to be from the Mississippi River, not the Mobile River. Further evidence for this was found in ponded turbidites whose source has been previously established as the Mississippi River.

Ages of the stratigraphic sequences were compared to changes in eustatic sea level. The formation stratigraphic sequences appear decoupled from sea level change with “pseudo-highstands” forming condensed sections during pronounced Pleistocene sea level lowstands. Miocene and Pleistocene depositional analogues suggest the location of the shifting Mississippi River Pleistocene depocenter is a more dominant influence on sequence formation. Thus, the application of traditional sequence interpretation with respect to sea level change should be reconsidered to also account for the shifting depocenter for both the study area as well as the broader Eastern Mississippi Fan.

DEDICATION

This dissertation is completed in service to Jesus Christ. This dissertation is also dedicated to my parents, Thomas and Georgina Brand, whose constant support and timely vigilance, throughout my life, has made the completion of this endeavor a reality.

ACKNOWLEDGMENTS

I thank God for this life and His continued grace and guidance in this and the rest of my endeavors.

I am sincerely grateful to my Advisory Committee Chair, Dr. William Bryant, for his advice and guidance throughout the course of this work. Thank you, along with Dr. David Prior, for pushing me to pursue my doctoral degree rather than settle for a masters.

I would like to thank Drs. William Sager and Niall Slowey for acting as members of my committee, particularly Niall Slowey who provided much needed guidance in the early part of my graduate experience. Dr. Sager provided invaluable guidance on editing and improvement of the manuscript.

A special thank you to ExxonMobil for their courteousness in permitting me to use their seismic dataset for this research, specifically Mr. Stephen J. Ledet without whom the use of the seismic data would not have been possible.

I sincerely thank the entire staff at Geoscience Earth and Marine Services, Inc. for their support, encouragement, and at times, joking sarcasm in pushing me to complete this research. I would like to specifically acknowledge Mr. Michael J. Kaluza and Alan G. Young for their guidance, support, timely patience, and confidence in my abilities to complete this research. Special thanks to Daniel Lanier for all of your help and camaraderie; you are not only my co-worker but also my friend.

There are many individuals in the graduate program at Texas A&M who indirectly contributed to the completion of this dissertation. In particular, Christopher Spagnoulo, my best friend while at Texas A&M who endured with me the many frustrations of the graduate experience and shared a common respect for the ocean and a love of surfing. Thank you Sandy Drews and Barbara Childress for your patience and tolerance with me getting blocked every semester, changing my course of study about 5 times, changing my degree plan, and always registering at the last minute. Both of you always solved my administrative problems with a laugh and a smile. Thanks to Laura Caldwell up on the 12th floor for your kindness and long conversations about autoracing, etc.

There have been many individuals in my life before graduate school who were instrumental in the completion of this dissertation. Thank you Mom and Dad for raising me the way you did. Thank you to Dr. Raymond Nighan of St. John's College High School who was the best teacher I ever had. With excitement, he opened a world of knowledge, literature, and inquisitive thinking to me that I still use every day. Thank you to coach Peter Karl for teaching me the value of dedication, hard work, and expecting nothing less than a 100% effort all the time. Thank you to coach Kevin Gilson for getting me to believe in myself, for teaching me the benefit of sacrifice and commitment, for demanding only the best from myself and others, and for proving that the only thing limiting me from achieving my goals is me.

Last but certainly not least, I thank myself, for persevering through thick and thin and finally getting this thing done.

TABLE OF CONTENTS

	Page
ABSTRACT	iii
DEDICATION	v
ACKNOWLEDGEMENTS	vi
TABLE OF CONTENTS	viii
LIST OF FIGURES	xi
LIST OF TABLES	xviii
 CHAPTER	
I INTRODUCTION	1
Objectives	4
II DATA AND METHODS	10
Data	10
Methods	11
A. Bathymetry Map	12
B. Isopach Map	13
C. Thickness Maps	14
D. Enhanced Seafloor Rendering and Seafloor Amplitude Rendering	15
E. Seismic Data Examples	16
F. RMS Volume Calculations	16
III BACKGROUND	18
Gulf of Mexico Geologic Setting	18
Regional Geologic Setting	43
A. Geologic Structure	43
B. Stratigraphy	47
C. Geohazards	49
Slope Gradient and Slope Stability	50
Hydrocarbon Vents	51
Chemosynthetic Communities	52

CHAPTER	Page
Hydrates	53
Carbonates	54
Faults	55
Salt	55
Gas	56
Shallow Water Flow	57
Exploration and Production Activity	60
Previous Work	61
A. Regional Salt Tectonics	61
B. Depositional Processes	68
IV SALT TECTONICS	74
Introduction	74
Mechanisms of Salt Movement	77
Seismic Recognition of Salt	85
Observations	87
A. Distribution of Salt in the Study Area	87
B. Morphology: Salt Body I	87
C. Morphology: Salt Body II	106
D. Morphology: Salt Body III	111
E. Morphology: Salt Body IV	115
F. Salt Basin Types	118
V SEISMIC STRATIGRAPHY	130
Seismic Sequence Definition	130
Seismic and Geologic Facies	136
A. Sequence I: Horizon C' to Top of Salt/4.00 Seconds	137
B. Sequence II: Horizon C to Horizon C'	144
C. Sequence III: Horizon B' to Horizon C	152
D. Sequence IV: Horizon B to Horizon B'	160
E. Sequence V: Horizon A to Horizon B	171
F. Sequence VI: Seafloor to Horizon A	179
VI SEQUENCE STRATIGRAPHIC CORRELATION	186
VII GEOLOGIC MODEL	203
Introduction	203
Sequence I (1.1Ma to 0.45Ma, BP)	210
Sequence II (0.45Ma to 0.40Ma, BP)	211
Sequence III (0.40Ma to 0.071Ma, BP)	213

CHAPTER	Page
Sequence IV (0.071Ma to 0.055Ma, BP)	215
Sequence V (0.055Ma to 0.023Ma, BP)	217
Sequence VI (0.023Ma, BP to Present)	219
VIII GEOLOGIC HAZARDS	221
Introduction	221
A. Seafloor Morphology	221
B. Bathymetry and Seafloor Gradient	225
C. Seafloor Amplitude	227
D. Sequence VI: Seafloor to Horizon A	231
E. Sequence V: Horizon A to Horizon B	233
F. Sequence IV: Horizon B and Horizon B'	234
G. Sequence III: Horizon B' to Horizon C	235
H. Sequence II: Horizon C to Horizon C'	236
I. Sequence I: Horizon C' to Top of Salt/4.00 Seconds	237
IX OBSERVATIONS	239
X DISCUSSION	246
Introduction	246
Salt End-members and Shift in Mobilization History	247
Shift in Dominance from Salt Tectonics to Slope Depositional Processes	252
Correlation With and Extending the Eastern Mississippi Fan Westward	255
Mississippi River is Source of the Eastern Mississippi Fan	258
Eastern Fan Sensitivity to Depocenter Location and Sea Level Change	262
XI CONCLUSION	270
REFERENCES CITED	271
VITA	282

LIST OF FIGURES

FIGURE	Page
1 Gulf of Mexico deepwater production as % total GOM production	2
2 Gulf of Mexico seafloor rendering showing location of study area	5
3 Bathymetry map of study area	6
4 Seafloor rendering of the study area	7
5 Reconstruction of western Pangea (future Gulf of Mexico) in late Paleozoic/early Mesozoic time	19
6 Schematic diagram illustrating the early (pre-middle Cretaceous) evolution of the Gulf of Mexico	20
7 Reconstruction of western Pangea (future Gulf of Mexico) during late-Middle Jurassic	21
8 Distribution of Middle Jurassic salt deposits and oceanic crust in the Gulf of Mexico during the early Cretaceous	23
9 Diagram of carbonate ramp and platforms in the Gulf of Mexico during the early Cretaceous	24
10 Isopach map showing thickness and distribution of Upper Cretaceous sediments in the Gulf of Mexico basin	25
11 Generalized deposystems map showing location of primary Upper Cretaceous depocenters	27
12 Location of Cenozoic depocenters in the northwestern gulf of Mexico	28
13 Isopach map showing the thickness of Paleocene terrigenous clastic sediments in the Gulf of Mexico basin	29
14 Generalized deposystems map showing location of primary Paleocene depocenters	30
15 Isopach map showing the thickness of Eocene terrigenous clastic	

FIGURE	Page
sediments in the Gulf of Mexico basin	31
16 Generalized deposystems map showing location of primary Eocene depocenters	32
17 Isopach map showing the thickness of Oligocene terrigenous clastic sediments in the Gulf of Mexico basin	34
18 Generalized deposystems map showing location of primary Oligocene depocenters	35
19 Isopach map showing the thickness of Miocene terrigenous clastic sediments in the Gulf of Mexico basin	36
20 Generalized deposystems map showing the location of primary Miocene depocenters	37
21 Isopach map showing thickness of Pliocene terrigenous clastic sediments in the Gulf of Mexico basin	38
22 Generalized deposystems map showing location of primary Pliocene depocenters	40
23 Isopach map showing thickness of Pleistocene terrigenous clastic sediments in the Gulf of Mexico basin	41
24 Generalized deposystems map showing location of primary Pleistocene depocenters	42
25 Regional seafloor morphology	44
26 Gulf of Mexico tectonostratigraphic provinces	45
27 Western and Eastern Mississippi Fan systems	48
28 Modern-day distribution of shallow salt in the Gulf of Mexico	62
29 Palipinastic reconstruction of allochthonous salt in the Mississippi Canyon area	64
30 Model for salt sill formation	65

FIGURE	Page
31 Basic model of salt glacier propagation	67
32 Allochthonous salt end-member systems in the Gulf of Mexico	69
33 Cross-section model of Mississippi Fan depositional sequences	72
34 Cross-section model of Eastern Mississippi Fan depositional sequences	73
35 Tectonostratigraphic provinces of the Gulf of Mexico	75
36 Distribution of tectonostratigraphic provinces in relation to the study area	76
37 Proposed driving mechanisms for salt movement	78
38 Downbuilding model of shallow salt emplacement	82
39 First known illustration of allochthonous salt	83
40 Perspective view of principal types of salt structures	84
41 Seismic recognition and characters of salt	86
42 Distribution of shallow salt in the study area	88
43 Location of salt in study area relative to previously mapped salt in the Mississippi Canyon area	89
44 Structure map, top of salt	90
45 Perspective view, top of salt	91
46 Isopach map, top of salt	93
47 Locations of arbitrary seismic lines used in this study	94
48 Arbitrary Seismic Line A illustrating the character of SBI	95
49 Arbitrary Seismic Line E illustrating the character of SBI	96
50 Relationship of mapped salt bodies to a previously proposed thin-skinned, strike-slip boundary	98

FIGURE	Page
51 Location of SBI-SBIV to the strike-slip boundary and tectonostratigraphic provinces	99
52 Basic model of the Roho end-member system	101
53 Comparison of previously defined Roho end-member system to salt in the study area	102
54 Large-scale regional seismic line showing local Roho end-member salt and location of SBI	103
55 Regional palipinastic reconstruction from Miocene to present showing interpreted location of SBI	105
56 Arbitrary Seismic Line B illustrating the character of SBII	108
57 Arbitrary Seismic Line F illustrating the character of SBII	109
58 Arbitrary Seismic Line C illustrating the character of SBIII	112
59 Reconstruction of regional seismic line through Canopy I	114
60 Composite arbitrary seismic lines illustrating the character of SBIV	117
61 Arbitrary Seismic Line F illustrating typical Type I basin in the study area	119
62 Deeper seismic section illustrating full morphology of a Type I basin	120
63 Spindler's model for suprasalt basin formation	122
64 Arbitrary Seismic Line A illustrating the character of the Type II basins above SBI	124
65 Arbitrary Seismic Line E illustrating the character of the Type II basins above SBI	125
66 Arbitrary Seismic Line F illustrating the character of the Type II basins above SBII	126
67 Arbitrary Seismic Line C illustrating the character of the Type II basin above SBIII	127

FIGURE	Page
68 Identified Type II suprasalt basins in the study area	128
69 Structure map, Sequence I	138
70 Isopach map, Sequence I	139
71 Arbitrary Seismic Line F showing Sequence I facies	140
72 Arbitrary Seismic Line A showing Sequence I facies	141
73 Sequence I RMS amplitude display	145
74 Structure map, Sequence II	146
75 Isopach map, Sequence II	147
76 Thickness map, Sequence II	148
77 Arbitrary Seismic Line B showing Sequence II facies	151
78 Sequence II RMS amplitude display	153
79 Structure map, Sequence III	154
80 Isopach map, Sequence III	155
81 Thickness map, Sequence III	156
82 Arbitrary Seismic Line B showing Sequence III facies	158
83 Arbitrary Seismic Line A showing Sequence III facies	159
84 Sequence III RMS amplitude display	161
85 Structure map, Sequence IV	162
86 Isopach map, Sequence IV	163
87 Thickness map, Sequence IV	164
88 Arbitrary Seismic Line B showing Sequence IV facies	166

FIGURE	Page
89 Arbitrary Seismic Line F showing Sequence IV facies	167
90 Arbitrary Seismic Line E line showing Sequence IV facies	168
91 Sequence IV RMS amplitude display	170
92 Structure map, Sequence V	172
93 Isopach map, Sequence V	173
94 Thickness map, Sequence V	174
95 Arbitrary Seismic Line B showing Sequence V facies	176
96 Arbitrary Seismic Line F showing Sequence V facies	177
97 Arbitrary Seismic Line E showing Sequence V facies	178
98 Sequence V RMS amplitude display	180
99 Arbitrary Seismic Line B showing Sequence VI facies	181
100 Arbitrary Seismic Line F showing Sequence VI facies	182
101 Arbitrary Seismic Line A showing Sequence VI facies	183
102 Perspective view of Sequence IV channel structure with RMS overlay	194
103 Location of channel (this study) in relation to previously mapped fan channels	196
104 Deposition of ponded turbidites in salt-constricted basin in this study	197
105 Ponded turbidite facies in Sequence IV	199
106 Seafloor gradient map	200
107 General depositional patterns for the Gulf of Mexico	206
108 Recent modification to depositional systems and systems tracts with respect to sea level	207

FIGURE	Page
109 Basic model for interaction of sedimentation and salt movement in slope depositional systems	208
110 Miocene middle-lower slope deposystem analogous to the Plio/Pleistocene in the study area	209
111 Seismic line illustrating intact debris blocks in Sequence V	218
112 Seafloor perspective views	222
113 Seafloor amplitude map	228
114 Potential location of hydrocarbon seeps and chemosynthetic communities	229
115 Sequence I RMS amplitude display	232
116 Arbitrary Seismic Line B illustrating extent of normal faulting	249
117 Location of channel in Sequence IV	259
118 Composite Mississippi River Pleistocene deposystem	261
119 Comparison of oxygen isotope stages and sea level curve to ages of stratigraphic sequences III-VI in the study area.	264
120 Proposed Pleistocene deposystem analogue composite (this study)	269

LIST OF TABLES

TABLE		Page
1	Previously derived definitions of seismic sequence stratigraphy	132
2	Gulf of Mexico Basin Depositional Synthesis seismic stratigraphic facies identification chart	133
3	Sequence I seismic facies	142
4	Sequence II seismic facies	149
5	Sequence III seismic facies	157
6	Sequence IV seismic facies	165
7	Sequence V seismic facies	175
8	Sequence VI seismic facies	185
9	Sequence number and age of stratigraphic sequences defined by Dixon and Weimer (1994)	188
10	Sequence correlation and inferred ages of sequences between those defined by Dixon and Weimer (1994) and this study	190

CHAPTER I

INTRODUCTION

The Gulf of Mexico has a long-standing reputation as one of the most productive hydrocarbon regions in the world. Traditionally, hydrocarbon exploration and production was limited to the shallow waters (<1000 ft) of the continental shelf and upper continental slope. The relatively recent discovery of large hydrocarbon reserves in the deepwater Gulf of Mexico (>1000 ft) has revived large-scale exploration and development. The advent of new exploration and production technologies such as digital, high-resolution, 3-dimensional surveying and processing, tension-leg platforms and floating production systems, dynamically positioned drill vessels, riserless drilling, and subsea completions and tiebacks are now making exploration and production of these deepwater plays economically feasible. Current deepwater hydrocarbon reserves are estimated to be 3.2 billion BOE (Koen, 1995). Deepwater production has increased steadily in the last 10 years and in 1998 was responsible for 35% of the total oil production in the Gulf of Mexico (Minerals Management Service, 2000)(Figure 1). Ultimate production in the deepwater Gulf of Mexico could reach as high as 10 billion BOE (Watkins and Buffler, 1996).

The shallow (0 ft to 5000 ft below mudline, bml) subsurface geology in the deepwater Gulf of Mexico presents a unique suite of engineering and geologic hazards

This thesis follows the style of the AAPG Bulletin.

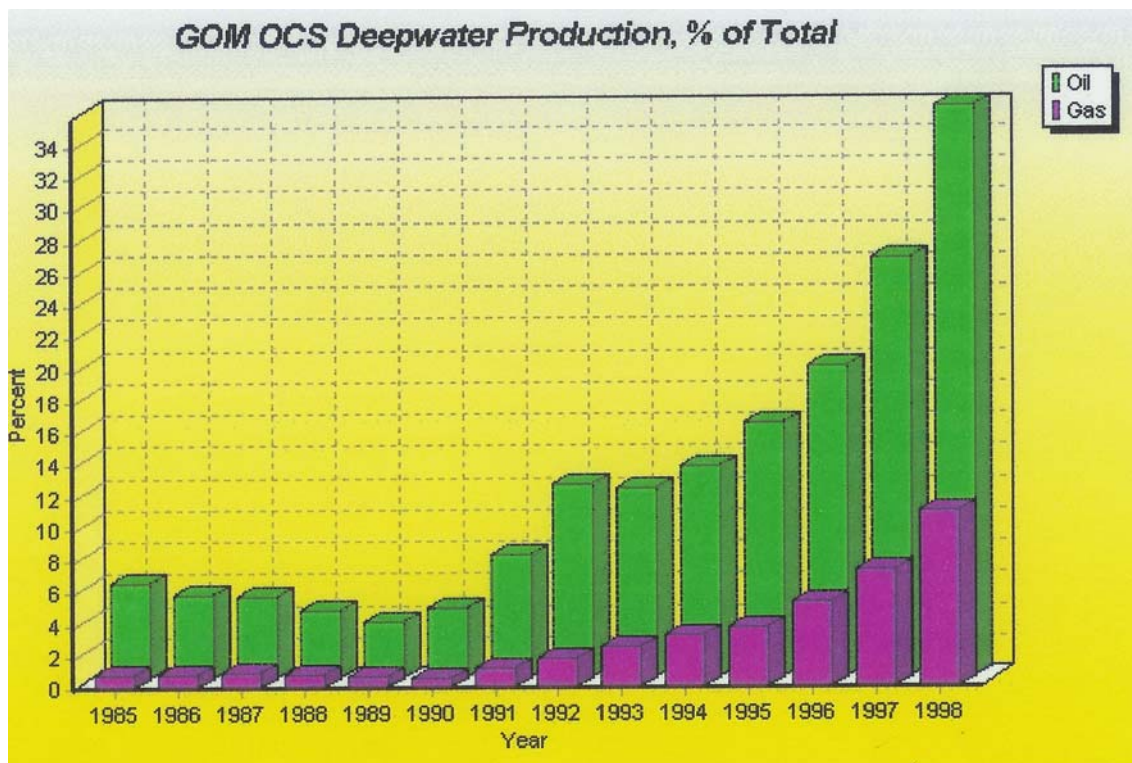


Figure 1. Gulf of Mexico deepwater production as % total GOM production (Minerals Management Service, 2000).

and/or constraints to hydrocarbon exploration and production. In many cases, these hazards/constraints have been the limiting factor in the pursuit of deepwater hydrocarbon plays. They not only present a literal threat to exploration activities, but also an economic threat as well, as mitigation techniques can be exceedingly costly.

Potential engineering or geologic hazards/ or constraints in the deepwater Gulf of Mexico include the following:

- Slope gradient and seafloor stability,
- Seafloor and buried faults,
- Strong bottom currents,
- Hydrocarbon seeps and vents,
- Chemosynthetic communities,
- Gas Hydrates,
- Carbonates,
- Salt,
- Mass-transport events,
- Shallow gas, and
- Shallow Water Flow (SWF)

A number of exploration and production wells have been delayed, forcibly abandoned, or completely lost in an encounter with one or many of these unique geologic conditions, particularly SWF.

Essential to the success of present and future deepwater development is the identification and understanding of the regional interaction between geologic processes

that lead to the formation of these hazards/constraints. An area of present interest for development is the central Mississippi Canyon area, Gulf of Mexico.

Objectives

The study area is located approximately 120 miles to 150 miles southeast of New Orleans, Louisiana, in the center of the Mississippi Canyon OCS area, on Louisiana continental slope (Figure 2). It covers a 73-block area of approximately 1,800 km² (720 mi²). Water depths in the study area range from 3,620 ft to 6,520 ft below sea level (Figure 3). The seafloor is varied with areas of irregular seafloor, the presence of seafloor valleys, and seafloor expression of buried salt structures (Figure 4). The most prominent seafloor features are Chandeleur Valley, Gulfport Valley, Redfish Valley, and seafloor expression of salt sills, ridges, spires, and canopies.

The analysis of modern, digital multi-fold 3-D seismic data should provide, for the first time, a high-resolution, regional perspective on the interaction between different structural and depositional processes that have produced the shallow geologic section of the present day. The following tasks will be used to analyze the data to form the basis of the interpretations:

- Visualization, mapping, and description of seafloor morphology in the study area,
- Identification and mapping of pertinent stratigraphic sequence in the study area,

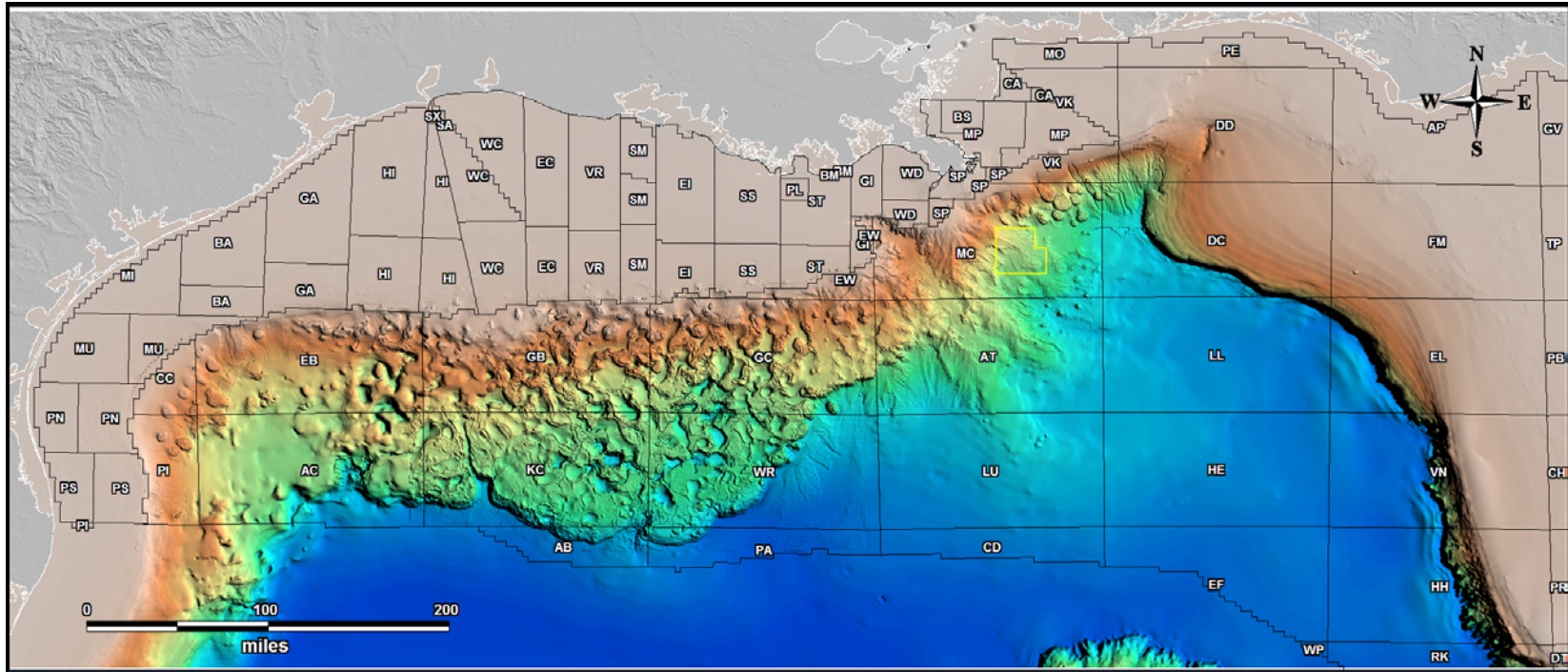


Figure 2. Gulf of Mexico seafloor rendering showing location of study area. Land is gray. Water depths increase from shallow (tan) to deeper (dark blue). Overlain areas are OCS protraction areas denoted by their area code. Study area outlined in yellow. Rendering courtesy of Geoscience Earth and Marine Services, Inc.

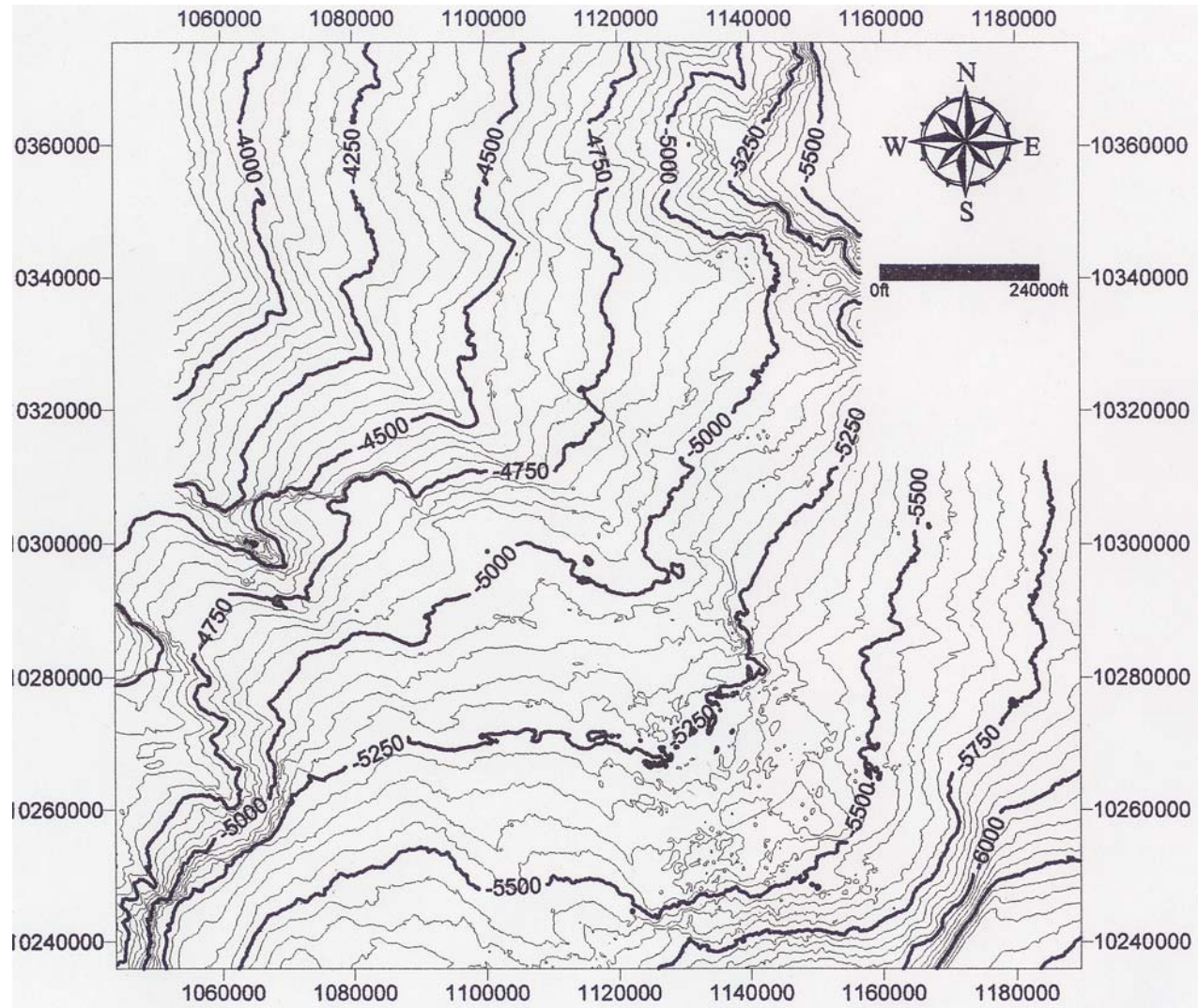


Figure 3. Bathymetry map of study area. Contour interval=50ft. Index Contours every 250ft. X/Y coordinates are NAD 27, UTM Zone 15, USFT.

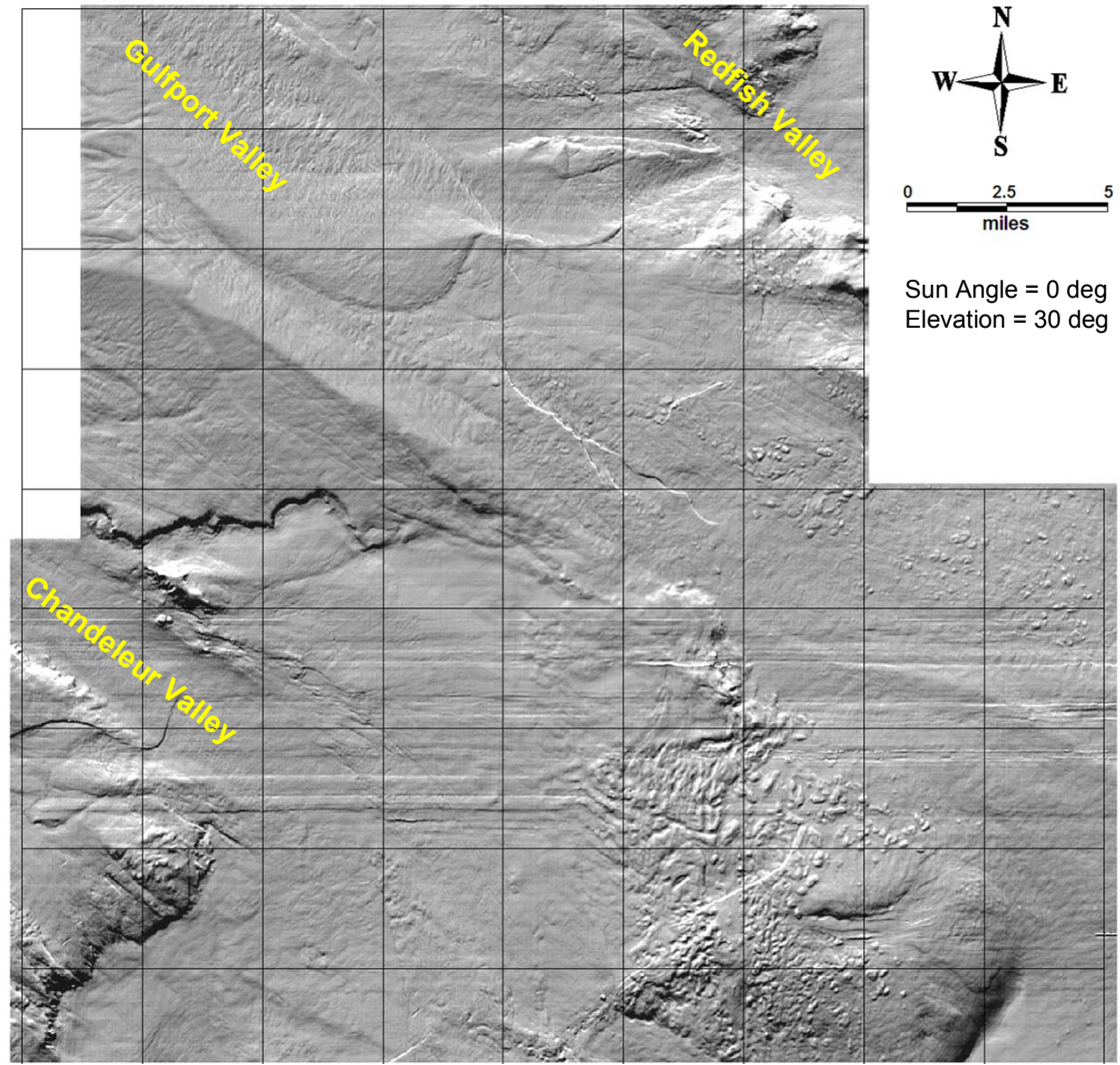


Figure 4. Seafloor rendering of the study area. Square regions represent 3x3 mile OCS lease blocks.

- Identification and mapping of shallow salt bodies in the study area,
- Identification of recent salt tectonic history in the study area,
- Identification of stratigraphy influenced primarily by salt tectonics in the study area,
- Identification of stratigraphy influenced primarily by slope depositional processes in the study area,

Accomplishing the above tasks will lay the groundwork for interpretations and analysis to pursue the following objectives:

- Evolution, on a relative times-scale, of the regional geology based on the interaction between salt tectonics and slope depositional processes in the study area,
- Correlate and where possible extend, confirm, or refute previous notable works conducted in this region of the Mississippi Canyon area on salt tectonics (Diegel et al., 1995; Peel et al., 1995; Schuster, 1995; Wu et al., 1990b) as well as those on sequence stratigraphy and the Mississippi Fan (Dixon and Weimer, 1994, 1998; Weimer, 1989; 1990, 1991).
- Extend sequences of Eastern Mississippi fan westward from the area previously defined by Weimer (1991) and Dixon and Weimer (1994, 1998).
- Confirm or refute the Mobile River as the established source of the Eastern Mississippi Fan (Weimer, 1991; Dixon and Weimer 1994, 1998)
- Examine interaction of salt tectonics and slope depositional processes for this portion of the continental slope.

- Place the evolution of the stratigraphic section for this portion of the slope within the greater context of the Gulf of Mexico depositional history such as the interaction of shifting depocenters and eustatic sea-level change.
- Provide the sequence stratigraphic basis to provide a cursory assessment of engineering/geologic hazards in the study area.

Accomplishing these objectives will hopefully result in new and significant insights into the geology and geological processes the study area as well as the greater northern Gulf of Mexico.

CHAPTER II

DATA AND METHODS

Data

Digital seismic, multi-fold data (3-D seismic) was provided on 8-mm digital tape to Geoscience Earth and Marine Services, Inc. (GEMS) by Mobil Oil Exploration & Producing Southeast Inc., (Mobil), now ExxonMobil. GEMS was contracted to assess the regional geology and stratigraphy for a 73 federal lease block area in the eastern Mississippi Canyon area. Mobil (ExxonMobil) was very courteous in allowing this dataset to be used for this purpose.

The digital seismic data, provided in a SEG-Y file format, on 8-mm digital tape, was loaded onto a PC based workstation to conduct the seismic interpretations and assessment. The study area encompasses a rectangular area of approximately 720 square miles. The inline spacing for the survey data is 65.64 ft, while the crossline spacing is 41.01 ft. The data is sampled at 4.0 milliseconds with a record length of 5.0 seconds from time zero. The data was loaded only for the upper 4.0 seconds from time zero to accommodate for the large size of the dataset as well as maintain interpretations for the upper 3000 ft, bml to 5000 ft, bml. The entire aerial extent of the 3-D volume was used for analysis and interpretation of the geologic conditions for the report and this proposed research.

Methods

The analysis of the data consisted of two steps: (1) Identification and mapping of salt structures and (2) seismic stratigraphic interpretation and facies analysis. The presence of salt is easily identifiable on the seismic record. Detailed analysis of the occurrence of salt in the study area provided confirmation of a number of previous works as well as refined the distribution and regional placement of the salt relative to tectonostratigraphic provinces in the Gulf of Mexico. Seismic stratigraphic and facies analysis was conducted using basic interpretation techniques (Vail, 1987; Vail and Mitchum, 1977; Vail and Wornhardt, 1991; Vail and Wornhardt, 1990; Van Wagoner et al., 1987; Wornhardt and Vail, 1990). These were further refined by recent work for this region of the Gulf of Mexico (Dixon and Weimer, 1994, 1998; Galloway and Buffler, 2004; Weimer, 1989, 1990; 1991).

The seismic program for this study is the Seismic Micro Technology (SMT) 2D/3D PAK®. The program was used to perform the seismic interpretations, map horizons, perform volume attribute analysis of the stratigraphic sequences, and produce the raw images for use in figures. Surfer®v.8.0 was used to grid horizon data and volume attribute data for visualization and input into MapInfo GIS. MapInfo GIS was used to visualize the grid data, produce Isopach, contour, and structure maps, create perspective views of surfaces, and georeferencing images of previous works with respect to this study's area and interpretations for insights into salt tectonics and sequence

stratigraphy. Corel Draw 7.0. and PowerPoint XP were used to finish the figures found in the text.

The maps and profiles used in this dissertation will reflect the reduction and interpretation of the 3-D digital seismic dataset. A concise description of how the data is analyzed to produce these maps and profiles follows.

A. Bathymetry Map

The bathymetric contours shown on the map are computer generated using the Golden Software Surfer®v.8.0 mapping program. The depth values are obtained using the SMT 2D/3D PAK® by picking the peak attribute of the seafloor return along an approximate 50-line by 50-line grid. Once these picks are completed, the remainder of the dataset is auto-volume picked. Erroneous picks are then corrected to produce a complete and accurate pick for every bin.

The time-value picks are transferred from the 2D/3D PAK® software to surfer and converted from time-pick values to depth (feet) values. The velocity corrections applied in this program are based on a seventh-order polynomial similar to a technique described by Advocate and Hood (1993). The equation is as follows:

$$\text{Depth}=0.1105-5066.913T-468.6693T^2-554.7107T^3+340.7019T^4-116.9910T^5+20.7280T^6-1.1658T^7$$

T = one way travel time

The Surfer program grids the water depth values on a 50 ft by 50 ft grid using a Kriging algorithm. This grid is then exported to MapInfo GIS and contoured at a 20 ft interval.

B. Isopach Map

Six prominent horizons were selected to separate the seismic volume into stratigraphic sequences. These horizons were selected according to their seismic attribute, or manually interpreted where necessary, using 2D/3D PAK®. The horizons are selected on every 10th inline and 20th crossline. These horizons are then "hunted" to get a 100% pick over the entire study area. The result of these endeavors are a files of time measurements from sea surface (time zero) for each horizon. The seafloor pick (in time) is then subtracted from the respective horizon time file to produce a thickness, in time, from the seafloor to the horizon.

A third-order polynomial is selected as the best fit curve to the raw checkshot values from wells within the study area (Figure 4). The polynomial is as follows:

$$y = 70.379x^3 + 0.8315x^2 + 2910.9x$$

$$y = \text{Depth below seafloor}$$

$$x = \text{time below seafloor (in seconds)}$$

The polynomial is used to generate an interpreted velocity curve for the conversion of time to depth.

The contour interval for these maps is chosen to best illustrate the change in sediment thickness above the horizons that reflect the structural and stratigraphic influences upon these sequences.

C. Thickness Maps

A thickness map between two prominent horizons is necessary for identifying the variation in thickness of a particular stratigraphic sequence which can provide insights into depositional processes and lateral distribution of facies. The horizons at the top and base of this sequence are mapped on every 50th inline and 50th crossline and then auto-volume picked. The result is two files of time measurements from sea surface (time zero). The seafloor pick (in time) is subtracted from the time pick to each horizon to produce a time value from the seafloor to each horizon.

Depth values are then calculated the same way described for the isopach maps. The xyz depth file for the shallower horizon is subtracted from the deeper horizon to produce a positive value of thickness between the two horizons. The resulting thickness file is then exported to Surfer® and gridded at a 50 ft by 50 ft grid spacing using a Kriging algorithm. This grid is then exported to MapInfo GIS for final preparation of the thickness map.

D. Enhanced Seafloor Rendering and Seafloor Amplitude Rendering

The Enhanced Seafloor Rendering is a visualization of the seafloor. Exporting the seafloor pick from the seismic dataset into Surfer for gridding, and subsequently to MapInfo GIS facilitates the rendering. The azimuth and elevation of the sun-angle are adjusted to filter out line bias, and at the same time retain any important seafloor features. Color enhancements of depth variation provide a graded depiction of the changes in seafloor depth.

The Seafloor Amplitude Rendering superimposes seafloor amplitudes over a greyscale seafloor rendering. To get these amplitude values, a time envelope around the seafloor peak is searched for the highest relative amplitude at each seismic trace. These amplitude values are exported to Surfer®, gridded on a 100 ft by 100 ft grid using a Kriging algorithm, and exported to MapInfo GIS for overlay and rendering.

The Seafloor Amplitude Rendering is used to identify possible areas of hydrocarbon seepage and/or carbonate hard grounds. Seabed amplitude anomalies may be related to the presence of venting hydrocarbons and/or authigenic carbonates as shown in various studies (Doyle et al., 1996; Roberts et al., 1992).

The renderings serve to highlight unique seafloor conditions related to the surface and subsurface geology of the study area. They also serve to highlight areas of potential hazards/constraints to hydrocarbon exploration and production operations.

E. Seismic Data Examples

The data examples are selected from the 3-D data volume to illustrate geologic conditions and stratigraphy pertinent to the objectives of this proposed research.

F. RMS Volume Calculations

The RMS, or root mean square, is a mathematical calculation performed on the seismic amplitude data using the following formula:

$$\text{RMS} = \sqrt{\frac{\sum p^2}{N}}$$

P= Seismic amplitude N= Number of sinusoids (seismic wavelets) in the time envelope

The horizons mapped in the study area are selected to define specific stratigraphic sequences. These horizons provide the upper and lower limit of the time envelope for each sequence. The number of seismic wavelets is dependent upon the time thickness of the envelope. The amplitude for each wavelet is squared to make all amplitudes positive; otherwise, positive and negative amplitudes would zero each other out when summed together. The squared values are summed and divided by the number of wavelets producing a positive mean square for each trace in the time envelope. The square root of the mean square is taken to return to a measure of amplitude.

The RMS value has unique properties when applied to shallow seismic amplitude data. Each stratigraphic sequence, or time envelope, has different ambient background amplitude particular to its seismic and stratigraphic properties. The RMS calculation tends to normalize the background amplitude of the sequence. This in turn allows traces having even a subtle RMS value greater or less than the background to become identifiable. Changes in sediment composition, depositional processes, and structure become apparent and better defined.

The RMS can also be considered an indirect representation of the variance when applied to an envelope of seismic data. The RMS is calculated for every trace in the dataset having its own unique value based upon the amplitude of the wavelets in that trace. When these values are displayed over the entire study area, such as in a RMS amplitude display, the lateral variance from trace to trace becomes apparent. This illustrates the variation in the amplitude envelope of each trace based upon changes in geologic structure or stratigraphy.

The RMS is beneficial to this proposed research in identifying specific structural and stratigraphic features. Application of this calculation to the seismic volume will provide insight into how structural and stratigraphic processes have interacted through time. It is also quite effective as an aid in identifying subsurface geologic hazards or constraints.

CHAPTER III

BACKGROUND

Gulf of Mexico Geologic Setting

Early studies of the Gulf of Mexico interpreted the basin to be an “ancient” feature, in existence since the Precambrian (Schuchert, 1909; Willis, 1909). Willis is quoted by Schuchert as describing the Gulf of Mexico as “a mass of basalt, which was erupted in the Pre-Cambrian time” and being of “great antiquity” (Schuchert, 1935).

Present day interpretations paint a much different picture of the development of the Gulf of Mexico. The formation of the modern day gulf was the result of the Mesozoic breakup of the supercontinent Pangea (Figure 5), during which the North American plate separated from the South American and African plate (Buffler and Sawyer, 1985; Pilger, 1981; Salvador, 1987). Triassic/Jurassic rifting associated with the supercontinent’s breakup resulted in the formation of a large area of transitional crust (Figures 6a and 6b) forming the gulf’s proto-basin (Buffler, 1989; Buffler and Sawyer, 1985).

Shallow and periodic flooding from the Pacific in the Middle Jurassic (Salvador, 1991), (Figure 7), in combination with an arid environment resulted in the formation of thick evaporite deposits known as the Louann salt (Liro, 1989; Salvador, 1991) (Figure 6b). Original thickness of the salt is estimated to be up to 4000 meters, or 13,000 ft

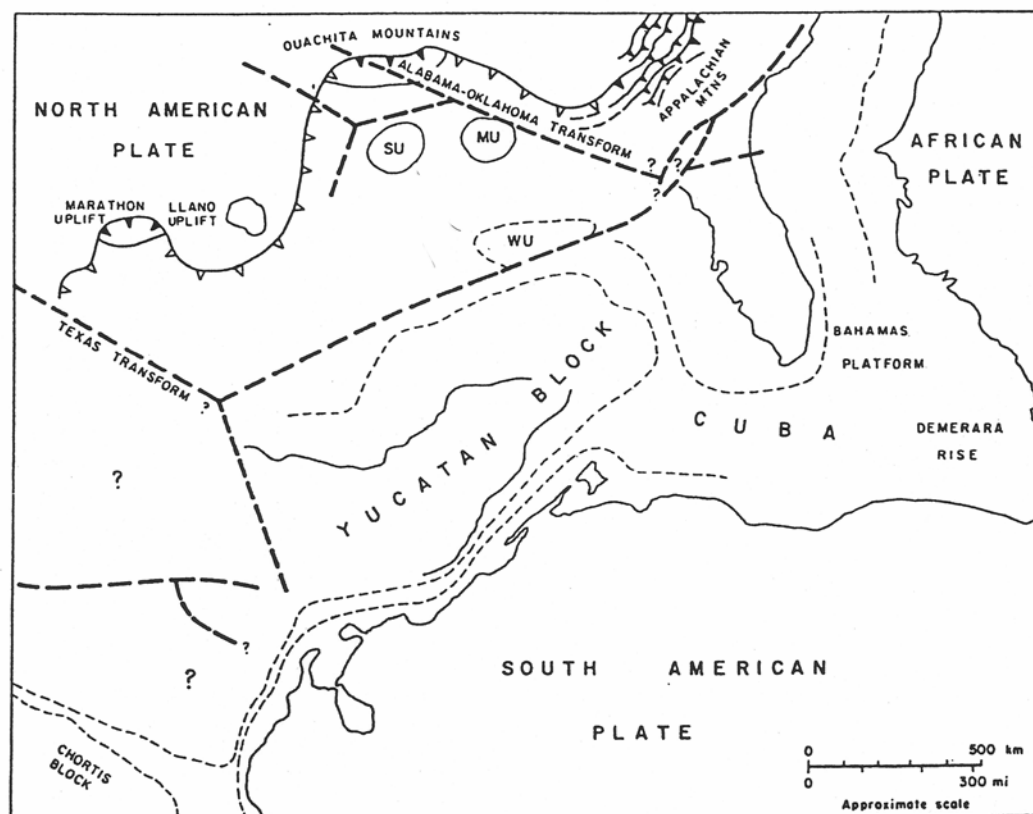


Figure 5. Reconstruction of western Pangea (future Gulf of Mexico) in late Paleozoic/early Mesozoic time (Salvador, 1991).

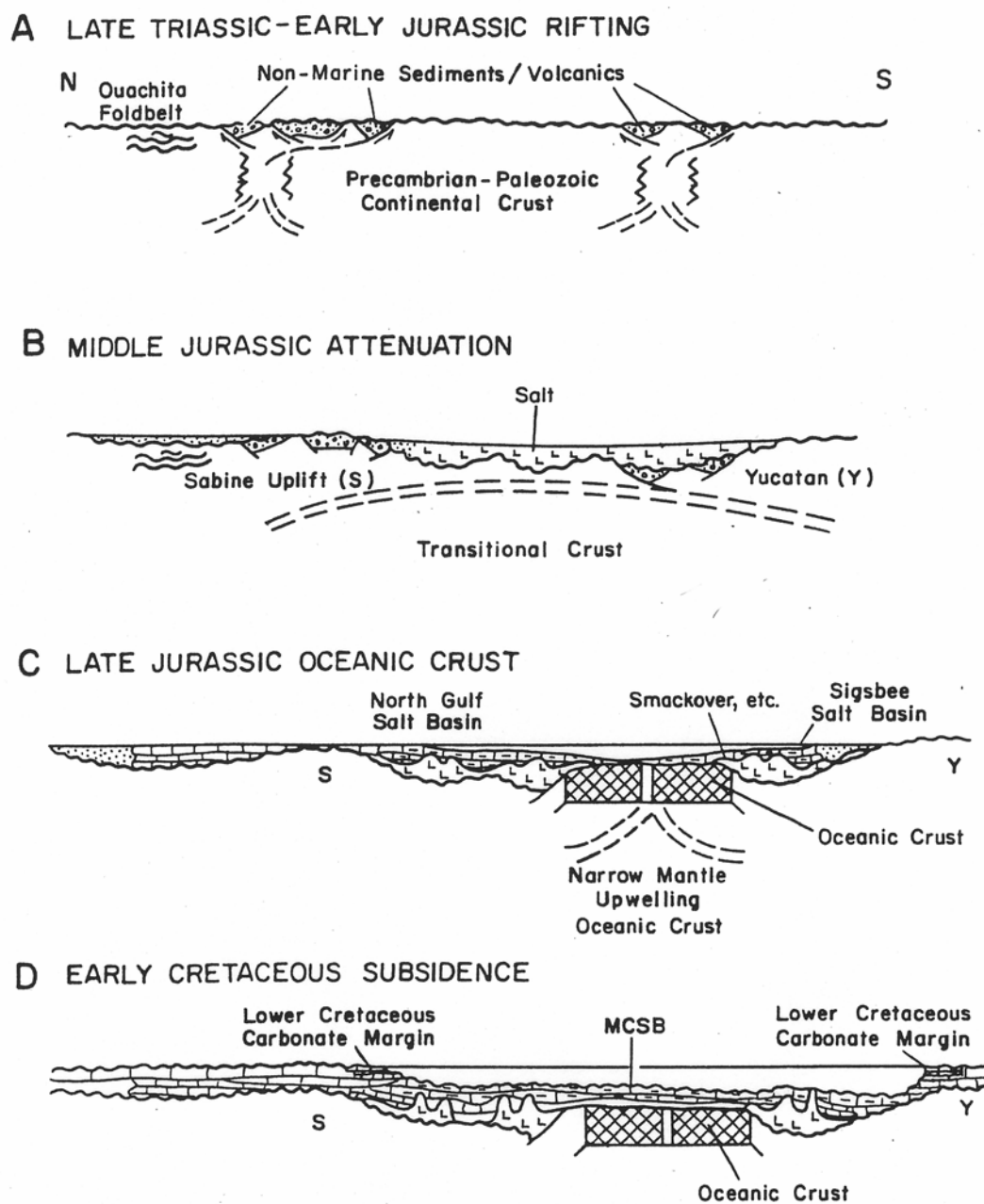


Figure 6. Schematic diagram illustrating the early (pre-middle Cretaceous) evolution of the Gulf of Mexico (Buller and Sawyer, 1985). Stages proceed from A to D.

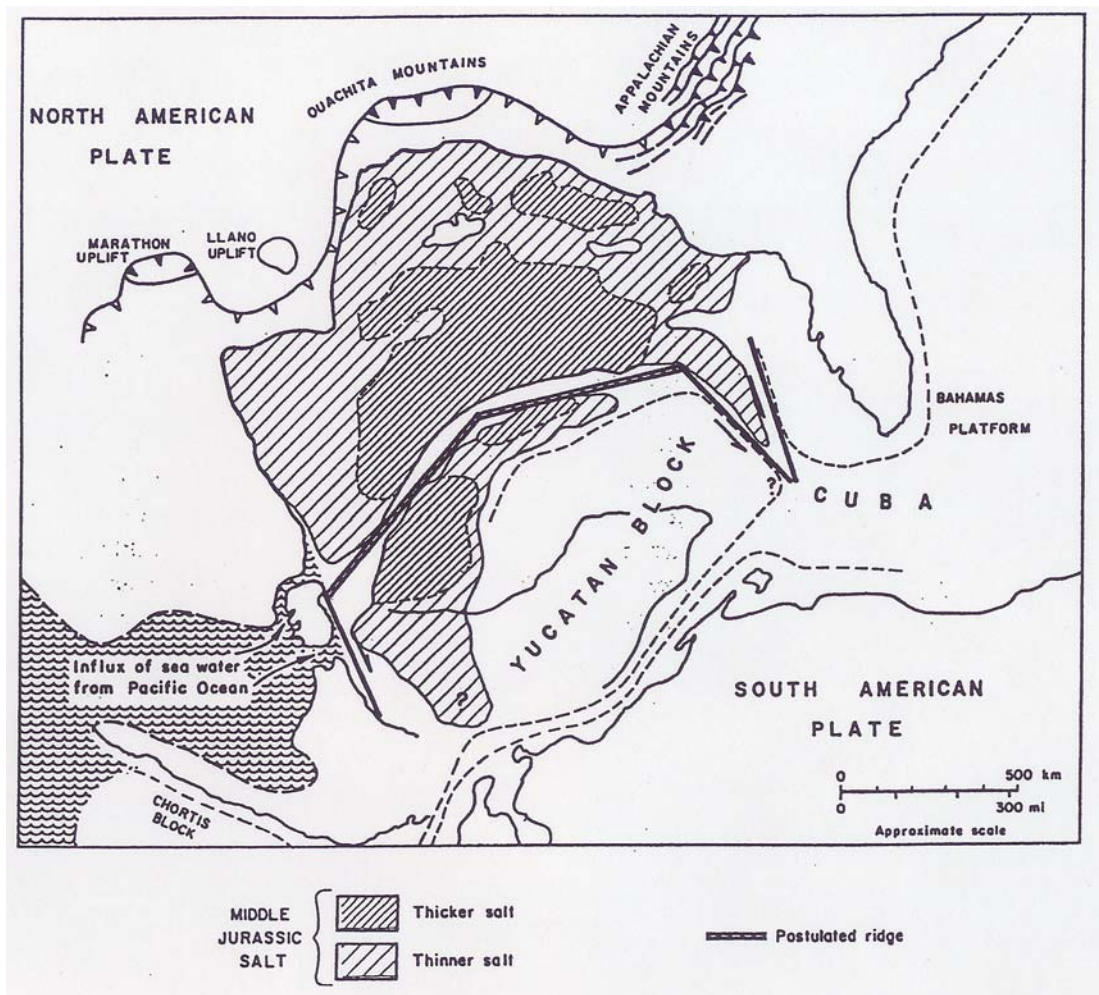


Figure 7. Reconstruction of western Pangea (future Gulf of Mexico) during late-Middle Jurassic (Salvador, 1991).

(Liro, 1989;Salvador, 1991). The salt is interpreted to have been deposited in gently subsiding grabens floored by transitional crust (Liro, 1989;Salvador, 1991). Continued rifting in the central gulf lead to seafloor spreading and the introduction of a narrow east-west trending band of oceanic crust (Figure 6c) during the Middle to Late Jurassic (Buffler, 1989;Buffler and Sawyer, 1985). The emplacement of oceanic crust split the Louann salt into a northern and southern segment (Lopez, 1989;Salvador, 1991) (Figure 8). Thermal subsidence of this oceanic crust resulted in formation of the modern modern basin, floored by the crust, into which approximately 3,000 to 6,000 meters (9,800 to 19,700 ft) of Jurassic and Cretaceous sediments have been deposited (Lopez, 1989), (Figure 6d). The subsidence reorganized the existing basin geometry with an evolving deepwater basin fringed by shallow water. This lead to the formation of carbonate platforms in the shallow waters that rimmed the deepening basin (Buffler and Sawyer, 1985) (Figure 9).

The depositional record of terrigenous clastic sediments into the Gulf of Mexico can be separated into two eras, the Late Mesozoic (Later Jurassic to Late Cretaceous), and the Cenozoic (Paleocene, Eocene, Oligocene, Miocene, Pliocene, and Pleistocene). Sediment influx during the Late Jurassic and Early Cretaceous was from the north, northeast, and northwest (Salvador, 1991). The source of terrigenous sediments during this period was from the Appalachian and Ouachita mountain ranges as well as the interior of the North American continent (Salvador, 1991). Later Cretaceous sedimentation became centered in the northwestern Gulf of Mexico (Figure 10) forming a thick wedge of sediment that extended into the deep basin (Feng and Buffler, 1996).

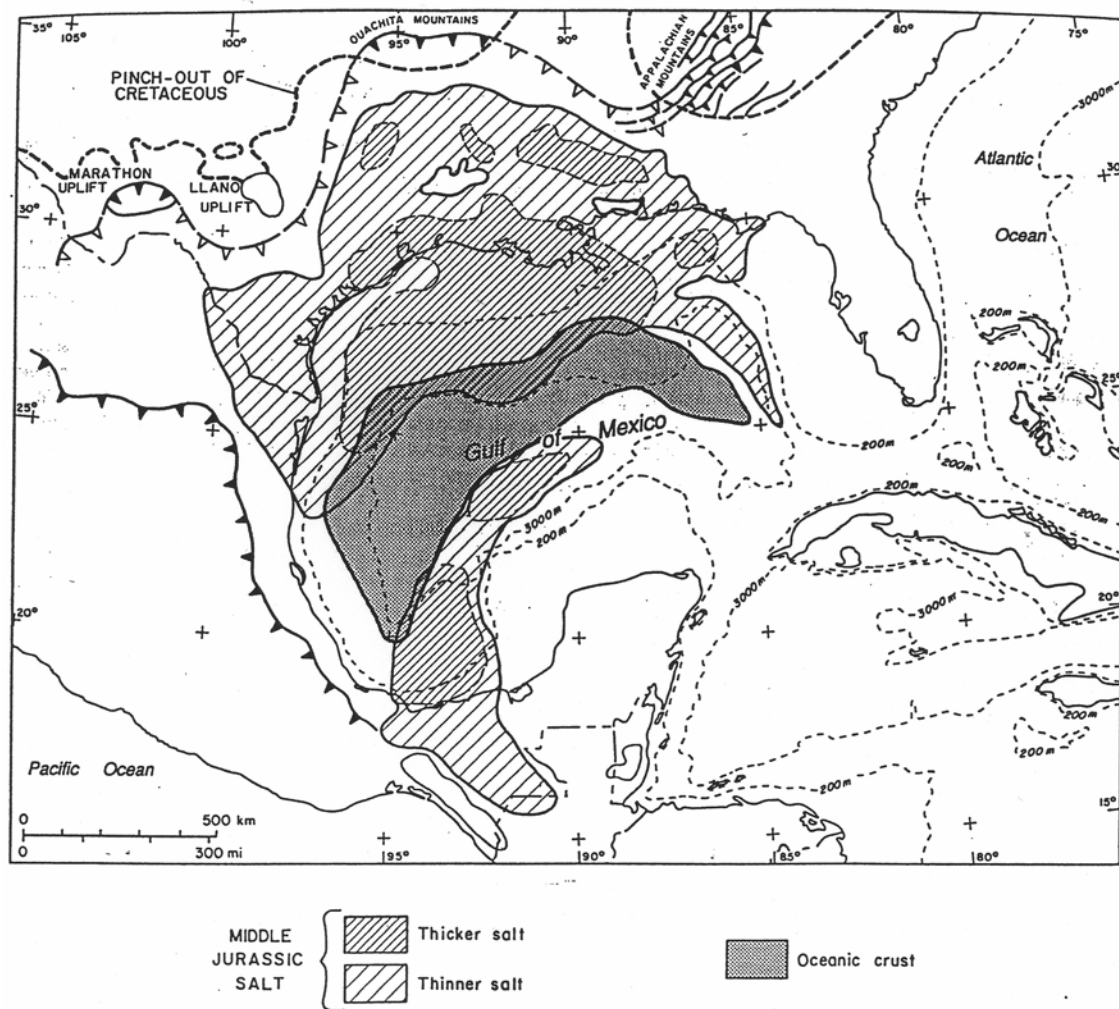


Figure 8. Distribution of Middle Jurassic salt deposits and oceanic crust in the Gulf of Mexico during the early Cretaceous (Salvador, 1991).

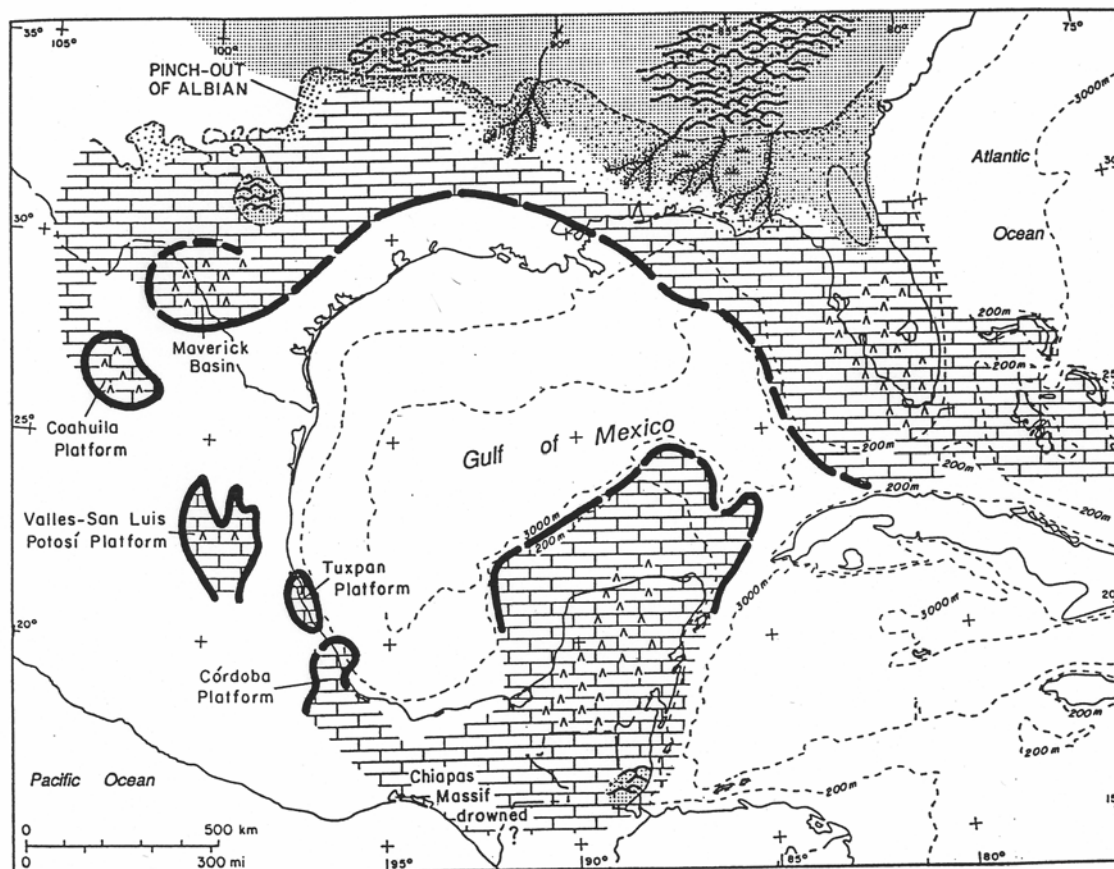


Figure 9. Diagram of carbonate ramp and platforms in the Gulf of Mexico during the early Cretaceous (Salvador, 1991).

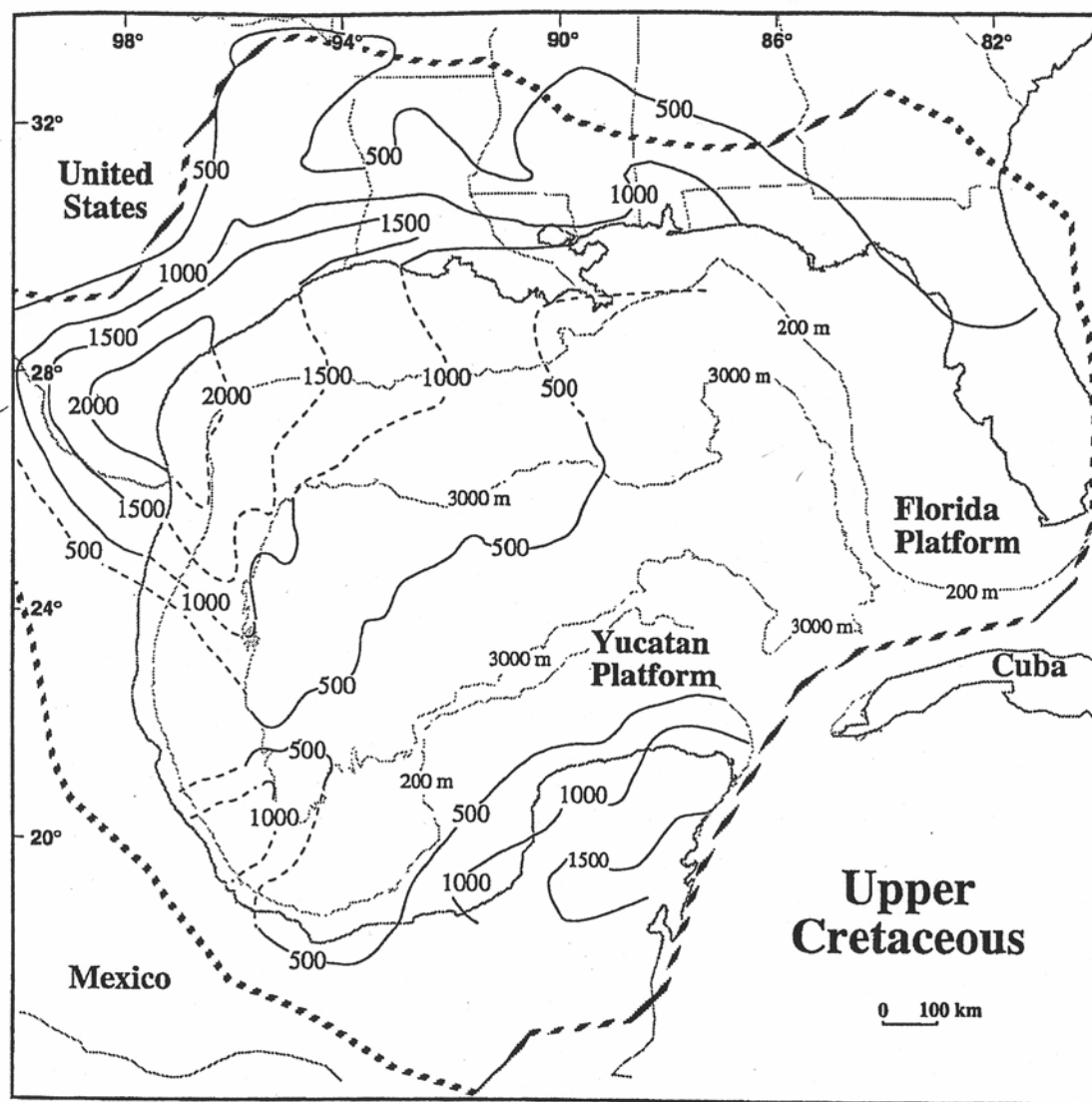


Figure 10. Isopach map showing thickness and distribution of Upper Cretaceous sediments in the Gulf of Mexico basin. Contours in meters. Dashed lines where interpolated. Structural limit of Gulf basin shown (Feng and Buffler, 1996)

Four major depocenters occurred along the northwest and southwest margins (Feng and Buffler, 1996)(Figure 11). Sedimentation into the Gulf basin during the Later Cretaceous is directly attributed to increased erosion due to uplift of the mainland associated with the initiation of the Laramide orogeny (mountain-building) along the western gulf basin (Feng and Buffler, 1996).

Cenozoic sedimentation into the Gulf of Mexico, beginning in the Paleocene, can be characterized by an eastward shift in depocenters (Figure 12) and changing terrigenous sediment sources. Large volumes of sediment were deposited into the northwestern and western gulf during the Paleocene (Feng and Buffler, 1996), (Figure 13). A dramatic increase in sedimentation is also evident in the northern and northwestern gulf (Figure 13 and 14). The Paleocene also marked the first notable episode of continental margin/shelf building (Galloway, 1989b; Rainwater, 1964; Salvador, 1991) (Figure 14).

High rates of sedimentation continued in the northwestern and western Gulf of Mexico during the Eocene. The Eocene depocenter remained the same as in the Paleocene but was much thicker and concentrated in the northwestern gulf where the deltaic margin/ shelf building begun in the Paleocene continued (Galloway, 1989b; Rainwater, 1964; Salvador, 1991) (Figure 15). During the late Eocene, there was an eastward shift in deep submarine fans probably related to the continued deltaic outbuilding in the northwestern Gulf (Feng and Buffler, 1996) (Figure 16).

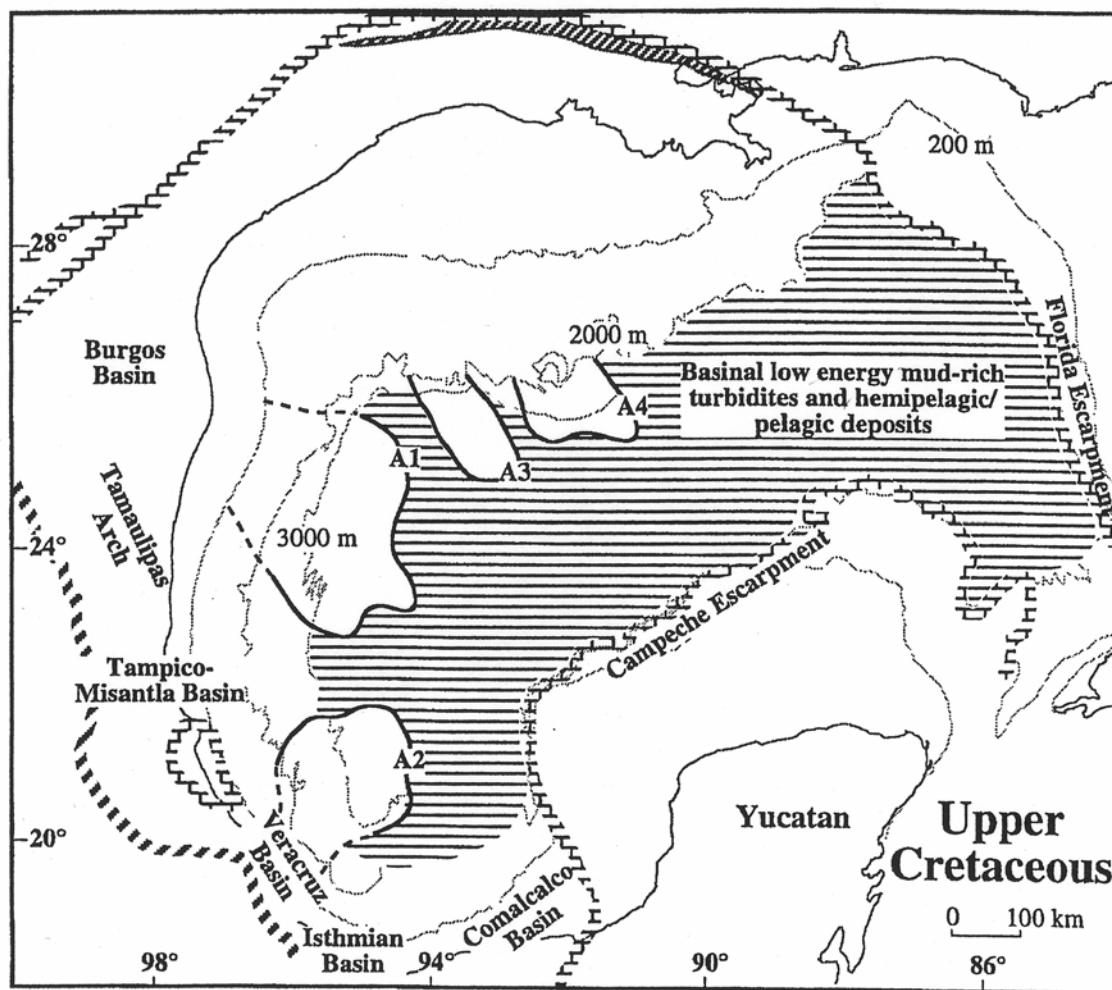


Figure 11. Generalized deposystems map showing location of primary Upper Cretaceous depocenters (Feng and Buffler, 1996). A1-A4 are Cretaceous submarine fan lobes (Feng, 1995).

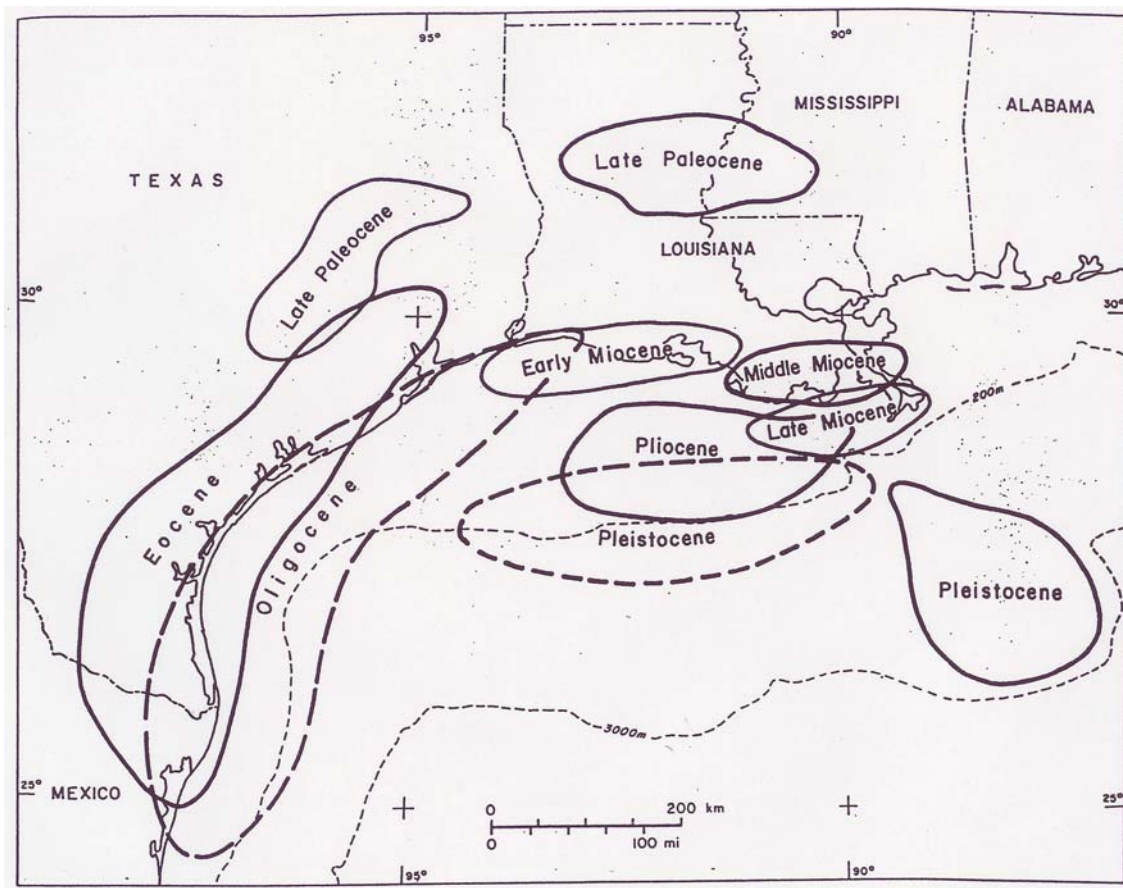


Figure 12. Location of Cenozoic depocenters in the northwestern Gulf of Mexico (Salvador, 1991).

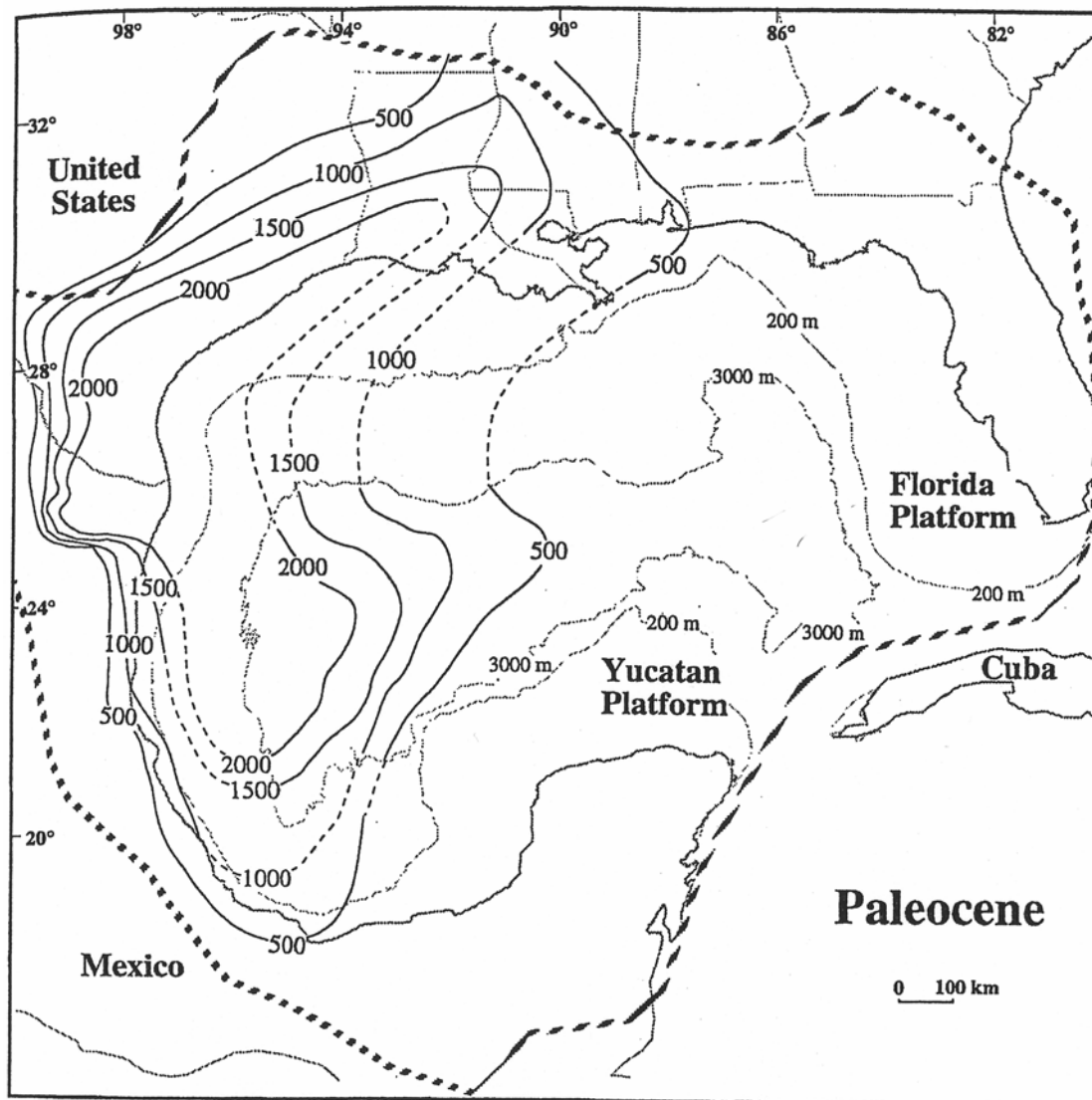


Figure 13. Isopach map showing the thickness of Paleocene terrigenous clastic sediments in the Gulf of Mexico basin. Contours in meters. Dashed lines where interpolated. Structural limit of Gulf basin shown (Feng and Buffler, 1996).

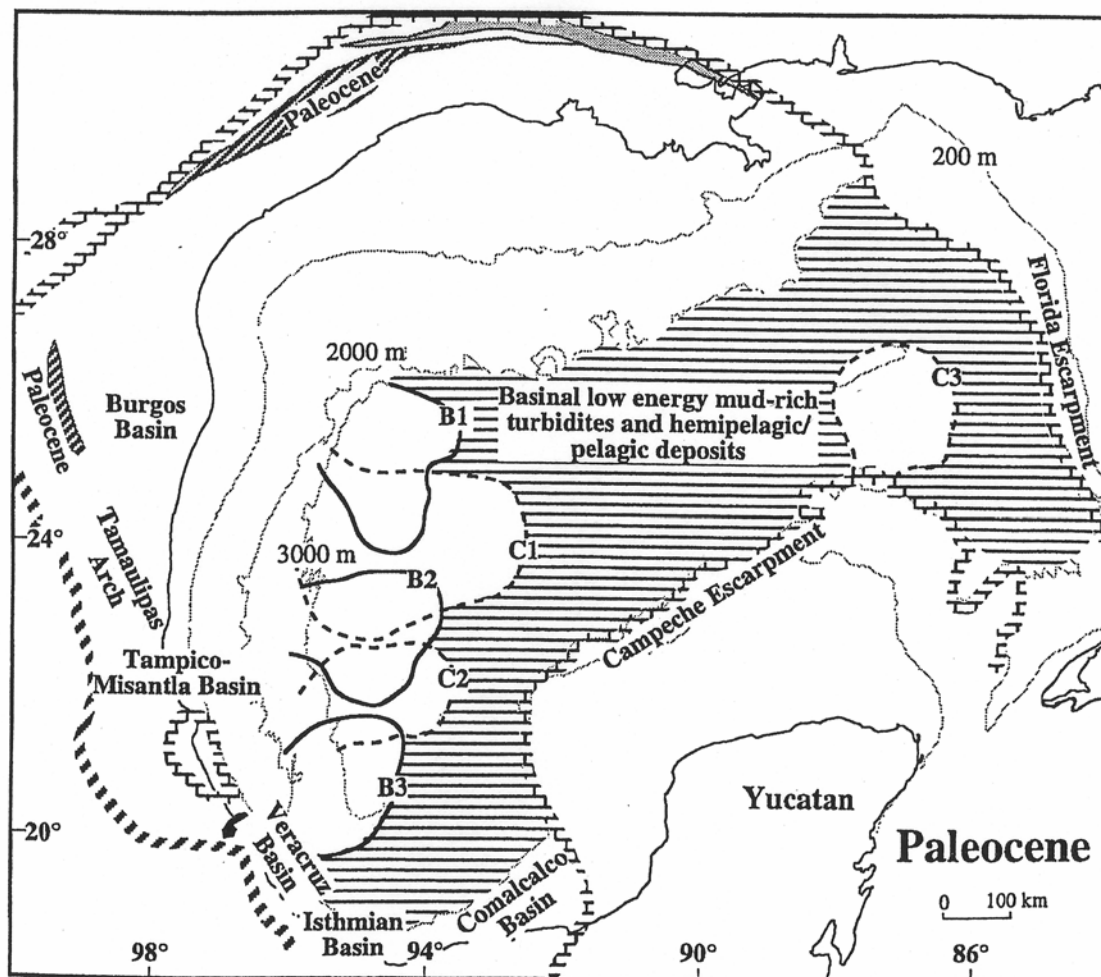


Figure 14. Generalized deposystems map showing location of primary Paleocene depocenters (Feng and Buffler, 1996). B1 through C3 are Paleocene submarine fan lobes (Feng, 1995).

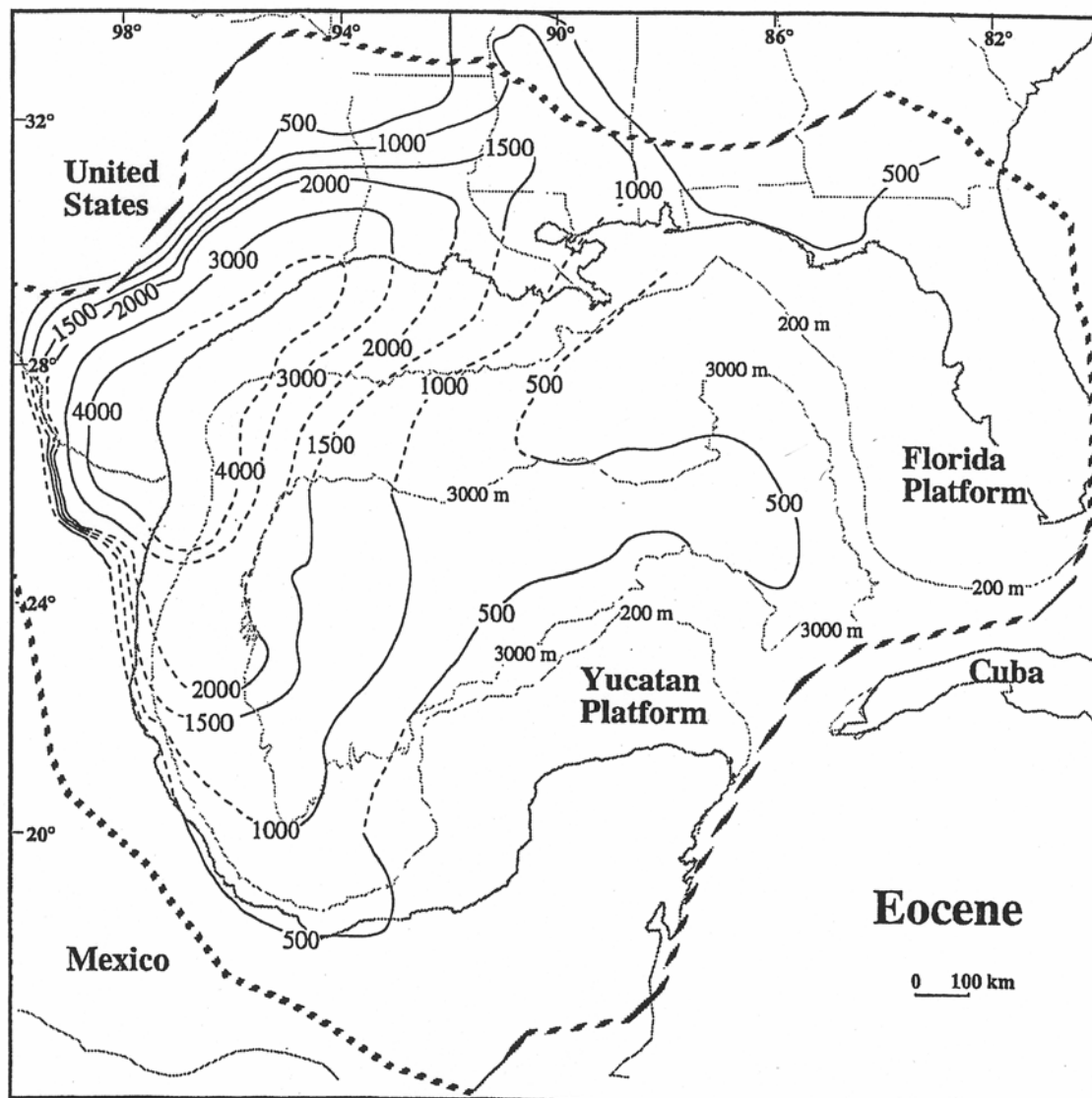


Figure 15. Isopach map showing the thickness of Eocene terrigenous clastic sediments in the Gulf of Mexico basin. Contours in meters. Dashed lines where interpolated. Structural limit of Gulf basin shown (Feng and Buffler, 1996).

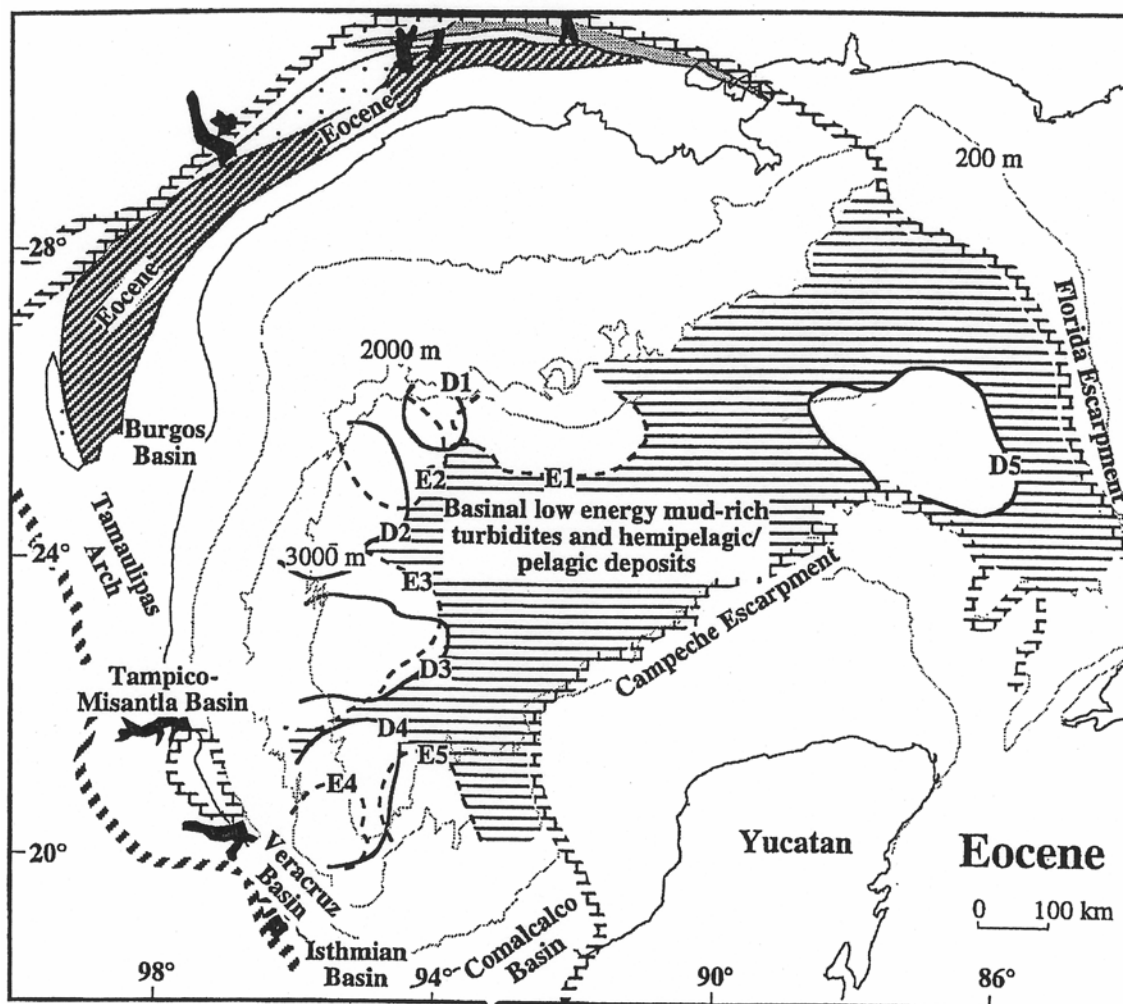


Figure 16. Generalized deposystems map showing location of primary Eocene depocenters (Feng and Buffler, 1996). D1-E5 are Eocene submarine fan lobes (Feng, 1995).

The Oligocene marks a major episode of margin/shelf building in the Gulf of Mexico (Galloway, 1989b; Rainwater, 1964; Salvador, 1991) where large volumes of sediments were deposited in the northwestern Gulf (Figure 17). A pronounced eastward shift in the depocenter along the northwest margin probably resulted from the change in source areas related to a pronounced fall in eustatic sea level (Coleman, 1990) and the emergence of an organized Mississippi River drainage system. As a result, a large clastic wedge of sediments prograded more than 80 kilometers seaward of the pre-existing shelf margin (Galloway, 1989b; Salvador, 1991) (Figure 18).

The eastward shift of depocenter in the Oligocene continued into the Miocene and was focused in the northwestern gulf offshore of what is now Texas and Louisiana (Feng and Buffler, 1996) (Figure 19). High sedimentation rates continued as the deltaic shelf margin continued to prograde seaward by another 80 kilometers (Figure 20). This eastward and basinward shift of depocenter signifies the organization and establishment of the Mississippi River as the primary source of terrigenous sediments to the Gulf of Mexico basin (Winker, 1982).

The Pliocene marked a continued eastward shift in depocenter focused on the northern basin margin offshore modern day Louisiana and Texas (Feng and Buffler 1996) (Figure 21). High volumes of sediments were deposited offshore Louisiana during the early Pliocene while sedimentation was low in areas offshore of Texas. during the late Pliocene, sedimentation resumed in areas of offshore Texas due to a fall in eustatic sea level (Galloway, 1989a). Eustatic changes in sea level during the Pliocene

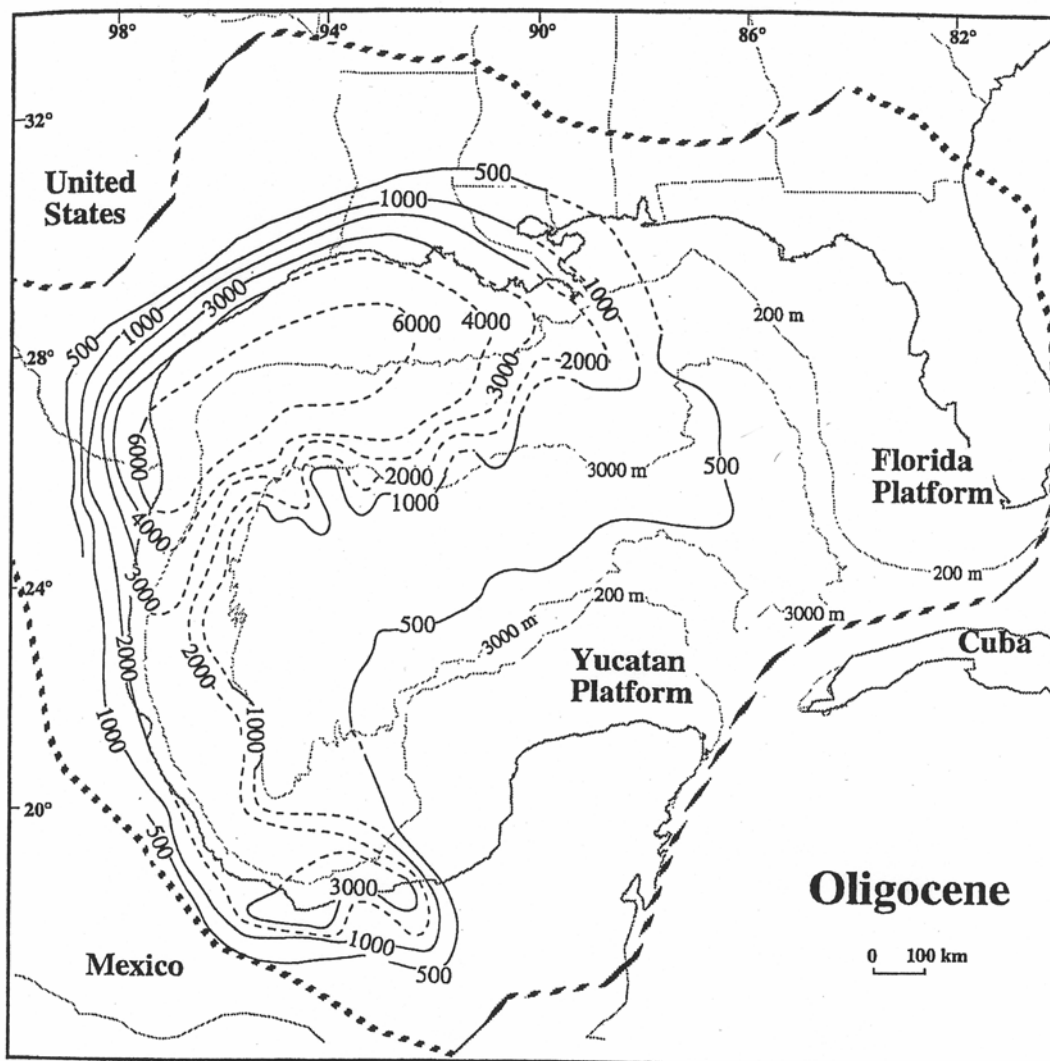


Figure 17. Isopach map showing the thickness of Oligocene terrigenous clastic sediments in the Gulf of Mexico basin. Contours in meters. Dashed where interpolated. Structural limit of Gulf basin shown (Feng and Buffler, 1996).

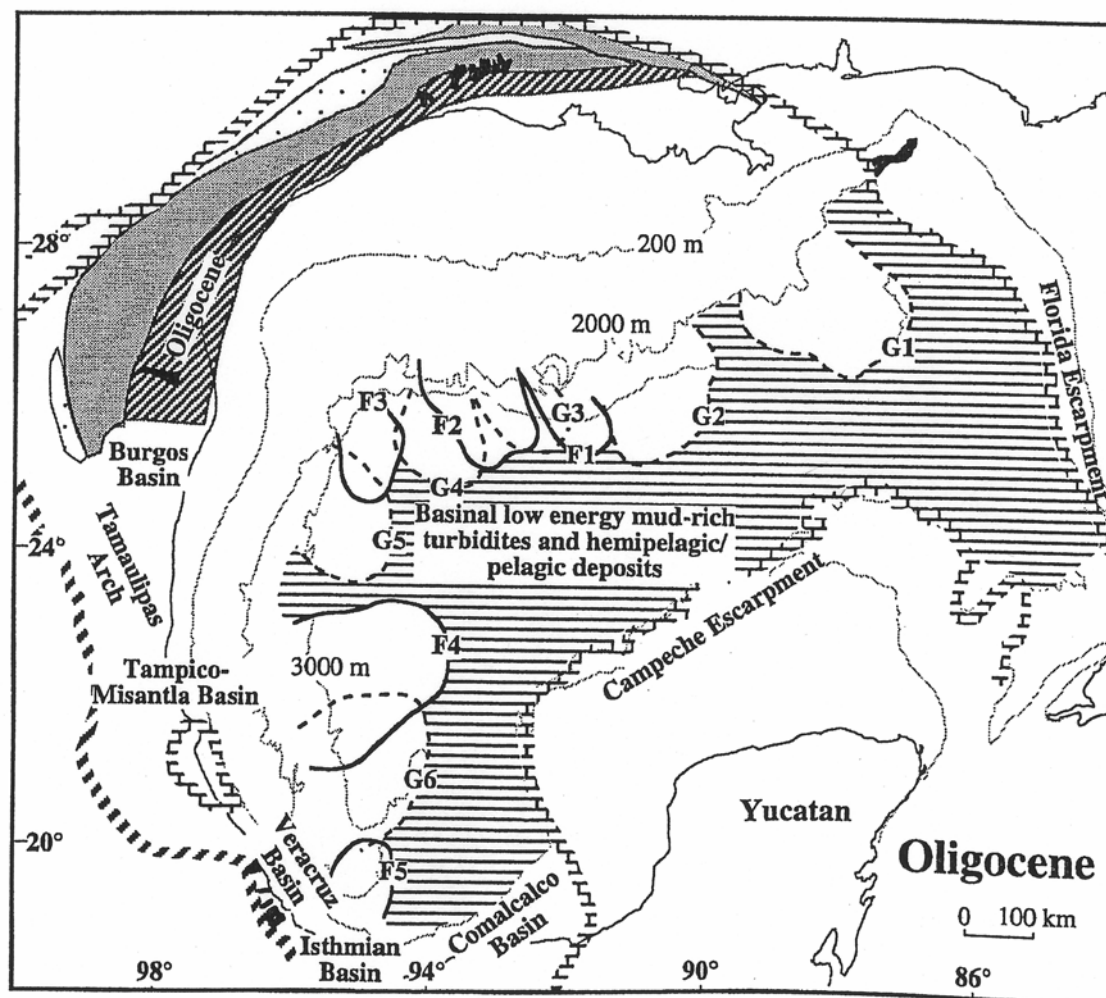


Figure 18. Generalized deposystems map showing location of primary Oligocene depocenters. Prograding shelf edge is evident (Feng and Buffler, 1996). F1-G6 are Oligocene submarine fans (Feng, 1995).

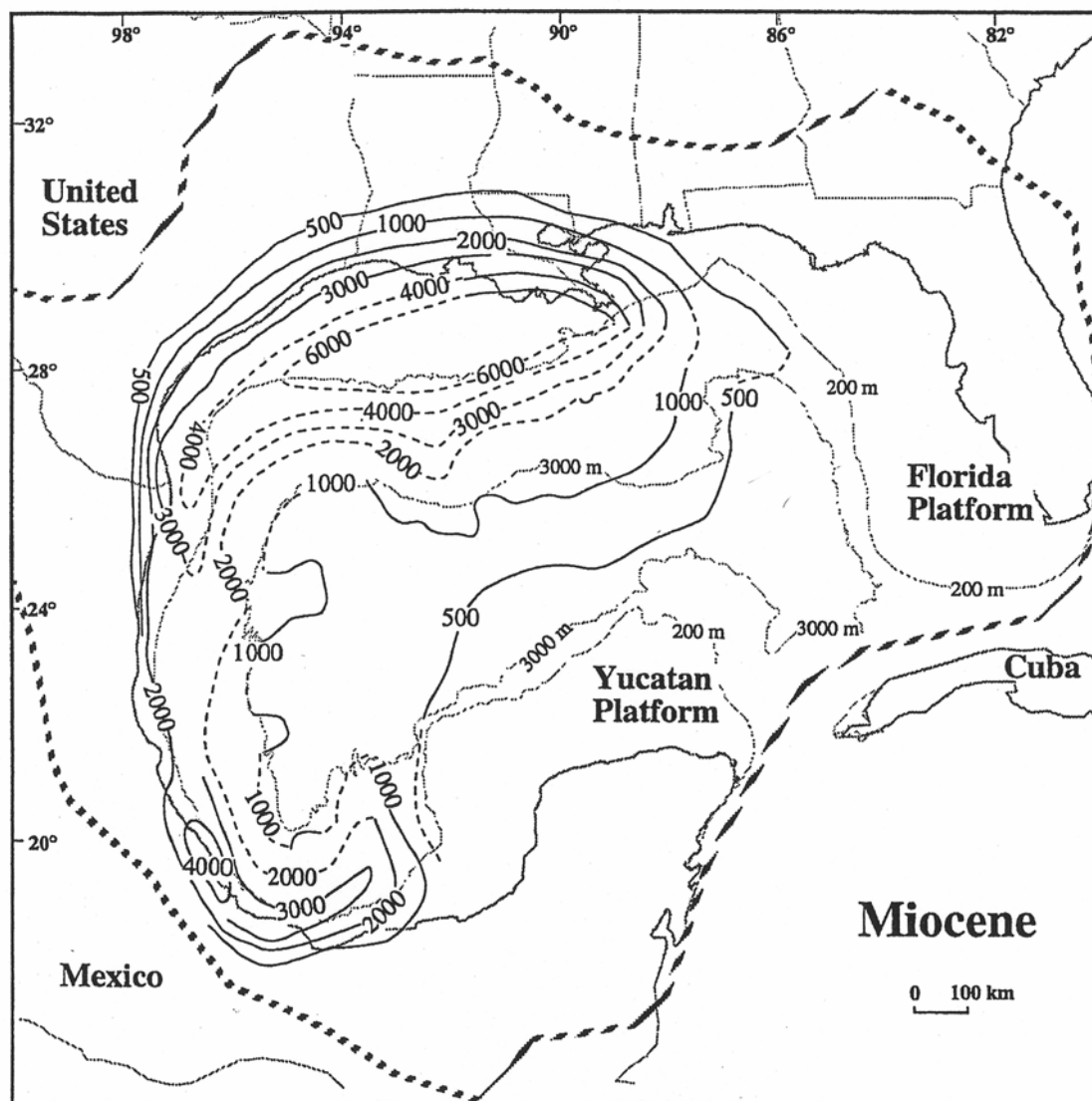


Figure 19. Isopach map showing the thickness of Miocene terrigenous clastic sediments in the Gulf of Mexico basin. Contours in meters. Dashed where interpolated. Structural limit of Gulf basin shown (Feng and Buffler, 1996).

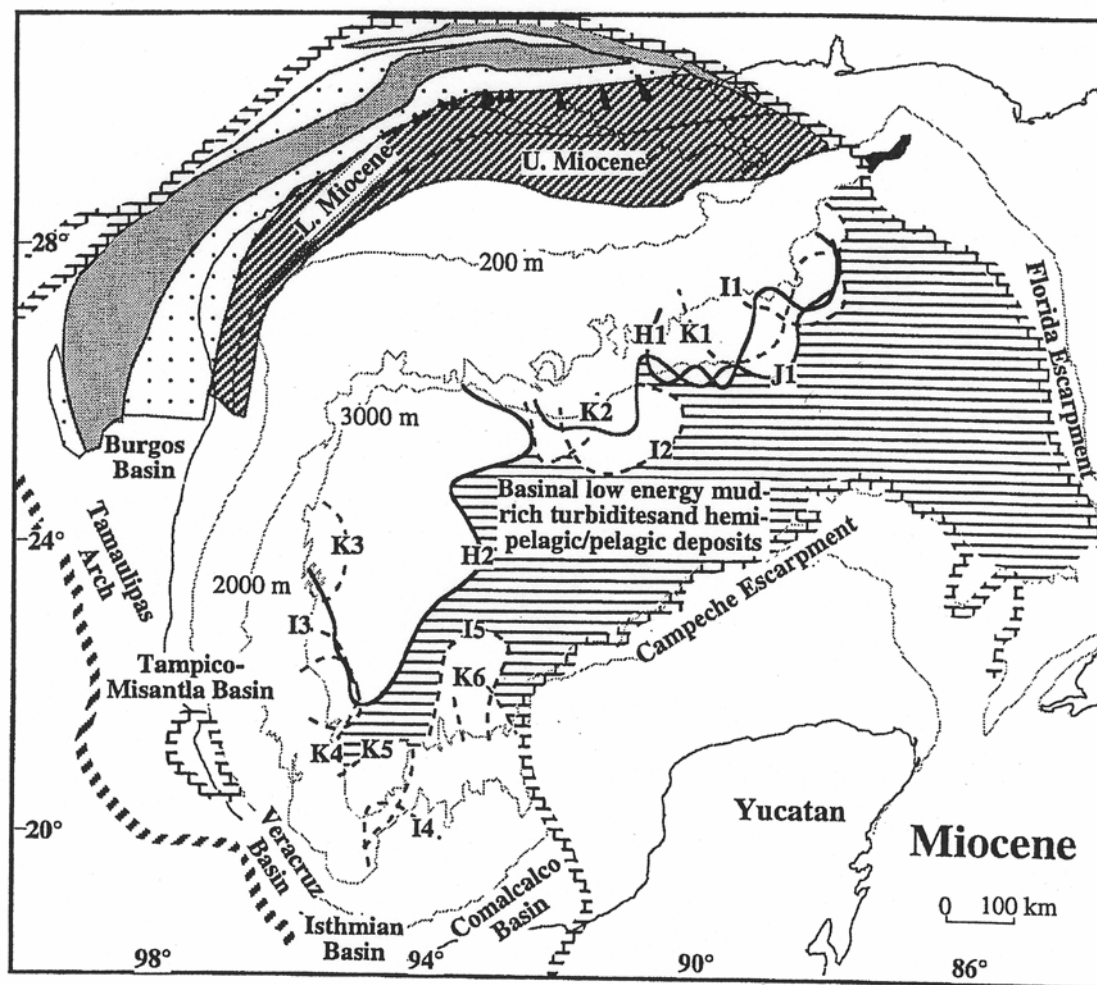


Figure 20. Generalized deposystems map showing the location of primary Miocene depocenters. Prograding northern shelf margin evident (Feng and Buffler, 1996). H1-K6 are Miocene submarine fan lobes (Feng, 1995).

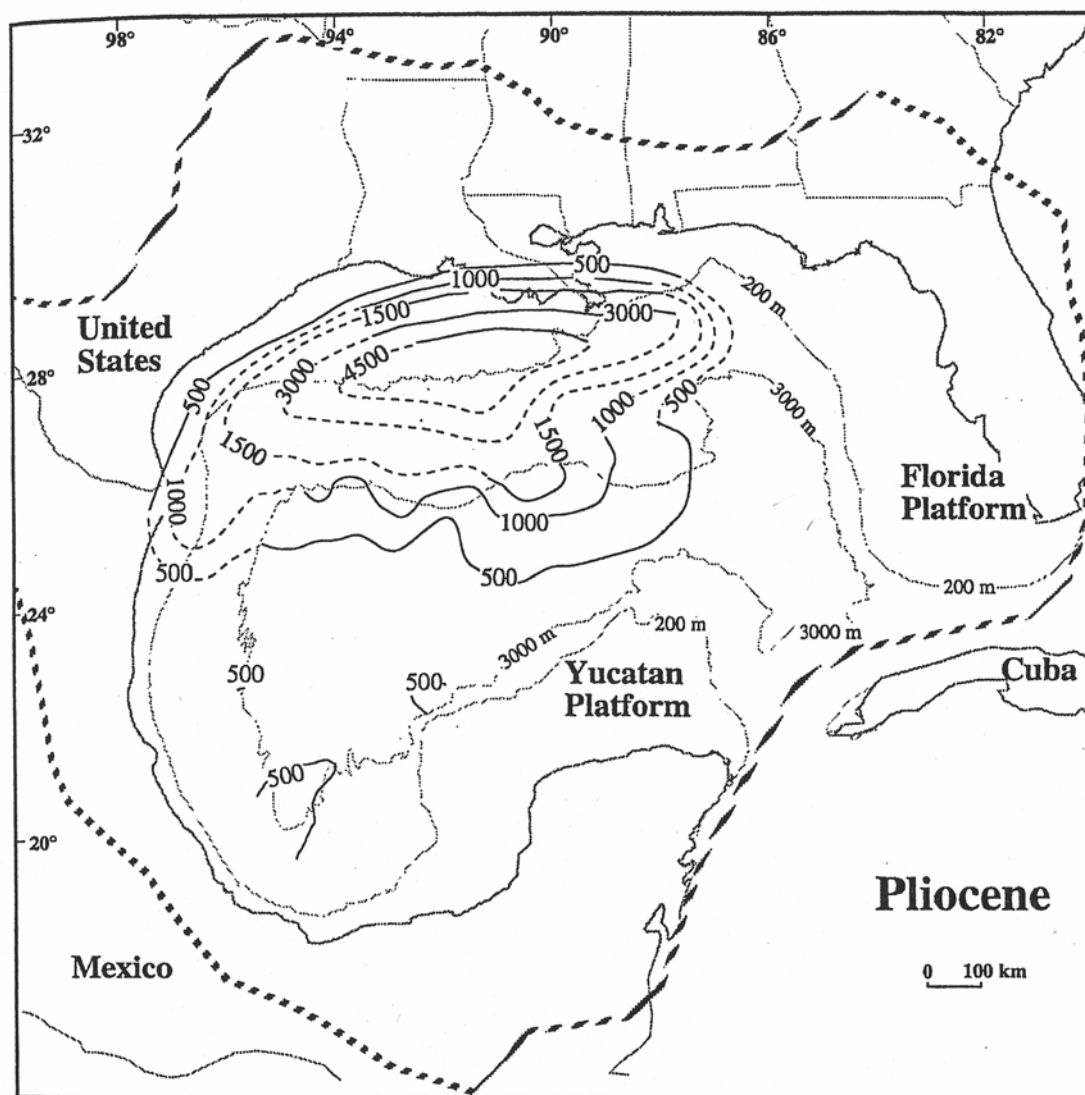


Figure 21. Isopach map showing thickness of Pliocene terrigenous clastic sediments in the Gulf of Mexico basin. Contours in meters. Dashed where interpolated (Feng and Buffler, 1996).

are thought to be the primary factor controlling the rate and location of sedimentation into the Gulf of Mexico (Galloway, 1989a, 1989b; Morton and Galloway, 1991). Shelf margin outbuilding continued as the Mississippi Fan prograded into the deep northern basin (Feng and Buffler, 1996), (Figure 22).

During the Pleistocene, the Mississippi River continued its dominance as the primary source of sediment to the Gulf of Mexico (Feng and Buffler, 1996). The Mississippi River continued to shift to the east resulting in a southeast shift in the Pleistocene depocenter (Feng and Buffler, 1996), (Figure 23). This southeastern shift in depocenter was likely related to the eastward shift of the Mississippi deltaic region and a progradation of deltaic sediments approximately 8- km seaward over older Oligocene and Pliocene shelf margins (Feng and Buffler, 1996), (Figure 24), which together, had already extended the shelf margin 160 km seaward.

The rapid rates of sediment accumulation in the northwestern Gulf of Mexico since the Eocene has resulted in the mobilization of the Jurassic age Louann Salt. Salt mobilization from sediment loading has led to the formation of regional growth faults on the Texas/Louisiana shelf (Worall and Snelson, 1989). On the continental slope, large allochthonous salt sheets have moved seaward since the Late Paleocene/Early Eocene (Worral and Snelson, 1989). The geologic structure in the Gulf of Mexico is, therefore, largely the result of the interaction between the location and rates of sedimentation, changes in eustatic sea level, and the deformation, mobilization, and re-mobilization of the Louann salt.

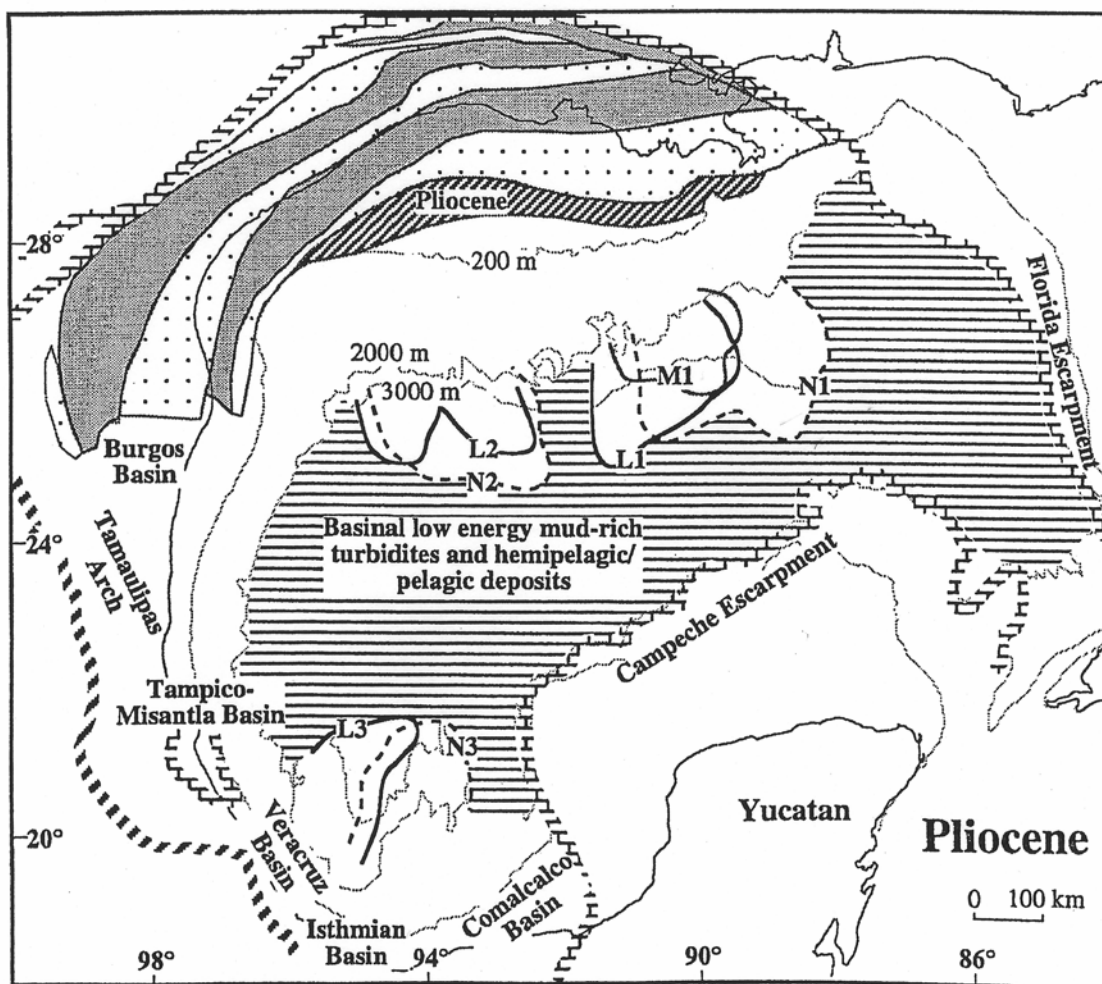


Figure 22. Generalized deposystems map showing location of primary Pliocene depocenters. Prograding northern shelf margin evident (Feng and Buffler, 1996). L1-N3 are Pliocene submarine fan lobes (Feng, 1995).

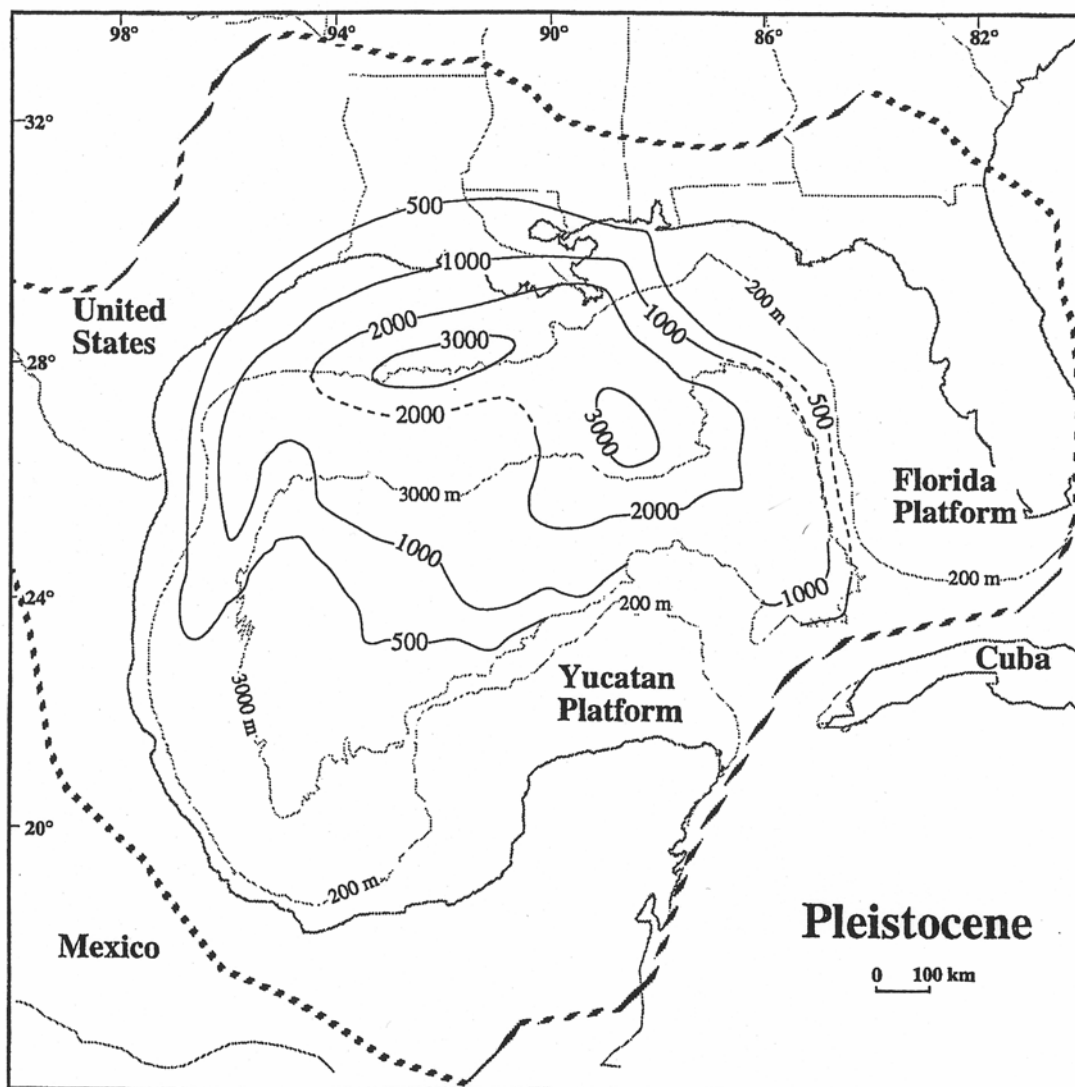


Figure 23. Isopach map showing thickness of Pleistocene terrigenous clastic sediments in the Gulf of Mexico basin. Contours in meters. Dashed where interpolated. Structural limit of the Gulf basin shown (Feng and Buffler, 1996)

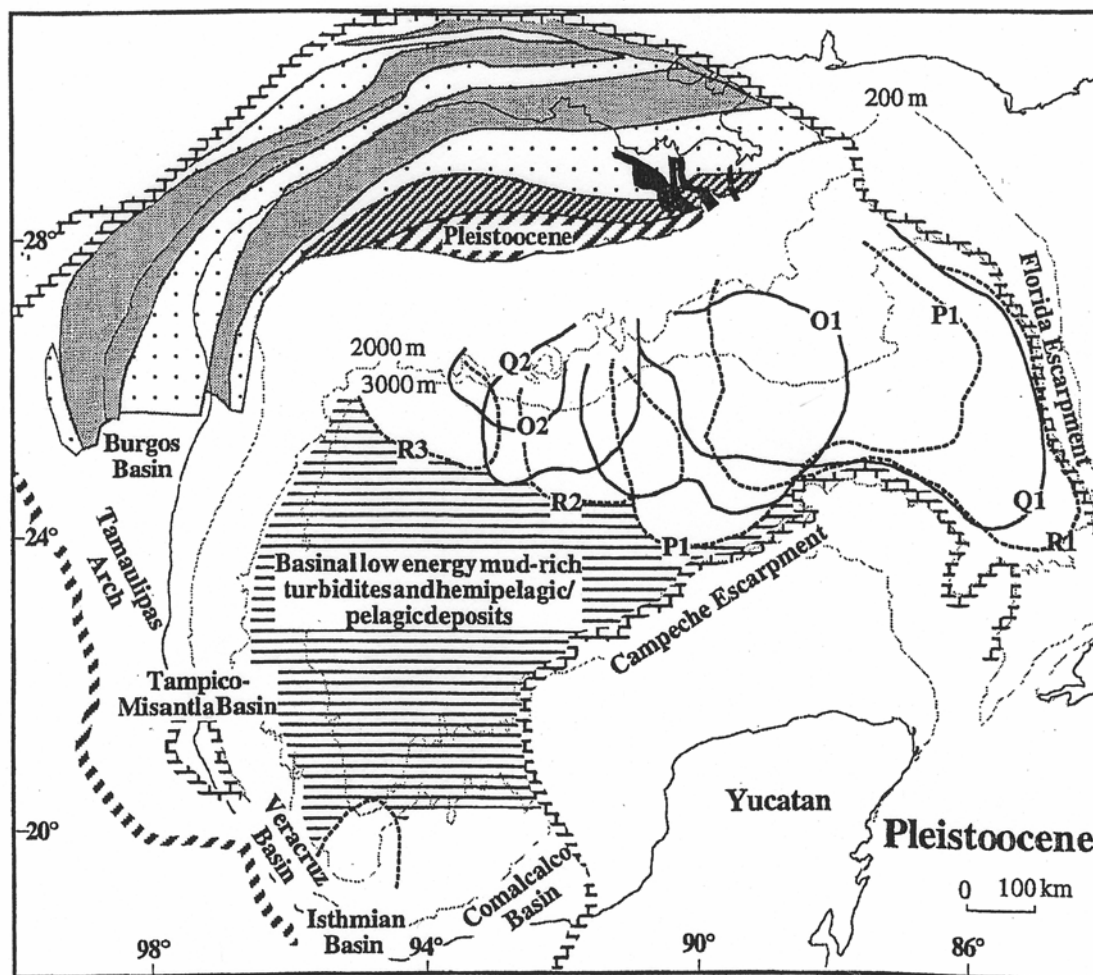


Figure 24. Generalized deposystems map showing location of primary Pleistocene depocenters. Prograding northern shelf margin evident (Feng and Buffler, 1996). O1-R3 are Pleistocene submarine fan lobes (Feng, 1995). Black areas are known submarine canyons.

Regional Geologic Setting

The study area is located in the center of the Mississippi Canyon OCS area on the eastern Texas-Louisiana continental slope (Figure 25). The region is a 75,000 square mile area of hill and basin morphology (Martin and Bouma, 1978) produced by the interaction of depositional processes and the movement of underlying salt. The average seafloor gradient ranges between 1° and 2° but can be greater than 20° around salt or shale diapirs, knolls, faults, and salt withdrawal basins (Coleman et al., 1986).

A. Geologic Structure

The study area lies in a transition zone between three major tectonostratigraphic provinces in the northern Gulf of Mexico (Diegel et al., 1995) (Figure 26). These provinces are a Salt Dome/Minibasin Province, Plio-Pleistocene Detachment Province, and a Tabular Salt/Minibasin Province.

Thick accumulations of probably Jurassic age (195 Ma to 145 Ma, BP) salt underlie much of the upper continental slope. The accumulation of late Mesozoic (140 Ma to 65 Ma, BP) and Cenozoic (65 Ma, BP to Present) sediments overlying the salt has caused the salt to flow laterally seaward. This squeezing effect has deformed the salt, producing lows where the salt has vacated, and diapiric uplifts where the salt is protruding upward through the shallower sediments. The result is a middle to lower continental slope composed of intraslope basins, valleys, and canyons intermixed with

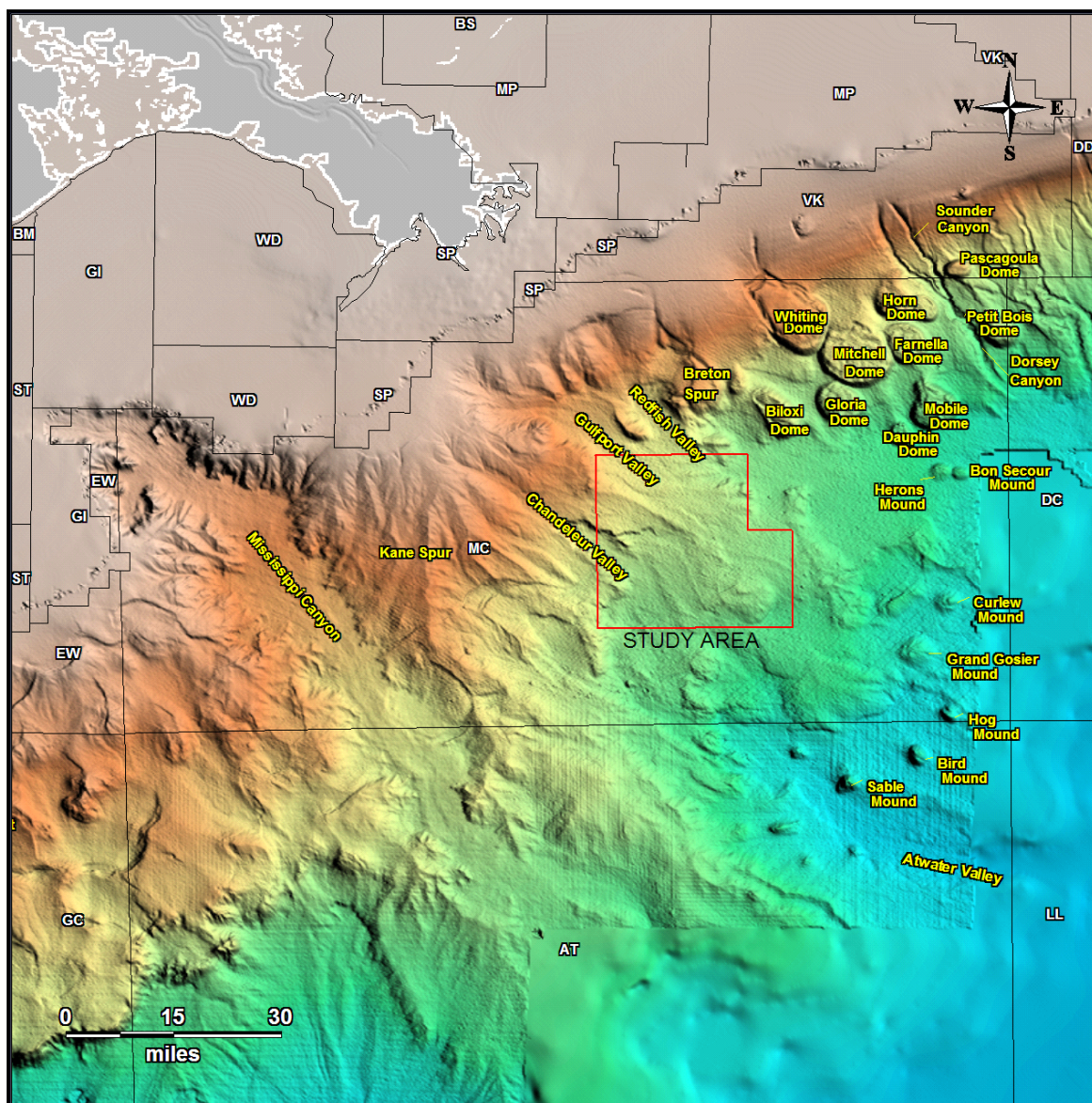


Figure 25. Regional seafloor morphology. Land is gray. Water depth deepens from shallow (tan) to deeper (blue). Significant regional feature names in yellow. Study area outlined in red. Rendering courtesy of Geoscience Earth and Marine Services, Inc.

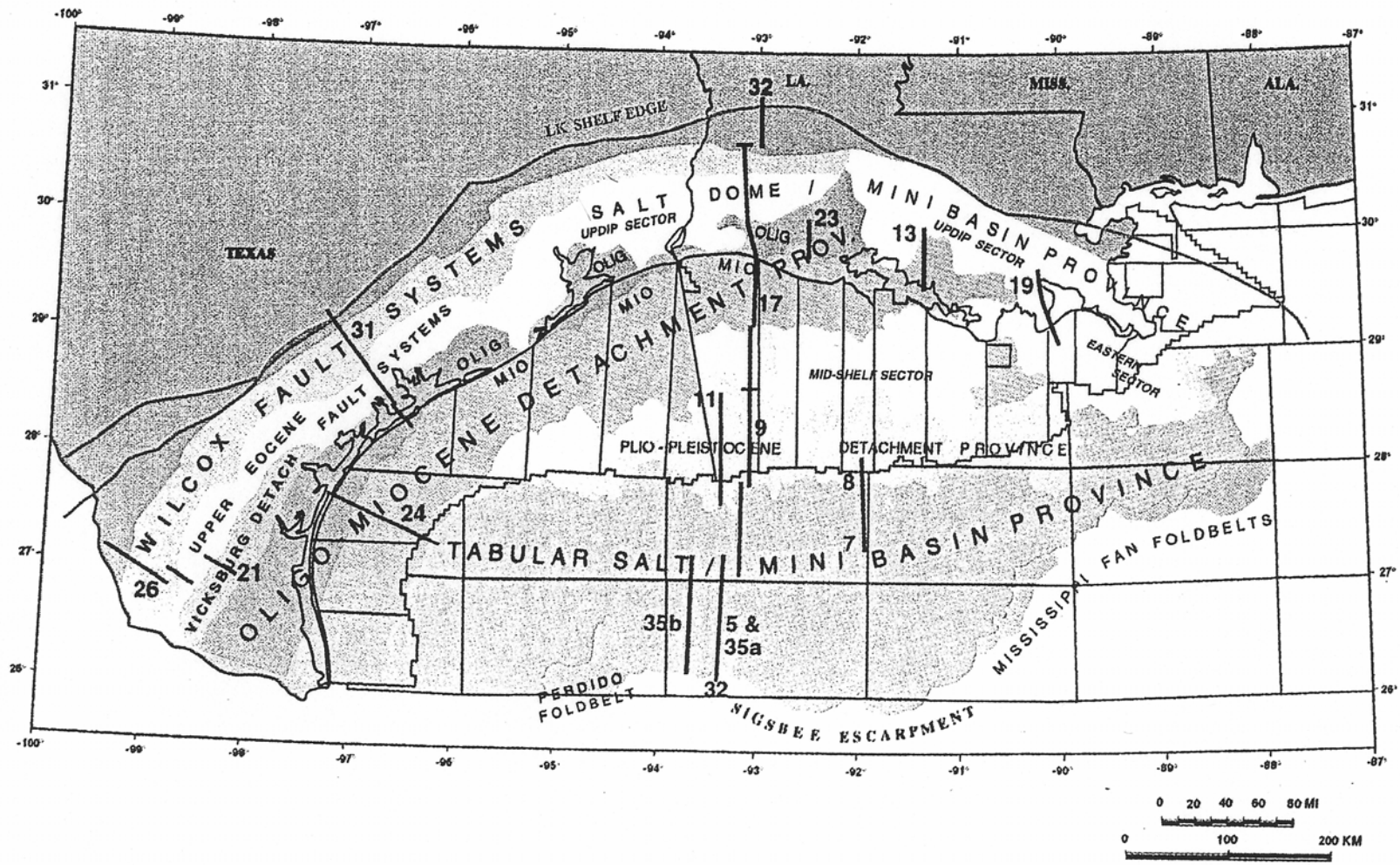


Figure 26. Gulf of Mexico tectonostratigraphic provinces (Diegel et al., 1995).

topographic high ground (Martin, 1978). Horizontal bodies of salt present in young sediments are relatively common (Nelson and Fairchild, 1989). The majority of allochthonous salt migration and emplacement occurred in this region of the Mississippi Canyon area from the Middle Miocene to the Plio Pleistocene, approximately 15Ma to 2 Ma, BP (Wu et al., 1990b).

Allochthonous salt refers to sheet or tongue-like, Jurassic salt bodies tectonically emplaced at stratigraphic levels above its origin, such that it overlies stratigraphically younger strata (Seni, 1994; Wu et al., 1990a). These salt bodies can be present less than 1,000 ft below the seafloor. Sill thickness can range from 2,000 ft to 11,000 ft. Increase in sill thickness is accommodated by compaction of underlying sediments, a rise or uplift of the section above the top of the sill, and by collapse of the underlying section (Nelson and Fairchild, 1989). Bathymetric highs associated with salt tongues in this region indicate the feeder stocks of salt are deeply rooted and probably still actively supplying salt to the present day structures (Wu et al., 1990b).

The lateral and vertical migration of salt bodies has placed a structural control on the distribution of sediment in the central Mississippi Canyon area. Topographic highs related to vertical salt migration, often in the form of diapirs or sills, block the downslope transport of sediments. Structural lows around salt related topography act as conduits for the transport of sediment downslope and out onto the continental rise. Salt withdrawal basins act as traps for the ponding and accumulation of large volumes of sediment.

B. Stratigraphy

The Mississippi Canyon area is seaward of the Mississippi River birdfoot delta. The area is in the general path of some 860 billion kilograms of sediment that is discharged annually from the Mississippi River (Coleman et al., 1983). Most of the discharge falls from the water column near the coast. However, much of the fine-grained sediments reach the upper slope province and form a series of offlapping, progradational bedforms.

The study area lies to the north/northwest of the Eastern Mississippi Fan (Figure 27) as defined by Dixon and Weimer (1998). This fan is interpreted to consist of sedimentary sequences whose primary source was from the Appalachian drainage area, whereas the ancestral Mississippi River provided sediments to the Western Mississippi Fan. Weimer (1989) identified 17 seismic packages of late Pliocene to Pleistocene (~3Ma to 0.015Ma) in the deeper stratigraphic sequence across the Mississippi Fan. Dixon and Weimer (1998) also recognized channel fill, levee overbank, mass-transport deposits, and submarine slide facies within eight major sequences in the region. Some of these sequences may correlate to sequences within the study area covered in this research. Correlation of these sequences into the study area would serve to extend the previous interpretations north, into areas previously not identified.

The major sequences discussed by Dixon and Weimer (1998) generally represent deposition during low stands of sea level and are separated by high-amplitude, laterally

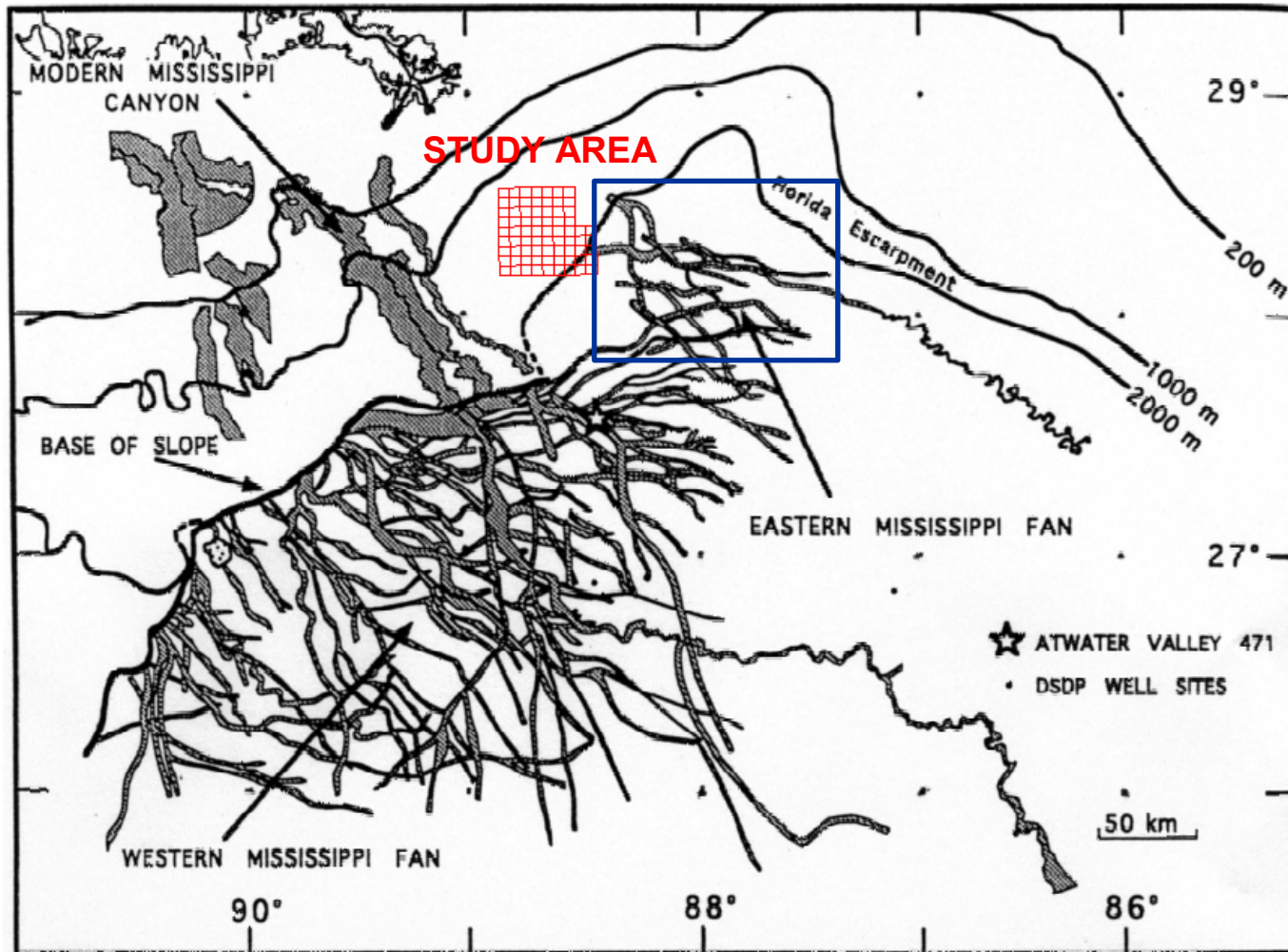


Figure 27. Western and Eastern Mississippi Fan systems (Weimer, 1990 and Dixon and Weimer, 1994). Gray areas in the Eastern Fan and below Base of Slope in the Western Fan are defined channels. Gray areas above Base of Slope in the Western Fan, in the upper left of the image, are known shelf/slope canyon systems. Eastern Fan coverage in Blue. Study area in Red.

continuous reflectors representing condensed sections deposited during high stands of sea level (Roberts and Coleman, 1988). The low-stand sequences are generally composed of mass-movement or turbidite deposits and can be sand-prone. The high stand sequences, or condensed sections, represent clay-rich, hemipelagic sedimentation. Condensed sections normally form thin, high-amplitude stratigraphic marker horizons that separate expanded sections (Roberts and Coleman, 1988). These condensed sections also form regional seals to the underlying, potentially sand-prone, expanded sections, thus contributing to the formation of overpressured fluid zones related to shallow water flow.

C. Geohazards

The shallow (0 to 5000 ft, below mud line; bml) subsurface geology in the deepwater Gulf of Mexico presents a unique suite of engineering and geologic hazards or constraints to hydrocarbon exploration and production. In many cases, these hazards/constraints have been the limiting factor in the pursuit of deepwater hydrocarbon plays. Potential engineering or geologic hazards/constraints in the deepwater Gulf of Mexico include slope gradient and stability, hydrocarbon seeps and vents, chemosynthetic communities, gas hydrates, carbonates, seafloor and buried faults, salt, mass-transport events, shallow gas, and shallow water flow. A number of exploration wells have been delayed, lost, or forcibly abandoned because of these unique geologic

conditions, particularly shallow water flow. Previous human activities and existing infrastructure may also constrain drilling operations.

Slope Gradient and Slope Stability

The gradient of the seafloor and its stability are important factors that may limit or constrain drilling. Steep slopes, such as those found associated with fault scarps, slump scarps, rims of salt withdrawal basins, and around the perimeter of salt structures may be too steep to drill a well. Steep seafloor gradient may also place a constraint on anchoring of the anchors of the drilling rig. It also constrains other seafloor infrastructure, in particular, production and export pipelines. Steep slopes affect the latter by creating a condition where potential, undesirable spans (an area where the pipeline is “hanging” off the bottom) in pipelines can occur.

Steep seafloor gradient may also be a factor in slope stability. Slope stability is of primary concern to exploration drilling and production because of its potentially catastrophic impact on manmade seafloor structures. Slope instability is both a function of the gradient of the seafloor and the composition of the shallow sediments. High seafloor gradients coupled with weak, shallow sediments may produce a condition at which the slope is unstable and could fail. However, high seafloor gradients are not necessary to produce slope instability and failures. Slope failures occur on a number of different scales both in size and in repeat interval. They may occur as small, very frequent events where their impact on infrastructure may be minute. Alternatively, they

may occur as one large, massive event where the impact on infrastructure may be disastrous. The size and frequency of occurrence of these events is a combination of numerous geologic and geotechnical factors, of which slope gradients and sediment composition are the most important.

Seafloor gradient and relative slope stability can be deduced from the seismic data. Gradient is calculated from the seafloor horizon pick from the data. Relative seafloor stability is inferred from not only the relative amplitude of the seafloor (which indicates harder or softer sediment cover) but also by observation of the character on composition of the shallow sediments from the seismic data. These data can then be correlated with other, higher resolution geophysical data, and then ground-truthed with geotechnical sampling and analysis.

Hydrocarbon Vents

Thermogenic hydrocarbons are generally believed to form at depths greater than 5 km in the Gulf of Mexico (Kornacki et al., 1994). These hydrocarbons subsequently migrate vertically along diapiric salt bodies and major, deep-seated faults. Some hydrocarbons migrate laterally into reservoirs, while some may actually migrate to the seafloor and are expelled. These hydrocarbons migrate toward the seafloor along faults or other fractures in the subsurface sediments. The expulsion or venting process is generally slow and imperceptible on the seabed. However, evidence of rapid and violent expulsions in the form of large blowout craters, mud volcanoes, and mud diapirs have

been attributed to the venting of gas or fluids (Neurauter and Bryant, 1990; Neurauter and Roberts, 1994; Prior and Bornhold, 1989).

Hydrocarbon vents may be identified on the seismic data by their anomalously higher seafloor amplitude and seismic cross-sections. Seabed amplitude anomalies possibly relate to the presence of venting hydrocarbons and/or authigenic carbonates as shown in various studies (Doyle et al., 1996; Roberts et al., 1992). Their physiographic features such as irregular seafloor from pockmarks, mounds, and craters may also identify hydrocarbon seeps.

Chemosynthetic Communities

Chemosynthetic communities, or those organisms that have a food source at least in part from chemosynthesis rather than terrestrial (plankton), or marine (algae) photosynthetic organic carbon, can form in areas of active hydrocarbon vents (Brooks et al., 1987; Kennicutt et al., 1985). Some communities consist of dense assemblages of tubeworms, clams, and mussels, while others consist of mats or traces of the bacteria “beggiatoa”. The Minerals Management Service (MMS) regulates exploration activity and their potential impact on these communities. These communities are designated “sensitive” biological zones and are considered an endangered species. Consequently, the MMS prohibits any exploration or production activities that may harm or destroy these communities where found, or implied, to be present.

Chemosynthetic communities in the Mississippi Canyon area have been reported in Blocks 709 and 929 (Kohl and Roberts, 1994), and Blocks 201, 282, and 839 (Brooks et al., 1987). Often, the presence of chemosynthetic communities is implied with the identification of hydrocarbon seeps, vents, or carbonate hardground based on seafloor amplitude. The actual presence of these communities cannot be confirmed by seismic data and alternative methods, such as seafloor sampling or ROV inspection, must be made to confirm or deny the presence relative abundance of these communities in these higher-amplitude areas.

Hydrates

Hydrates, a solid form of light gases that have been compressed in an ice matrix of water molecules (Kvenvolden and Barnard, 1983), form in areas of high pressure and low temperature. Gas hydrates generally have been found in water depths exceeding 1500 ft in the northern Gulf of Mexico (Brooks et al., 1987). Gas hydrates have been recovered in a piston core collected in a small mud mound located in MC 798 west of the study area (Neurauter and Bryant, 1990). If active venting is occurring within the study area, hydrates formation may be likely. Hydrates may pose a threat to drilling in the shallow subsurface due to their sublimation to gas when drilling activity disturbs in situ temperatures and pressures. Hydrates often form along a common temperature/pressure line at some depth below the seafloor. They are commonly

identified on seismic data as by a bottom-seismic-reflector, or, BSR. BSR's are high-amplitude reflectors that parallel the seafloor and cut across seismic strata.

Carbonates

Venting gasses can react with interstitial pore-water in shallow sediments to produce carbon dioxide and bicarbonates (Roberts et al., 1990). Under proper conditions, this reaction causes the production of calcium and magnesium carbonates. The result is an accumulation of authigenic carbonates cementing large caps or seals over gaseous sediments, and the generation of boulder-like, cemented hard rock outcrops. Authigenic rock outcrops have been recognized in many areas along the upper continental slope in association with diapiric uplifts, fault scarps, and known hydrocarbon vents. If active venting is occurring within the study area, the formation of carbonates may be likely. Carbonates also form a hard substrate to which chemosynthetic organisms may attach themselves. Thus, the presence of carbonates may also imply the presence of chemosynthetic or other biologically sensitive organisms. The presence of seafloor or shallow, buried carbonates may prohibit the jetting of wells and placement of seafloor founded infrastructure such as anchors.

Faults

Faults on the middle and lower continental slope are generally extensional over diapiric ridges or along the flanks of salt withdrawal basins (Swiercz, 1992). These faults are release mechanisms for the stresses created by the geologically rapid intrusion of salt into shallower, younger sediments. The overlying soils are typically more ductile than the viscous salt, thus causing soils to shear with vertical and lateral movement. As movement of salt continues, the faults may continue to move causing increased displacement of bedding planes. This produces a growth-like character in the faults. Seafloor displacements are common, and may show as much as 400 ft to 500 ft of vertical offset.

Faults commonly provide conduits for the upward migration and accumulation of hydrocarbons. Fluid charged faults and accumulations of hydrocarbons close to faults can pose a threat to drilling when associated with excess pressures. Faults are easily identified on the seismic data by the offset of strata across the fault. High amplitudes along or close to the fault are interpreted as fluid charging and migration along the fault plane.

Salt

Drilling through salt poses its own unique problems with drilling as isolated pressure pockets and dissolution from hypo-saline drilling fluids being common

problems. However, the greatest impact of salt is in its resulting structural deformation. The lateral and vertical migration of salt bodies has placed a structural control on the distribution of sediments in the eastern Mississippi Canyon area. Topographic highs related to vertical salt migration, often in the form of diapirs or ridges, block the downslope transport of sediments. Structural lows around diapirs or salt ridges act as conduits for the transport of sediment downslope and out onto the continental rise. Salt withdrawal basins act as traps for the ponding and accumulation of large volumes of sediments.

Movement of salt often results in faulting of the sediment column above the salt. Where the salt is shallow and has rapidly intruded (on a geologic time scale), numerous salt-seated faults may penetrate to the seafloor. Salt-rooted faults coupled with steep seafloor gradients may result in zones of inherent slope instability. The seismic identification of salt was covered in the chapter Salt Tectonics.

Gas

Faults may provide the conduit for gas to migrate from depth. The in situ formation of gas by biogenic bacteria is also common, particularly in the shallow sediments. Gas pockets are typically recognized and assessed on digital seismic data as “bright spot” phenomena, where the signal intensity of the reflected interface from non-gas to gas-charged sediment is greatly enhanced. This “bright spot” may also have a phase inversion of the wavelet, which is a strong indicator for the presence of gas.

The greater the depth of the gas zones beneath the seabed, the more likely that pressures greater than hydrostatic may occur. Shallower zones of gas accumulation (less than a few hundred feet below the mudline) generally are not expected to have a significant pressure gradient. The low shear strength of soils in these shallow zones prevents any appreciable buildup of pressure. In some instances the gas build up in shallower soils may reach a point where the pressures will exceed the holding capacity of the low shear strength seal; thus the gas will move upward or “bleed off” pressure. This gas migration can become trapped at a shallower level, if a more competent and impermeable seal is encountered. Increased formation pressure may sometimes lead to gas in solution. Solution gas may or may not be identifiable on the seismic data. Gas in solution may pose a threat to drilling when the drillstem pierces the sequence, relieving the pressure, resulting in the volumetric expansion of gas out coming out of solution. However, if there is no overlying seal present the gas can flow to the seafloor and vent into the water column and is fundamentally benign.

Shallow Water Flow

Shallow overpressured sands or “flowing water sands” are generally defined as water flowing outside of the wellbore casing and out onto the seafloor, are a significant constraint in the deepwater region of the Gulf of Mexico (Alberty et al., 1997). These flows are a particular problem when encountered in an open hole before the setting of the 20-inch casing, usually at about 2000 ft to 2500 ft below the mudline (bml). The

water flows originated from these overpressured zones can erode the structural support of the well and may lead to buckling of the casing, casing failure, and loss of the well.

These sands have been found to be isolated sandy layers of varying thickness, isolated between low permeability shales and clays. Rapid burial by fine-grained, hemipelagic clays increases the existing overburden, causing an increase in pore pressure within these sands. Low-permeability, condensed sections deposited during high stands of sea level form regional seals these sand-prone sections. An increase in the overburden above the seal transmits pressure into these sand-prone layers faster than the seal allows pore fluids to escape (Alberty et al., 1997). The faster the sediment deposition rate above the seal, the higher the pore water pressures within these sand-prone zones. Sedimentation rates for condensed sections have been estimated to be 5.0 to 30.0 cm/1000 yr (Roberts and Coleman, 1988). Sedimentation rates for expanded sections where these overpressured zones are located have been estimated to be 40.0 to 60.0 cm/1000 yr on the continental slope and be as high as 100m/1000 yr related to individual shelf delta lobes. Thus, alternating sequence of expanded and condensed sections may result in rapidly loaded sandy layers sealed by clay overburden resulting in excess pore-water pressures.

High-amplitude “bright spots” on seismic data often identify gas-charged sediments or overpressured sand units. However, water flow sands do not always correlate with high-amplitude anomalies (Byrd et al., 1996). Identification of sand-prone sections is facilitated using stratigraphic sequence analysis optimally correlated with well data. Sand-prone facies in the Mississippi Canyon area are commonly

associated with slope, fan-channel sequences. The sands occur within parts of channel-levee systems and lag-deposits at the base of channels and unconformities.

Overpressured sands can also occur within salt withdrawal basins where sheet or turbidite sands can become ponded behind the salt structure and rapidly buried (or subsided) like those associated with the basin floor fan in Sequence IV.

The present study area is located in a region of the Mississippi Canyon area that has experienced a number of shallow water flows. The most significant water flow events pertinent to this study area are those that occurred at the Mensa prospect in MC 686, 687, 730, and 731. The original exploration wells set 20 inch casing into a “chaotic sand” sequence at a depth of 1850 ft (bml) in MC 730 and 731 (Burman and Norton, 1998). Well tickets indicated water flows occurred when drilling at depths of 1855 ft and 2072 ft (bml), with the latter zone also producing biogenic gas. Both exploration wells experienced water flow problems during the entire drilling operation and were permanently abandoned (Burman and Norton, 1998).

Before drilling the production wells (MC 687, A-1 through A-3) a geotechnical soil boring was completed. The boring indicated highly plastic clays from the mudline to 690 ft (bml). At 690 ft, a section of alternating sand, sandy silt, and thin shale layers were encountered to a depth of 800 ft (bml). Hard clays were then identified in the sequence between 801 ft to 1199 ft (bml). The sand-rich layer at 690 ft to 800 ft (bml) was designated the Blue Unit. Two of the three production wells encountered water flows at the top of this sequence and lost circulation approximately halfway through the section (Burman and Norton, 1998). The Blue Unit flowed despite the conclusion from

the geotechnical investigation that flow would not be likely. Numerous well control and cementing strategies were implemented, subsequently stabilizing the wells which were then drilled to completion (Burman and Norton, 1998). The production wells set casing above the deeper “chaotic sand” sequence at 1700 ft (bml), thus negating the flow problems experienced with the exploration wells in MC 730 and 731.

Exploration and Production Activity

Pre-existing man-made infrastructure poses unique constraints and hazards and affects drilling, anchoring, and placement of seafloor infrastructure. Shell’s Mensa field is located in MC 686, MC 687, MC 730, and MC 731 (Figure 4). The flowlines for the sub-sea completions run to a central tie-in point in MC 685. An export pipeline runs northwest and out of the study area in MC 507. Chevron has drilled a well in MC 772 and BP Exploration is the operator of a well in MC 777. BP plans development of their Thunder Horse field in the near future with seafloor-founded production infrastructure to be associated with the developments. Of these known wells, only those associated with the Shell Mensa field had reported shallow water flow (Minerals Management Service, 2000).

Previous Work

A. Regional Salt Tectonics

Thick accumulations of probable Jurassic age (195 to 145 Ma, B.P.) salt underlie much of the upper continental slope. The presence and movement of salt at depth has been the primary structural control on the Texas-Louisiana slope (Worall and Snelson, 1989). Shifting terrigenous depocenters on the continental shelf and upper slope during the Miocene to the Pleistocene mobilized the salt, creating the complex structures observed in the present day (Woodbury et al., 1973) (Figure 28). Rapidly increasing sediment overburden in these depocenters caused the slopeward displacement of the underlying, viscous salt resulting in the formation of allochthonous salt masses (Humphris, 1978). Allochthonous salt refers to sheet or tongue-like Jurassic salt bodies tectonically emplaced at stratigraphic levels above the source layer, such that it overlies stratigraphically younger strata (Wu et al., 1990b, Seni, 1994). The result is a middle to lower continental slope composed of intraslope basins, valleys, and canyons intermixed with topographic high ground (Martin, 1978). The seaward extension of the allochthonous salt is the Sigsbee Escarpment, separating the lower continental slope from the continental rise (Humphris, 1978; Martin, 1978).

In the region of the Mississippi Canyon area, sub-horizontal allochthonous salt bodies emplaced in young sediments is relatively common. Wu et al. (1990b) used a

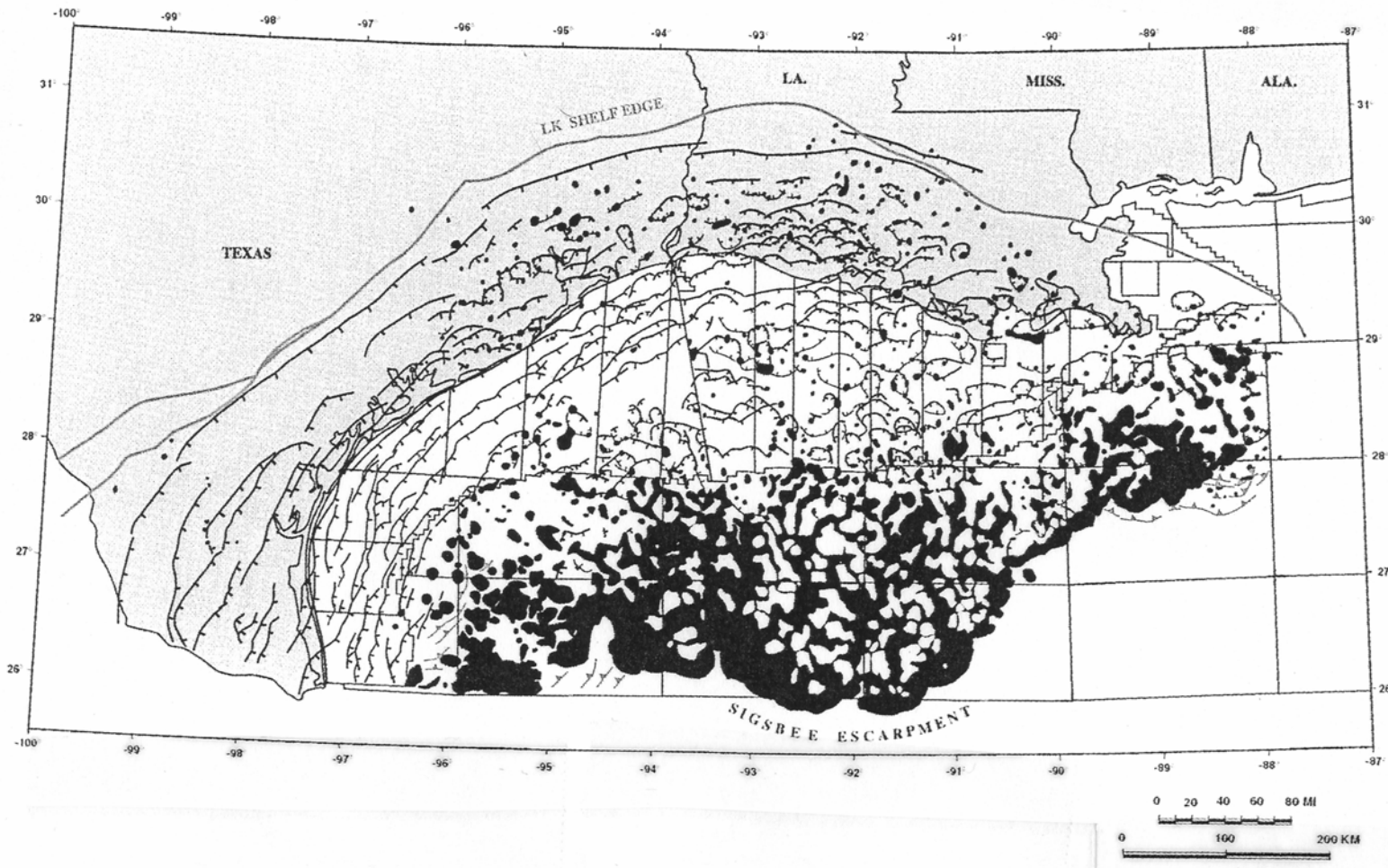


Figure 28. Modern-day distribution of shallow salt in the Gulf of Mexico (Diegel et al., 1995). Black areas are shallow salt bodies.

computer palimpsest reconstruction to study the evolution of allochthonous salt in the Mississippi Canyon area (Figure 29). He concluded that gravity spreading is the primary mechanism for the formation of shallow, laterally extensive allochthonous salt sills on the continental slope. According to his model, Jurassic aged salt approximately 2.6-3.0 km thick was buried by progradational sedimentation from 150 Ma to 94 Ma. The increasing overburden caused the lateral, basinward movement of salt forming large salt pillows, domes, and massifs. Growth faults, downdip both seaward and landward, also formed as the salt moved basinward. Between 94 Ma and 30 Ma the region underwent sediment starvation, allowing for the stabilization of the salt. Intense sedimentation affected the region between 30 Ma and 15.5 Ma resulting in rapid vertical growth of salt structures due in part to density inversion. This resulted in very shallow salt bodies which, between 15.5 Ma to the Plio-Pleistocene, formed lateral tongues and sills by downslope gravity spreading.

Nelson and Fairchild (1989) also studied the formation of allochthonous salt tongues, or sills, on the eastern Louisiana continental slope. They concluded that sills formed as salt at the top of shallow salt diapirs intruded through shallow, low-density slope sediments less than 1,000 ft below the seafloor (Figure 30). Studying 53 different sill edges, they found that intrusion occurred at depths less than 1,000 ft below the seafloor and had a mean depth of emplacement at 390 ft below the mudline. They believe the sills form by rapid intrusion of salt into almost pure mud and that the nature of sediments surrounding the salt is the key to formation. The sill thickens until the feeder stock is depleted or a new density inversion occurs. When silling ceases,

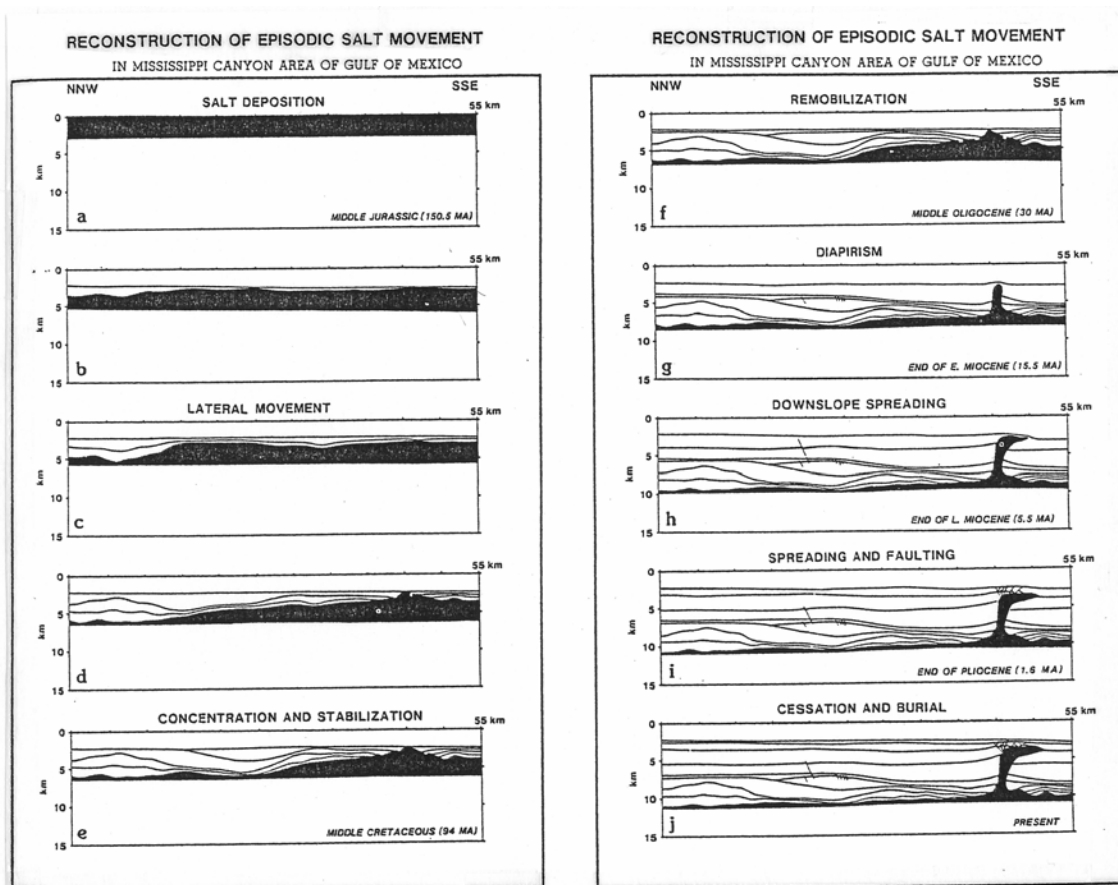


Figure 29. Palipinastic reconstruction of allochthonous salt in the Mississippi Canyon area (Wu et al, 1990b).

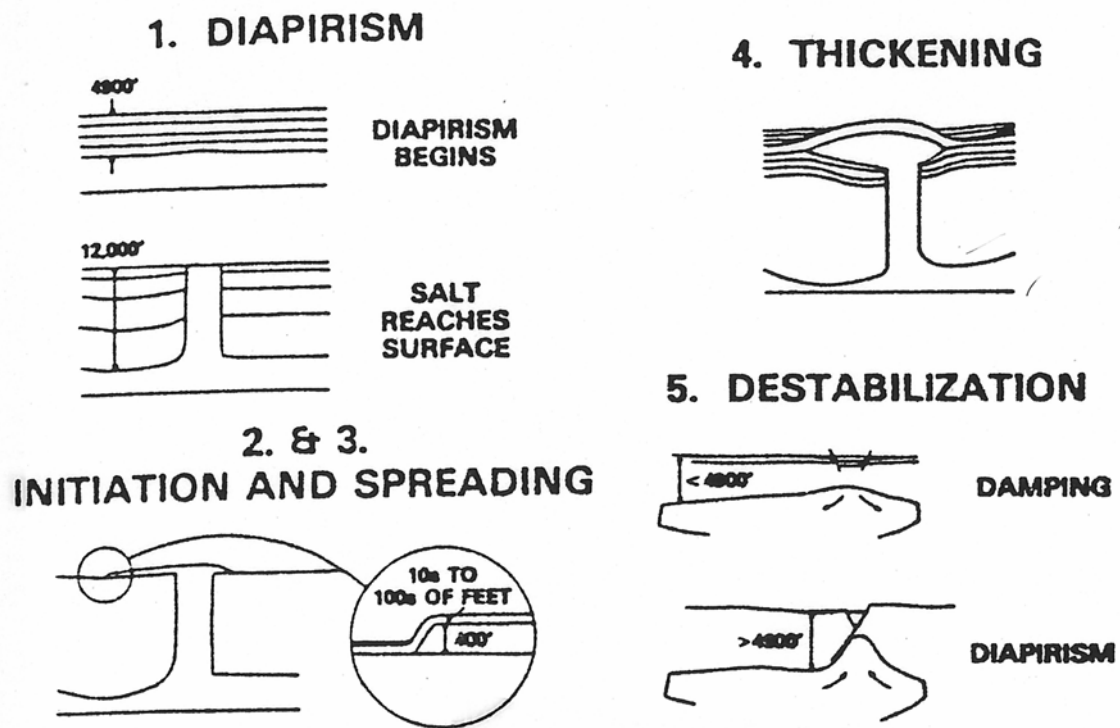


Figure 30. Model for salt sill formation (Nelson and Fairchild, 1989).

remobilization begins. If there is no density inversion, the sill is dampened and internally reworked. If a density inversion is present, irregularities on the upper surface of the sill become points where new diapirs may originate.

Fletcher (1995) posited that early emplacement and burial of allochthonous salt sheets on the eastern Louisiana continental slope occurred through extrusion of "salt glaciers" rather than salt intrusion. Their work cites other works on the extrusive nature of salt glaciers (Hudec et al., 1995; McGuinness and Hossack, 1993; Talbot, 1994). Their model has "salt glaciers" formed by the extrusion of salt at the sediment-water interface, protected from total dissolution by a thin veneer of pelagic sediments (Figure 31). During extrusion, a salt fountain resulted in high topographic relief. Sedimentation was limited to the glacial margins with most sediment deposited on the upslope side of the glacier. In this manner, the salt grew upward in the sedimentary section from the feeder stock with successive sedimentary horizons truncated against it. The fountain became laterally asymmetrical in the downslope direction due to a greater hydraulic differential resulting from less sedimentation on the downslope side. This allowed for the lateral downslope spreading of the salt and subsequent formation of detached allochthonous salt-sediment glaciers. The density differential between salt and sediment influence only late-stage development of the salt sheet.

Schuster (1995) described end-member systems that developed from the progradational loading and evacuation of allochthonous salt in onshore and offshore Louisiana. A focus of his studies was an area of the eastern Louisiana continental slope.

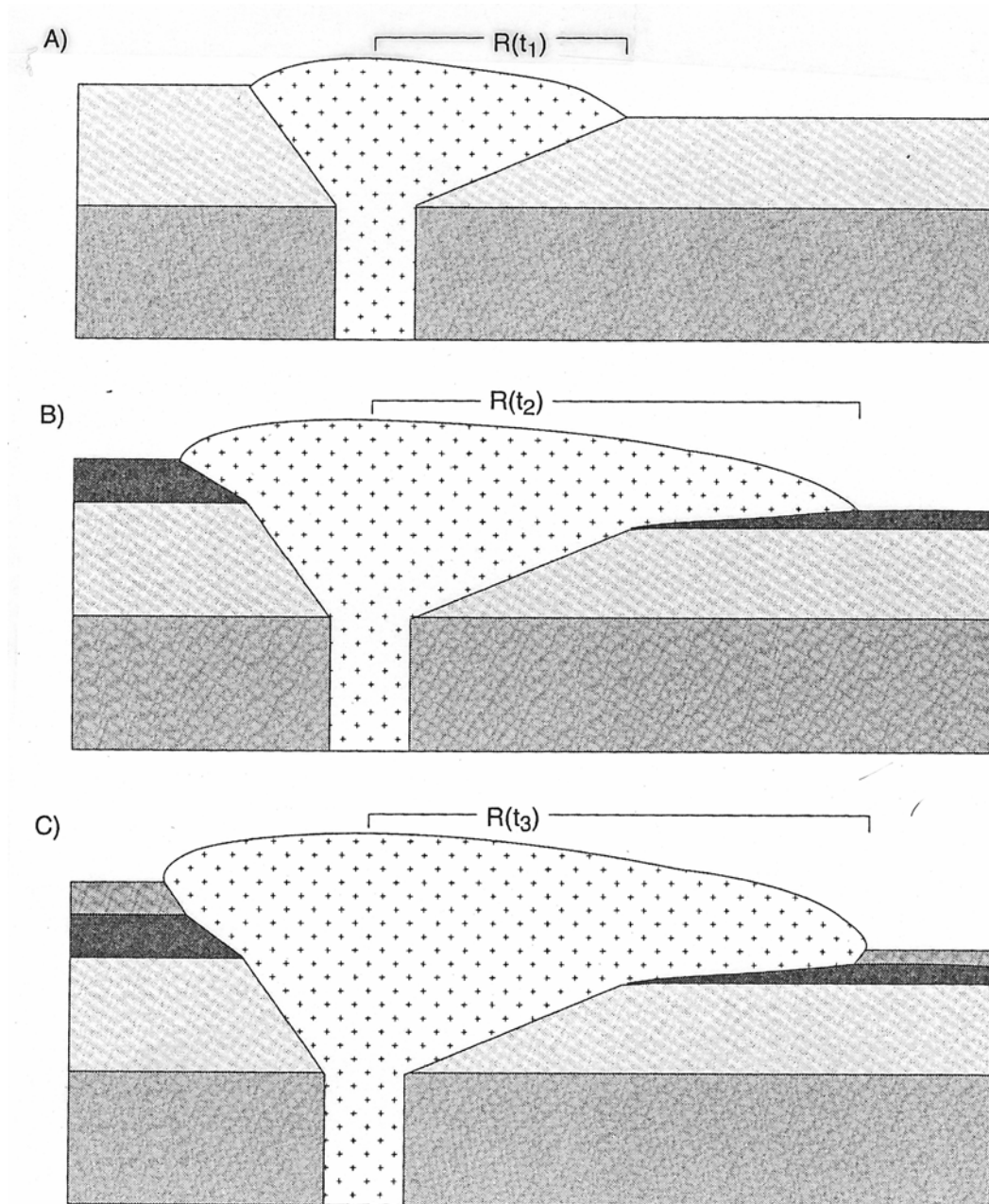


Figure 31. Basic model of salt glacier propagation (Fletcher, 1995). R is the radius from the center to the edge of the forming glacier. T denotes time. The model evolves through time from A to C.

Here, he defined the Roho (phrase derived from Shell's C.C Roripaugh's *Moho*) end-member system.

The Roho system (Figure 32b) is characterized by major listric, down-to-the-basin growth faults that sole into intra-Tertiary salt evacuation surfaces. These faults occur only on the up-dip end, whereas most of the salt has been evacuated downdip into various shallow salt structures.

B. Depositional Processes

Lehner (Lehner, 1969) conducted an exhaustive study of the Texas-Louisiana slope using high-resolution seismic data and core data. His findings suggested that the sediments on the continental slope are between Cretaceous and Pleistocene in age and that the outer part of the slope represents the seaward limit of the Pleistocene depocenter.

Others have also studied the sedimentology of the Texas-Louisiana slope (Stuart and Caughey, 1977; Woodbury et al., 1978). Their findings showed that turbidity flows and hemipelagic sediments were initially deposited in topographic lows, subsequently eroded or reworked by mass-transport events. Beard et al. (Beard et al., 1982) studied Quaternary chronology, depositional sequences, and eustatic cycles using seismic and geotechnical data from the Texas-Louisiana slope. He identified eight glacial-interglacial eustatic cycles during the last 2.5 Ma to 3.0 Ma. Seven corresponding Pleistocene sequences were identified for the lower continental slope. Glacial periods, representing a lowstand of sea-level may be recognized as variable amplitude, chaotic

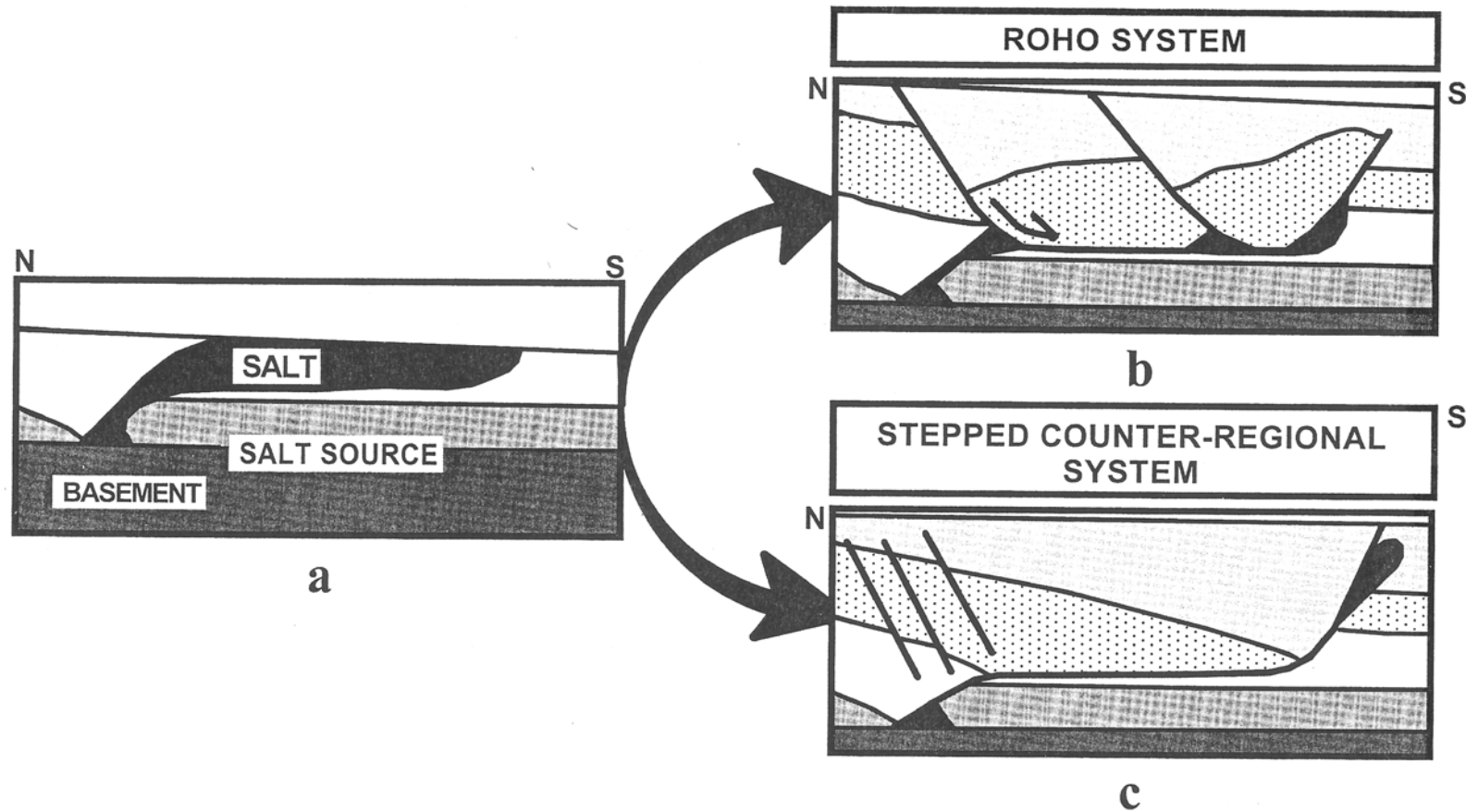


Figure 32. Allochthonous salt end-member systems in the Gulf of Mexico (Schuster, 1995). Shallow-emplaced allochthonous salt undergoes overburden loading via sedimentation resulting in mobilization through time toward one of the two salt end-member systems and associated overlying stratigraphic basin geometry.

bedding surfaces and associated cold-water fauna. Interglacial periods may display low to high-amplitude, parallel bedding with warm water fauna. These cycles were identified using paleontologic, seismic, and geotechnical evidence. Further evidence of the influence of sea level association with glacial and depositional cycles were identified by Behrens (1985) and Bouma (1981).

Roberts and Coleman (1988) also identified stratigraphic changes coincident with sea level changes. They showed that low-stands of sea level are characterized by chaotic, coarse-grained channel fill, levee overbank, mass-transport, and submarine slide deposits. These low-stand deposits are termed "expanded" sections.

Thin, high-amplitude, laterally continuous reflectors represent deposition during high-stands of sea-level. These high-stand deposits are termed "condensed" sections and are mostly composed of hemipelagic clays. Condensed sections normally form thin stratigraphic marker horizons that separate expanded sections as well as create regional seals. They are commonly expressed seismically as a single high-amplitude wavelet.

Sangree et al. (1988) applied sequence stratigraphic methods to interpret deep-water seismic facies in the Gulf of Mexico. Their studies resulted in three divisions of lowstand deposition, basin floor fans, slope fans, and prograding complexes. Basin floor fans form in topographic lows during sea level fall. Slope fans occur in salt-bounded topographic lows as the fall of sea level slows. Slope fans are identified by their seismic facies, which include channels, overbank deposits, and slumps. Prograding complexes form a basinward offlapping sequence as terrigenous sediments bypass the paleo-shelf edge during the early stages of sea-level rise.

The in-depth sequence stratigraphy of the Gulf of Mexico basin has been studied and adequately summarized in other notable works (Galloway, 1989a; Winker, 1982; Winker and Buffler, 1988).

The study area is located immediately west-northwest of the Eastern Mississippi Fan (Figure 27). Dixon and Weimer (1994) first identified the Mississippi Fan complex comprised of the Western Mississippi Fan and the Eastern Mississippi Fan (Figure 27). Previously, in 1989, Weimer had defined 17 seventeen depositional sequences of the Western Fan that were deposited between the Miocene (5.5 ma) to Present. He also identified at least seven submarine canyons that could be traced downslope in the equivalent channel-levee systems. They also found that sequences 8-11 and 13-16 of the Western Fan were coeval with eight depositional sequences in the Eastern Fan (Figures 33 and 34). Submarine canyons feeding the Eastern Fan were located east of the present day Mississippi bird-foot delta. They hypothesized that the ancestral Mississippi River during the Miocene fed the Western Fan to the present. On the other hand, rivers draining the southern Appalachian Mountains during the Pleistocene fed the Eastern Fan. This drainage system was located immediately east of the present Lagniappe Delta. In general, the mud-dominated Eastern Fan is thin and small when compared to the massive Western Fan. Dixon and Weimer attribute the small size of the Eastern Fan to be due to the smaller drainage area and less sediment supply than that of the Mississippi River fed Western Fan.

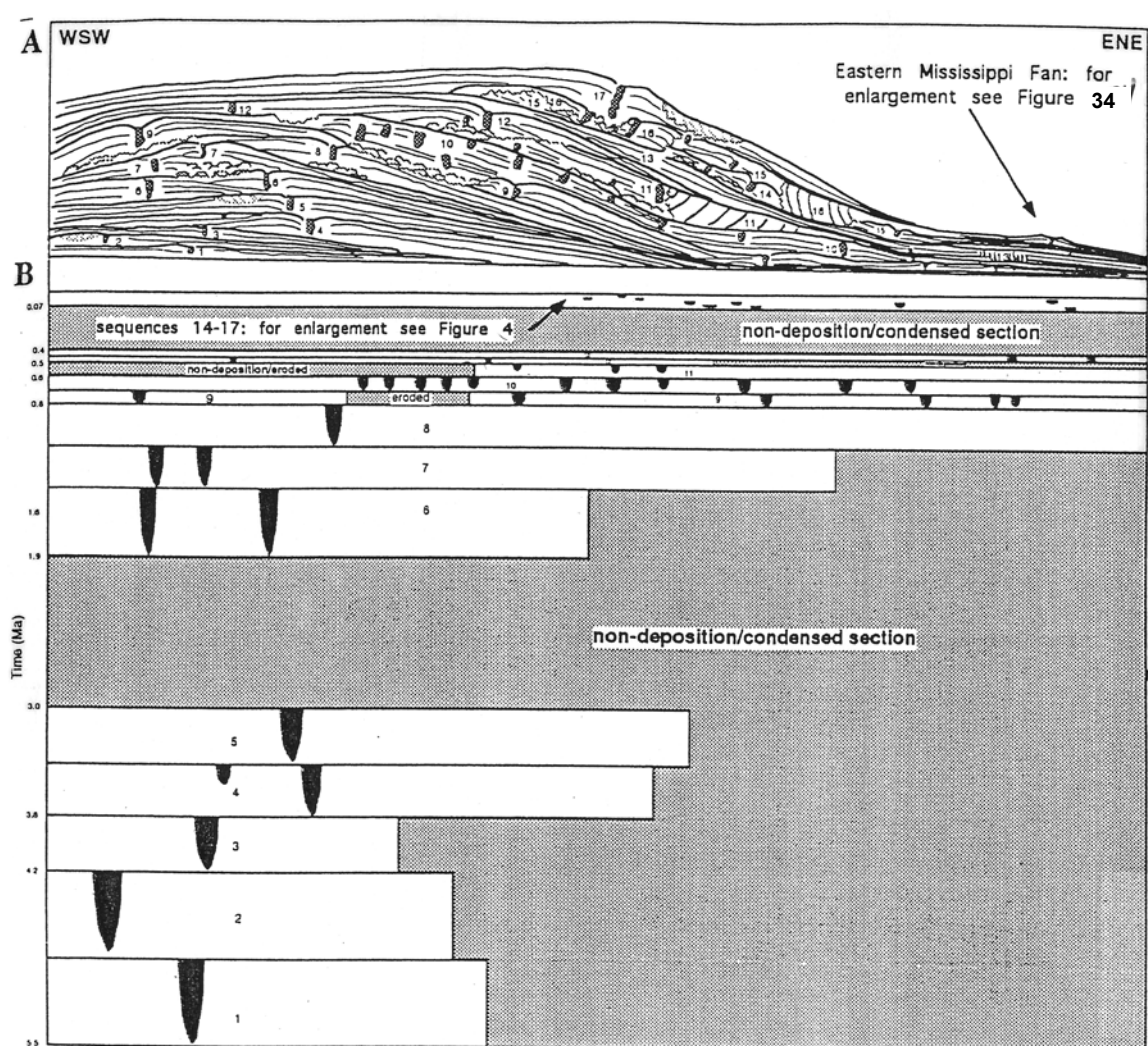


Figure 33. Cross-section model of Mississippi Fan depositional sequences (Dixon and Weimer, 1994). Section A denotes distribution of stratigraphic sequences across the fan complex. Section B denotes chronostratigraphic evolution of stratigraphic sequences across the fan complex. Black, V-type features in both images denote channels. Gray areas in Section B denote periods of either non-deposition, or reduced sedimentation, leading to formation of a condensed section.

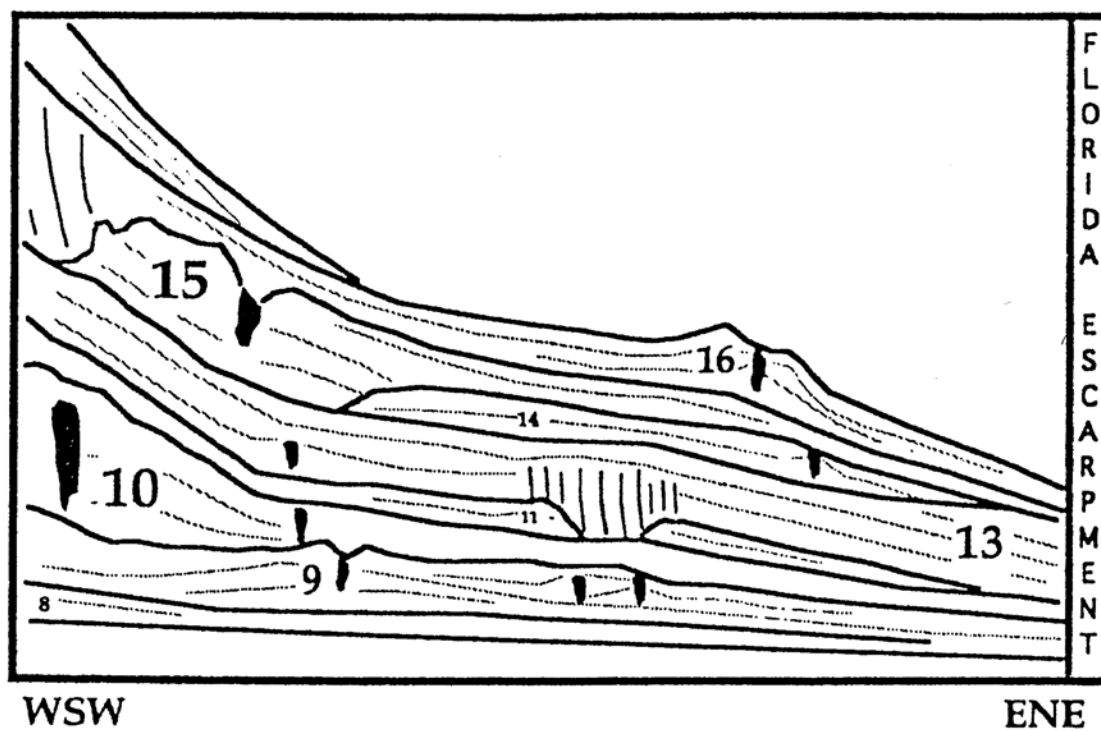


Figure 34. Cross-section model of Eastern Mississippi Fan depositional sequences (Dixon and Weimer, 1994). Numbers denote stratigraphic sequences identified in the Western Mississippi Fan and correlated and extended to the Eastern Mississippi Fan. Black areas denote location of channels.

CHAPTER III

SALT TECTONICS

Introduction

The northern Gulf of Mexico can be divided into eight nongenetic tectonostratigraphic provinces (Diegel et al., 1995; Minerals Management Service, 2000), (Figure 35): (1) a contractional foldbelt province at the toe of slope; (2) a tabular salt-minibasin province on the slope; (3) a Plio-Pleistocene detachment province on the outer shelf and upper slope; (4) a salt dome/mini-basin province; (5) an Oligocene-Miocene detachment province onshore/shelf; (6) an Oligocene-Vicksburg detachment province onshore Texas; (7) an upper Eocene detachment province, and (8) the Paleocene-Eocene aged Wilcox growth fault province.

The study area lies in a transition zone between three of these tectonostratigraphic provinces (Figure 36): a salt dome/mini-basin province, a Plio-Pleistocene detachment province, and a tabular salt/mini-basin province. Salt stocks characterize the salt dome/mini-basin province and the intervening minibasins are bounded by large-displacement, arcuate, and dominantly counter-regional growth faults. The province contains numerous different salt structures linked to depocenters of Eocene to Pleistocene age (Diegel, 1995). The Plio-Pleistocene detachment province contains areas of evacuated allochthonous salt as well as remnant allochthonous or "secondary"

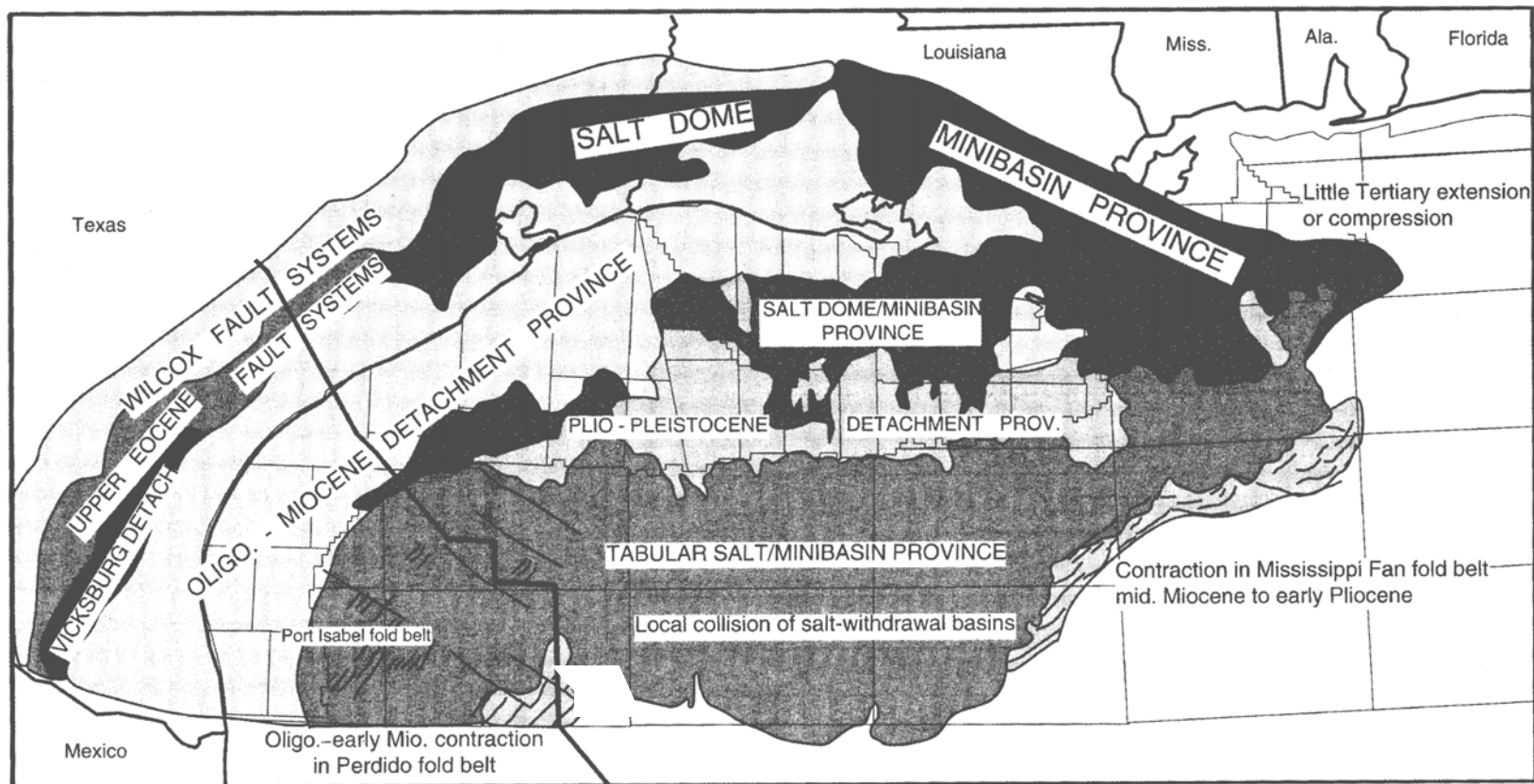


Figure 35. Tectonostratigraphic provinces of the Gulf of Mexico (Diegel, 1995).

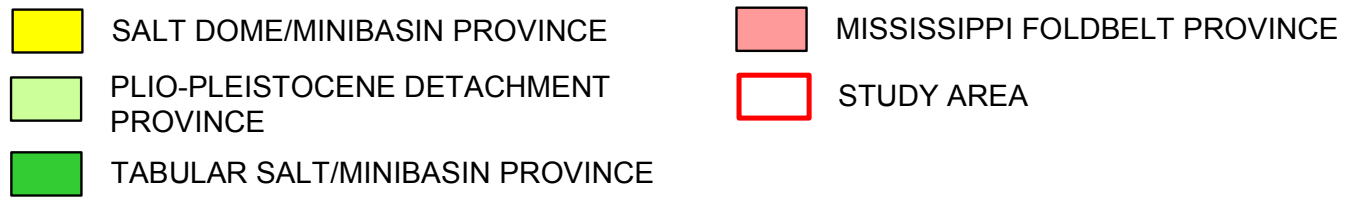
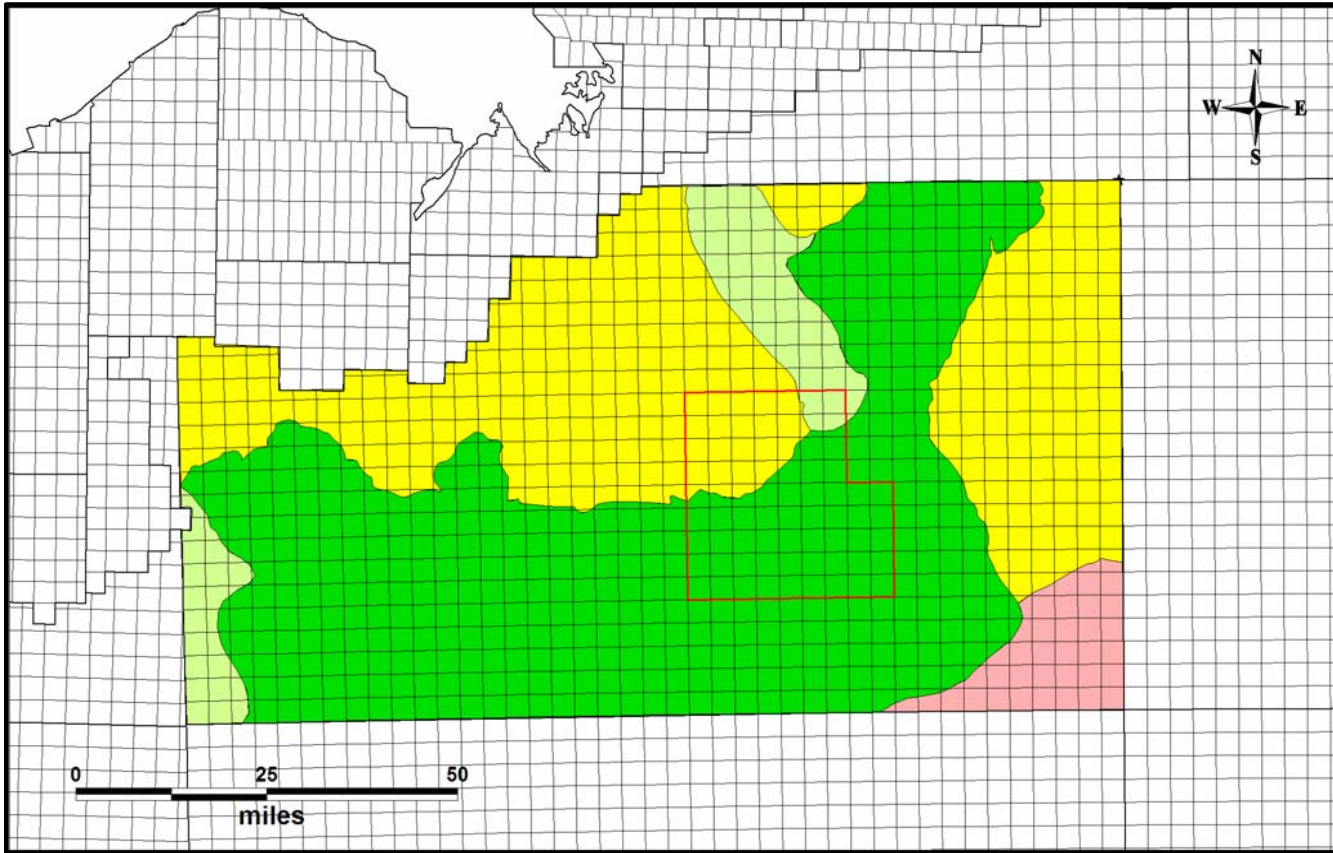


Figure 36. Distribution of tectonostratigraphic provinces in relation to the study area (provinces originally from Diegel, 1995).

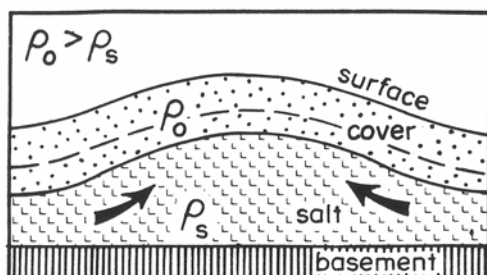
salt domes and wings near Pliocene-Pleistocene depocenters (Diegel, 1995). The tabular salt/mini-basin province is characterized by large salt sheets with intervening deep-water sediment-filled basins (Diegel, 1995).

This chapter describes the distribution and morphology of salt and identifies the character of associated basins in the study area.

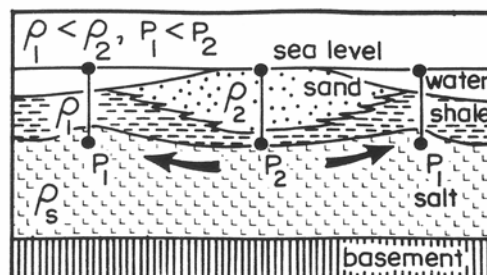
Mechanisms of Salt Movement

A number of mechanisms have been proposed to explain salt movement. These mechanisms include buoyancy, differential loading, gravity spreading, thermal convection, tectonic compression, and tectonic extension (Figure 37). These mechanisms arise from the following fundamental properties of salt: (1) Salt, on a geologic time-scale, can act as a viscous fluid, capable of flowing under the influence of outside stresses; (2) the density of salt does not change with depth; and (3) at some depth the density of salt becomes less than that of the overburden resulting in a density differential.

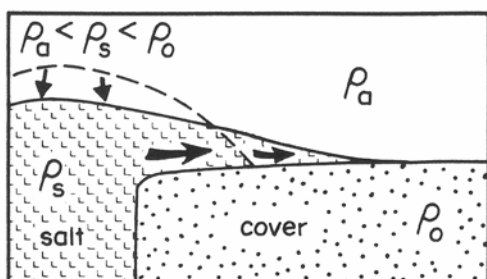
The buoyancy model (Figure 37A) is one of the oldest models for salt mobilization and has been studied extensively (Dobrin, 1941;Hubbert, 1937;Lachmann, 1910;Nettleton, 1934). In buoyancy, salt is buried deeper by sedimentation. While the density of salt remains constant, the density of the overburden increases with depth. At the critical depth a density inversion occurs with the density of salt being less than that of the surrounding sediment. At this point the salt becomes buoyant and, given



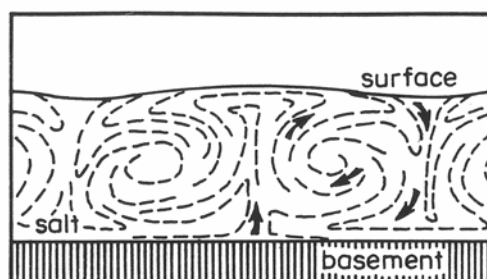
A. BUOYANCY



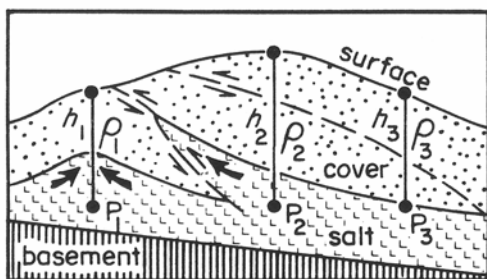
B. DIFFERENTIAL LOADING



C. GRAVITY SPREADING

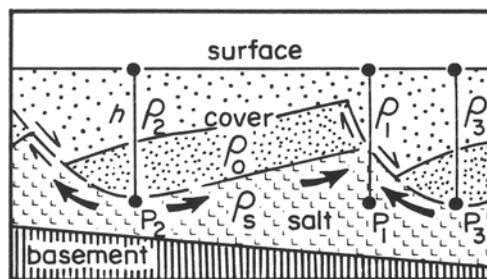


D. THERMAL CONVECTION

E. COMPRESSION $h_2 > h_1 = h_3$

Stable: $\rho_s > \rho_o \therefore \rho_1 > \rho_2 > \rho_3$ and $P_3 < P_1 < P_2$

Unstable: $\rho_s < \rho_o \therefore \rho_1 < \rho_2 < \rho_3$ and $P_1 < P_3 < P_2$



F. EXTENSION

Stable: $\rho_s > \rho_o \therefore \rho_1 > \rho_2 > \rho_3$ and $P_1 > P_2 > P_3$

Unstable: $\rho_s < \rho_o \therefore \rho_1 < \rho_2 < \rho_3$ and $P_1 < P_2 < P_3$

Figure 37. Proposed driving mechanisms for salt movement. P denotes a point or to the lithostatic pressure at that point. ρ denotes mean bulk density of a unit. A, B, D, E, and F modified from (Jackson and Talbot, 1986). C modified from (Ramberg, 1980) and Jackson and Talbot (1986).

continued sedimentation, will rise to maintain density equilibrium.

The differential loading model is not dependent on deep burial and can account for salt motion with little overburden. The model is based upon the lateral variations, thickness, density, and strength of the overburden (Jackson, 1995). Two types of differential loading are accepted: (1) erosional differential loading (Figure 37); and (2) depositional differential loading (Figure 37B). Erosional differential loading (Harrison, 1927) involves the removal of overburden over part of the salt. This removal locally decreases the pressure over the salt. The weight of the surrounding, un-eroded overburden pushes the salt into the eroded, low-pressure area. (Bailey, 1931) and (Rettger, 1935) recognized depositional differential loading in the early 1930's. Humphris (1978) attributed the mobilization of salt in the Gulf of Mexico basin to differential loading. Sediments are differentially deposited on top of salt. The salt will migrate from zones of high load (thick overburden) to zones of low load (thin overburden).

Gravity sliding (Figure 37C) results from the vertical collapse of salt (Ramberg, 1981; Ramberg, 1980). With the salt volume remaining constant, the vertical collapse of the salt results in the horizontal, downslope movement. The vertical collapse is driven by a reduction or depletion of the volume of the feeder salt source coupled with a difference in elevation between the center and spreading edge of the salt. Gravity spreading generally occurs after salt reaches density equilibrium. In a shelf/slope environment, salt may be emplaced higher than the deeper seafloor. In this case, gravity will aid in "pulling" the salt basinward. Gravity sliding usually results in an upper zone

of extension and downdip zone of contraction (Crans et al., 1980; Letouzey et al., 1995). In a marine environment, gravity sliding is divergent off coastal salients and convergent off coastal re-entrants (Cobbold and Szatmari, 1991). Divergent gliding causes strike-parallel extension whereas convergent gliding produces strike-parallel contraction.

Thermal convection (Figure 37D) is a theory based on the thermal expansion of salt. (Talbot, 1978) proposed that thermal expansion in salt would allow salt diapirs to rise as thermal plumes. Temperature increases with increasing depth. As salt becomes hotter and weaker, it expands due to heat. The expansion of the salt is greater than the compression due to increasing pressure at depth. At 5,000 m depth, with a geothermal gradient of 30°C/km, salt expands 2% but contracts only 0.5% due to pressure resulting in an overall expansion of 1.5% (Jackson and Galloway, 1984). Hot, deep salt would expand, lose density, and rise while shallow, cooler, denser salt would sink to replace it, thus establishing a convective cell.

Salt deformation can also occur in compressive or extensive tectonic regimes (Figure 37E and 37F). In compression, the salt can act as a basement detachment for compression of the overburden. In extension, salt can act as a decollement below listric normal faults allowing for extension of the overburden.

Extensive research and observations on the mechanics of salt tectonics have led to the conclusion that: (1) differential loading is the most effective mechanism in the early stage of salt deformation (Humphris, 1978); (2) buoyancy is not an effective mechanism unless the salt has pre-existing relief under denser overburden; (3) Gravity sliding is an important mechanism in the formation of shallow, horizontal salt bodies

(Nelson and Fairchild, 1989; Wu et al., 1990b); and (4) active tectonics are, in some part, responsible for some types of salt deformation.

There is ongoing debate on whether salt bodies form by intrusion, downbuilding, or extrusion. (Nettleton, 1955) and (Bishop, 1978) have theorized that salt structures grow intrusively. Wu et al (1990a) and Nelson and Fairchild (1989) provided models of horizontal intrusion of allochthonous salt in the Gulf of Mexico basin. (Barton, 1933) concluded that salt structures maintain their relative level with the base "downbuilding" with increased sedimentation (Figure 38). (Amery, 1969) produced the first known illustration of allochthonous salt illustrating an extrusive wedge of salt over flat-lying reflectors (Figure 39). Fletcher (1995) proposed that emplacement of allochthonous salt sheets was via an extrusive salt glacier that continued to "flow" even after burial. (Jackson et al., 1988) and (Jackson and Talbot, 1989) realized the existence of a number of growth modes that exist between intrusion, downbuilding, and extrusion. Jackson and Talbot (1986, 1989) also examined the relationship between the shape and maturity of salt structures (Figure 40). They hypothesized that structures grow from low-amplitude, concordant to high-amplitude, discordant through their evolution. Salt structures can halt growth at any stage dependent upon salt supply and surrounding geologic conditions. Immature structures include salt anticlines, domes, or pillows. Mature structures include attached or detached salt tongues and individual or coalesced salt canopies.

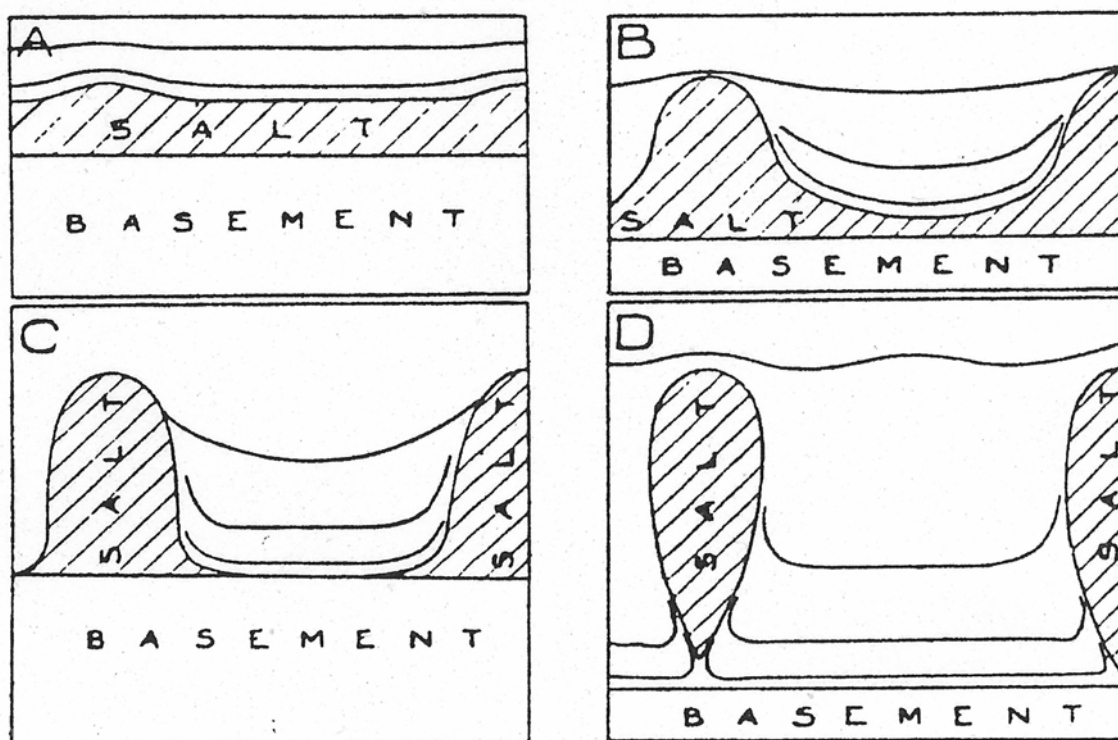


Figure 38. Downbuilding model of shallow salt emplacement (Barton, 1933). The salt height remains constant and the basin downbuilds as the volume of the salt reorganizes to accommodate the increasing overburden.

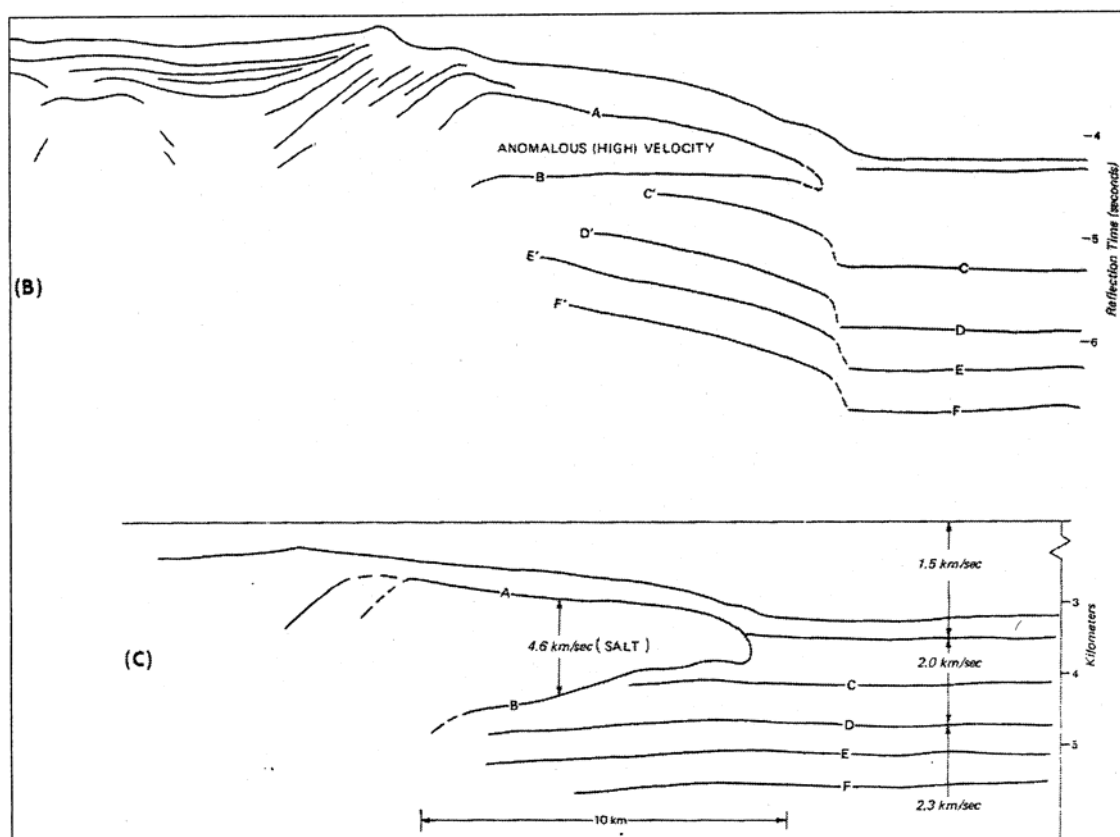


Figure 39. First known illustration of allochthonous salt (Amery, 1969). B represents a stratigraphic interpretation from a seismic time section. C represents the same interpretations now shown on a seismic velocity section illustrating proper salt geometry when the anomalously high salt velocities are factored in.

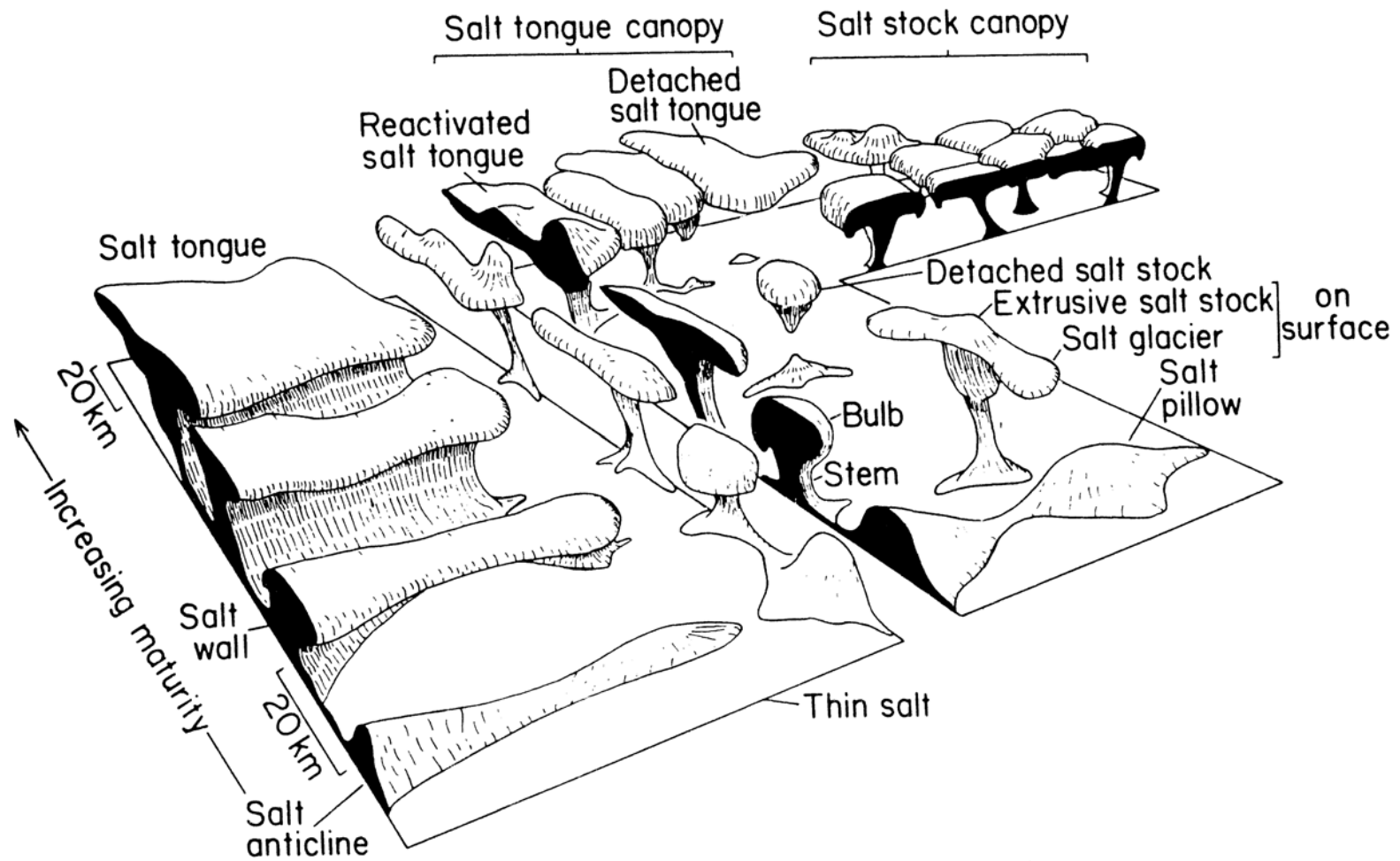


Figure 40. Perspective view of principal types of salt structures (Jackson and Talbot, 1986).

Seismic Recognition of Salt

Salt can be recognized on seismic data in three ways: (1) Seismic character at the salt-sediment interface; (2) Seismic character within the salt; and (3) Seismic character of sediments surrounding the salt. The high-impedance contrast between high-velocity salt and the overlying low-velocity sediments produces a high-amplitude reflector (Figure 41). This can be a single reflector or a well-pronounced seismic doublet.

An important attribute of salt is that it possesses little or no porosity (Yorston and Fox, 1985). This contributes to salt only compressing slightly when subjected to pressure. In addition, the density of salt remains relatively unchanged at depth. Since seismic velocity is primarily dependent upon density of the medium, the velocity of salt (~4,500 m/sec) also remains unchanged. Minor impedance changes within the salt are not large enough to produce coherent seismic reflections (Jenyon, 1986). Thus, the seismic response through salt is seen as a wipeout zone, acoustic void, or zone of multiple, low-amplitude incoherent reflections (Figure 41). This velocity wipeout zone, coupled with the high-amplitude reflector at the salt-sediment interface is the best seismic indicator that salt is present (Figure 41).

Seismic indications in sediments surrounding salt include: (1) velocity pull-up/or pull-down up reflectors underlying the salt (2) faulting above the salt resulting from the tension of salt movement; and (3) heavily deformed sediments just above the salt sediment interface. Dragging and rotation have deformed these sediments as the salt has moved immediately underneath them.

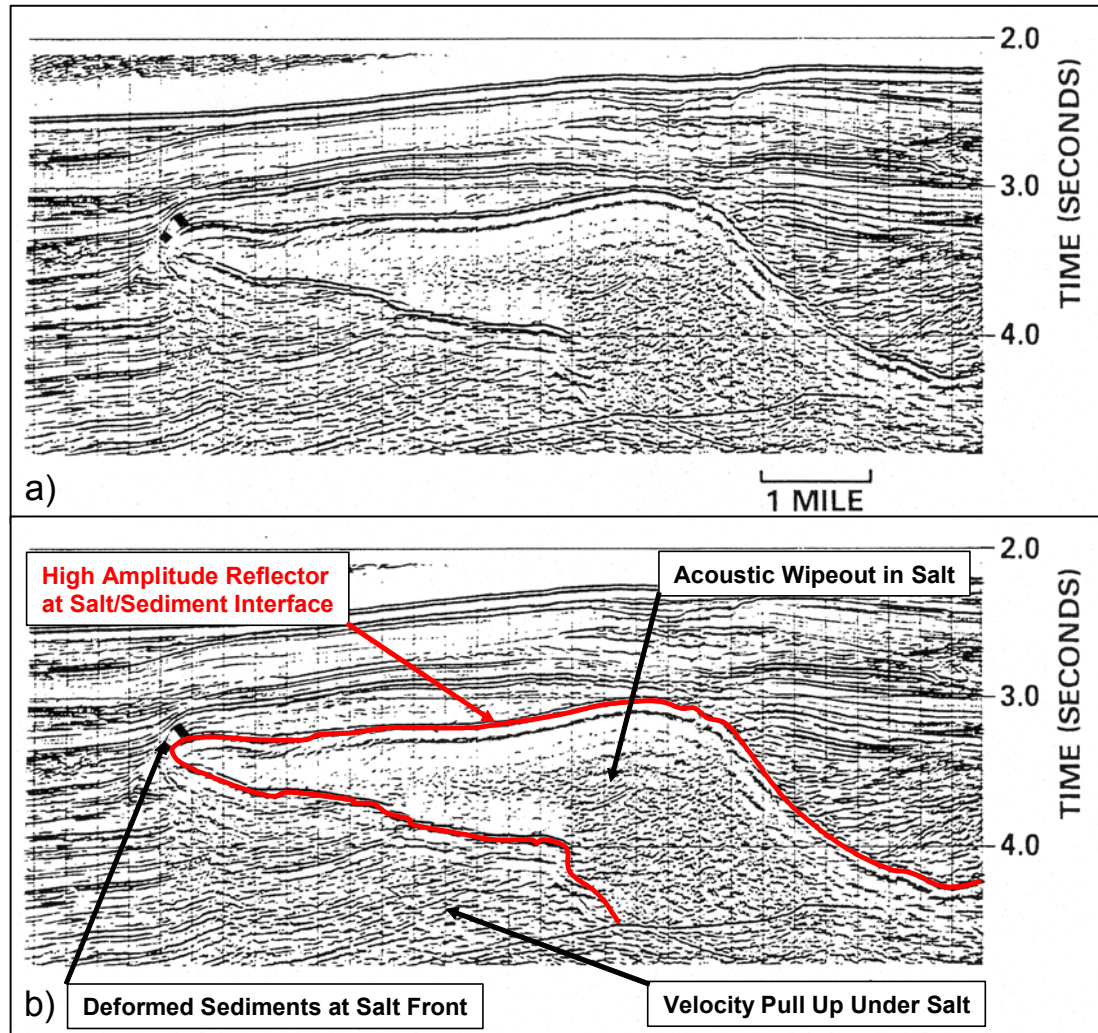


Figure 41. Seismic recognition and characters of salt (Nelson, 1991). A is an uninterpreted seismic section. B is an interpreted seismic section.

Observations

A. Distribution of Salt in the Study Area

Salt is present in the northeast, southeast, and southwest quadrants of the study area and along the central western perimeter of the study area. These salt bodies are labeled I-IV respectively (Figure 42). The distribution of salt above 4.00 seconds (time depth limit of the data) is shown in comparison to salt bodies previously mapped in the Mississippi Canyon area (Figure 43). There is an excellent correlation between the previously mapped salt and the salt mapped in this study. The distribution of salt above 4.00 seconds in the study area is also shown on the depth-structure map and salt surface rendering (Figure 44) and perspective view (Figure 45).

In areas not mapped as salt, the salt was either not present, not mappable, or was deeper than 4.00 seconds. The morphology of the four individual salt bodies is presented in the following discussions.

B. Morphology: Salt Body I

Salt Body I (SBI) is located in the northeast quadrant of the study area and covers an area of approximately 122 square miles (Figure 42). The salt trends in a northwest to southeast direction and appears to be the southern extent of a larger, linear salt body

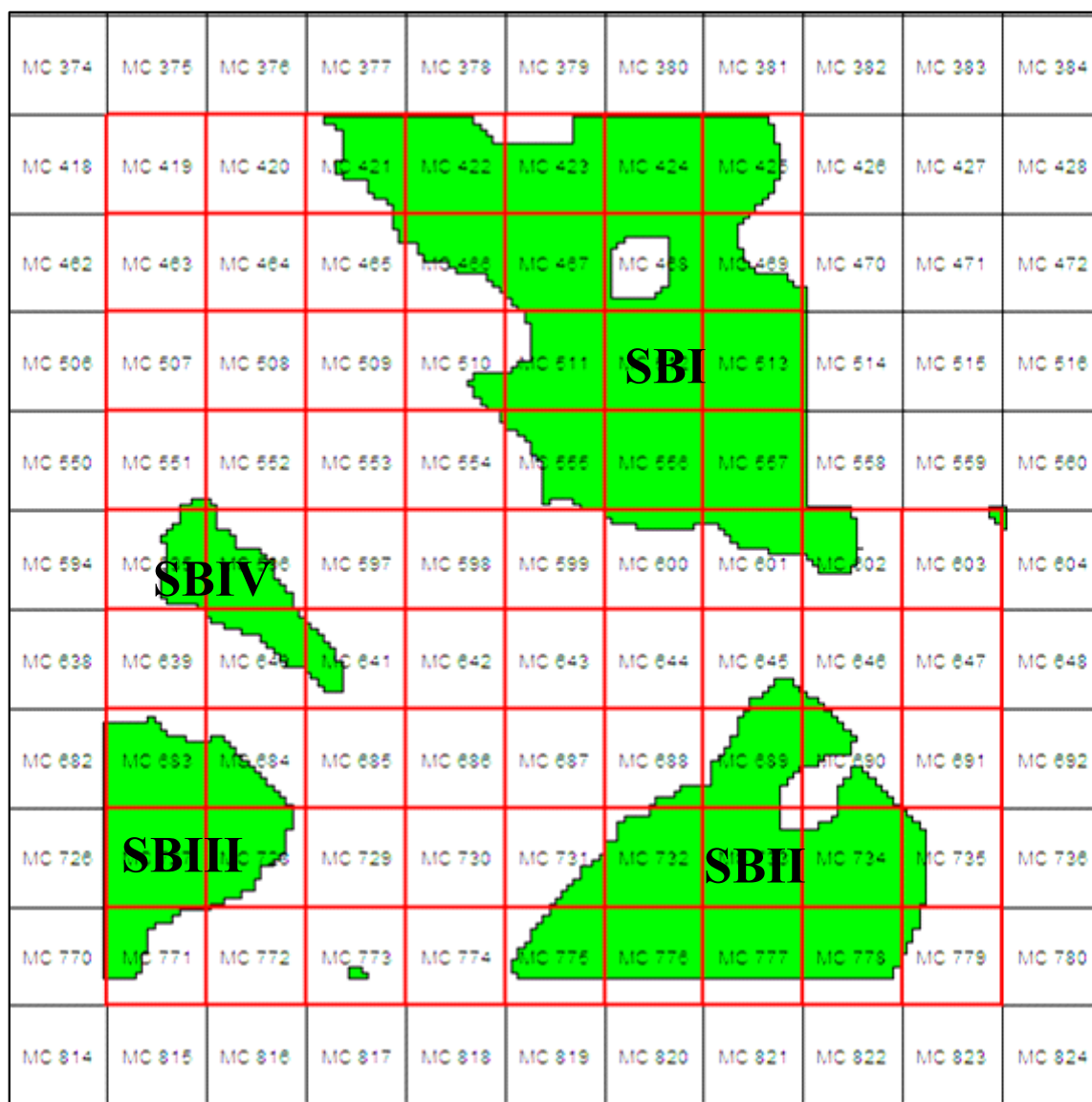


Figure 42. Distribution of shallow salt in the study area.

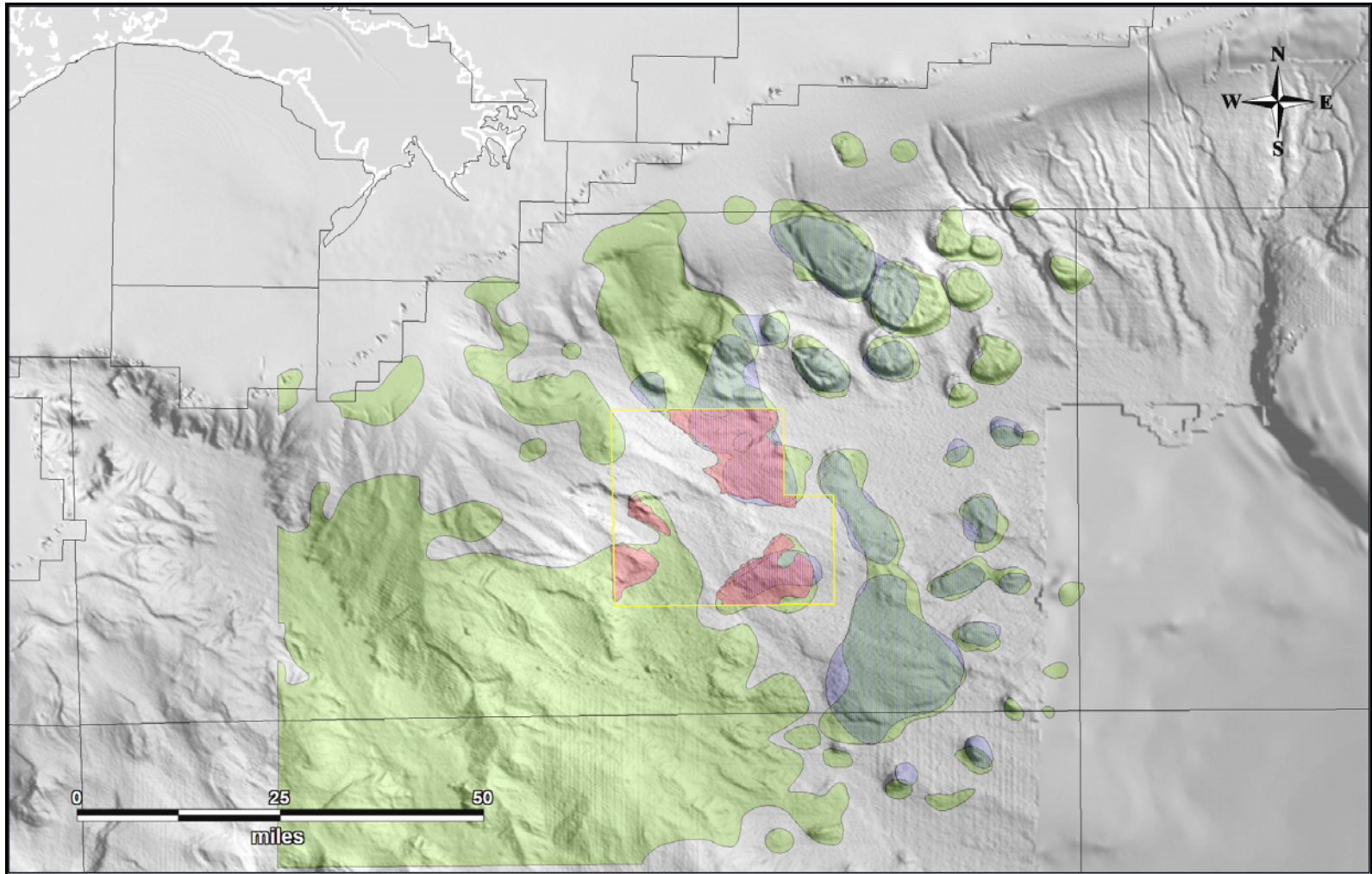


Figure 43. Location of salt in study area relative to previously mapped salt in the Mississippi Canyon area. Blue areas from Wu et al (1990a). Green areas from Fletcher (1995). Red areas denote salt mapped from this study. Outline of study area in yellow. Rendering courtesy of Geoscience Earth and Marine Services, Inc.

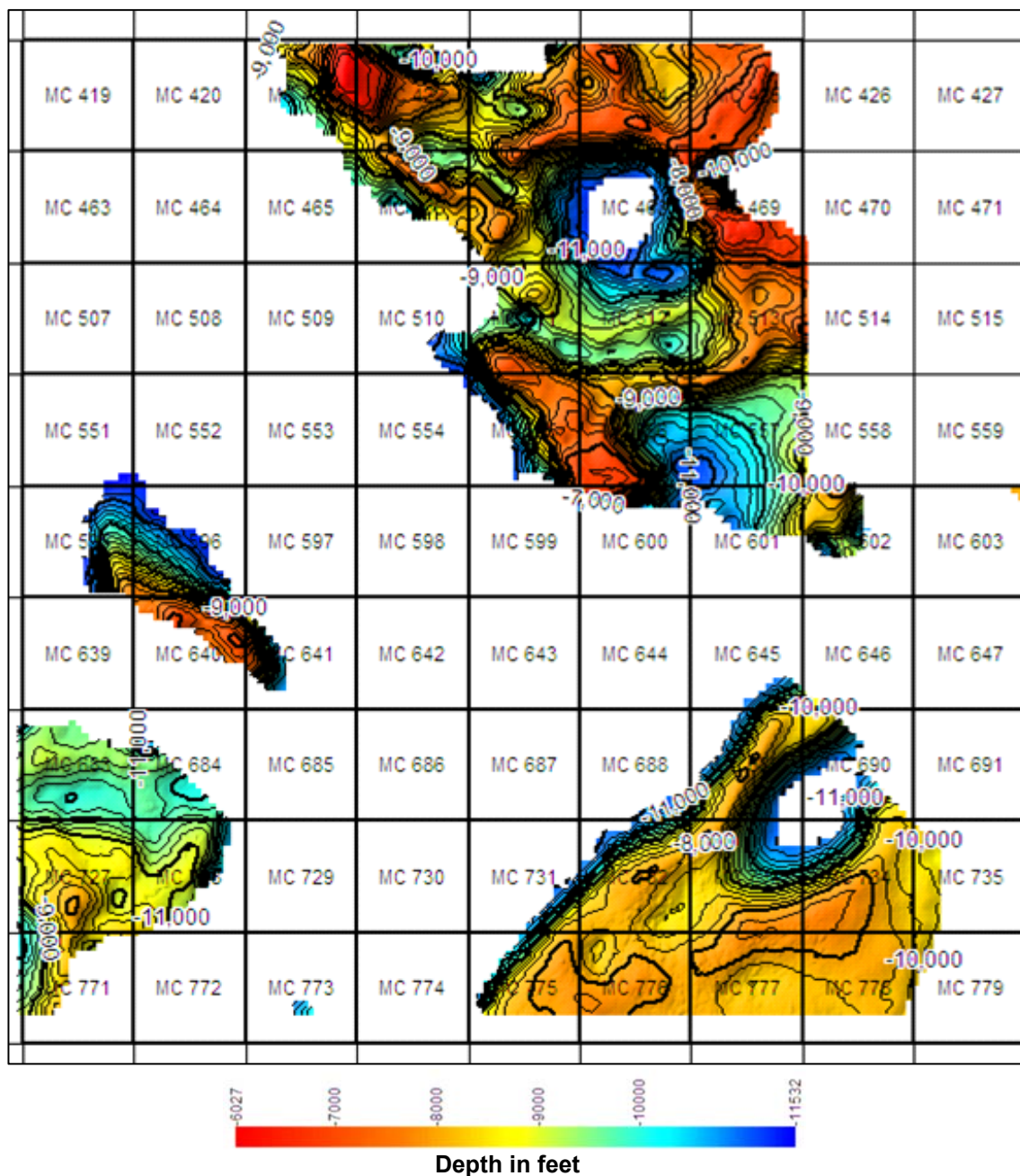


Figure 44. Structure map, top of salt. Contour interval = 200ft. Index Contours every 1,000ft.

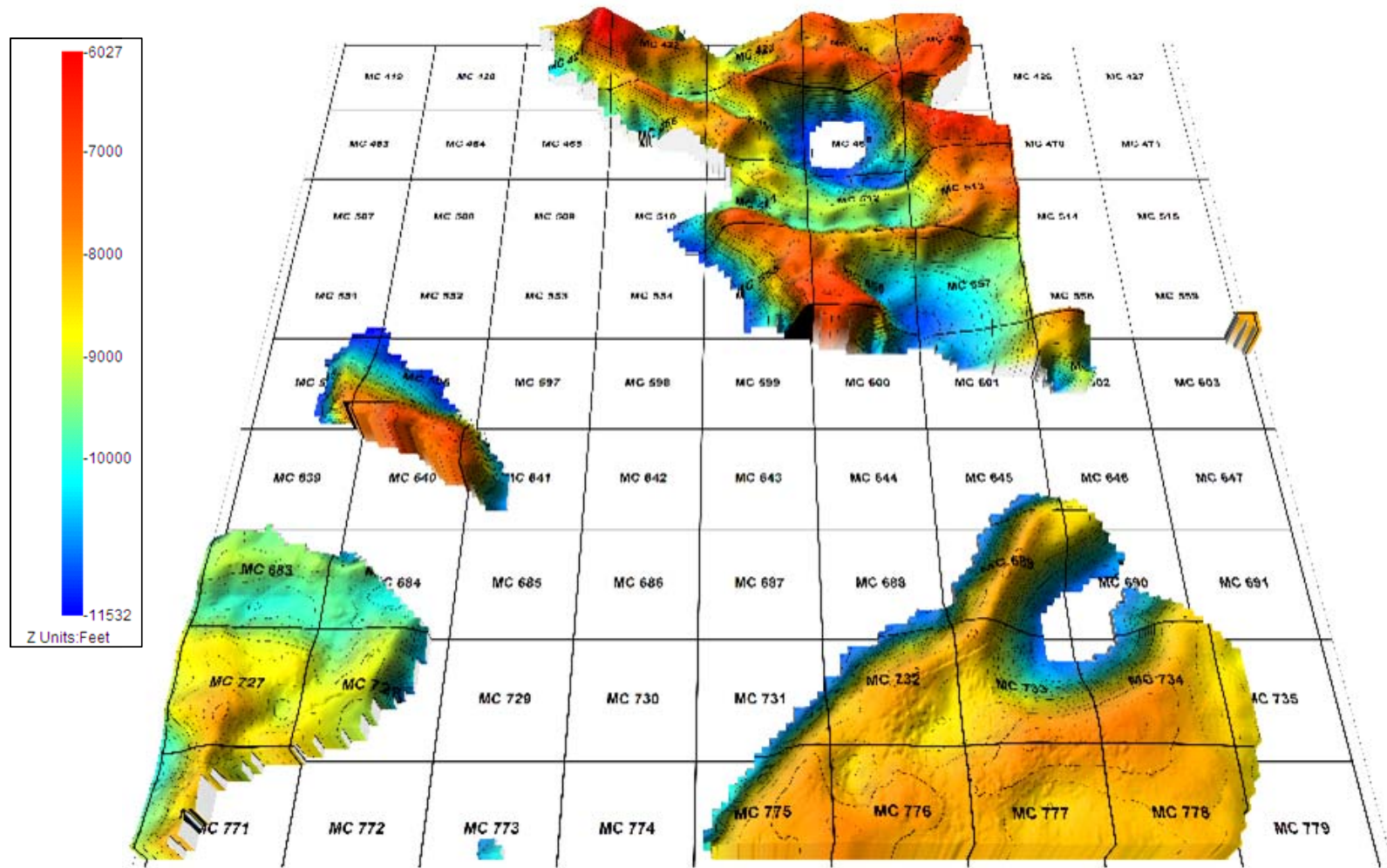


Figure 45. Perspective view, top of salt. Perspective looking south to north from a 35 degree elevation. Sun angle is from 0 degrees (north).

extending southeast from the northern border of Mississippi Canyon (Figure 43). This larger salt body covers an approximate area of 519 square miles.

The depth structure map and salt surface rendering (Figure 44) illustrate the irregular surface of the top of SBI. The depth to the top of SBI ranges from approximately 6000 ft to 11,000 ft, below sea level (bsl). The isopach map to the top of salt (Figure 46) correspondingly illustrates the irregular thickness distribution of sediments above the salt. Sediment thickness from the mudline to the top of SBI range between 1200 ft to 6200 ft. Sediments are thickest in two deep basins along the northwest to southeast axis of SBI (Figure 46). Smaller, shallower basins flank these larger basins with sediments thinnest along basin rims.

The salt structure and isopach maps reveal a rugose top of salt which in turn dictates the overlying sediment thickness. Figure 47 illustrates the arbitrary seismic lines used in this study to display the type sections for both the salt morphology and shallow stratigraphy. Two seismic lines (Figures 48 and 49) pass through SBI and illustrate the observed irregular character of the salt top as well as display the distribution of sediments in the mini-basins above the salt surface. The differential loading of sediments above the salt has caused the salt to remobilize and subside resulting in a series of small, deep basins surrounded by pointed rims of salt. This remobilization correlates with theories of late stage allochthonous salt sheets proposed by Nelson and Fairchild (1989), Liro (1989), and Diegel (1995) whereby the salt volume is re-organized by salt withdrawal underneath basins and inflation (or diapirism) in areas of thinner overburden.

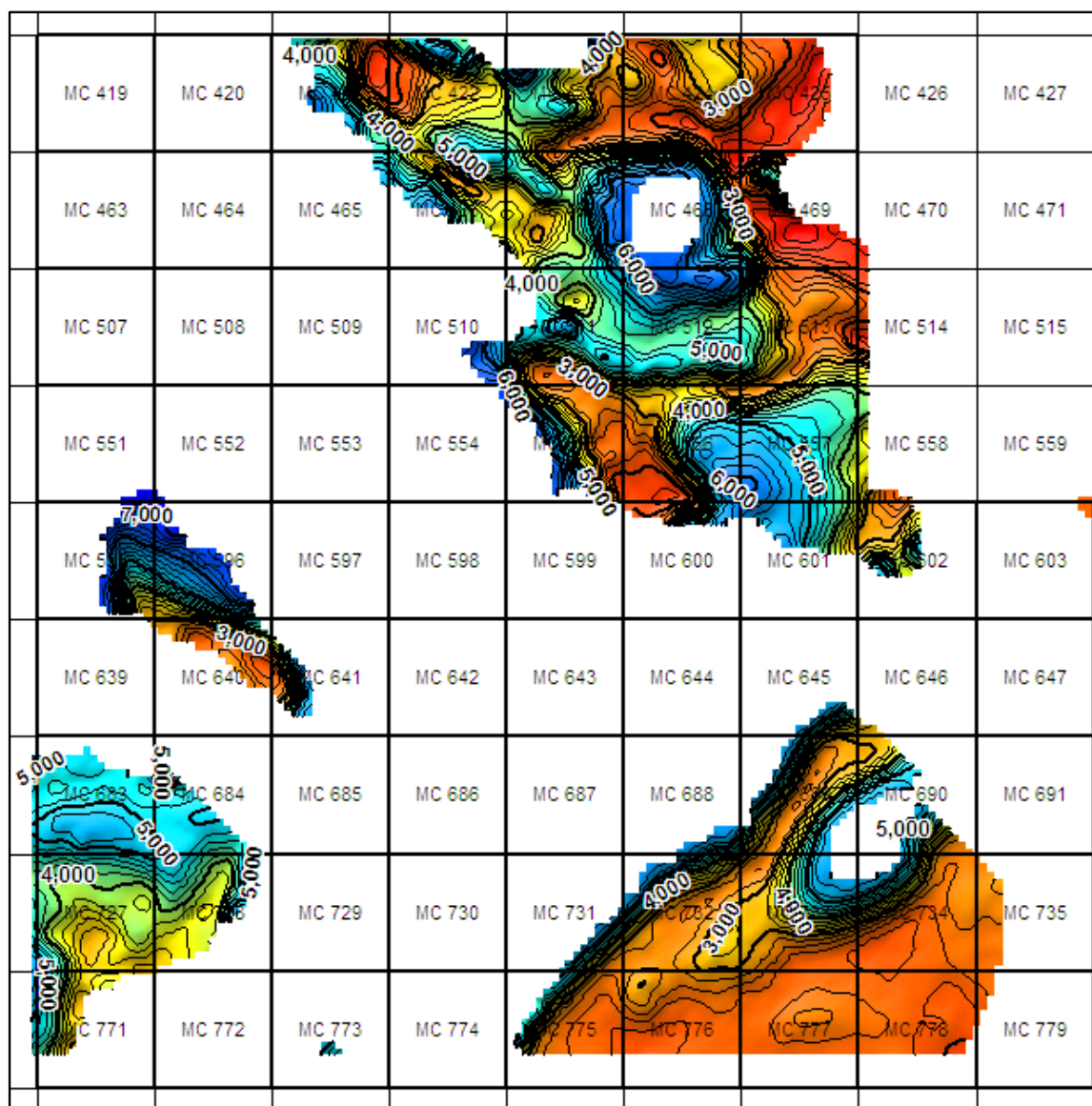


Figure 46. Isopach map, top of salt. Contour interval = 200ft. Index Contours every 1,000ft.

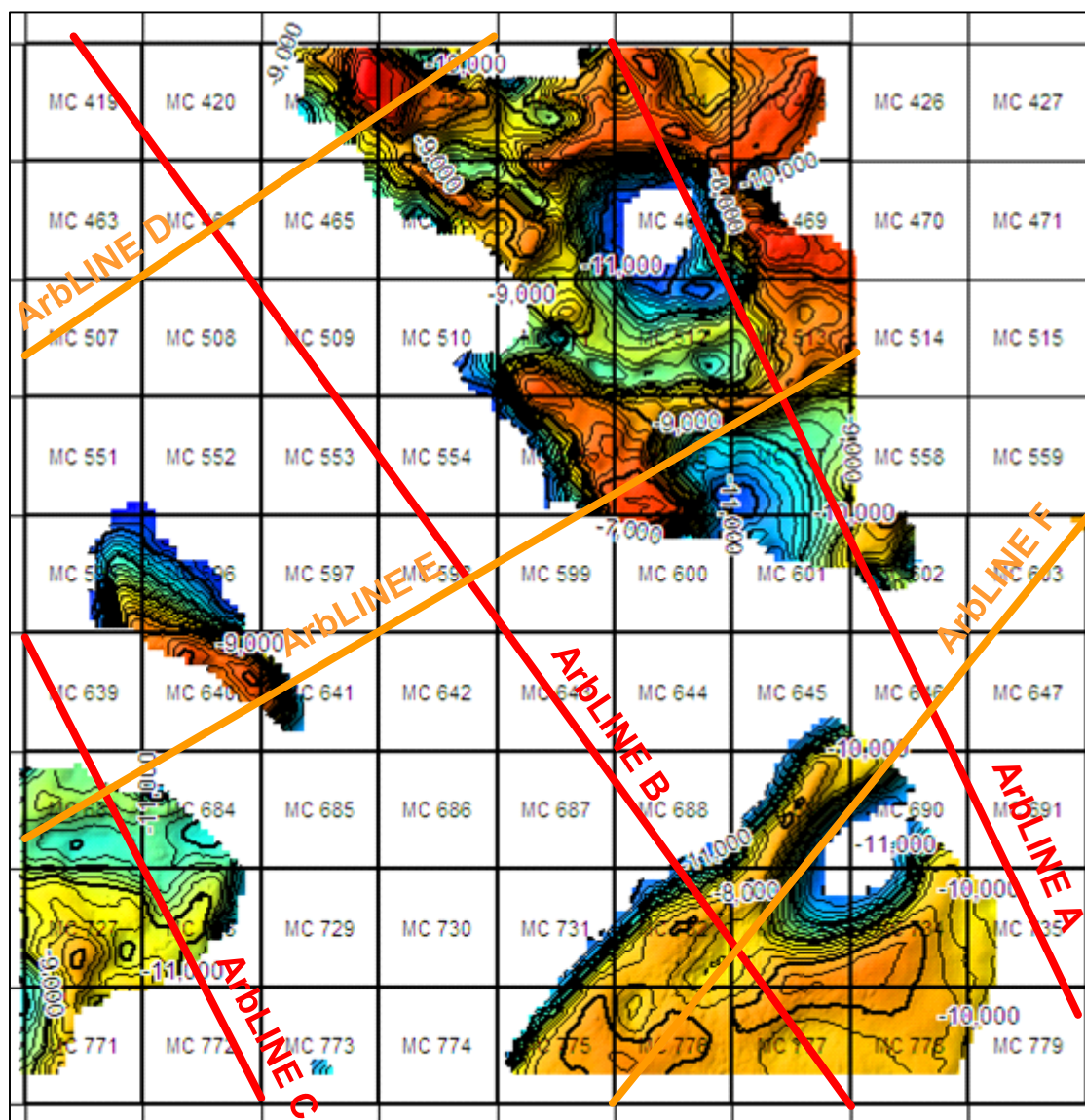


Figure 47. Locations of arbitrary seismic lines used in this study. Lines chosen to show seismic data along the regional strike and dip. Background image is top of salt structure map. Contour interval = 200ft. Index Contours every 1,000ft.

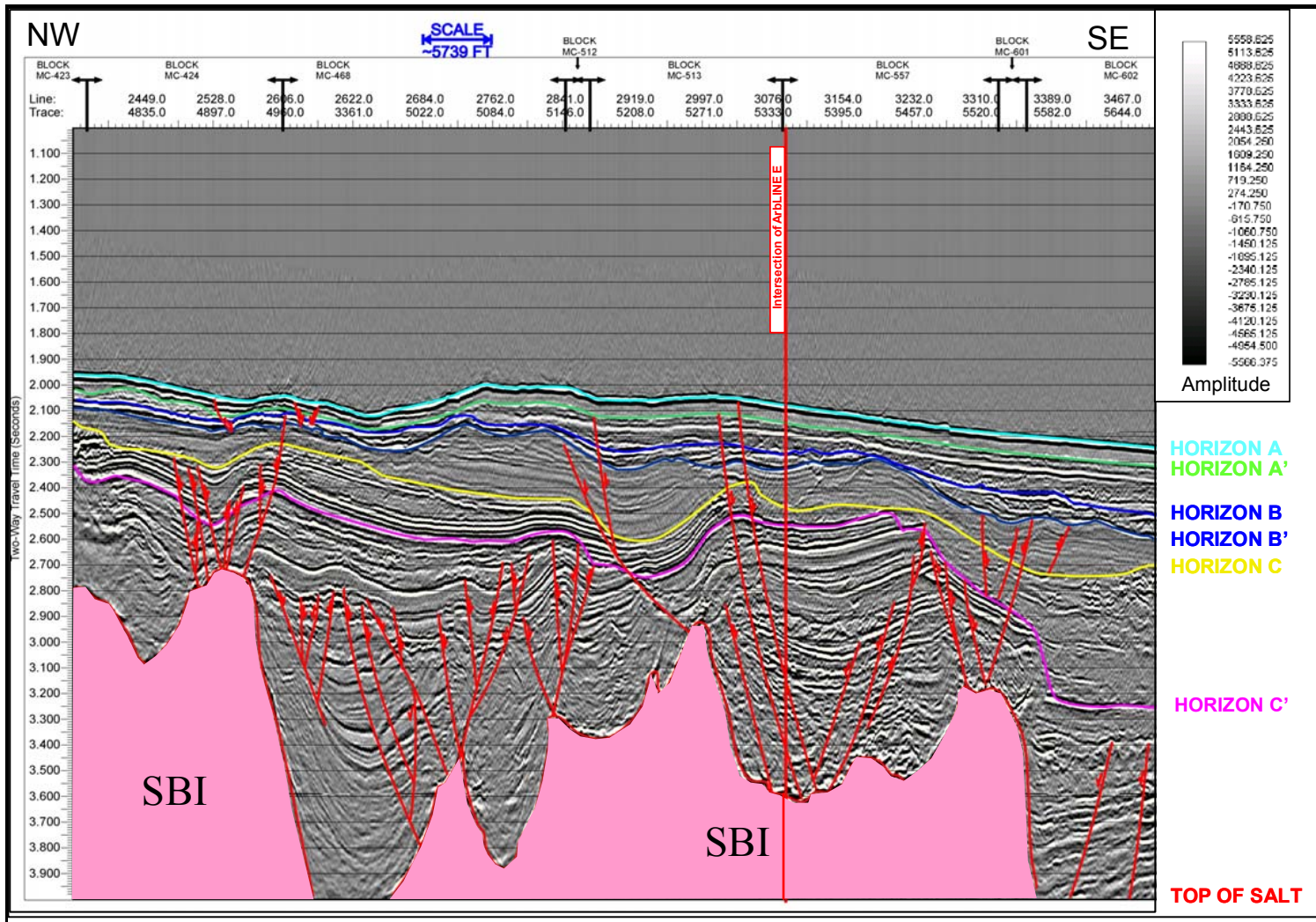


Figure 48. Arbitrary Seismic Line A illustrating the character of SBI. Pink shaded area is SBI. Colored lines denote mapped horizons annotated to the right of the seismic image. Red lines denote faults.

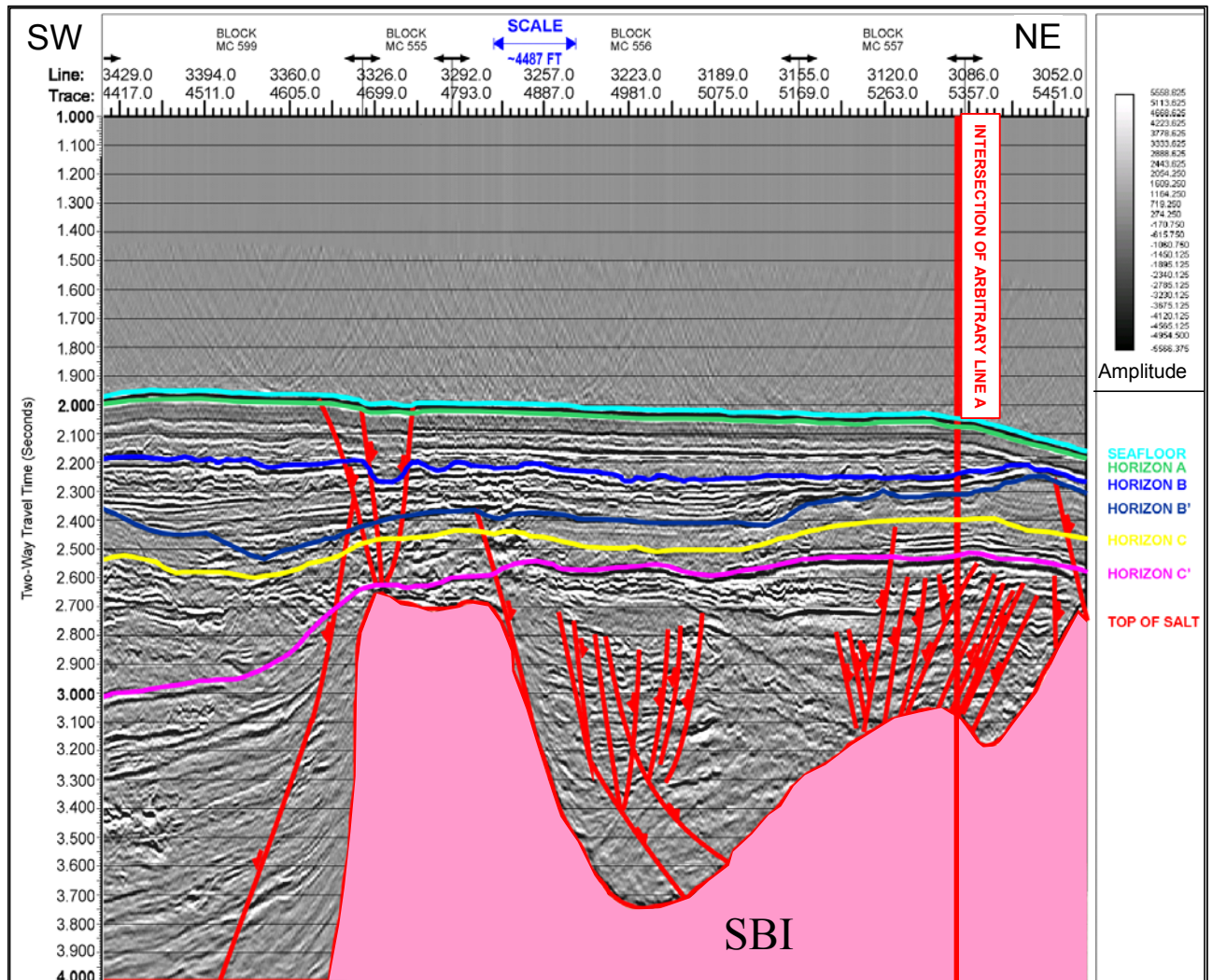


Figure 49. Arbitrary Seismic Line E illustrating the character of SBI. Pink shaded area is SBI. Colored lines denote mapped horizons annotated to the right of the seismic image. Red lines denote faults.

The original topography of the salt surface probably plays an important role in the initial and continued formation of these mini-basins. It is expected that the salt will continue to be slowly remobilized in adjustment to the overburden.

The larger salt body, of which SBI is part, may lie along a thin-skinned, strike-slip boundary as proposed by Peel et al. (1995). Figure 50 illustrates the relationship of the salt bodies mapped by Fletcher (1995) to the strike-slip boundary proposed by Peel et al. (1995). The northwest to southeast, dip elongate salt body may define a transfer zone between a Far-Eastern province with little or no Cenozoic extension and an Eastern Province of Mid-Miocene to Pliocene extension. Deformation of the stratigraphy, in the form of faulting, within the strike-slip transfer zone would provide a preferential path for the upward migration of salt. SBI could have formed from the coalescence of dip elongate shallow salt bodies that migrated into the shallow section along this strike-slip transfer zone to form the original allochthonous salt mass which has been subsequently remobilized.

SBI also lies at the transition between two of the tectonostratigraphic provinces proposed by Diegel (1995). Figure 51 illustrates the distribution of Salt Bodies I-IV in relation to salt mapped by Fletcher (1995), the strike-slip boundary proposed by Peel et al. (1995) and Diegel's tectonostratigraphic provinces for the study area. The northeast corner of SBI is a supposed part of the Plio-Pleistocene Detachment province previously discussed as a potential dip-elongate, strike boundary between a region of little or no Cenozoic extension and Mid-Miocene to Pliocene extension. This correlates well with Diegel's designation of this province as Plio-Pleistocene Detachment whereby the

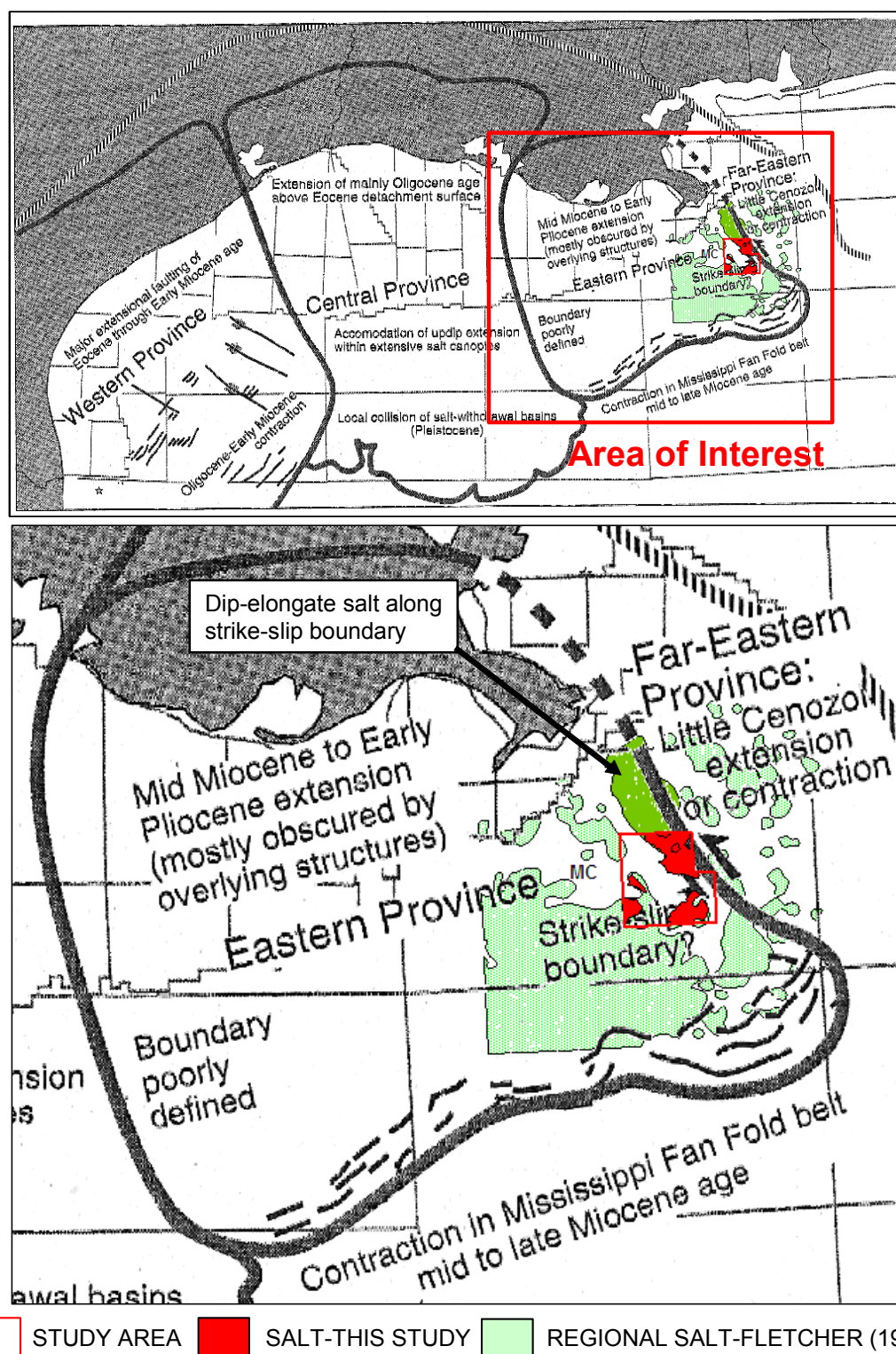


Figure 50. Relationship of mapped salt bodies to a previously proposed thin-skinned, strike-slip boundary. Provinces from Peel et al (1995).

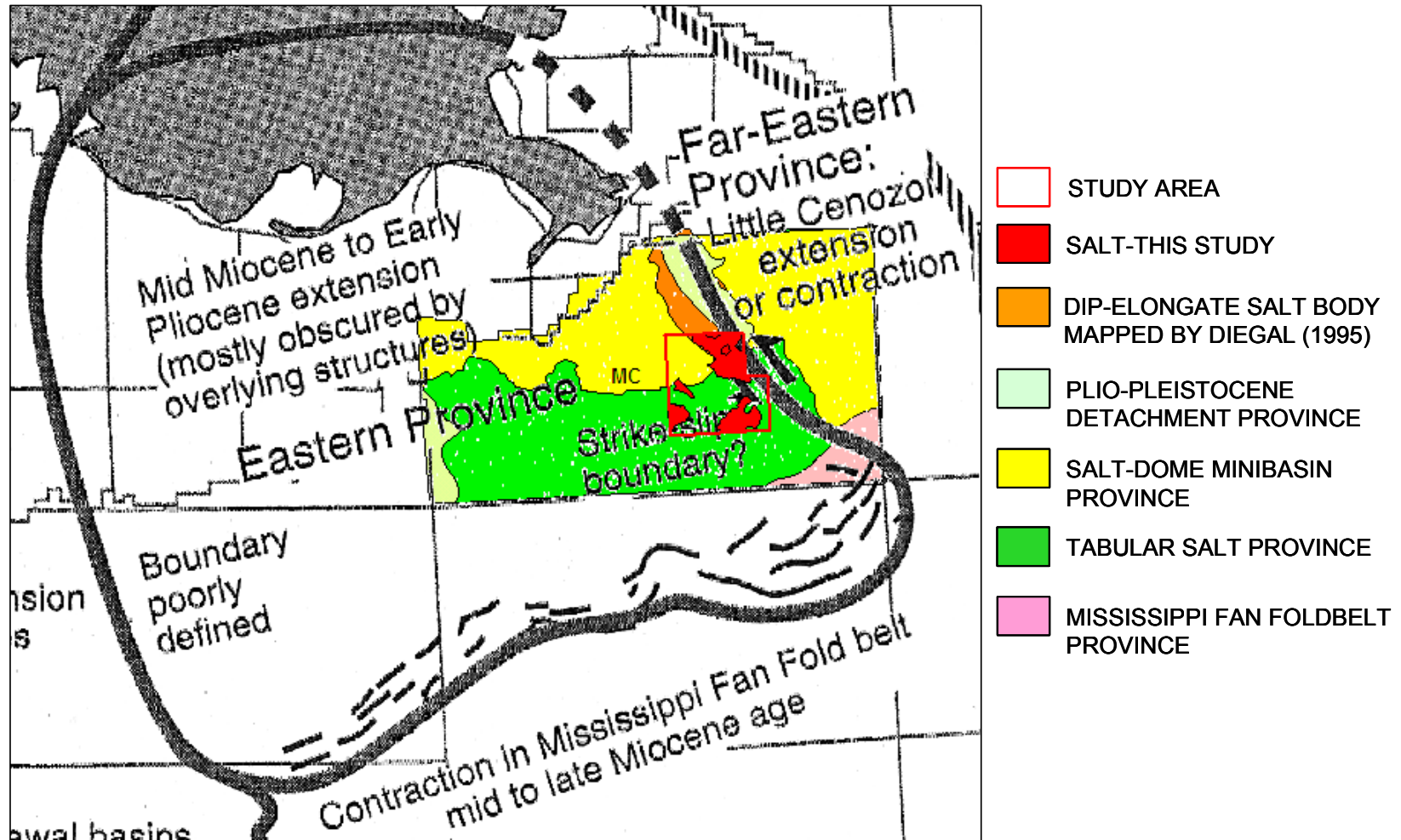


Figure 51. Location of SBI-SBIV to the strike-slip boundary and tectonostratigraphic provinces. Strike-slip boundary from Peel et al (1995). Tectonostratigraphic provinces originally from Diegel (1995).

detachment could in part be facilitated by extension and subsequent inflation of salt along the strike-slip-boundary.

The remainder of SBI lies in the Salt Dome-Minibasin province. At first glance this interpretation appears acceptable as the morphology of SBI could be primarily characterized as a salt dome/minibasin allochthonous salt sheet. However, the two provinces are decidedly different in their formation. Therefore further discussion on the possible origin of SBI is necessary.

Diegel (1995) proposed the Plio-Pleistocene detachment province in this region as an "organized" Roho system. Further research by Schuster (1995) indicates that SBI may be the downdip extent of a Roho system. The presence of a strike-slip transfer zone would facilitate the formation of a Roho system by allowing for the vertical migration and coalescence of salt to form the original shallow allochthonous salt mass. Figure 52 illustrates the basic model of evolution to the end-member Roho system (Schuster, 1995). Figure 53 shows the salt body used by Schuster as a model Roho end-member system. This salt body is the dip-elongate salt previously discussed where SBI is the southern most extension of this salt body. Figure 54 is a dip oriented seismic line through the Roho system and shows the position of SBI within that system. The seismic example provided by Schuster is a large-scale regional line that images far below the 4.00 seconds of data used for this research. The resolution of Figure 54 allows for the identification of the salt sill that SBI may be part of as well as the tertiary salt-weld up-dip of the study area. The incremental extensional faults associated with a Roho system are also evident.

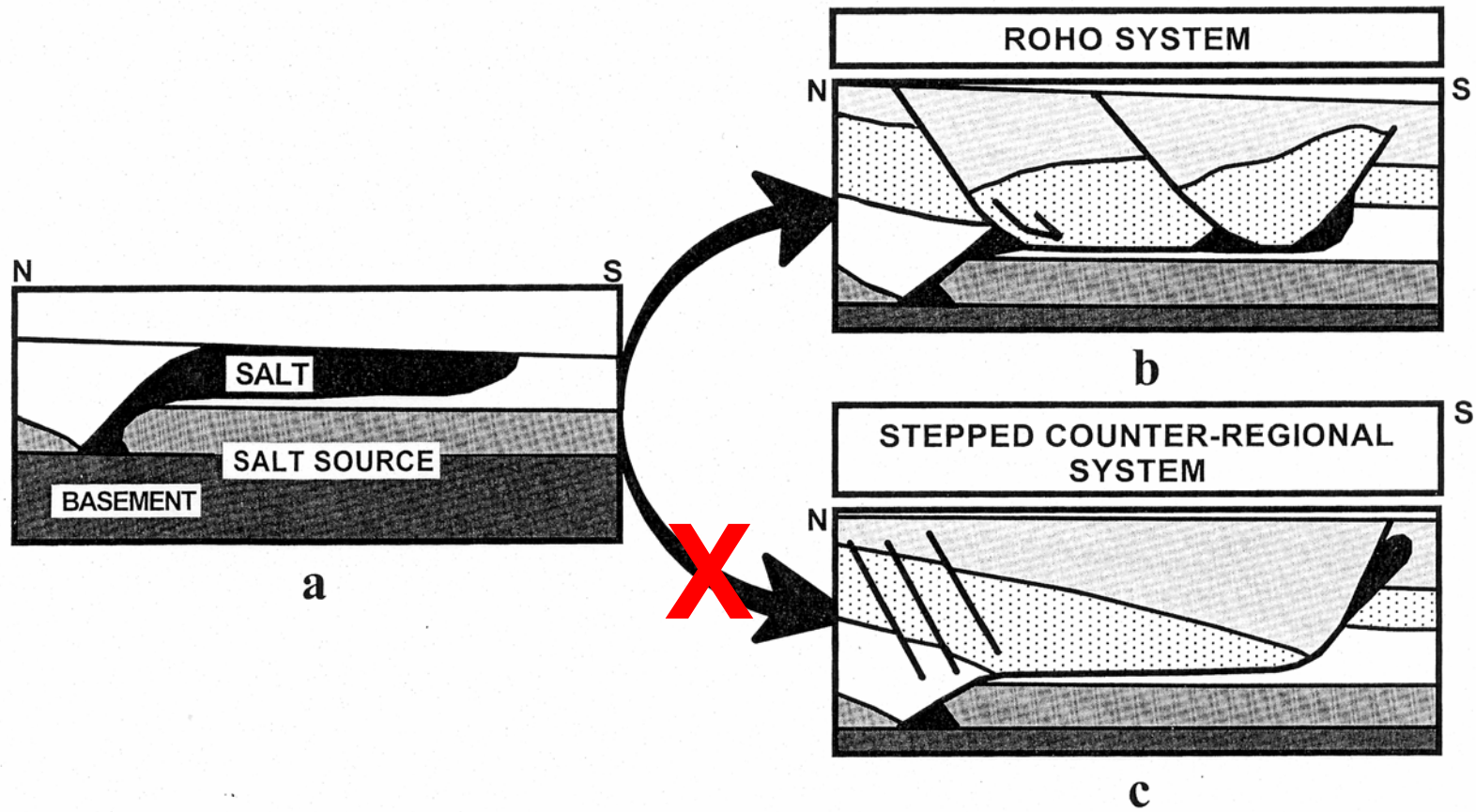
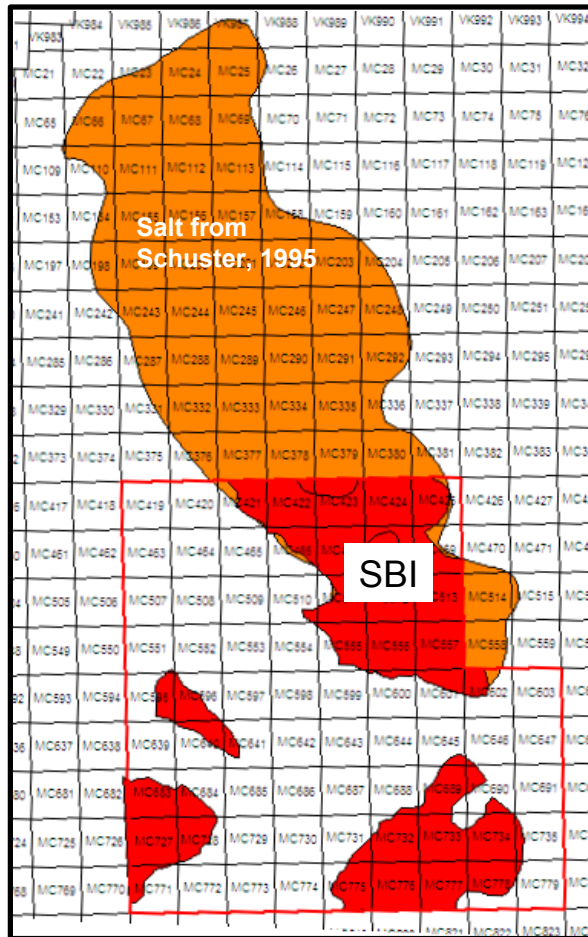
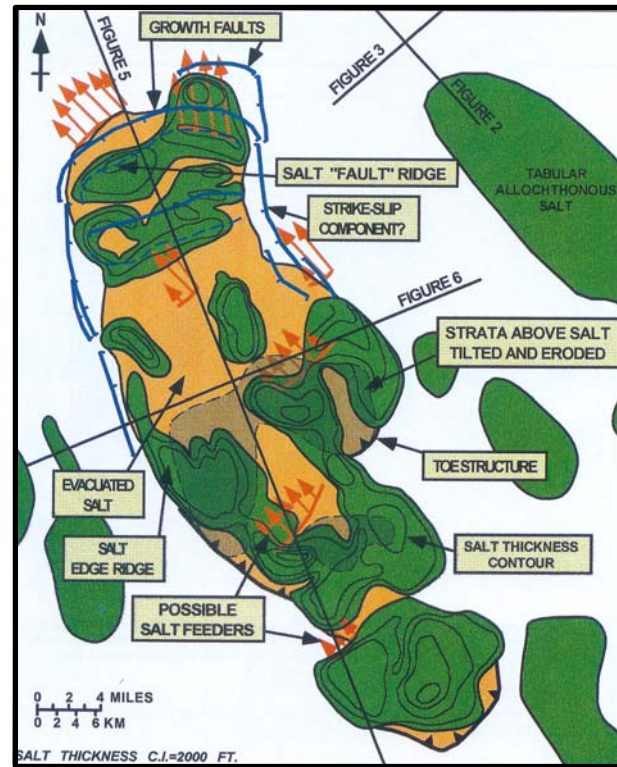


Figure 52. Basic model of the Roho end-member system (from Schuster, 1995). Note the variation in the geometry of faults and orientation of stratigraphic within the section between the two end-members systems.



STUDY AREA



SCHUSTER, 1995

Figure 53. Comparison of previously defined Roho end-member system to salt in the study area (Schuster, 1995). SBI lies at the seaward end of the Roho end-member system identified by Schuster (1995).

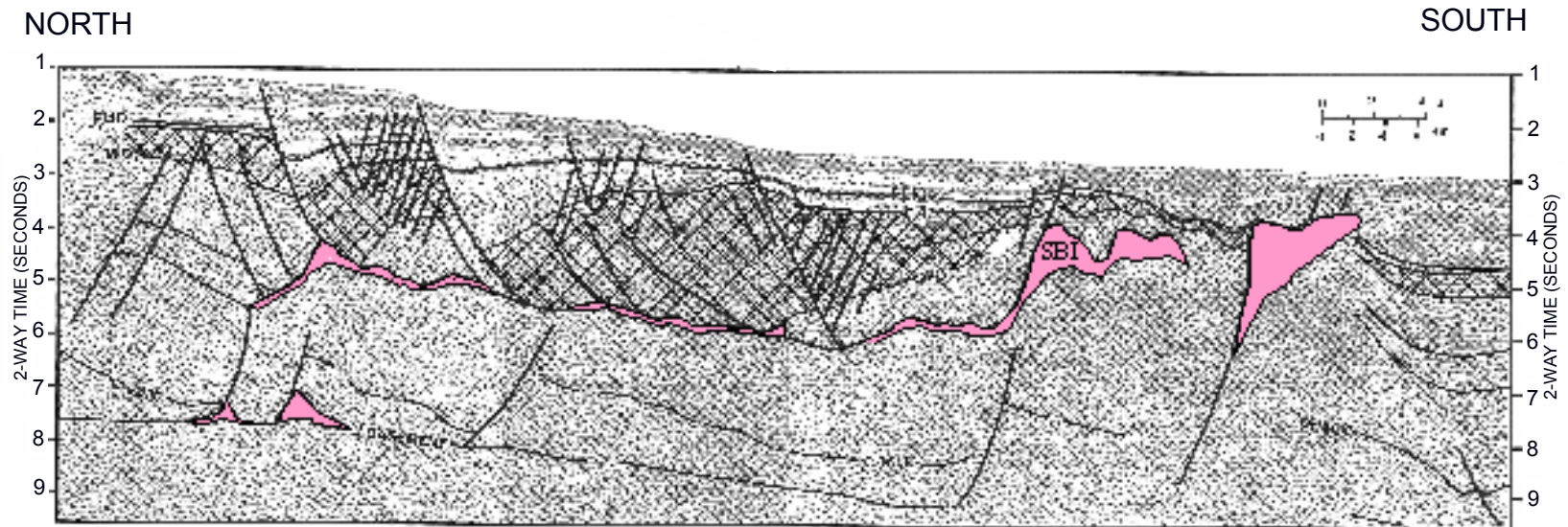


Figure 54. Large-scale regional seismic line showing local Roho end-member salt and location of SBI (modified from Schuster, 1995). Pink shaded areas are salt. Black, vertically oriented lines denote faults. Horizontal lines denote horizons. Note geometry of faults and overlying stratigraphic section above the salt weld in comparison to the idealized Roho end-member model by Schuster (1995) in Figure 52.

This is important in defining the salt system as a Roho end-member as opposed to a stepped counter-regional system which differs in that the overlying stratigraphic section within the evolving basin rolls into the seaward counter-regional extensional fault to accommodate the extension caused by evacuation of salt and associated basin subsidence. Figure 54 also shows the top of the salt, as mapped by Schuster, to be at about the same time-depth (~2.8 to 3.0 seconds) as SBI in Figure 44. The southernmost salt body in Figure 54 may actually be SBII, not intersected by the seismic line in Figure 48. A palipinastic reconstruction (Schuster, 1995) from the Miocene to Present illustrates one possible evolution of the regional salt system resulting in the present day morphology of SBI (Figure 55). This reconstruction will also have implications later on for understanding the sequence stratigraphy in the study area. The data suggests that SBI is part of the Roho system presented by Schuster (1995) that has been, in part, facilitated by the transfer zone proposed by Peel et al. (1995), and is the southern expression of Diegel's Plio-Pleistocene Detachment province. This leads to a necessary local adjustment to those tectonostratigraphic provinces. Considering the mode of formation and end-member system, SBI should be entirely part of the Mississippi Canyon Plio-Pleistocene Detachment province and not part of the Salt Dome/Minibasin province (Figure 36). This would imply that the salt was allochthonously emplaced in the Miocene and subsequently remobilized to a Roho end-member as a response to sediment loading during the Plio-Pleistocene (see Figure 55 illustrating position of Miocene and Plio-Pleistocene boundaries relative to salt evolution in the palipinastic reconstruction as well as formation of the Roho end-member style basin above the salt).

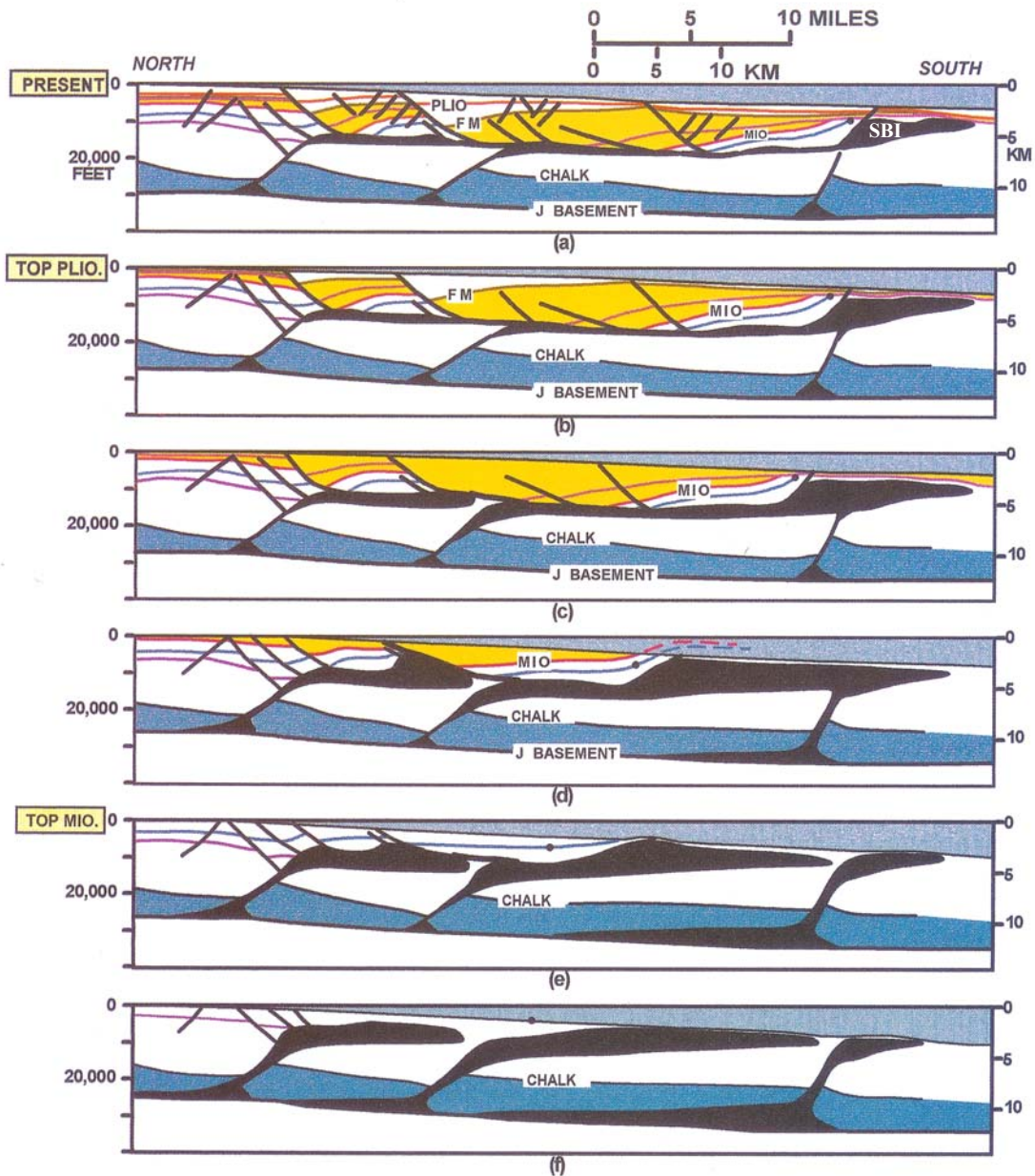


Figure 55. Regional palipinastic reconstruction from Miocene to present showing interpreted location of SBI (modified from Schuster, 1995). Section evolves through time from bottom to top panel. Note positions of salt with respect to Miocene and Plio-Pleistocene boundaries as well as the Roho end-member system that results as the section evolves.

It should be noted that SBI I does indeed lie at the transition between two tectonostratigraphic provinces which cannot be exactly defined. Also, the present day morphology of SBI is more typical of the Salt Dome/Minibasin province. The plausible conclusion to this discussion is that the modern morphology of SBI is dictated by secondary mobilization of the salt to the loading of Plio-Pleistocene sediments.

C. Morphology: Salt Body II

Salt Body II (SBII) is located in the southeast quadrant of the study area and covers an area of approximately 66 square miles (Figure 42). The salt is an oblong shaped body that trends northeast to southwest. SBII correlates well with salt bodies mapped by Wu et al (1990a) and Fletcher et al. (1995), Figure 43. Their areas for this salt body were approximately 45 square miles and 81 square miles, respectively. The mean area of their salt bodies is 63 square miles, which closely matches the 66 miles measured in this study, and illustrates the variation in mapping and interpretation that can occur through the use of only widely-spaced, regional 2-dimensional seismic data.

The depth structure map and salt surface rendering (Figure 44) and perspective view (Figure 45) illustrate the topographic character of the top of SBII. The depth to the top of SBII ranges from approximately -7800 ft to -10,800 ft, below sea level (bsl). The isopach map to the top of salt (Figure 46) correspondingly illustrates the thickness distribution of sediments above the salt. Sediment thickness from the mudline to the top

of SBII range between 2200 ft to 5200 ft. Sediments thicken toward a basin in the northeast corner of the salt and thin southwest across a broad salt top.

Two seismic lines (Figures 56 and 57) through SBII illustrate the character of the top of salt as well as display the distribution of sediment above the salt. Unlike SBI, SBII does not have a very thick sediment cover and has only one small, possible salt basin. Differential loading of overburden has caused only minor concave inflection in the top of the salt. Loading remobilization is therefore considered minimal in SBII.

The present morphology of SBII is likely the result of salt emplacement and gravity sliding like that proposed by Wu et al. (1990a) in Figure 29 where the palipinastic reconstruction illustrates a phase of vertical, shallow emplacement of salt above regional dip followed by gravitational collapse at the rear of the salt and seaward horizontal extension via gravity sliding at the salt front. Wu et al.'s palipinastic construction was derived from a seismic line that dissects SBII. Thus, the salt modeled by Wu et al. is SBII.

Palipinastic reconstructions for this area by Schuster (1995) in Figure 55 and Wu et al. (1990a) in Figure 29 show the feeder stock for the ridge was probably emplaced in during Miocene and evolved toward an end-member geometry during the Pliocene-Pleistocene. Reduction of the salt supply from the feeder stock (evidenced by subsidence at the northern extent of the salt), coupled with shallow emplacement of the salt above the regional dip and the force of gravity, a horizontal component of movement initiated during the mid-Pliocene to Pleistocene. Further reduction of the feeder stock has caused subsidence above the feeder (probably along the northern limit

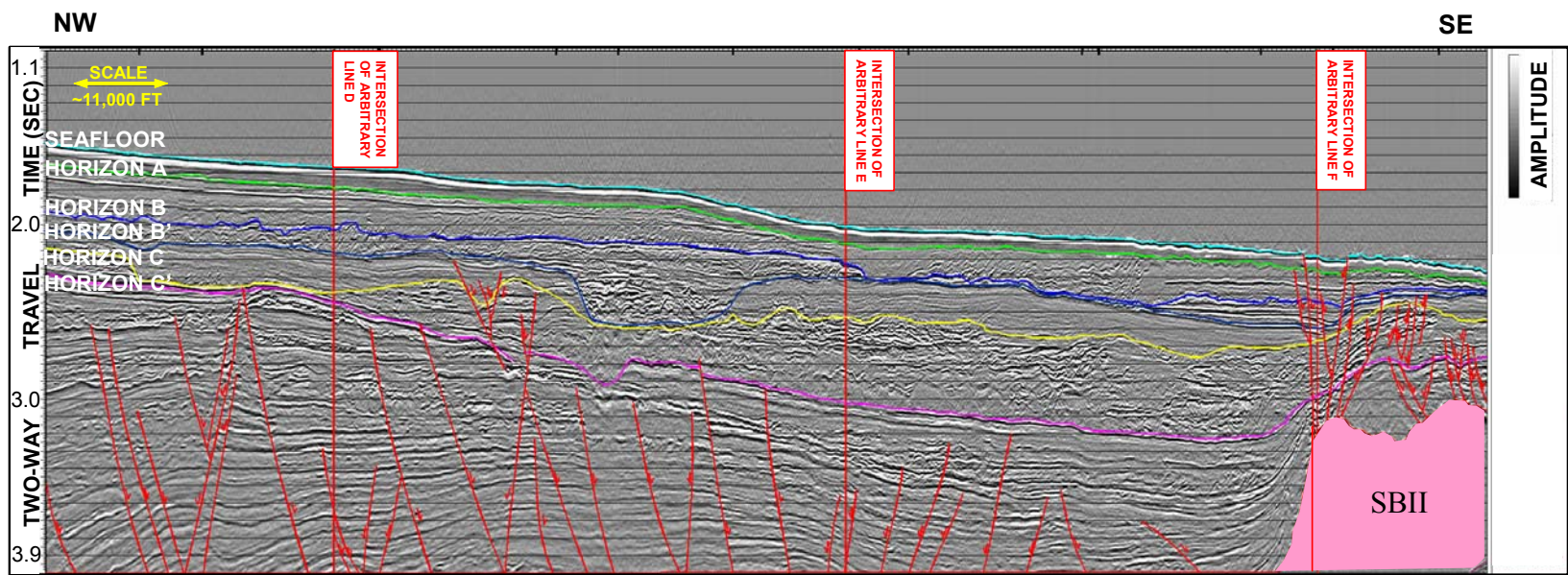


Figure 56. Arbitrary Seismic Line B illustrating the character of SBII. Pink shaded area denotes salt. Colored lines denote mapped horizons. Red lines denote faults.

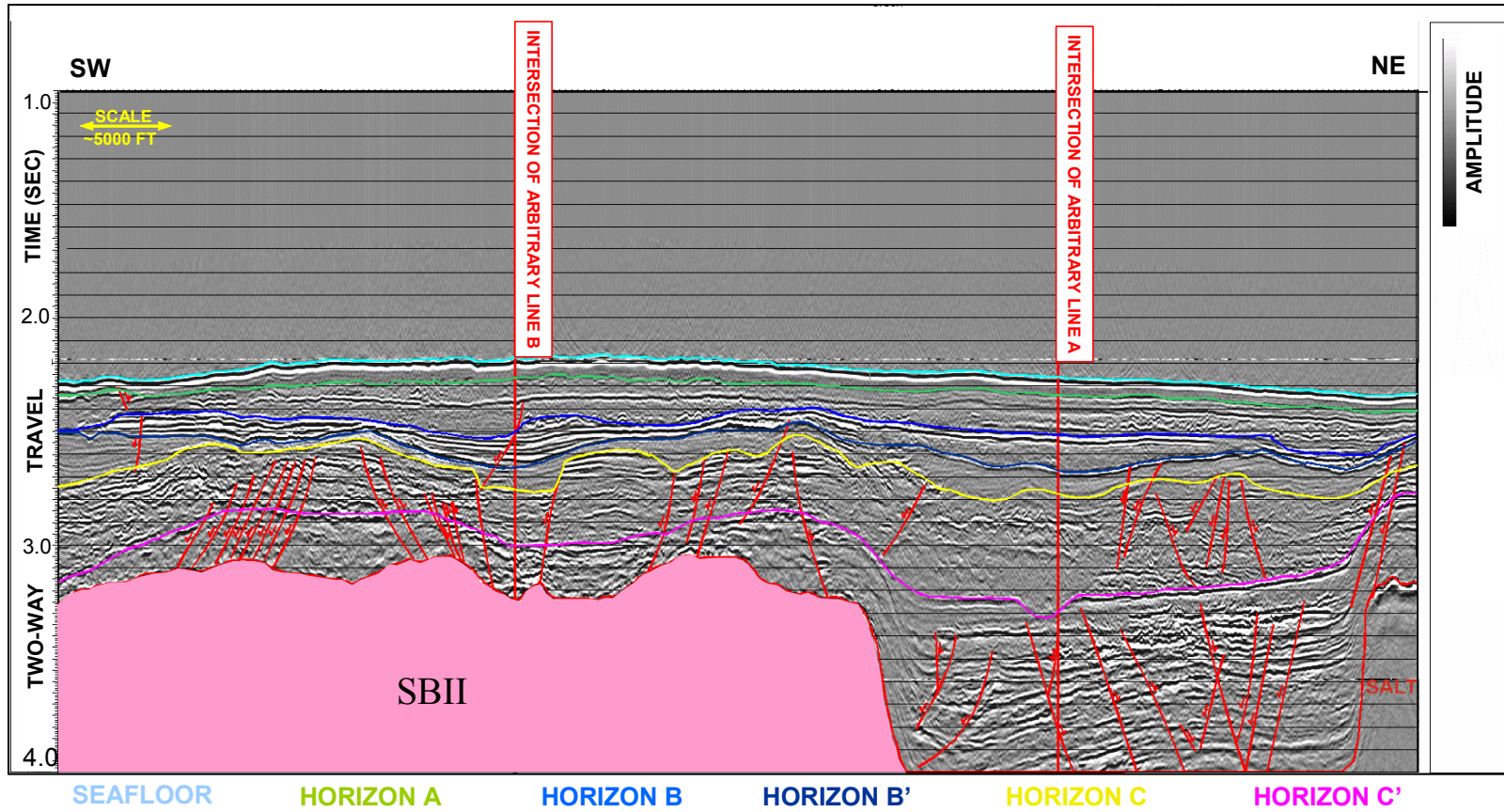


Figure 57. Arbitrary Seismic Line F illustrating the character of SBII. Pink shaded area denotes salt. Colored lines denote mapped horizons. Red lines denote faults.

of the salt) in Figure 56. This subsidence may still be occurring today, albeit at a slower rate, as extensional normal faults pierce the seafloor above the structure (Figure 57).

SBII could be considered a salt plug if the feeder stock has been completely pinched off. This is illustrated in Figure 54 where SBII has the same geometry as the southernmost salt plug in Figure 54. The morphology of SBII suggests the salt body has been detached from its feeder stock (Figure 54). Given the location of SBI relative to SBII in Figure 54, it is unlikely that the two salts are part of the same Roho end-member system. Rather, SBII may be a separate salt body not related to SBI. SBII was probably originally emplaced as a vertical, northeast to southwest trending salt ridge that formed along the seaward normal fault within an end-member system. A ridge rather than a dome is hypothesized because of the linear nature of northern limit of the salt body. The strike of regional extension (strike of basinward end-member fault) is parallel to the strike of the northern limit of the salt. The salt would have migrated up the fault forming a ridge that subsequently has undergone horizontal extension and gravity sliding as previously explained above.

SBII is part of the tabular salt minibasin province (Diegel, 1995) composed of allochthonous or "tabular" salt tongues (Figure 54). Diegel uses "tabular" to refer to laterally extensive salt bodies with flat tops. Liro (1989) posits that shallow salt tongues are sourced from updip, domed features (although SBII is a ridge) with lateral salt motion appearing to be only tens of miles or kilometers. SBII is interpreted to be in the moderate stage of allochthonous salt body formation and early-stages of tabular salt

formation. If SBII is not in equilibrium at present, it is expected the lateral extension of salt will continue seaward due to gravity sliding.

D. Salt Morphology: Salt Body III

Salt Body III (SBIII) is located in the southwest corner of the study area and covers an area of approximately 28 square miles. SBIII is probably a small, allochthonous salt body that is part of a large salt canopy covering most of the southwestern Mississippi Canyon area (Figure 43). This larger canopy has an aerial extent of approximately 2720 square miles.

The depth-structure map salt surface rendering (Figure 44) illustrates the shallow character of SBIII. Figure 45 is a perspective view of the salt. The depth to the top of SBIII ranges from approximately -8000 ft to 10,800 ft, bsl. The isopach map to the top of salt (Figure 46) correspondingly illustrates thickness distribution of sediments above the salt. Sediment thickness from the mudline to the top of SBIII ranges between 3200 ft to 5200 ft. Sediments thicken north from the salt front into a small, east-west trending, shallow basin in the center of the salt.

Figure 58 is a seismic line illustrating the character of the salt top as well as highlighting the sediment above the salt. There is evidence that SBIII has undergone

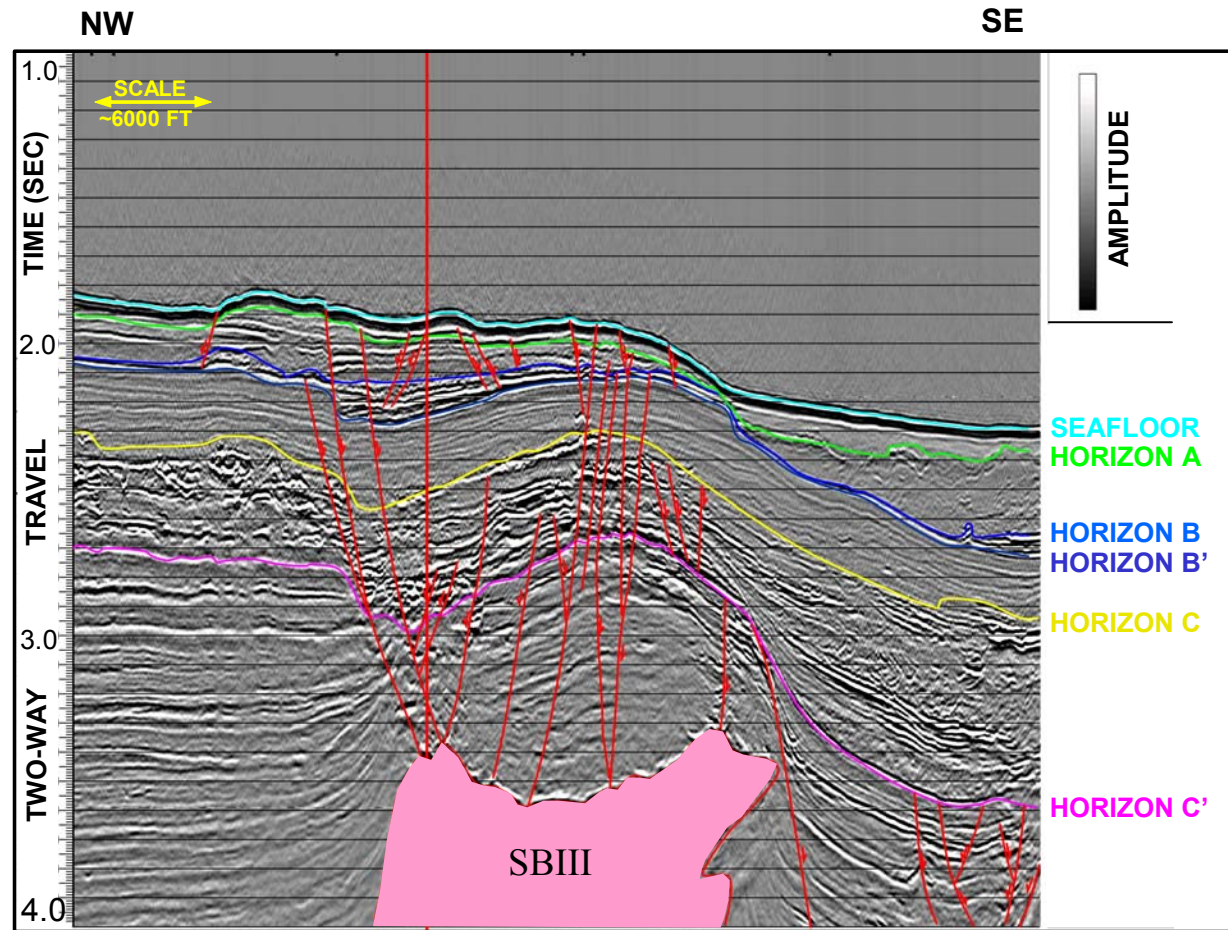


Figure 58. Arbitrary Seismic Line C illustrating the character of SBIII. Pink shaded area denotes salt. Colored lines denote mapped horizons. Red lines denote faults.

differential loading with sediments causing the concave down-warping of salt in the center of the salt. Differential remobilization is therefore considered an influence on the present day morphology of the salt top as the salt volume is locally remolded to accommodate the focused load of the overburden.

SBIII is part of the tabular salt minibasin province (Diegel, 1995) described for SB II. It is also part of the Canopy I salt complex proposed by Peel et al. (1995), Figure 59. Canopy I is a large salt body that partly overlies the Mississippi Fan foldbelt (well south of the study area). The canopy initiated in the Middle Miocene and continued spreading into the late Miocene. Figure 59 also shows the location and reconstruction of a regional seismic line through Canopy I (Peel et al., 1995). The Cenozoic of the upper slope (likely to extend eastward to the study area) is primarily composed of salt stocks and small isolated salt sheets. The morphology of SBIII corresponds to the isolated salt stock in the middle of the reconstruction (Figure 59). SBIII is either a secondary or an isolated salt stock originally derived from Canopy I. This segmentation from the canopy could explain emplacement followed by differential loading and collapse. The concave top of salt coupled with extensional, normal faults that pierce the seafloor (Figure 58) support the theory that the salt body is currently undergoing collapse with SBIII's feeder stock either fully depleted or cutoff. It is plausible that Cenozoic sedimentation along the eastern periphery of Canopy I caused salt withdrawal and formation of isolated salt stocks similar to the isolated salt stocks of Canopy I on the central Louisiana upper slope (Figure 59). It is likely these salt stocks (or sheets) have been permanently segmented

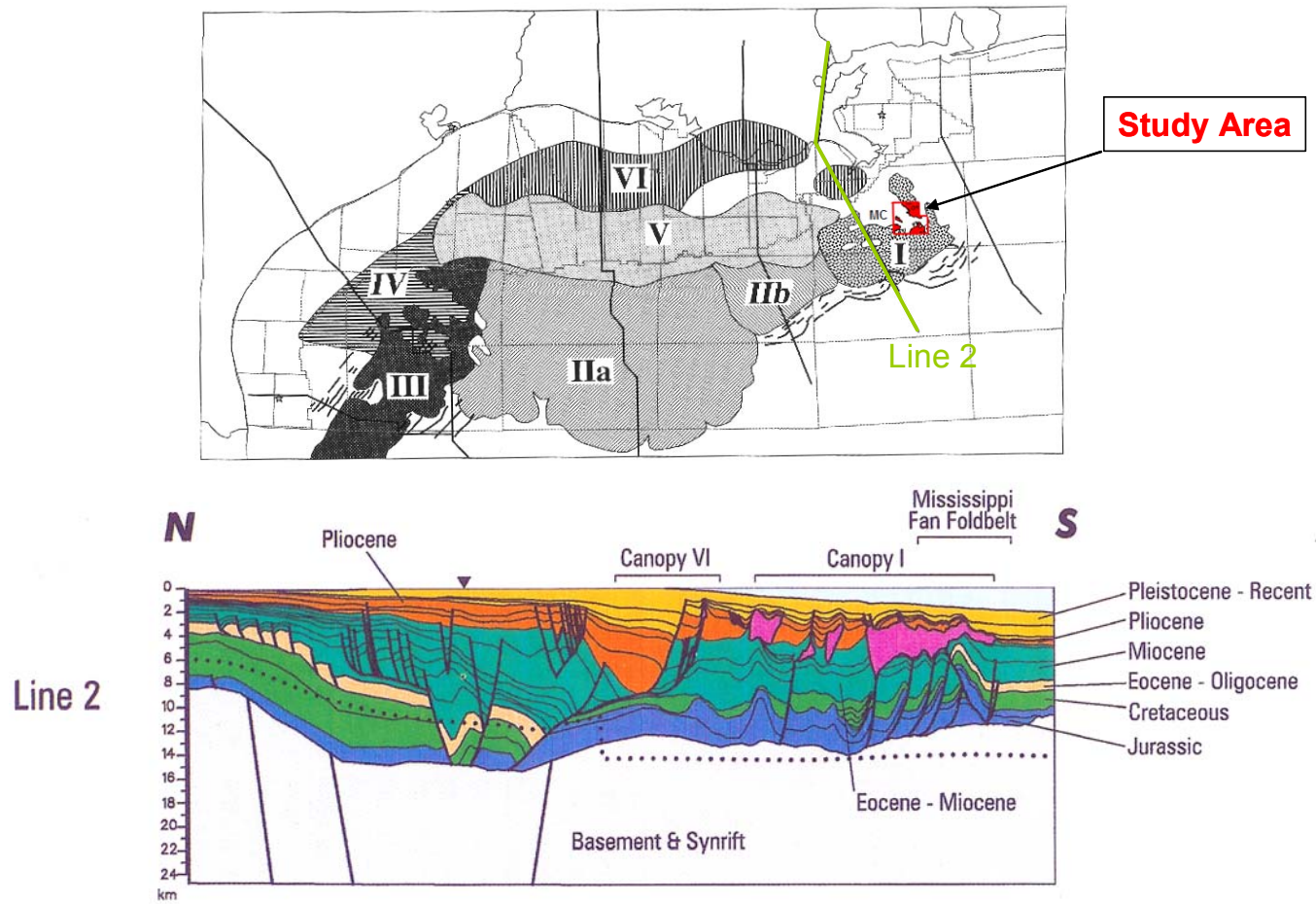


Figure 59. Reconstruction of regional seismic line through Canopy I (Peel et al., 1995). SBIII is posited to have originally been part of Canopy I but has subsequently been separated from the rest of the salt mass.

from Canopy I with as sediment/sediment suture lying somewhere below the extent of the data used in this study.

There also appears to be a rotational component of the block of sediment directly above SBIII (Figure 58). Sediments become rotated and remolded as the salt moves moves out from underneath the overburden to accommodate the overburden load. This remolding of the salt volume provides accommodation space into which the overburden can sink, commonly rotating, tilting, or remolding the stratigraphy of the overburden. The location of the salt within the stratigraphic sequence, coupled with the age and position of strata in the regional reconstruction by Peel et al. (1995) in Figure 59, suggests emplacement during the very late Miocene or early Pliocene followed by remobilization and segmentation from Canopy I during the Plio-Pleistocene.

E. Salt Morphology: Salt Body IV

Salt Body IV (SBIV) is located along the central-western perimeter of the study area and covers an area of approximately 12 square miles. Figure 43 illustrates SBIV in relation to the salt previously mapped by Fletcher (1995) and Wu (1990a). The depth structure map and salt surface rendering (Figure 44) illustrates the character of SBIV. SBIV is shown in perspective view in Figure 45. The depth to the top of SBIV ranges from approximately -7000 ft to -11,400 ft. The isopach map to the top of SBIV (Figure 46) correspondingly illustrates thickness distribution of sediments above the salt.

Sediment thickness from the mudline to the top of SBIV range between 2600 ft and 7000 ft. Sediments thicken off the northern flank of the salt.

Figure 60 has composite arbitrary seismic lines illustrating the character of the salt top as well as highlighting the sediment above the salt. SBIV is essentially a relatively thin, vertical, northwest to southeast trending, salt spire. There is no evidence of differential loading or remobilization affecting the top of SBIV.

SBIV is part of the tabular salt minibasin province (Diegel, 1995) described for SBII. It also may be considered part of the Canopy I salt complex proposed by Peel et al. (1995), discussed for SBIII (Figure 59). Minimal uplift and offlap of thin, overlying sediments (Figure 60) may suggest the structure was emplaced later than SBIII. This would support the theory that SBIV is a younger structure than SBIII and may possibly be the youngest structure in the study area. Findings by Wu et al. (1990a) support this theory. His work concluded that salt structures are first vertically emplaced due to differential loading and then flow laterally via gravity sliding. The fact that SBIV is the only salt body with a purely vertical component (lacking evidence of horizontal movement) component supports this "younger" theory in that SBIV is an immature structure that has not evolved to the point where it is undergoing evident collapse or gravity gliding (horizontal component). If the salt body is indeed the latest to be emplaced in the study area, it is quite plausible that this emplacement occurring sometime during the Pleistocene as there is very little uplift or deformation of the late Pleistocene stratigraphy. SBIV may still be attached to its feeder stock as there are no

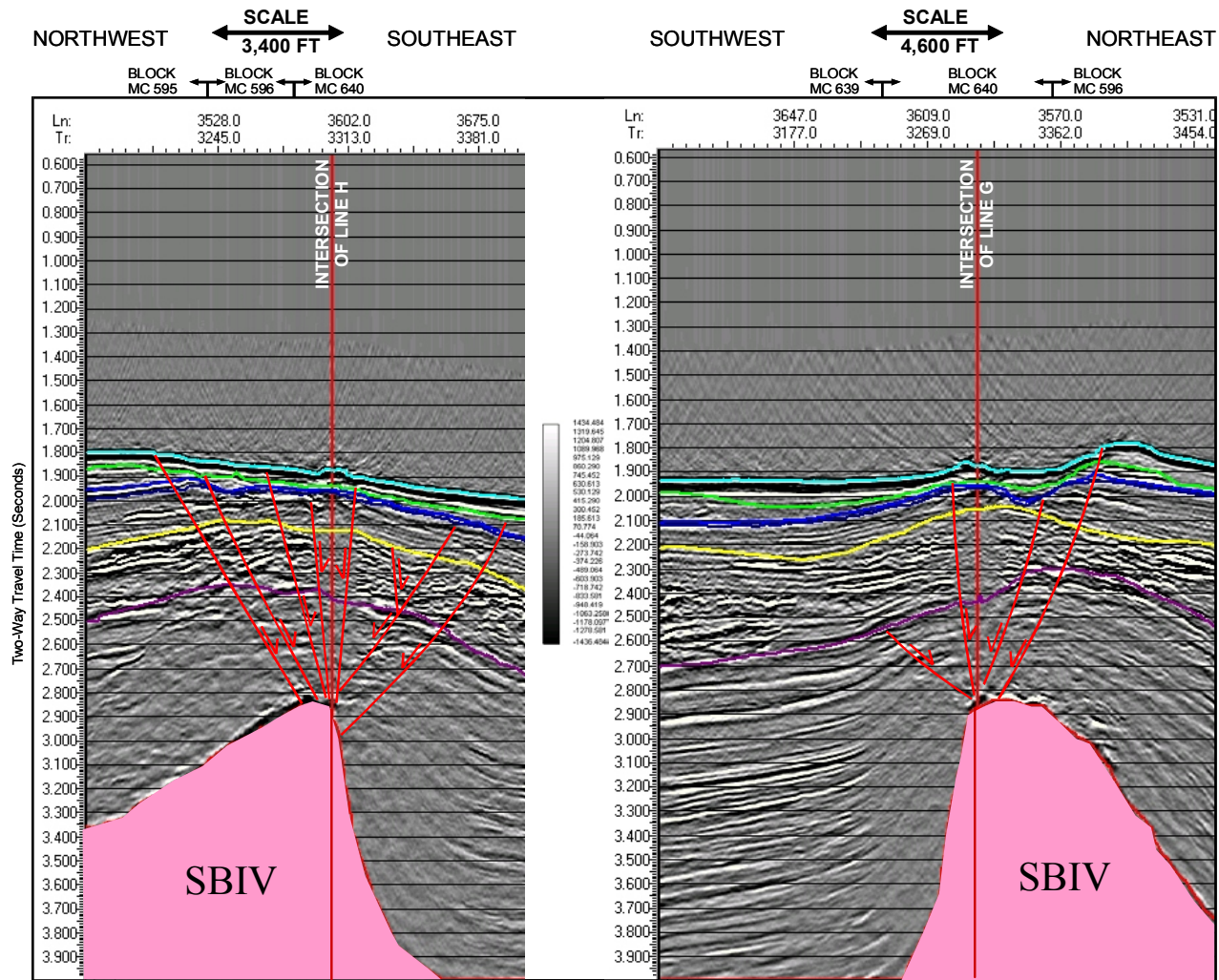


Figure 60. Composite arbitrary seismic lines illustrating the character of SBIV. Pink shaded area denotes salt. Colored lines denote mapped horizons. Red lines denote faults.

signs of collapse or withdrawal that are normally associated with depletion of or disconnection from the feeder stock.

F. Salt Basin Types

The movement of salt and subsequent interaction with sediments has resulted in the formation of two different types of basins identified in the study area. These basins are defined in this study as Type I Basins (TI) and Type II Basins (TII).

Type I Basins (BI) are identified as deep basins present between the salt bodies (SBI-SBIV) identified in the study area. The basins are commonly deeper than the 4.00 second time-depth cutoff of the data. TI basins contain thick accumulations of sediments and are floored by either very thin salt or a salt weld. This is plausible and derived from the previous discussion of the salt tectonic end-member geometry of the salt in the study area where salt is fully mobilized into shallow salt bodies with little to no salt left in the basin behind the salt front (see Figure 52 and 54). The salt once flooring the basin has evacuated under loading to form the diapirs, ridges, and/or sills that fringe the basin. Figure 61 illustrates a seismic section typical of the Type I basins from the seismic data in the study area. Figure 62 is a deeper seismic section from Schuster (1995) and illustrates the full morphology of the Type I basins below the 4.00 seconds of seismic data. Note the very thin, nearly depleted salt that floors the basin.

The sediments in a TI basin are generally parallel to semi-parallel and continuous in the basins. Local variations in the seismic reflections in these sediments probably

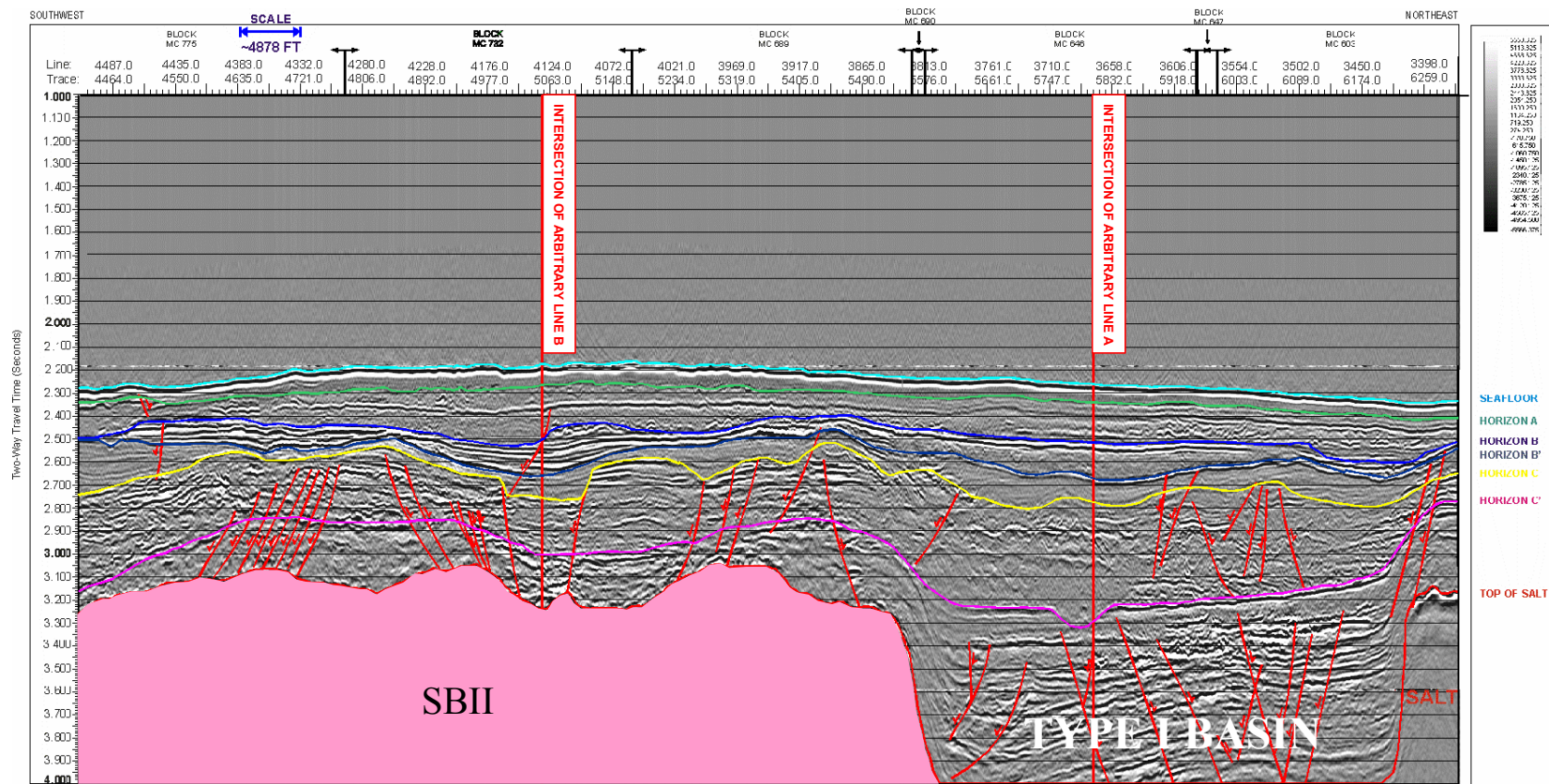


Figure 61. Arbitrary Seismic Line F illustrating typical Type I basin in the study area. Pink shaded area denotes salt. Colored lines denote mapped horizons. Red lines denote faults. Note depth of basin with respect to thickness of strata overlying salt.

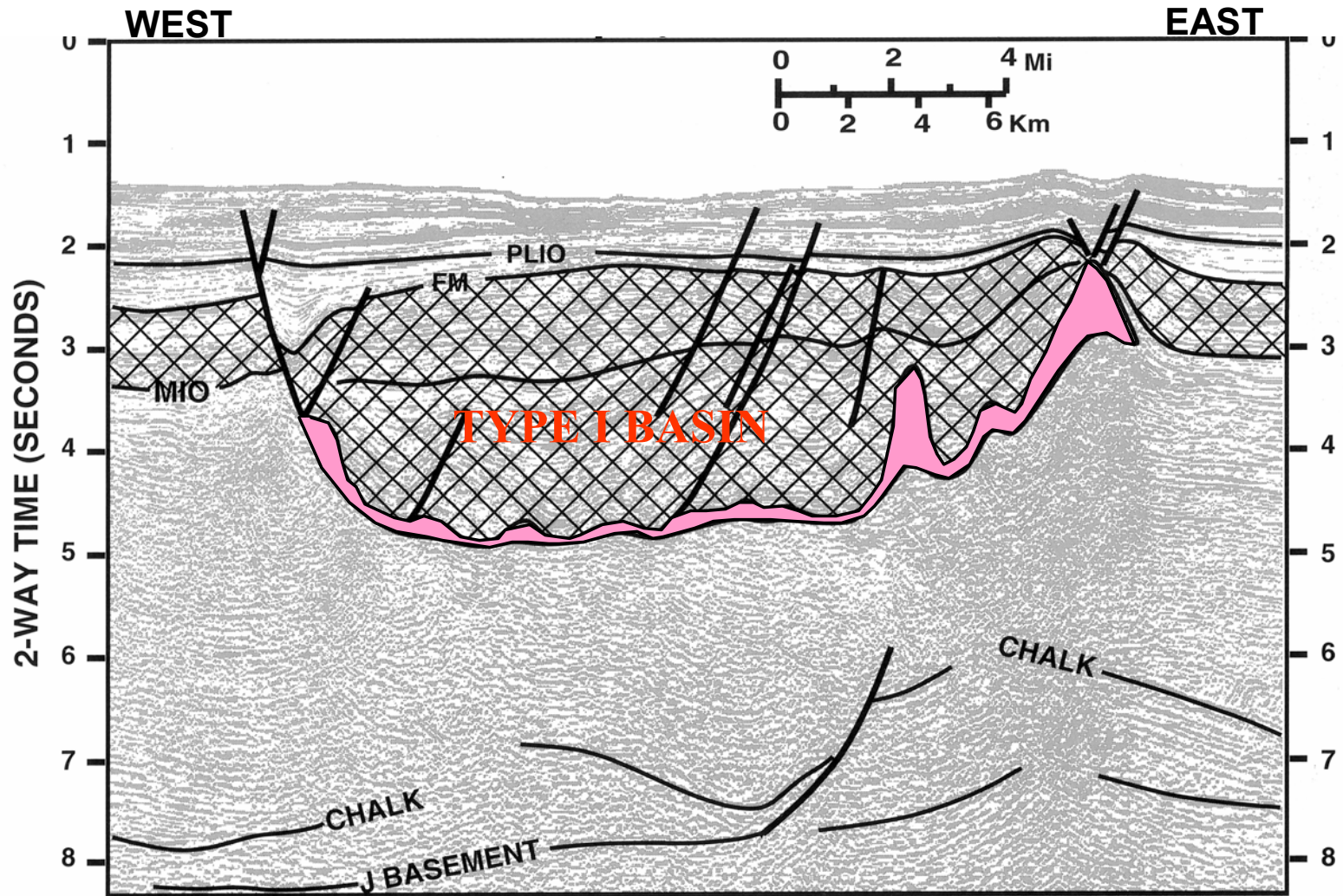


Figure 62. Deeper seismic section illustrating full morphology of a Type I basin (Schuster, 1995). Note the very thin salt (pink) that floors the basin

represent different types of stratigraphic facies deposition. TI basin sediments show displacements due to faulting which is probably associated with extension resulting from lateral movement of salt that flooded the basin as it evacuated. The evacuation of salt would have created accommodation space for the overlying stratigraphic section, expressing itself through extension and normal faulting as the section subsided. The edge of TI basins exhibit steep uplift or truncations of strata against shallow salt bodies present in the area (SBI-SBIV). TI basins may in fact be regional, end-member expressions of original suprasalt basins discussed in the following segment.

Type II basins (TII) are identified as suprasalt basins. TII basins exist entirely on top of shallow salt in the study area. (Spindler, 1977) proposed that subsidence of sediments into shallow salt masses is the major mechanism for basin formation on the northern Gulf of Mexico continental slope. Figure 63 illustrates his model for suprasalt basin formation. In this model, pre-existing lows on the salt surface allow for the local accumulation of sediments. Nelson and Fairchild (1989), who indicated that the topography of an allochthonous salt tongue was a factor in the remobilization and formation of secondary salt structures (and thus basins), also suggested this premise. Once small, local basins are established on top of the salt, continued sedimentation produces differential loading. This differential loading causes the salt to subside and be squeezed into areas of thinner sediments forming deep, suprasalt basins rimmed by steep walls of salt. Once a basin is formed, active mass-transport events may preferentially be deposited in these basins with deposition bypassing the basin rims. Basin rims themselves may become over steepened as

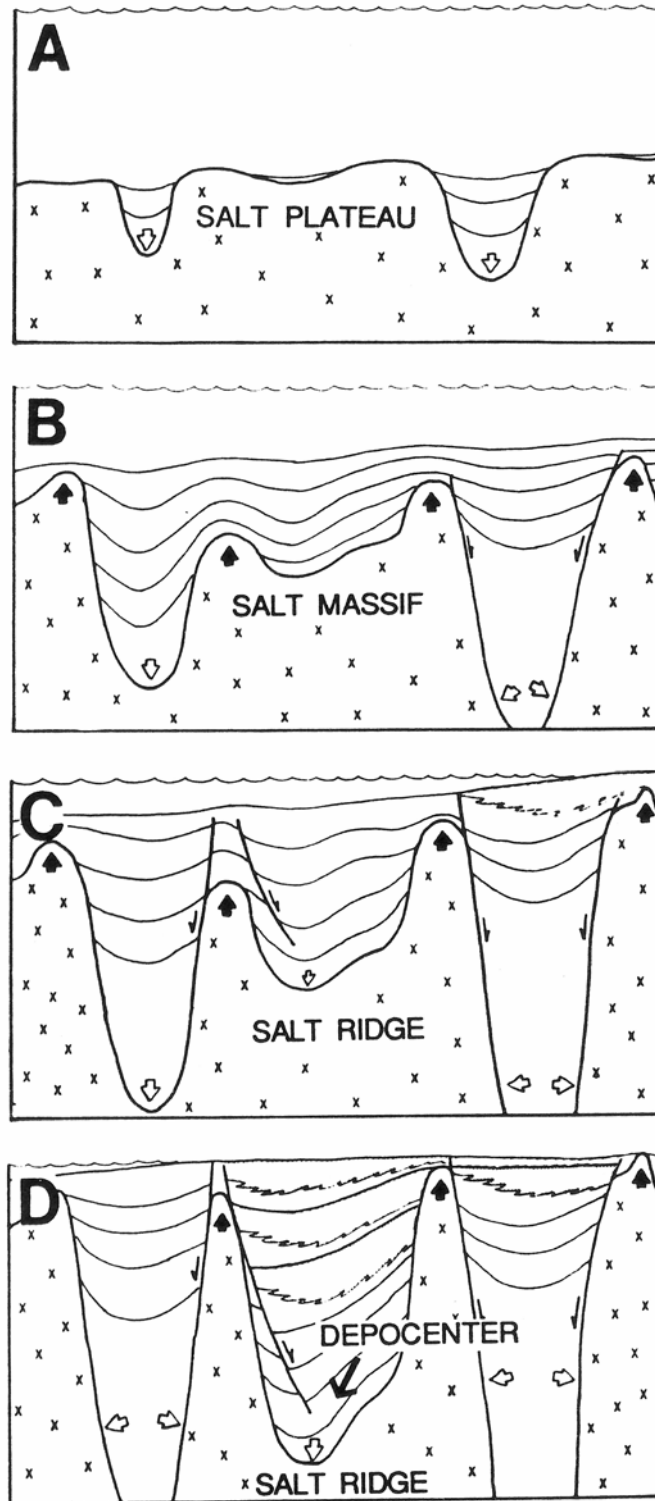


Figure 63. Spindler's model for suprasalt basin formation (Spindler, 1977). Section evolves from A to D.

the basins subside resulting in slope failures adding to the stratigraphic sequence in the basins. The interaction of the rate of subsidence (directly associated with deposition) with the rate of secondary salt inflation has an impact on the overall basin structure. (Apps et al., 1994) propose that, for a given amount of time, if the rate of growth of the structure is faster than sedimentation, the seabed topography amplifies with time. If the rate of sedimentation is faster than structure growth then the topography will be drowned by the stratigraphy. Any single basin may undergo different amounts of surface expression at different times thus affecting the rate at which basin formation and surrounding structures occur.

Figures 64, 65, 66, and 67 are seismic lines illustrating the nature of TII basins in the study area. Subtle to steep walls of salt flank these mini-basins. The sediments within the basin are bowed down as the basin gets deeper. In some cases sediments within the basin have been rotated and greatly deformed in adjustment to the underlying withdrawal of salt. The morphology of basins within each individual salt body is indicative of its state of development. If allowed to continue, these basins would likely continue to deepen, eventually driving out the salt and becoming end-member Type I basins.

The distribution of TII basins identified in the study area is presented in Figure 68. The greatest concentration of TII basins is associated with SBI. These basins are well developed and in some places are deeper than the 4.00 second time-depth cutoff of the data (Figure 64). Sediments within these deeper basins are more deformed and bowed down than in other TII basins present in the study area. It is hypothesized that

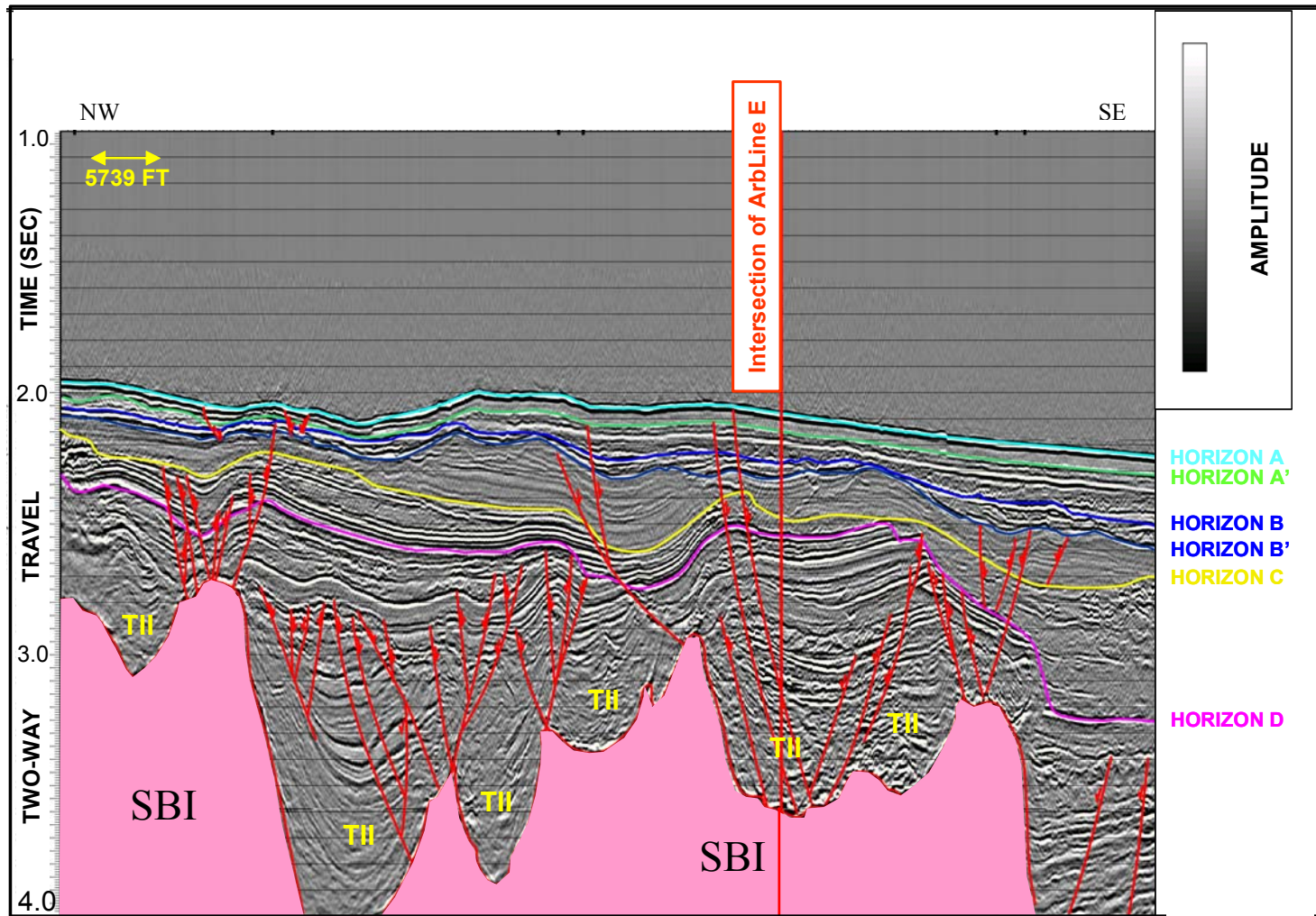


Figure 64. Arbitrary Seismic Line A illustrating the character of the Type II basins above SBI. TII annotation denotes location of Type II basin. Pink shaded area denotes salt. Colored lines denote mapped horizons. Red lines denote faults. .

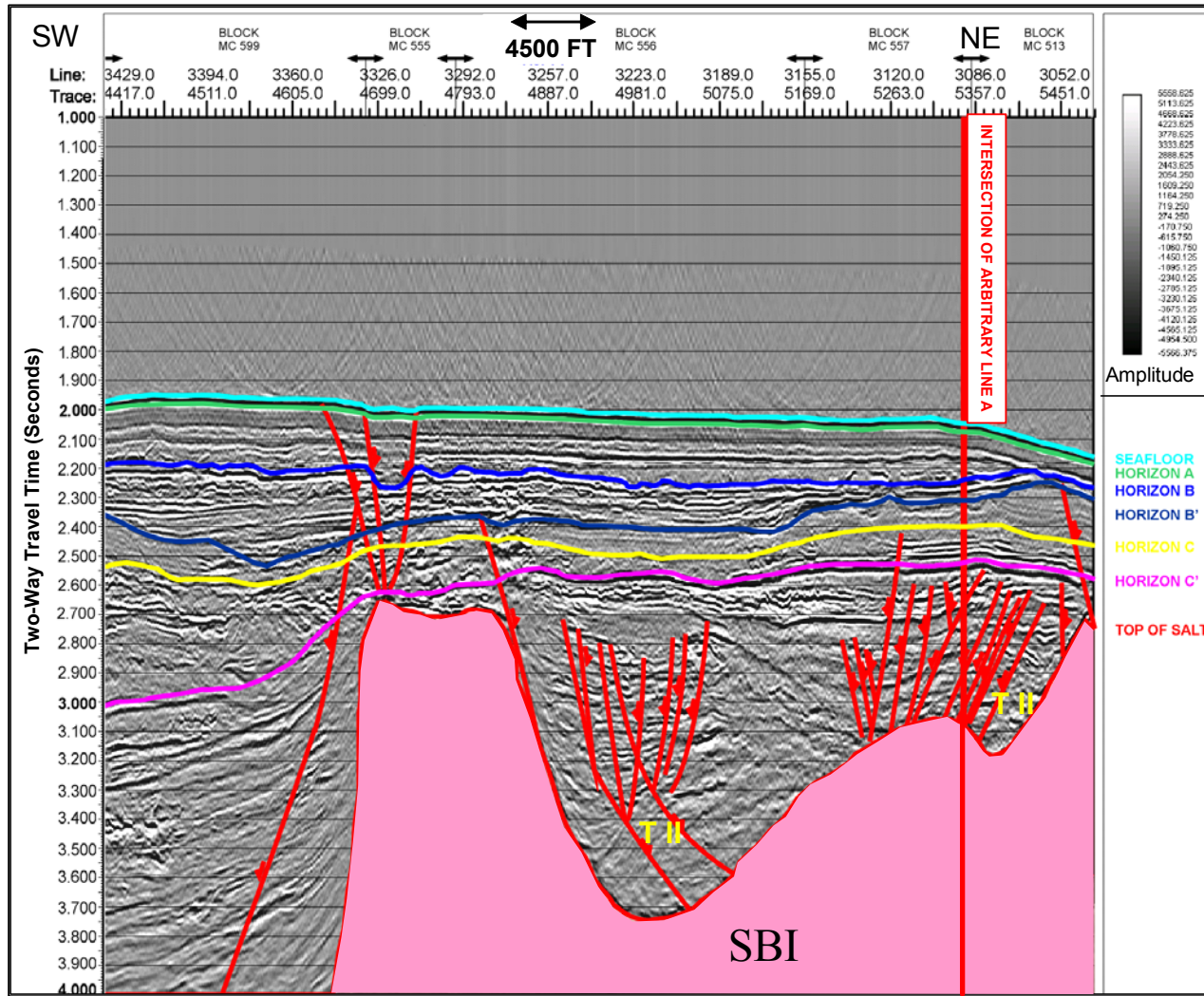


Figure 65. Arbitrary Seismic Line E illustrating the character of the Type II basins above SBI. TII annotation denotes location of Type II basin. Pink shaded area denotes salt. Colored lines denote mapped horizons. Red lines denote faults.

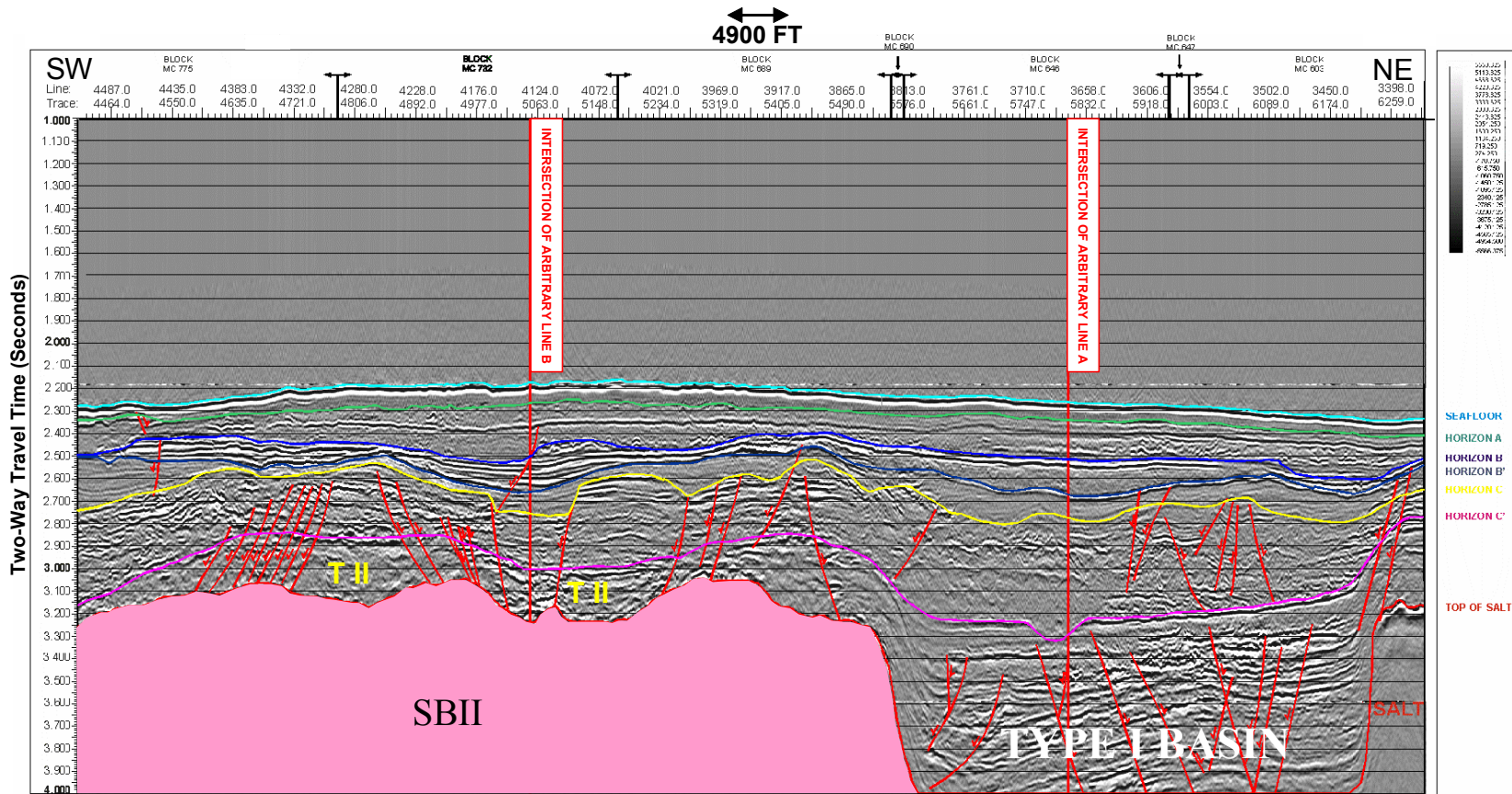


Figure 66. Arbitrary Seismic Line F illustrating the character of the Type II basins above SBII. TII annotation denotes location of Type II basin. Pink shaded area denotes salt. Colored lines denote mapped horizons. Red lines denote faults.

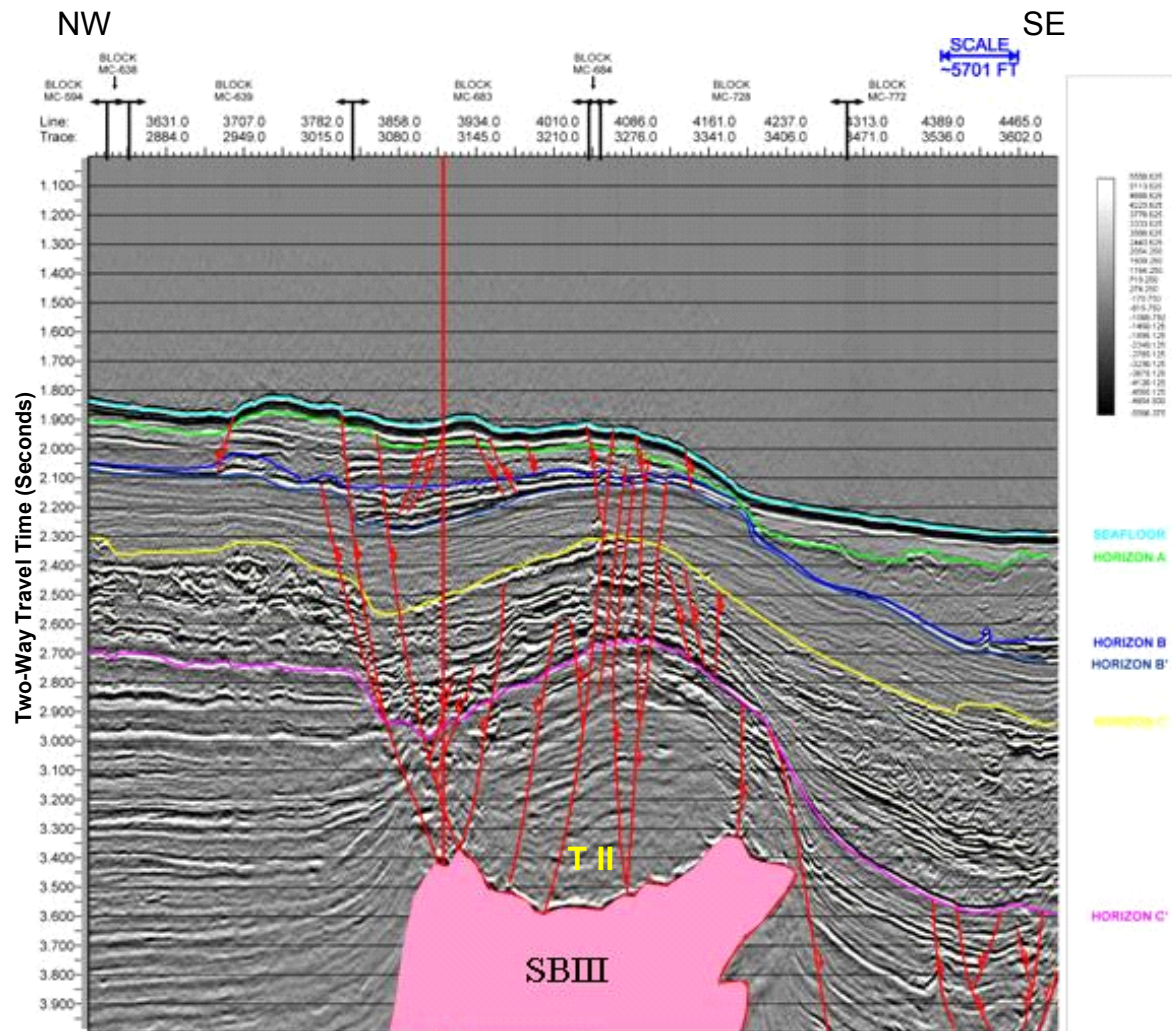


Figure 67. Arbitrary Seismic Line C illustrating the character of the Type II basin above SBIII. TII annotation denotes location of Type II basin. Pink shaded area denotes salt. Colored lines denote mapped horizons. Red lines denote faults.

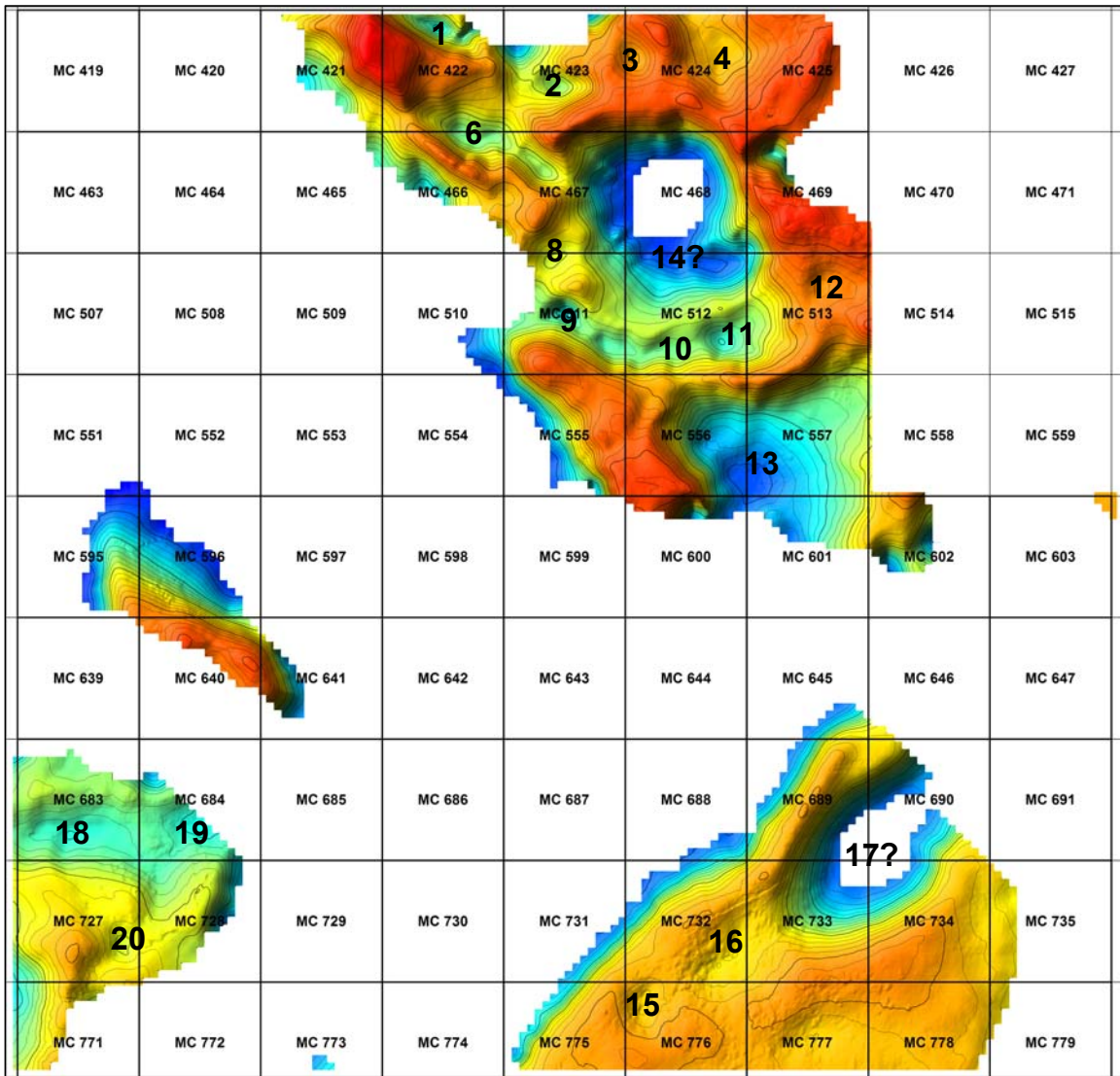


Figure 68. Identified Type II suprasalt basins in the study area. Image is structure map of top of salt (sea surface to top of salt). Numbers indicate Type II basins identified on the salt surfaces.

the basins associated with the SBI are the most mature TII basins in the study area. TII basins are also associated with SBII and SBIII. These basins are shallow with thin sediment accumulations. Figure 65 illustrates the nature of the basin above SBII. The sediment affected by basin formation is relatively thin but appear to be moderately deformed. Figure 67 illustrates the nature of the basin above SBIII. This is a very shallow basin and is only designated as such by the concave nature of the salt top. Only a thin section of sediment seems to have bowed down into this basin. These sediments may actually be deformed because of a rotational component resulting from initial salt subsidence and evident by numerous extensional faults on the up-dip side of SBIII. The shallow character of the basins above SBII and SBIII, coupled with thin sediment cover and little or no structural deformation of the stratigraphic section above, indicates these are immature TII basins. SBIV is a vertical salt spire and thus has no associated TII basins.

CHAPTER V

SEISMIC STRATIGRAPHY

Seismic Sequence Definition

Advances in the acquisition and analysis of digital seismic data have allowed for the high-resolution study of seismic stratigraphy. Seismic stratigraphy can be defined as the study of stratigraphy and depositional facies interpreted from seismic data (Mitchum and Vail, 1977). The depositional sequence is an objectively defined stratigraphic unit composed of genetically related strata and bounded by unconformities and their correlative conformities (Mitchum et al., 1977). Seismic facies are groups of reflections, within a sequence, whose parameters differ from adjacent groups (Mitchum et al., 1977). These parameters include (1) reflector continuity, (2) reflector amplitude, (3) geometric relations between reflectors, (4) overall reflector form, and (5) three-dimensional associations of groups of reflections (Stuart and Caughey, 1977). The identification of seismic facies allows for the interpretation of sedimentary processes and depositional environment allowing for the formation of a depositional model for a given area of study.

Exhaustive work on the fundamentals and tools of seismic stratigraphy have been carried out by numerous studies. (Mitchum and Vail, 1977; Ramsayer, 1979; Sangree and Widmier, 1977; Stuart and Caughey, 1977; Vail, 1987; Vail and Mitchum, 1977; Vail and

Wornhardt, 1991; Vail and Wornhardt, 1990; Van Wagoner et al., 1987; Wornhardt and Vail, 1990). Others studies (Beard et al., 1982; Bouma, 1981; Bouma and Stelting, 1984; Walters, 1985) have undertaken further modifications in the application of seismic stratigraphy related to eustatic sea level change to the geology of the northern Gulf of Mexico. Weimer (1989, 1990) and Dixon and Weimer (1994, 1998) conducted an in depth analysis of the seismic sequence stratigraphy of the Mississippi Fan Complex (Western and Eastern Fan) using a modification of the seismic stratigraphic tools defined by the aforementioned authors (Table 1). Recently, the Gulf of Mexico Basin Depositional Synthesis conducted by Galloway and Buffler (2004) produced a seismic stratigraphic facies identification chart for the deep Gulf of Mexico basin (Table 2). The works by Weimer, Dixon and Weimer, and Galloway and Buffler form the basis for the identification and interpretation of the seismic stratigraphic sequences and component facies in the study area.

Traditionally, stratigraphic sequences and facies were identified and correlated by the nature of their reflectors on a line by line basis. However, it was not possible to quantitatively analyze the attributes of those reflectors from line to line. With the advent of digital, 3-D multifold seismic data, it is now possible to view seismic data in a three-dimensional cube, or volume. The ability to analyze the attribute of a volume of seismic data has opened a new avenue of seismic stratigraphic facies interpretation. The presence of different facies within a stratigraphic sequence can be further defined using Volumetric Seismic Amplitude Analysis (VSAA). In general, this analysis provides a "snapshot" of the entire stratigraphic sequence, based on a seismic attribute, allowing

Table 1. Previously derived definitions of seismic stratigraphy (Weimer, 1989).

Depositional Environment	External Form	Reflection Configuration	Amplitude	Continuity	Lateral Distribution	Nature of Lower Boundary
Channels	Lens, sheet, fill	Subparallel, to slightly hummocky in the upper fan	High, becoming low to moderate vertically	Fair	Narrow, linear, sinuous downfan	Erosive upfan, becoming conformable downfan
Levees	Wedge	Subparallel to slightly divergent toward channel	Low to fair, sometimes higher at base	Moderate to fair, becoming fair farther from channel	Parallel the channels, high depositional relief upfan, to low relief downfan	Generally conformable local downlap
Overbank	Sheet	Subparallel, with interbedded hummocky and mounded	Low to fair, locally higher	Fair, locally poor	Areally widespread away from channel	Generally conformable, local downlap
Basinal, unchannelized (lobe?)	Sheet	Subparallel, occasional hummocky and mounded	Low to moderate, generally fair	Fair to moderate	Widespread	Conformable, local downlap
Mass transport complex	Mound	Mounded, hummocky subparallel	Generally low to fair, locally moderate to high	Poor, occasionally fair	Upfan: underlies and subparallel to channel; downfan; fan shaped becoming wider downfan	Lower erosive upfan becoming downlapping or conformable downfan
Debris apron	Mound, wedge	Hummocky, mounded, chaotic, reflection free, subparallel	Generally low to fair; locally high	Fair to poor	Areally limited	Erosive upfan: locally conformable
Deformed levee-overbank	Wedge	Mounded, hummocky	Generally low to fair	Poor to fair	Areally limited	Downlap

Table 2. Gulf of Mexico Basin Depositional Synthesis seismic stratigraphic facies identification chart (Galloway and Buffler, 2004).



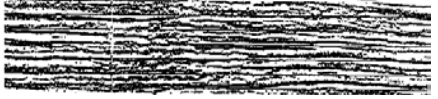

SESIMIC FACIES EXAMPLES	SESIMIC FACIES	SESIMIC FACIES DESCRIPTION	GEOLOGIC INTERPRETATION	OCCURENCE IN DEEP BASIN	DEPOSYSTEMS
<p style="text-align: center;">CHAOTIC</p> 	Chaotic	Disorganized, discontinuous, high or low amplitude reflections with mounded external configuration	slump, debris, flow, creep	Along western and northern deep basin margins or on flanks of submarine fans in NE deep basin	fasl slump, debris flow, creep
<p style="text-align: center;">VARIABLE AMPLITUDE, VARIABLE CONTINUITY</p> 	Variable amplitude variable continuity	Lateral variation in both amplitude and continuity within a short distance Wedge shaped external configuration	Channel/overbank- lobe complexes/ mass transport	Mainly in NE deep basin Representing Mississippi Fan sediments	fach channel/overbank- lobe complexes/mass transport
<p style="text-align: center;">SEMI-CONTINUOUS HIGH AMPLITUDE</p> 	Semi-continuous high amplitude	Subparallel, semi-continuous high amplitude reflections Concave-up high amplitude reflections are dominant Wedge shaped external configuration	Sand-rich channel/ lobe complexes /Sandy lobe complexes	Mostly in deep basin and along NE and N deep basin margins. Associated with depocenters	dfach sand-rich channel/lobe complexes
<p style="text-align: center;">SEMI-CONTINUOUS HIGH AMPLITUDE ALTERNATING WITH LOW AMPLITUDE</p> 	Semi-continuous high amplitude alternating with low amplitude	Subparallel, semi-continuous high amplitude reflections alternating with low amplitude reflections Contains concave-up high amplitude reflections Wedge shaped external configuration	Partially channelized turbidite/lobe complexes	Mainly in NE deep basin and along northern margin	dfatl partially channelized turbidite/lobe complexes

Table 2 (Continued).


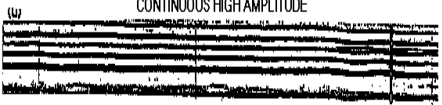


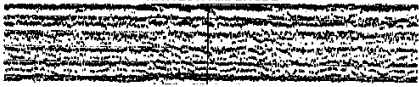

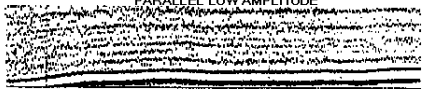
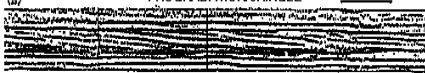
SESIMIC FACIES EXAMPLES	SESIMIC FACIES	SESIMIC FACIES DESCRIPTION	GEOLOGIC INTERPRETATION	OCCURENCE IN DEEP BASIN	DEPOSYSTEMS
	<p>Overlapping mound</p>	<p>Consisting of numerous overlapping mounds, each mound contains concave-up, bi-lateral downlap semi-continuous high amplitude reflections Mound-shaped external configuration</p>	<p>Sand-rich mounded turbidite/lobe complexes</p>	<p>Only in western deep basin and along NW and W deep basin margins Associated with depocenters</p>	<p>dfamtl sand-rich mounded turbidite/lobe complexes</p>
	<p>Continuous high amplitude</p>	<p>Parallel, continuous, high amplitude reflections dominant</p>	<p>Sand-rich sheet turbidites</p>	<p>Along western and northern deep basin margins Often associated with depocenters</p>	<p>dfast sand-rich sheet turbidite</p>
	<p>Divergent variable amplitude</p>	<p>Wedge-shaped in dip view and mounded-shaped in strike view Subparallel variable amplitude reflections</p>	<p>Heterolithic sheet turbidites</p>	<p>Along western and northern deep basin margins Associated with depocenters</p>	<p>dfahst heterolithic sheet turbidites</p>
	<p>Continuous high amplitude alternating with low amplitude</p>	<p>Contains three or more cycles, each cycle is dominated by low amplitude reflections, which is capped by a continuous high amplitude reflection Wedge-shaped external form</p>	<p>Heterolithic sheet turbidites hemipelagic drape</p>	<p>Only in western basin Closely associated with depocenters</p>	<p>bhsthd heterolithic sheet turbidites/hemipelagic drape</p>

Table 2 (Continued).

SESIMIC FACIES EXAMPLES	SESIMIC FACIES	SESIMIC FACIES DESCRIPTION	GEOLOGIC INTERPRETATION	OCCURENCE IN DEEP BASIN	DEPOSYSTEMS
<p>CONTINUOUS VARIABLE AMPLITUDE ALTERNATING WITH LOW AMPLITUDE</p> 	<p>Continuous variable amplitude alternating with low amplitude</p>	<p>Contains three or more cycles, each cycle is dominated by low amplitude reflections, which is capped by a continuous high amplitude reflection Wedge-shaped external form</p>	<p>Mud-rich sheet turbidites and hemipelagic drape</p>	<p>Only in western deepbasin Associated with depocenters</p>	<p>bthd mud-rich sheet turbidites/hemipelagic drape</p>
<p>DIVERGENT LOW AMPLITUDE</p> 	<p>Divergent low amplitude</p>	<p>Subparallel low amplitude reflections Wedge-shaped external form</p>	<p>Mud-rich sheet turbidites</p>	<p>Along western and northern deep basin margins Associated with depocenters</p>	<p>bt mud-rich sheet turbidites</p>
<p>PARALLEL LOW AMPLITUDE</p>  <p>DOUBLE WAVELET</p>	<p>Parallel low amplitude</p>	<p>Parallel, continuous low amplitude reflections One of the dominant facies in deep basin</p>	<p>Mud-rich sheet turbidites</p>	<p>Remote basinal areas Particularly in southern and southeastern deep basin</p>	<p>bt mud-rich sheet turbidites</p>
<p>PROGRADATION/SHINGLE</p> 	<p>Progradation/ shingle</p>	<p>Basinward progradation reflections geometry Change undip and downdip into parallel low amplitude facies</p>	<p>Mud-rich prograding lobes</p>	<p>Only in western deep basin along western margin</p>	<p>bpl mud-rich prograding lobes</p>

for the identification and interpretation of facies within the sequence. This is achieved by analyzing a desired seismic attribute on a trace by trace basis. For example, the Root Mean Square (can) is used to analyze seismic amplitude within a sequence. The RMS is computed for each trace in the sequence as defined by the horizons that bound the sequence. The variation in the value of the RMS represents both the vertical and horizontal variation of the volume of the sequence. This variation correlates to changes in the seismic facies which in turn represents changes in depositional facies and thus processes within the sequence. When coupled with traditional seismic stratigraphic methods, VSAA (such as RMS), provides a powerful tool for the true high-resolution interpretation in 3 dimensions of stratigraphic facies and associated depositional processes and environment for data coverage.

This chapter identifies and discusses the individual seismic sequences and component seismic facies of the study area.

Seismic and Geologic Facies

Seven prominent reflectors or horizons have been mapped in the study area. These horizons were selected to divide the stratigraphy into 6 major stratigraphic sequences. The stratigraphic horizons have been labeled Seafloor, A, B, B', C, C', and Top of Salt in order of increasing depth on the seismic record. The nature of the salt present in the area has been described previously in Chapter III.

The following sections describe and discuss the major seismic stratigraphic sequences. These descriptions also include reference to the RMS VSAA displays used to aid in the identification and interpretation of seismic facies within these sequences. The RMS, or root mean square, displays are an analysis used to represent the relative variance of amplitudes within an envelope (stratigraphic sequence) and are normalized to a positive amplitude spectrum. A further discussion on the definition and application of the RMS is provided in the Appendix. The sequences are numbered in order starting with the deepest sequence and ending with the shallowest sequence.

A. Sequence I: Horizon C' to Top of Salt/4.00 Seconds

Sequence I is present throughout the study area (Figures 69 and 70). The sequence has been mapped from Horizon C' to the top of salt or the bottom of the data at 4.00 seconds. The top of the sequence, Horizon C', lies between 5000 ft and 9600 ft below the sea surface (structure map, Figure 69) and 600 ft to 4000 ft below the seafloor (isopach map, Figure 70). The deepest and thickest parts of the sequence are located in basins between the salt bodies present in the study area. The shallowest and thinnest parts of the sequence occur on top of these salt bodies.

Sequence I contains six seismic and geologic facies. These facies are shown in Table 3. Seismic examples illustrating these facies are presented in Figures 71 and 72. Facies 1 occurs in the suprasalt basins present in the study area. It is seismically recognized as variable amplitude, inclined and divergent reflectors. These reflectors are

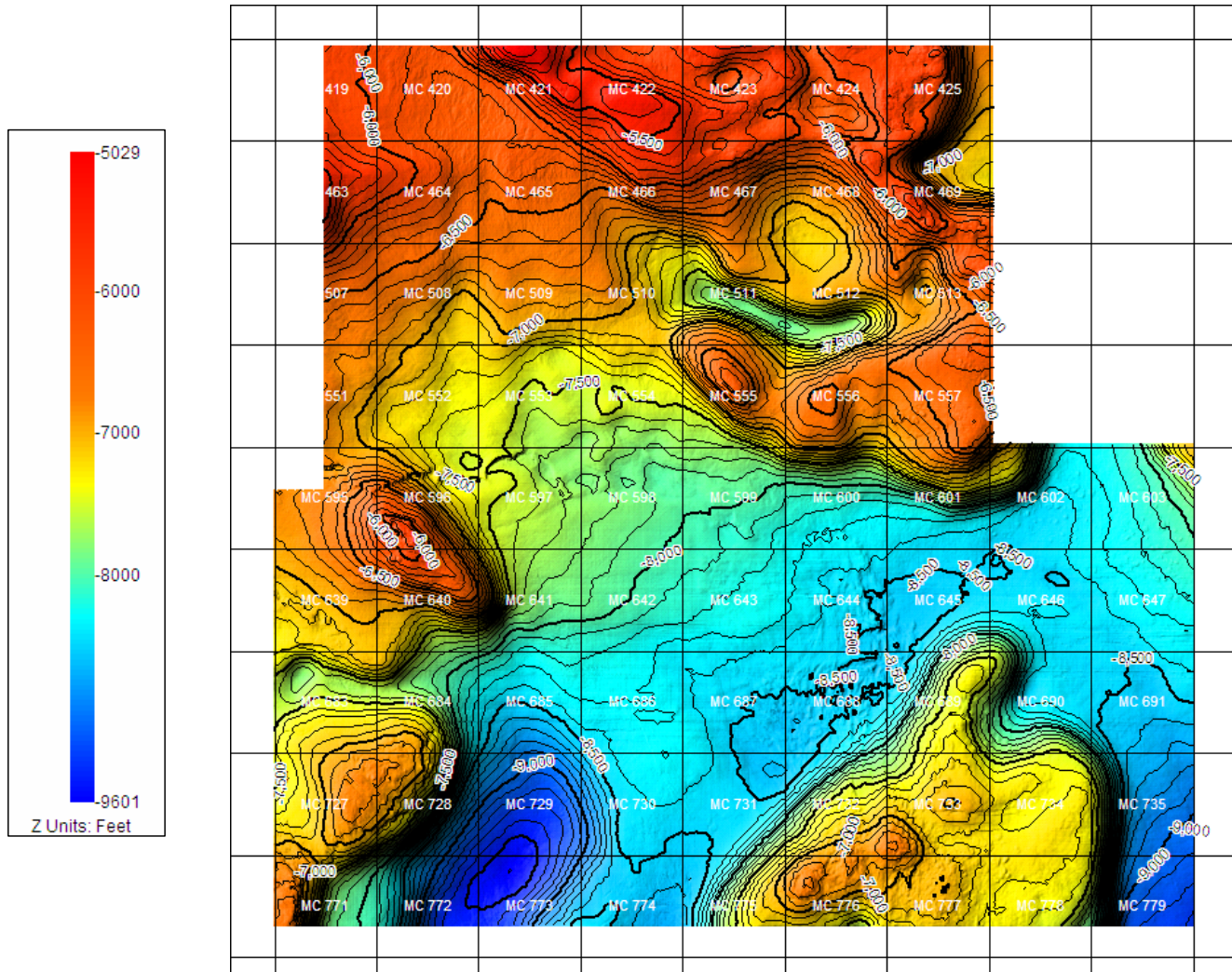


Figure 69. Structure map, Sequence I. Surface defined as depth from sea-surface to the top of sequence I (Horizon C'). Contour interval = 100ft. Index Contour every 500ft.

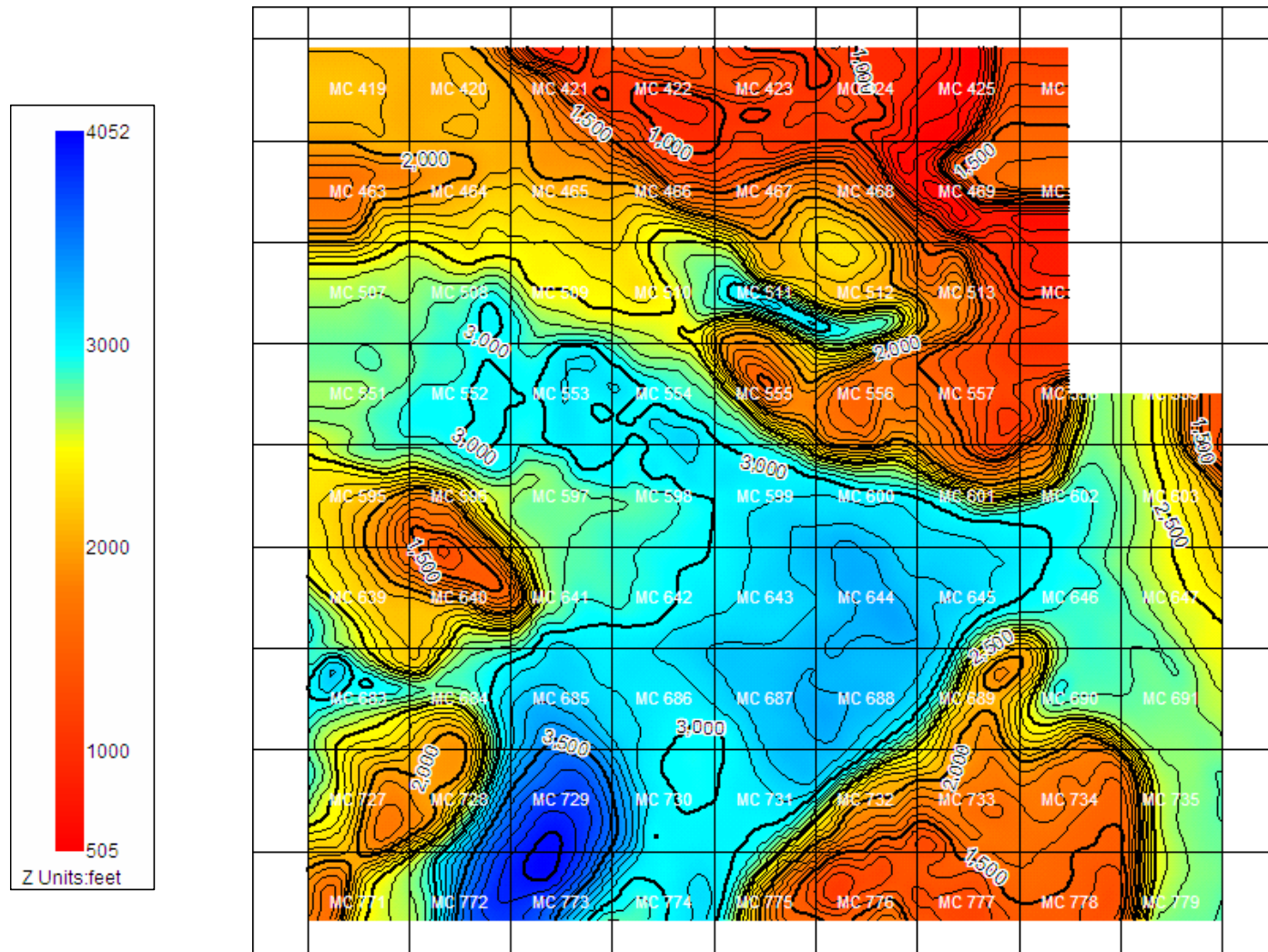


Figure 70. Isopach map, Sequence I. Image depicts thickness of sediment from seafloor to the top of sequence I (Horizon C'). Contour interval = 100ft. Index Contour every 500ft.

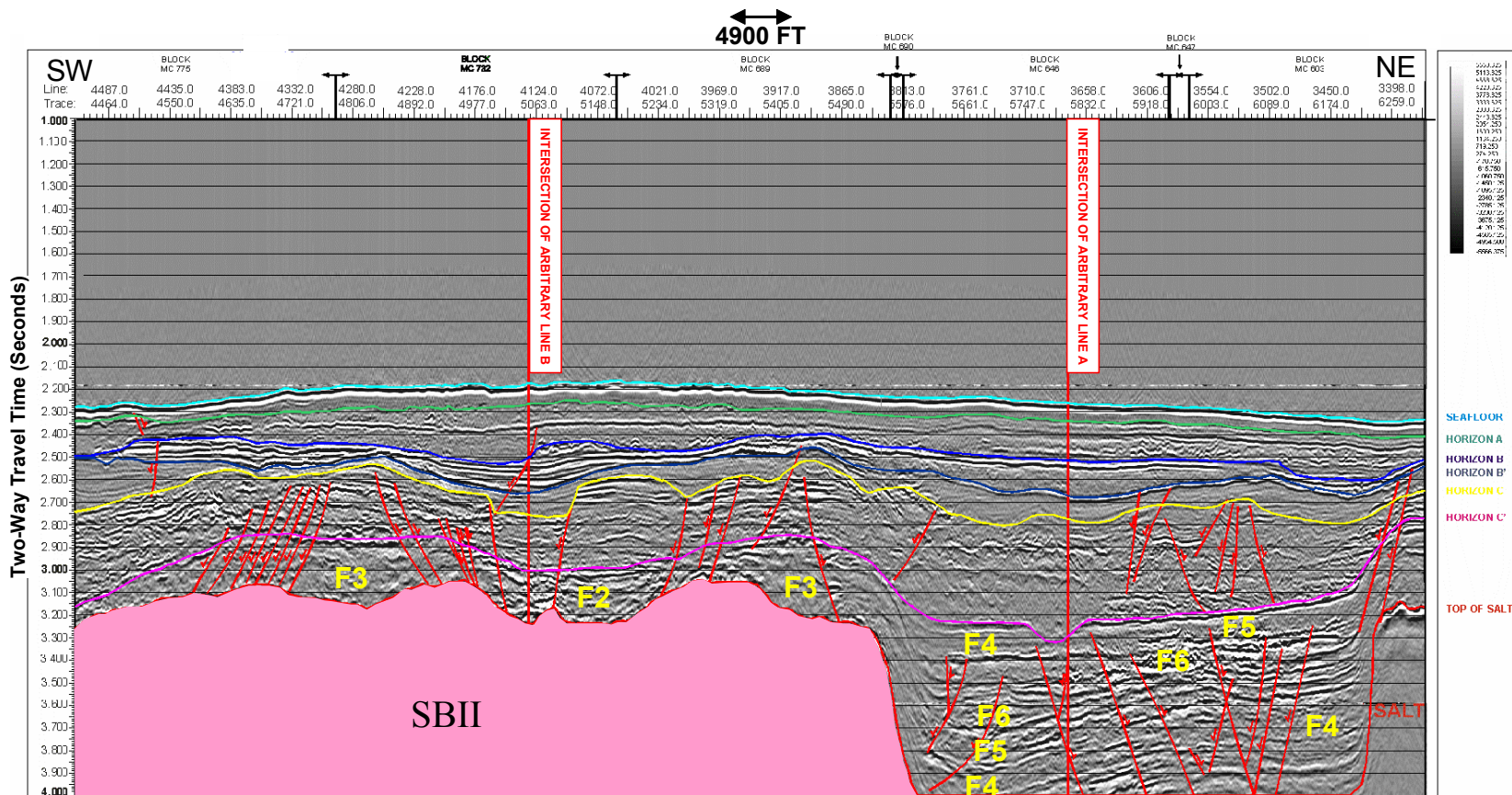


Figure 71. Arbitrary Seismic Line F showing Sequence I facies. F2-F6 represent Facies 2-Facies 6 as defined in Table 3. Pink shaded area denotes salt. Colored lines denote mapped horizons. Red lines denote faults.

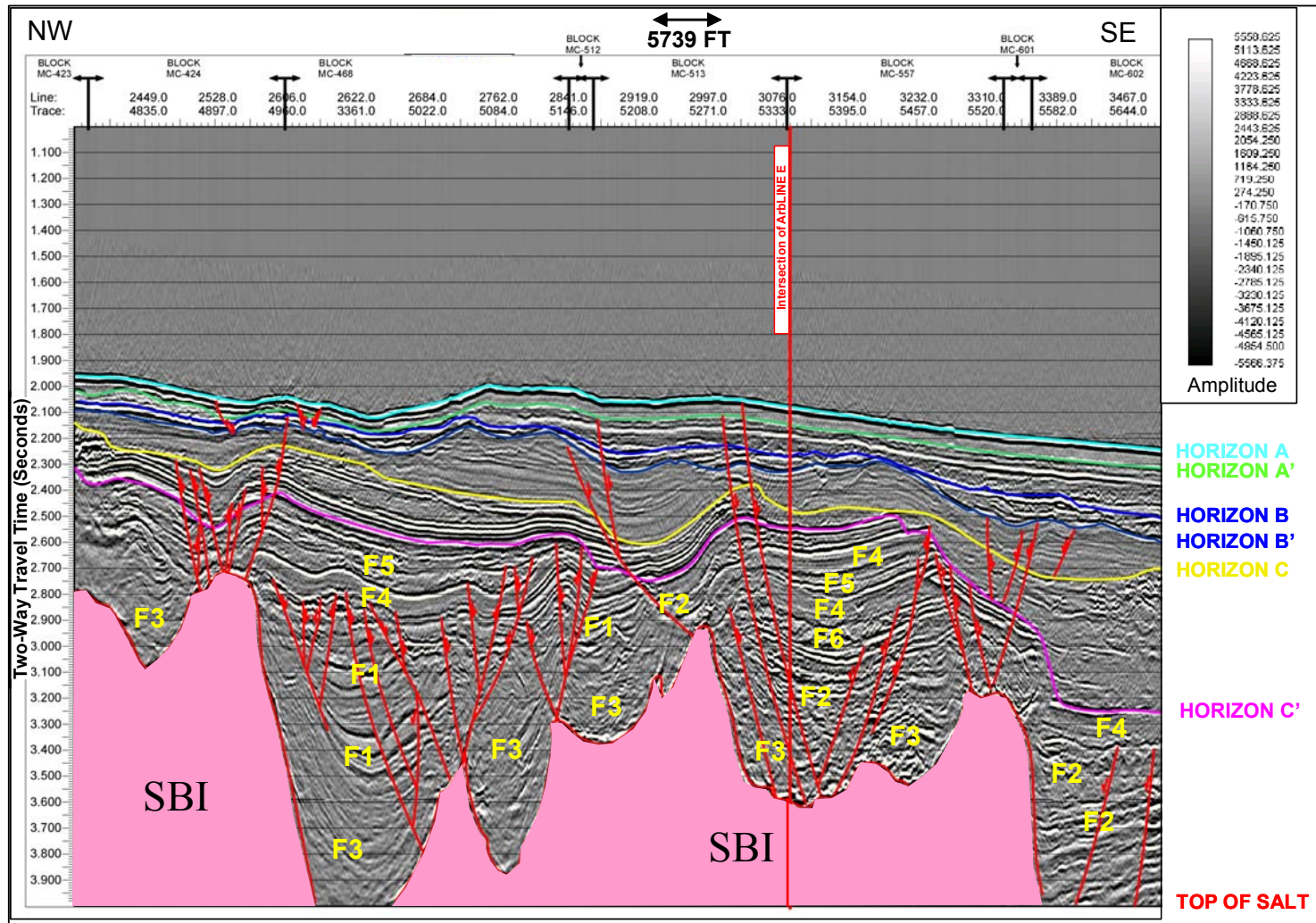

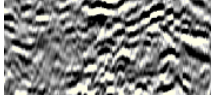

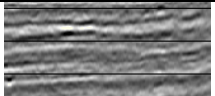
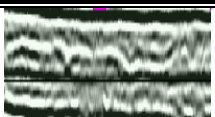
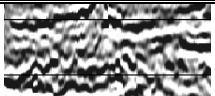


Figure 72. Arbitrary Seismic Line A showing Sequence I facies. F2-F6 represent Facies 2-Facies 6 as defined in Table 3. Pink shaded area denotes salt. Colored lines denote mapped horizons. Red lines denote faults.

Table 3. Sequence I seismic facies.

Sequence I Facies Designation	Seismic Character	Seismic Interpretation	Geologic Interpretation
Facies 1		Variable-amplitude, inclined, divergent reflectors.	Suprasalt basin fill deposits.
Facies 2		High-amplitude, chaotic reflectors.	Mass-transport deposits.
Facies 3		Variable-amplitude, chaotic reflectors.	Heterogeneous sediments deformed by salt movement.
Facies 4		Low to moderate-amplitude, parallel, continuous reflectors.	Hemipelagic sheet drape interbedded with mudflow deposits.
Facies 5		Moderate to high-amplitude, hummocky or shingled reflectors.	Thin, inter-fingered mudflow and debris slide deposits.
Facies 6		High-amplitude, chaotic reflectors.	Overlapping mass-transport deposits.

interpreted to be suprasalt-minibasin fill. Semi-parallel and divergent reflectors probably represent hemipelagic or fine-grained strata. Local amplitude variations within these reflectors may represent slightly varying sediment composition and/or competence. Locally high amplitudes within this facies may indicate the presence of gas trapped along faults that pierce not only this facies, but also the entire sequence. Facies 2 is composed of chaotic, higher amplitude reflectors than Facies 1 and probably represents coarser grained sediments possibly related to individual isolated high-energy mass-transport events, capable of transporting coarser sediments such as sand, deposited in the topographic lows of these suprasalt basins. The high-amplitude character of these reflectors may also represent gas migration along faults and localized charging in these coarser grained sediments. Facies 3 is interpreted to be very chaotic and/or seismically amorphous reflectors located directly above the salt at the bottom of these suprasalt basins. These reflectors are interpreted to represent a heterogeneous mix of sediment that has been internally deformed and rotated resulting from the upward movement of the salt during basin formation. The amplitude is generally lower than that of Facies 2 and probably represents a more heterogeneous sediment matrix. It may also represent a loss of reflective seismic energy from almost vertical, remnant inclined bedding within this facies.

Facies 4, 5, and 6 are generally located in intrasalt basins in the study area, and, in some places, may overlie Facies 1 through 3. Facies 4 is present throughout the study area. It is composed of low to moderate amplitude, parallel continuous and discontinuous reflectors. These reflectors probably represent silts and hemipelagic clays

as suggested by the body of low to moderate amplitude facies definitions in Table 2. Facies 5 is also present throughout the study area but is more confined toward the center of the intrasalt basins. The facies is composed of variable amplitude, shingled, hummocky, and chaotic reflectors. These reflectors are interpreted to represent multiple, thin, interfingering mudflow and debris slide deposits as defined in Table 2. The variable amplitude probably represents a change in sediment composition associated with deposits from each individual event. Facies 6 is confined to the centers of the intrasalt basins. The facies is composed of very high-amplitude, chaotic reflectors. These reflectors are interpreted to be represent numerous and overlapping, coarse grained mass-transport events in the form of local debris slides, slumps, or turbidites, deposited in the topographic lows of these intrasalt basins.

The aforementioned lateral distribution of these seismic and geologic facies within the sequence is illustrated in the RMS display in Figure 73.

B. Sequence II: Horizon C to Horizon C'

Sequence II is present throughout the study area (Figure 74 and 75). The top of the sequence, Horizon C, lies between 4900 ft and 7900 ft below the sea surface (structure map, Figure 74) and between 300 ft and 2200 ft below the seafloor (isopach map, Figure 75). The base of the sequence, Horizon C', lies between 600 ft and 4000 ft below the seafloor (Figure 70). The sequence ranges between 0 ft to 2300 ft thick (Figure 76). Sediments of the sequence thicken in areas associated with basin features

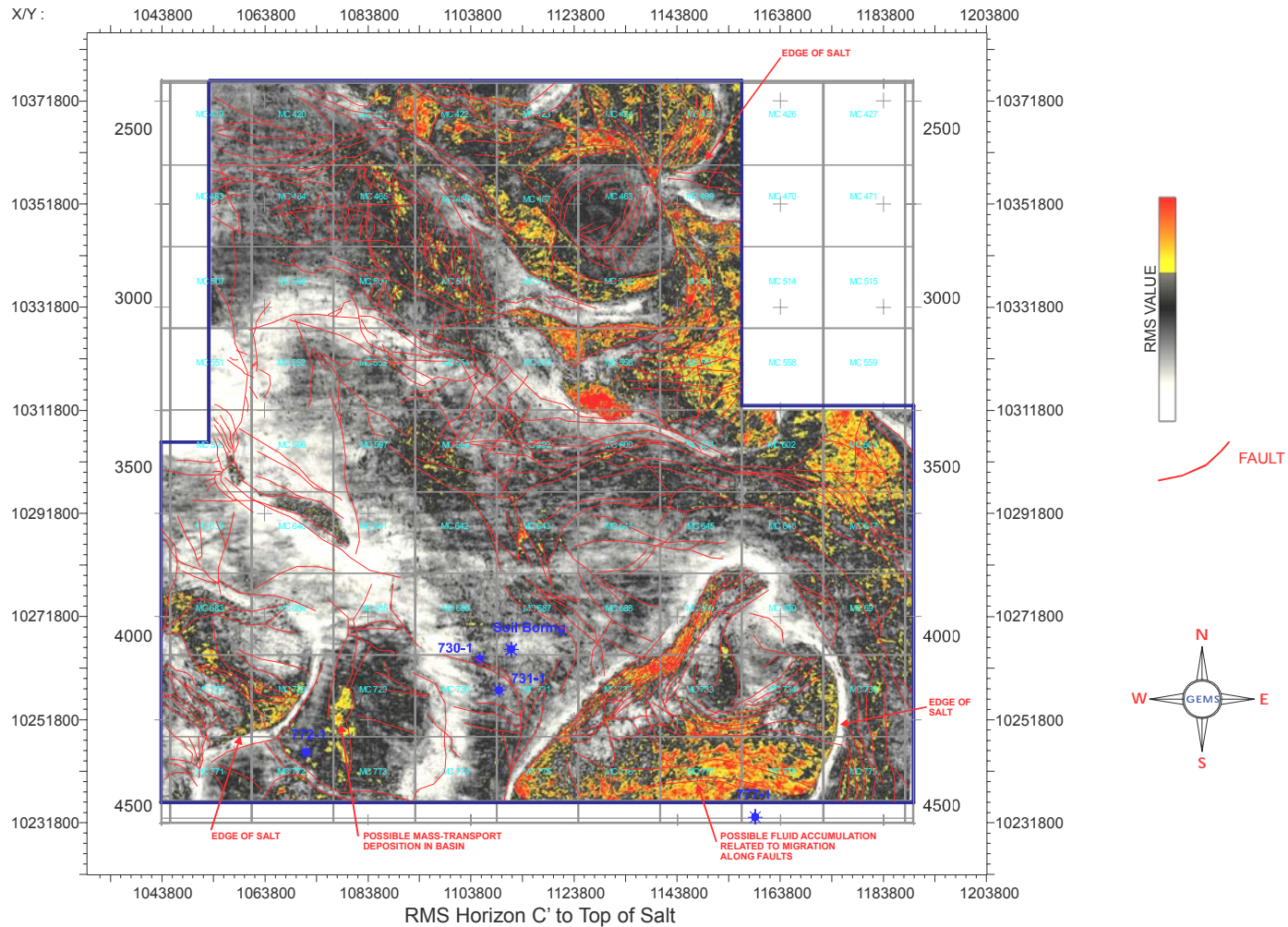


Figure 73. Sequence I RMS amplitude display. Higher RMS values (yellow to orange) represent higher seismic amplitude within the seismic volume of Sequence I. Note the concentration of high RMS values above salt likely indicative of fluid accumulation related to migration along faults above the salt. Also note the “halo” effect that marks the edge of salt within the sequence. X/Y coordinates are NAD 27, UTM 16, USFT. Red lines denote faults in the sequence identified from the RMS. Note extensive amount of faulting in the sequence.

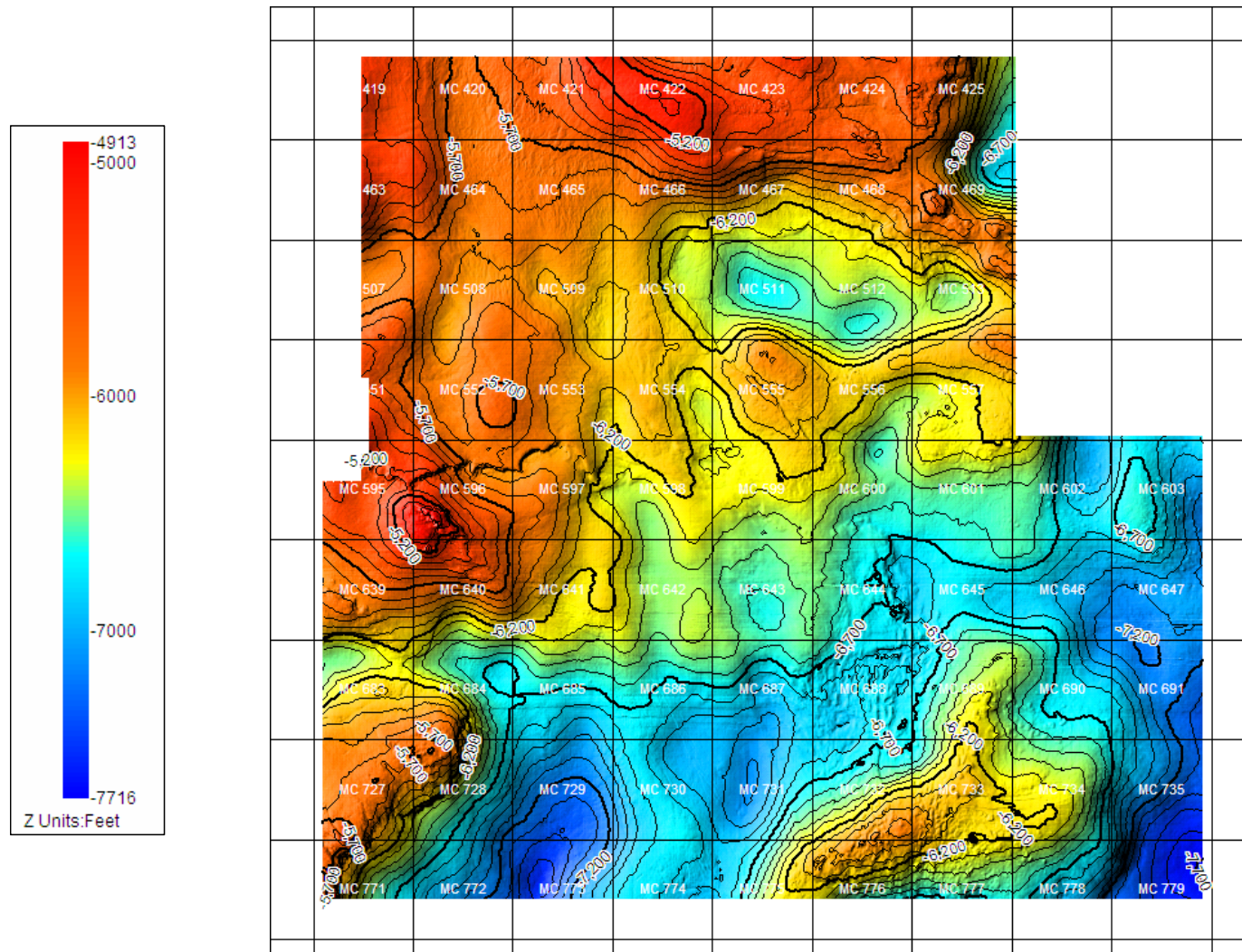


Figure 74. Structure map, Sequence II. Surface defined as depth from sea-surface to the top of sequence II (Horizon C). Contour interval = 100ft. Index Contour every 500ft.

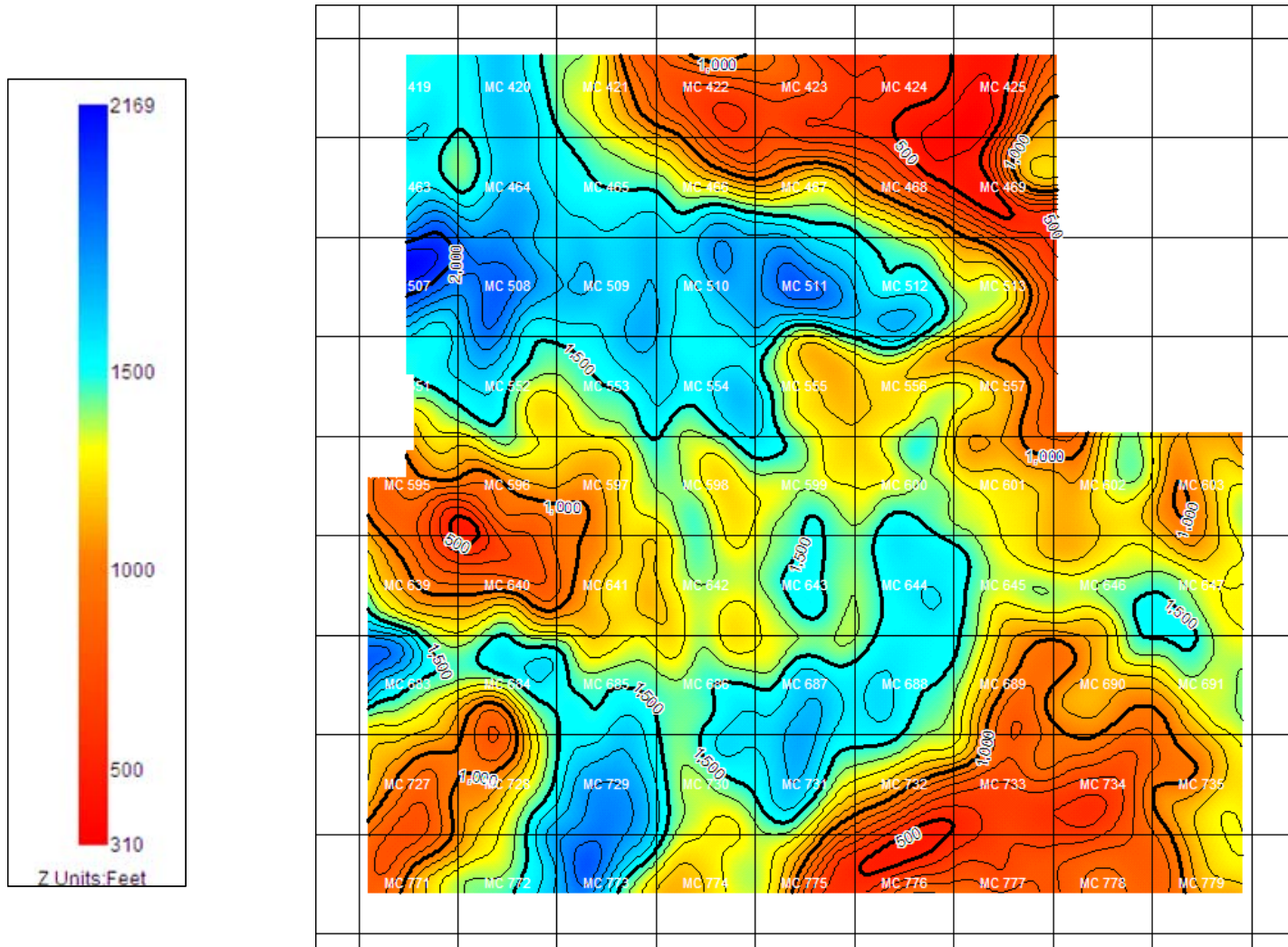


Figure 75. Isopach map, Sequence II. Image depicts thickness of sediment from seafloor to the top of sequence II (Horizon C). Contour interval = 100ft. Index Contour every 500ft.

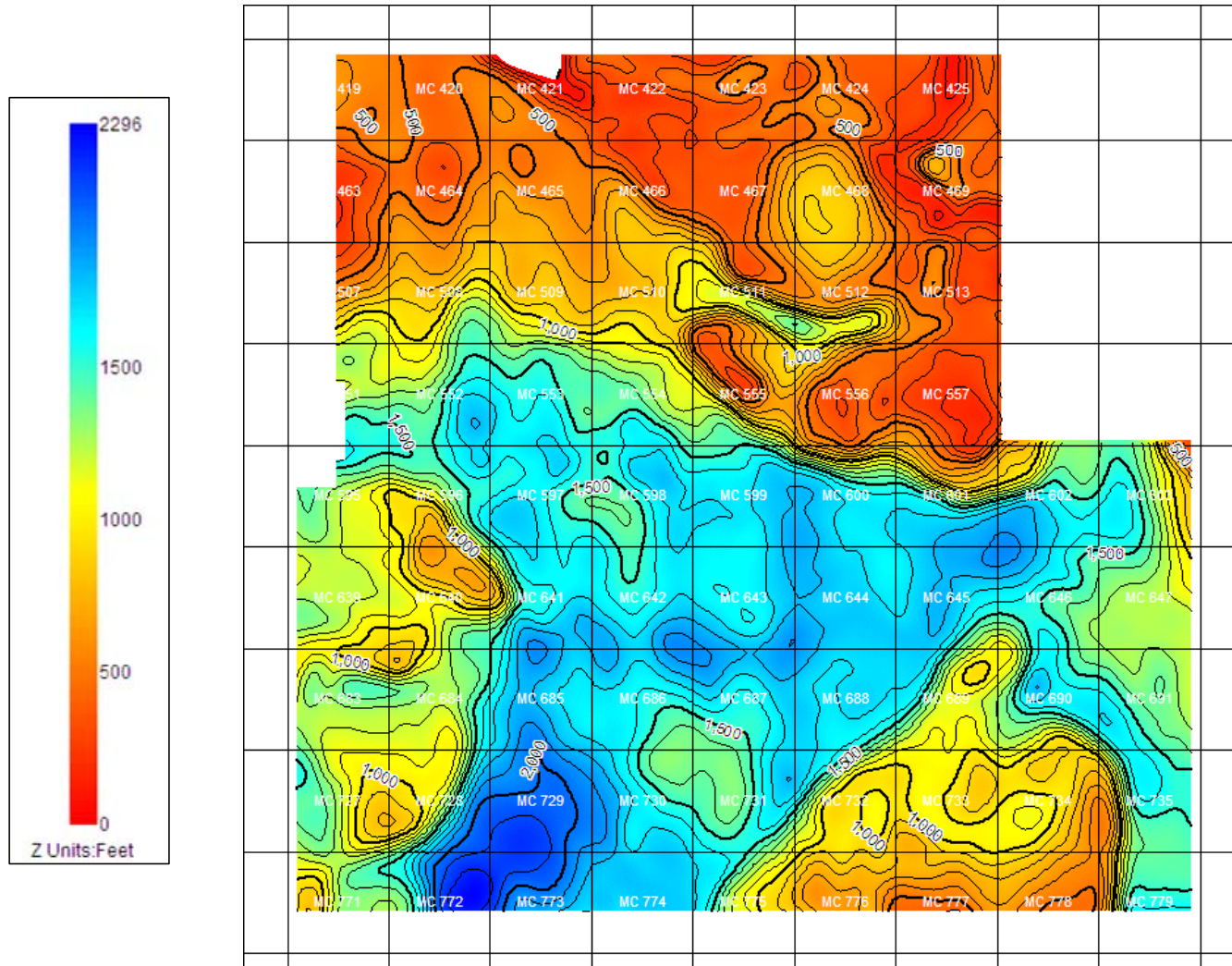
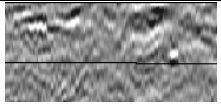
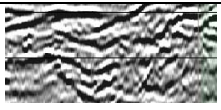


Figure 76. Thickness map, Sequence II. Image depicts thickness of Sequence II (Horizon C to Horizon C'). Contour interval = 100ft. Index Contour every 500ft.

Table 4. Sequence II seismic facies.

Sequence II Facies Designation	Seismic Character	Seismic Interpretation	Geologic Interpretation
Facies 1		Low-amplitude to amorphous, chaotic reflectors.	Low-energy, internally deformed, mass transport complex.
Facies 2		High-amplitude, hummocky and chaotic reflectors.	High-energy, partially channeled, mass transport complex.

and structural lows surrounding the uplifted salt bodies in the study area. Sediments are thinner in areas associated with these salt uplifts. Sequence II contains two seismic and geologic facies. These facies are shown in Table 4.

A seismic example illustrating these facies is presented in Figure 77. The chaotic, variable amplitude seismic character of Sequence II (Facies 1 and Facies 2) suggests the sequence is composed entirely of large mass-transport complex (MTC) deposits. Facies 1 is composed of chaotic, seismically amorphous and low-amplitude reflectors generally present in the lower half of the sequence. Facies 1 probably represents a number of large debris slide events. The overall low to seismically amorphous amplitude character of the facies may be an indication of a heterogeneous mix of fine and coarse-grained sediments. It may also be indicative of a complex, near vertically inclined geometry of the sediments within the facies which would significantly reduce the seismic energy reflected back to the source necessary to establish a reflector in time at that position.

Facies 2 is composed of high-amplitude contorted and chaotic reflectors. Facies 2 is generally present in the upper half of the sequence, and, in some areas has partially or completely eroded Facies 1. The higher amplitude character of the facies is interpreted to be a result of heterogeneous, coarser-grained sediment composition and may indicate a higher energy regime of deposition. The geometry of the reflectors is interpreted to be combinations of deposition under a high-energy regime as well as a localized internal deformation probably resulting from differential compaction. This is.

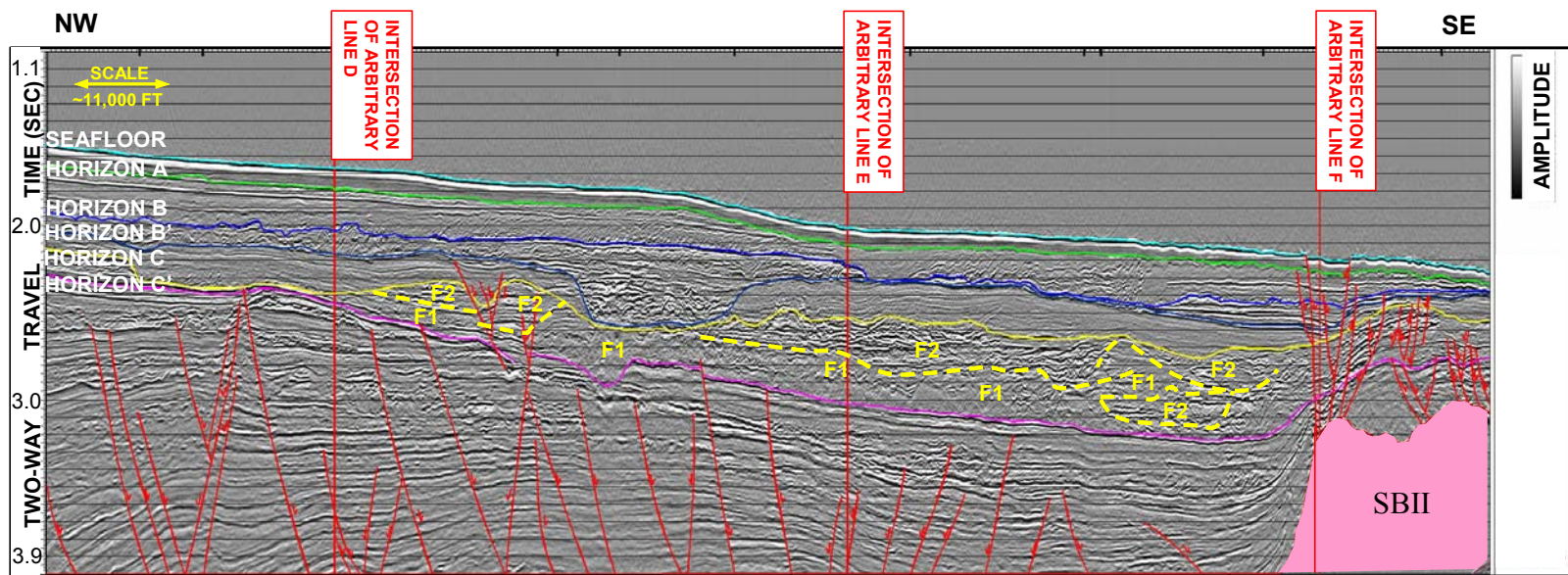


Figure 77. Arbitrary Seismic Line B showing Sequence II facies. F1 and F2 are Facies 1 and Facies 2 as defined in Table 4. Pink shaded area denotes salt. Colored lines denote mapped horizons. Red lines denote faults.

based on both the seismic facies and implied soils characteristics derived from both interpretation and seismic facies definitions in Table 2. The aforementioned lateral distribution of these seismic and geologic facies within the sequence is illustrated in the RMS display in Figure 78.

C. Sequence III: Horizon B' to Horizon C

Sequence III is present throughout the study area (Figure 79 and 80). The top of the sequence, Horizon B,' lies between 4600 ft and 6900 ft below the sea surface (structure map, Figure 79) and between 100 ft and 2200 ft below the seafloor (isopach map, Figure 80). The base of the sequence, Horizon C, lies between 310 ft and 2170 ft below the seafloor (Figure 75). The sequence ranges between 0 ft and 950 ft thick (Figure 81), thickening to the southeast and thinning in the center of the study area where it has been eroded via channel incision during deposition of the overlying stratigraphic sequence, Sequence IV. Sequence III contains one seismic and geologic facies. The facies is shown in Table 5. Seismic examples illustrating this facies are presented in Figures 82 and 83. Facies 1 is composed of low-amplitude to seismically amorphous, parallel and continuous reflectors. Facies 1 represents a thick condensed section composed of hemipelagic clays interbedded with thin mudflow deposits. In some areas, the facies is structurally deformed over areas of Sequence II that are interpreted to have undergone internal rotation or differential compaction.

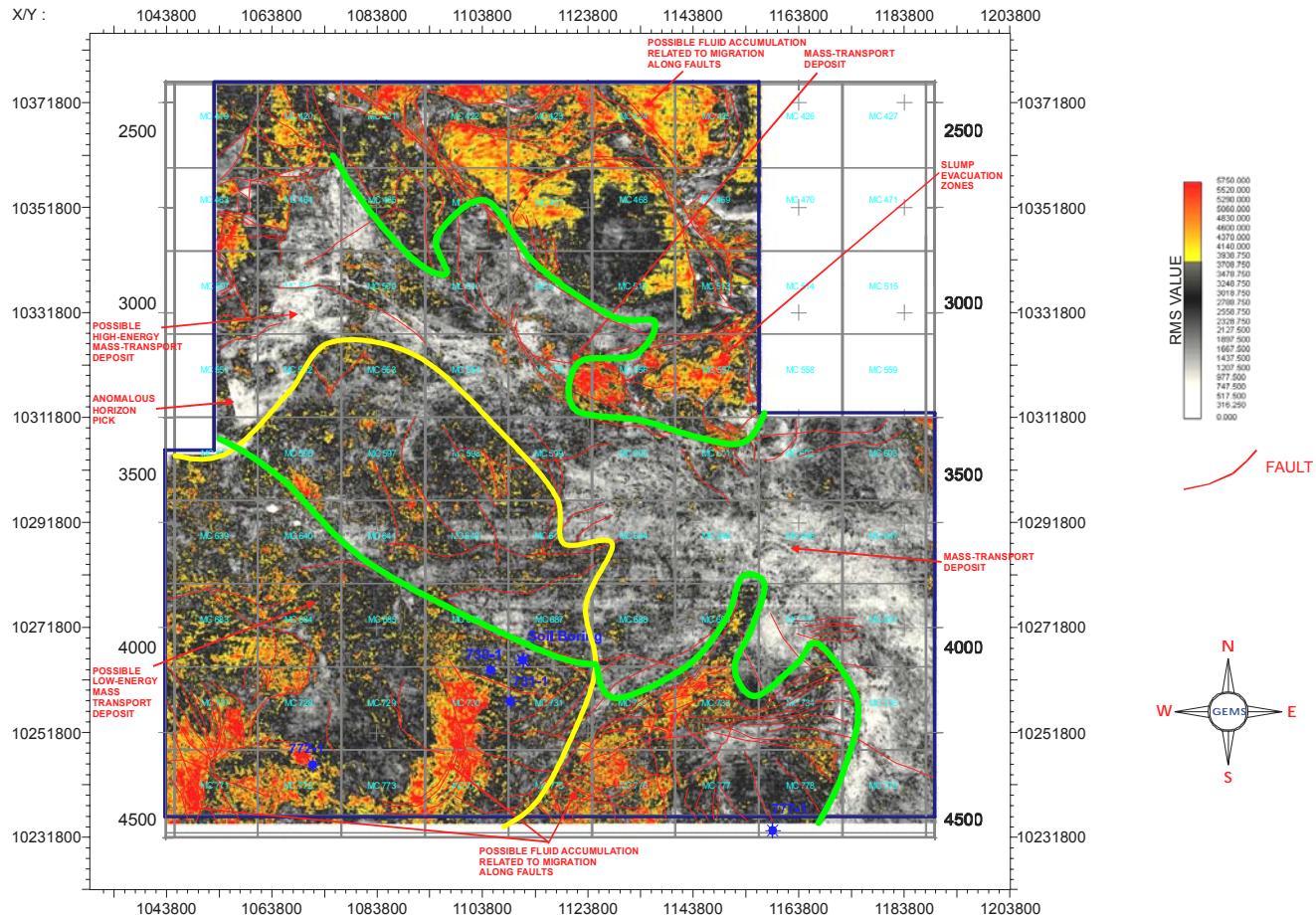


Figure 78. Sequence II RMS amplitude display. High RMS values (yellow to orange) above salt likely indicate migration of fluids into the sequence along faults. High RMS values in basins between salt indicate possible presence of fluids in coarser grained soils within massive slide deposits. Variation in moderate RMS values (white to black) across the image show variation in slide facies within the sequence. The extent of the slides are identified by the yellow and green boundary lines. The higher amplitude slide facies appear focused in the southwest portion of the study area and are found west of the yellow line. The lower amplitude slide facies appear through the center of the study area and are bounded on each side by the green lines. X/Y coordinates are NAD 27, UTM 16, USFT. Red lines denote faults in the sequence identified from the RMS.

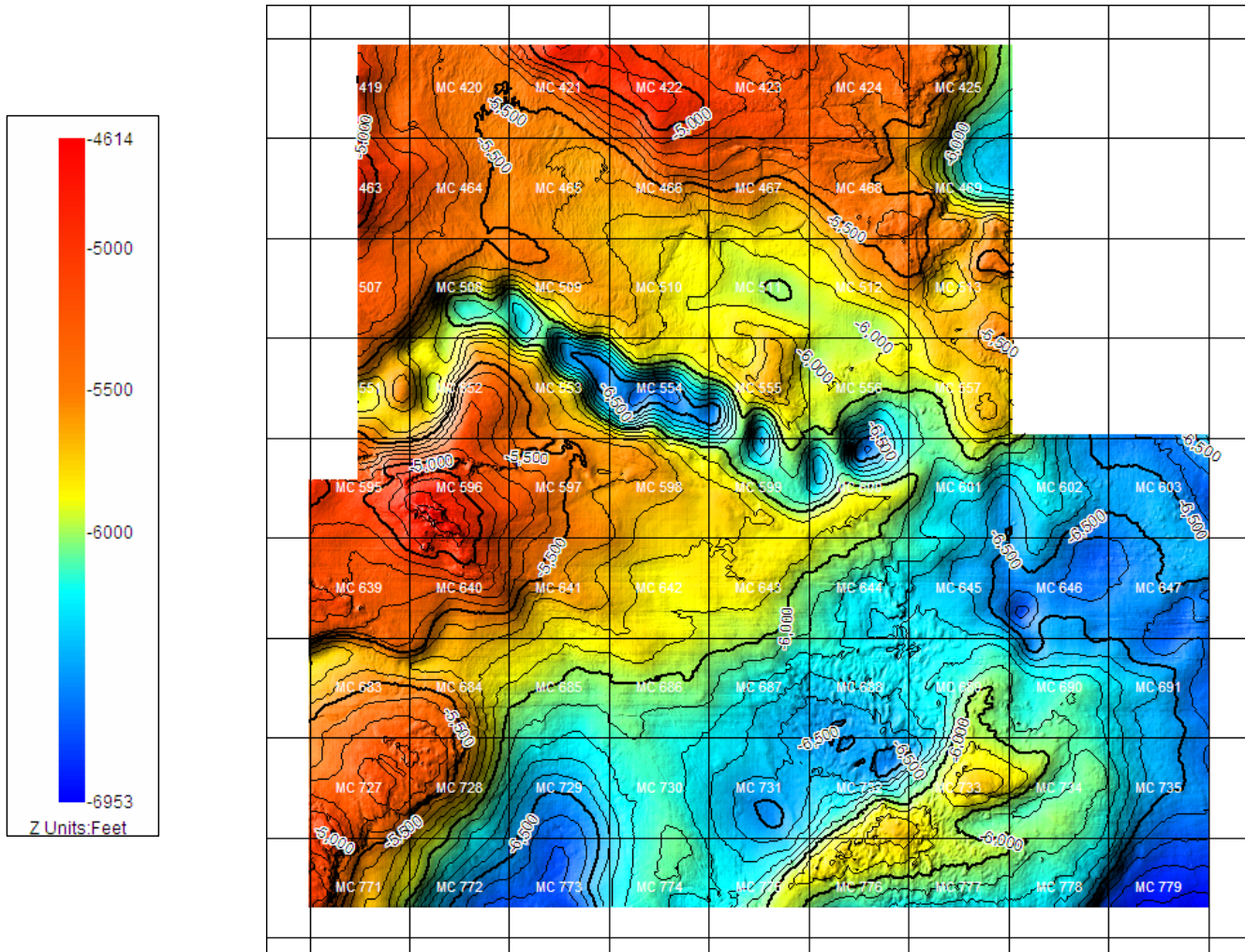


Figure 79. Structure map, Sequence III. Surface defined as depth from sea-surface to the top of sequence III (Horizon B'). Contour interval = 100ft. Index Contour every 500ft. Note the deep lineament in the middle of the study indicative of channel incision during formation of the overlying Sequence IV.

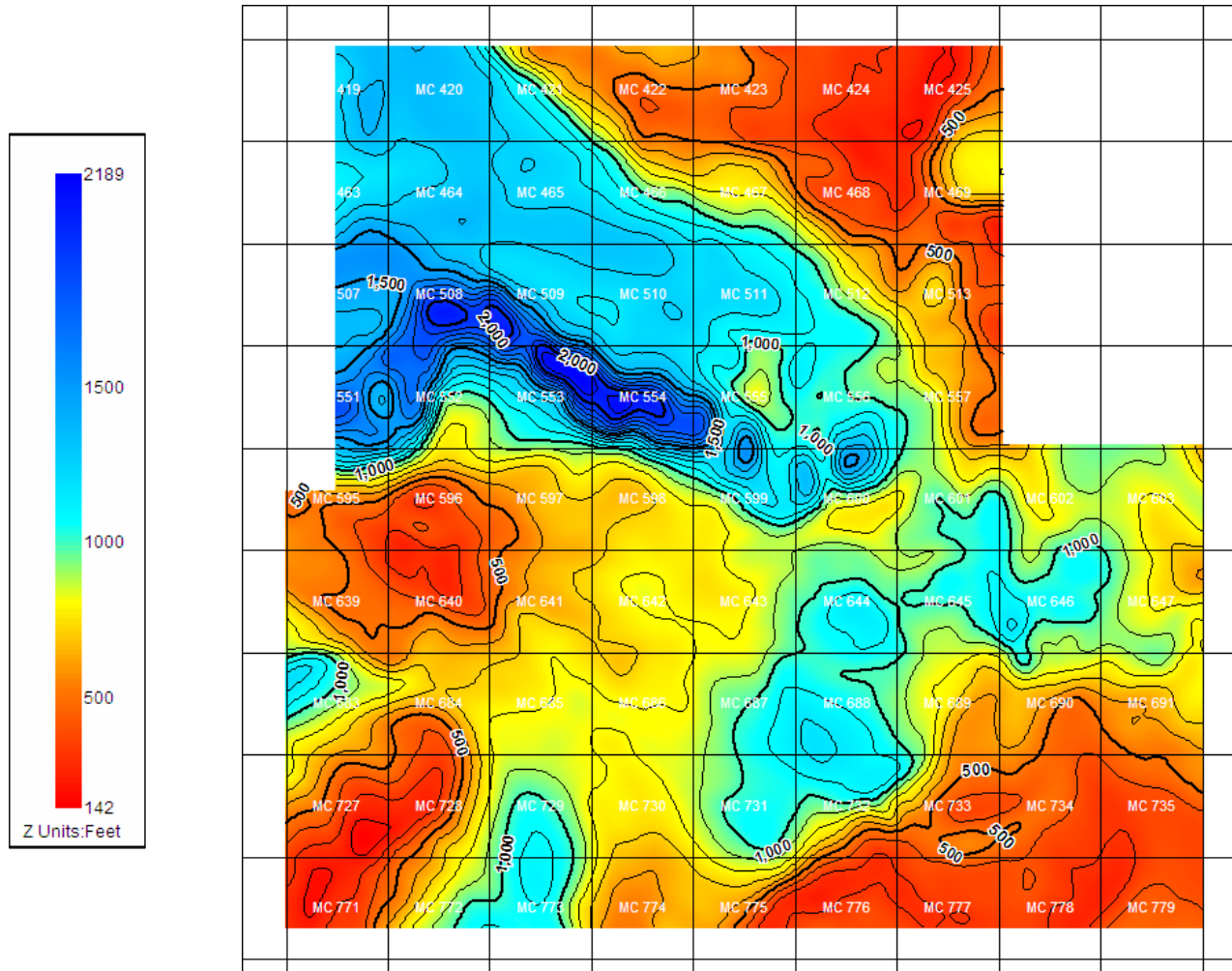


Figure 80. Isopach map, Sequence III. Image depicts thickness of sediment from seafloor to the top of sequence III (Horizon B'). Contour interval = 100ft. Index Contour every 500ft. Note the corresponding increase in thickness at the location of the channel incision from the overlying Sequence IV in the middle of the study area.

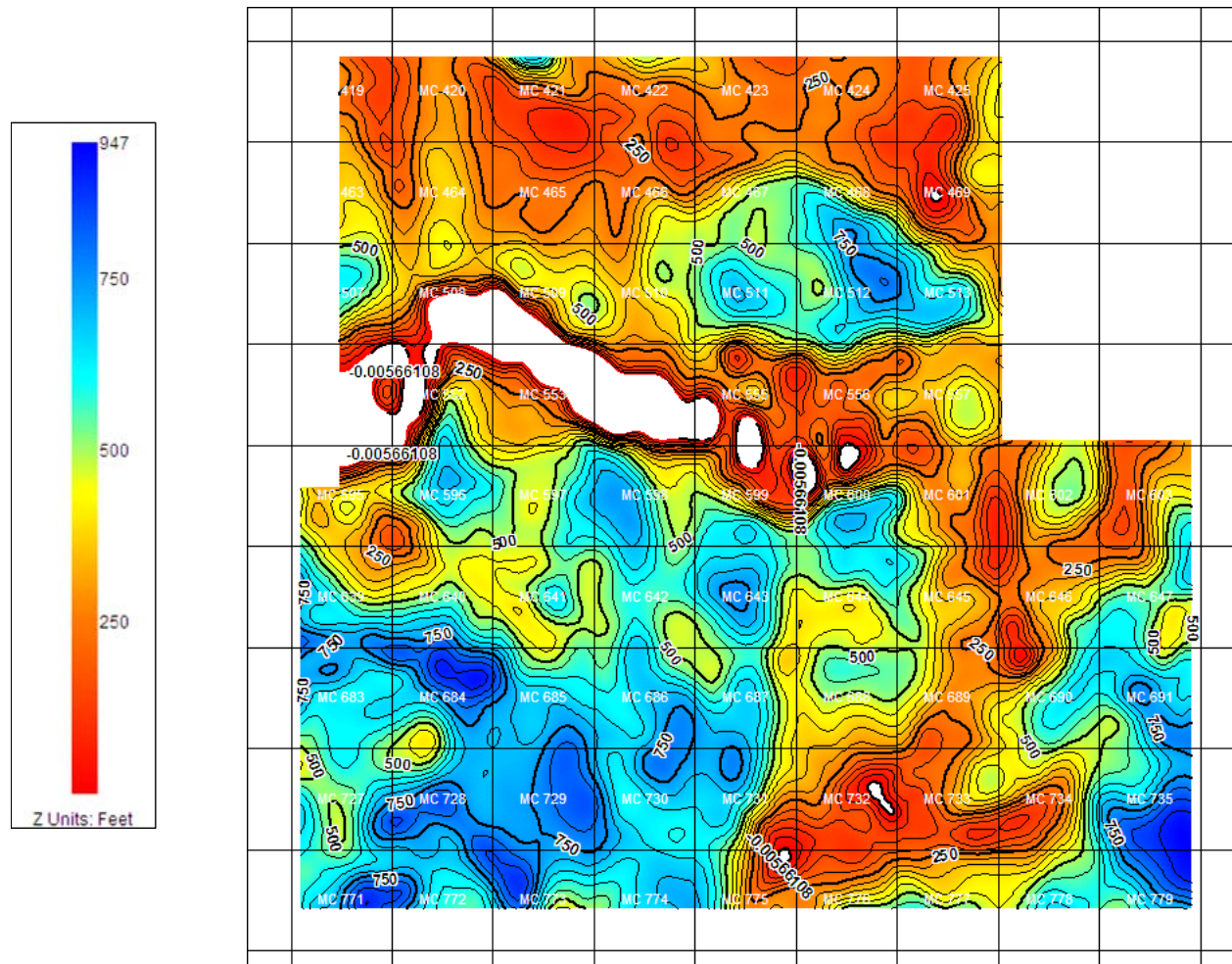



Figure 81. Thickness map, Sequence III. Image depicts thickness of Sequence III (Horizon B' to Horizon C). Contour interval = 50ft. Index Contour every 250ft. Note middle of study area where Sequence III has been completely removed in areas of channel incision during formation of the overlying Sequence IV.

Table 5. Sequence III seismic facies.

Sequence III Facies Designation	Seismic Character	Seismic Interpretation	Geologic Interpretation
Facies 1		Low-amplitude to amorphous, parallel, continuous reflectors.	Hemipelagic sheet drape interbedded with thin mudflow deposits.

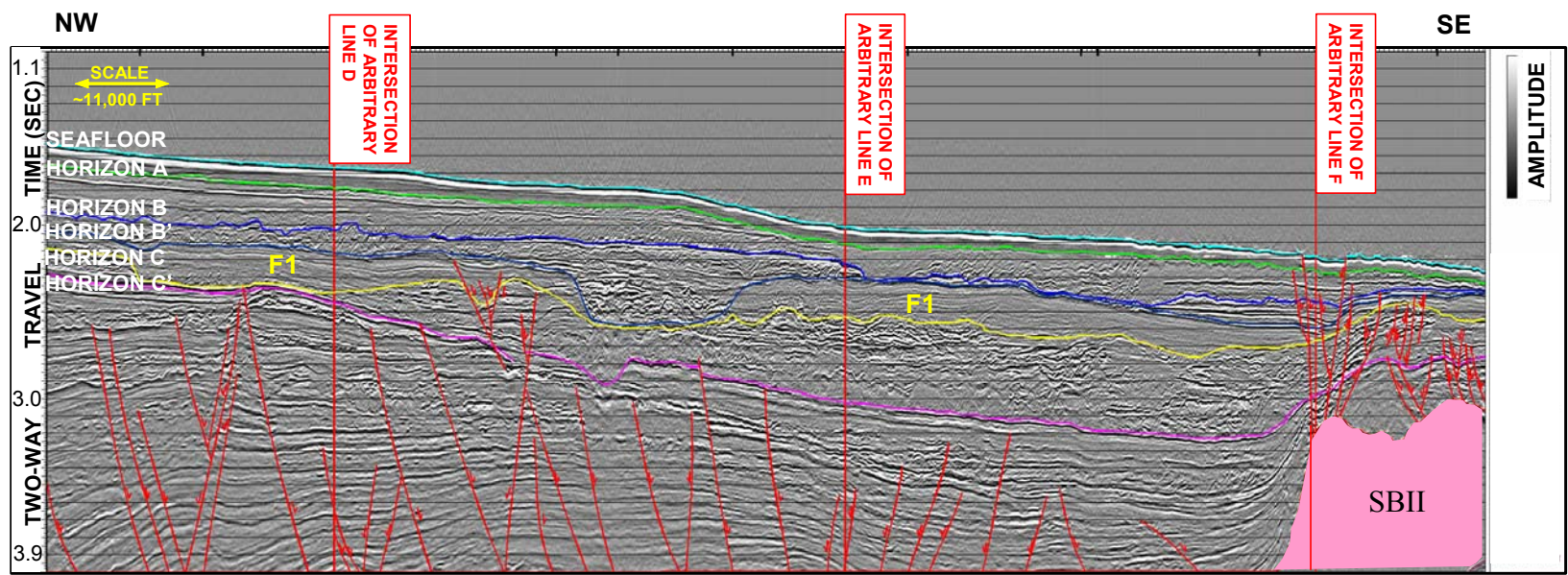


Figure 82. Arbitrary Seismic Line B showing Sequence III facies. F1 is Facies 1 as defined in Table 5. Pink shaded area denotes salt. Colored lines denote mapped horizons. Red lines denote faults.

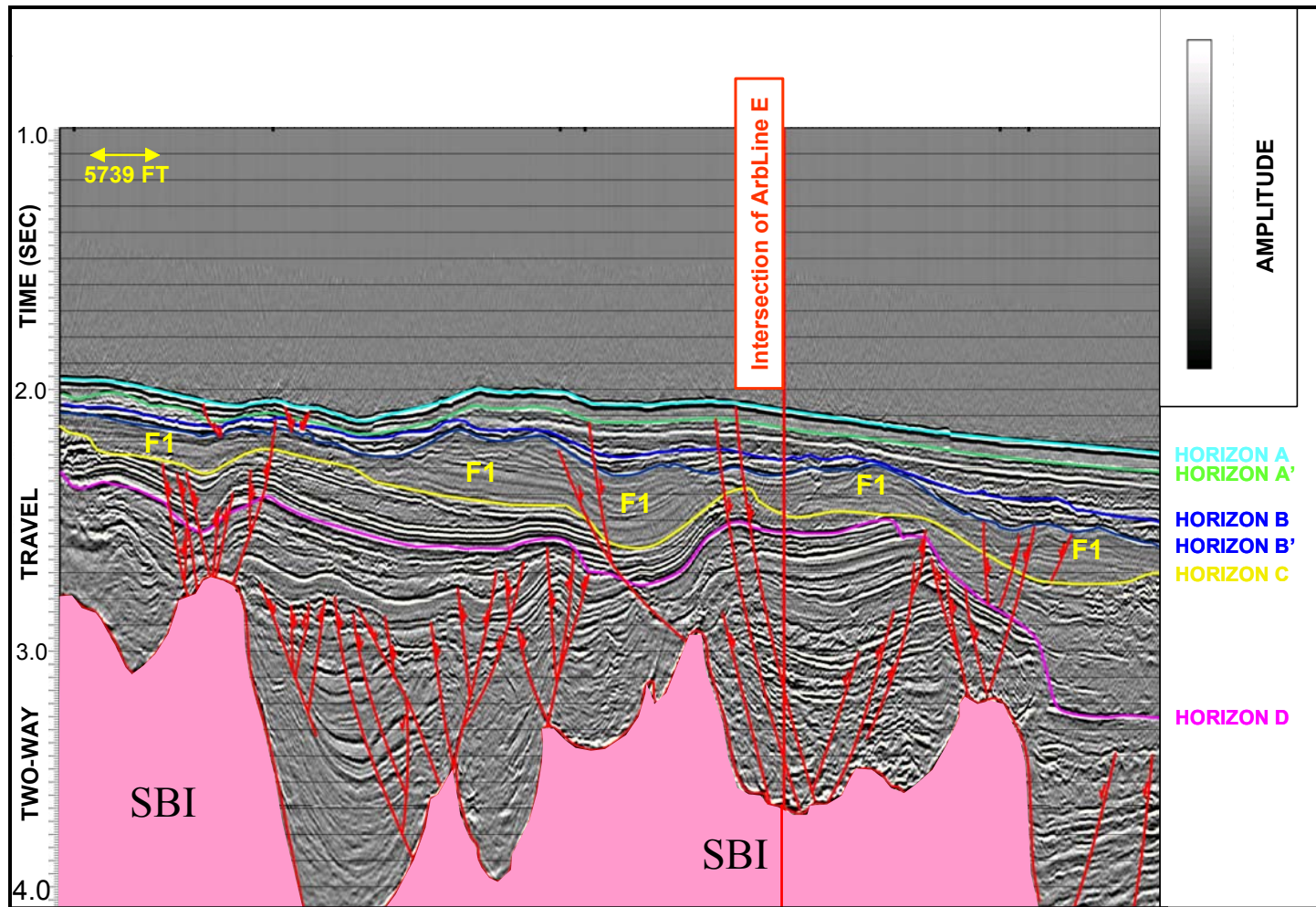


Figure 83. Arbitrary Seismic Line A showing Sequence III facies. F1 is Facies 1 as defined in Table 5. Pink shaded area denotes salt. Colored lines denote mapped horizons. Red lines denote faults.

The distribution of these seismic and geologic facies within the sequence is illustrated in RMS display of the sequence Figure 84.

D. Sequence IV: Horizon B to Horizon B'

Sequence IV is present throughout the study area (Figure 85 and 86). The top of the sequence, Horizon B, lies between 4500 and 6900 below the sea surface (structure map, Figure 85) and between 114 ft and 1262 ft below the seafloor (isopach map, Figure 86). The base of the sequence, Horizon B', lies between 200 ft and 2100 ft below the seafloor (Figure 80). The sequence ranges between 0 ft to 1400 ft thick (Figure 87). Sediments of the sequence thicken in areas associated with basin features and structural lows surrounding the uplifted salt bodies in the study area. The thickest sediments occur in a channel/slump feature that runs through the center of the study area (Figure 87). Sediments are thinner in areas associated with salt uplifts.

Sequence IV contains three seismic and geologic facies. These facies are illustrated in Table 6. Seismic examples illustrating this facies are presented in Figures 88, 89, and 90. Facies 1 is composed of high-amplitude, subparallel reflectors. Facies 1 represents sediments composed of thick, high-energy, ponded turbidite deposits. The facies is present through a channel/fill feature that runs through the center of the area. However, the type section of the geologic and seismic character for this facies occurs in a shallow basin in the southern half of the survey. Both SBII and SBIII flank this basin with their corresponding topographic highs constricting the open downslope movement

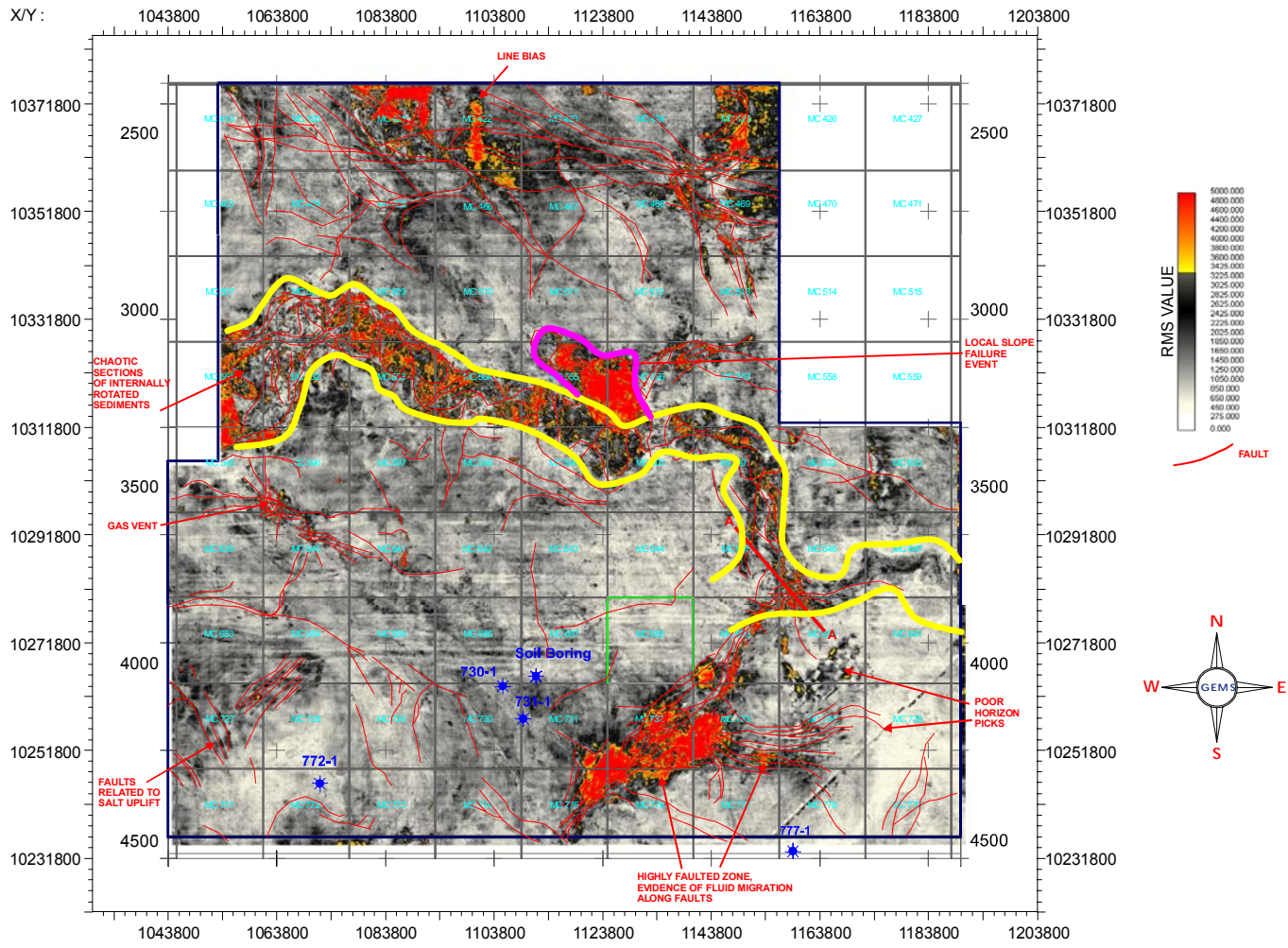


Figure 84. Sequence III RMS amplitude display. The overall low background RMS values (white to black) are consistent with a low-amplitude, clay-rich, condensed section. High RMS values (yellow to orange) and faults (red lines) are concentrated both above the salt and where the channel from overlying Sequence IV has incised Sequence III. The base of the channel is bounded by the yellow lines. A channel sidewall failure marked by high RMS values is outlined by the magenta line. X/Y coordinates are NAD 27, UTM 16, USFT. .

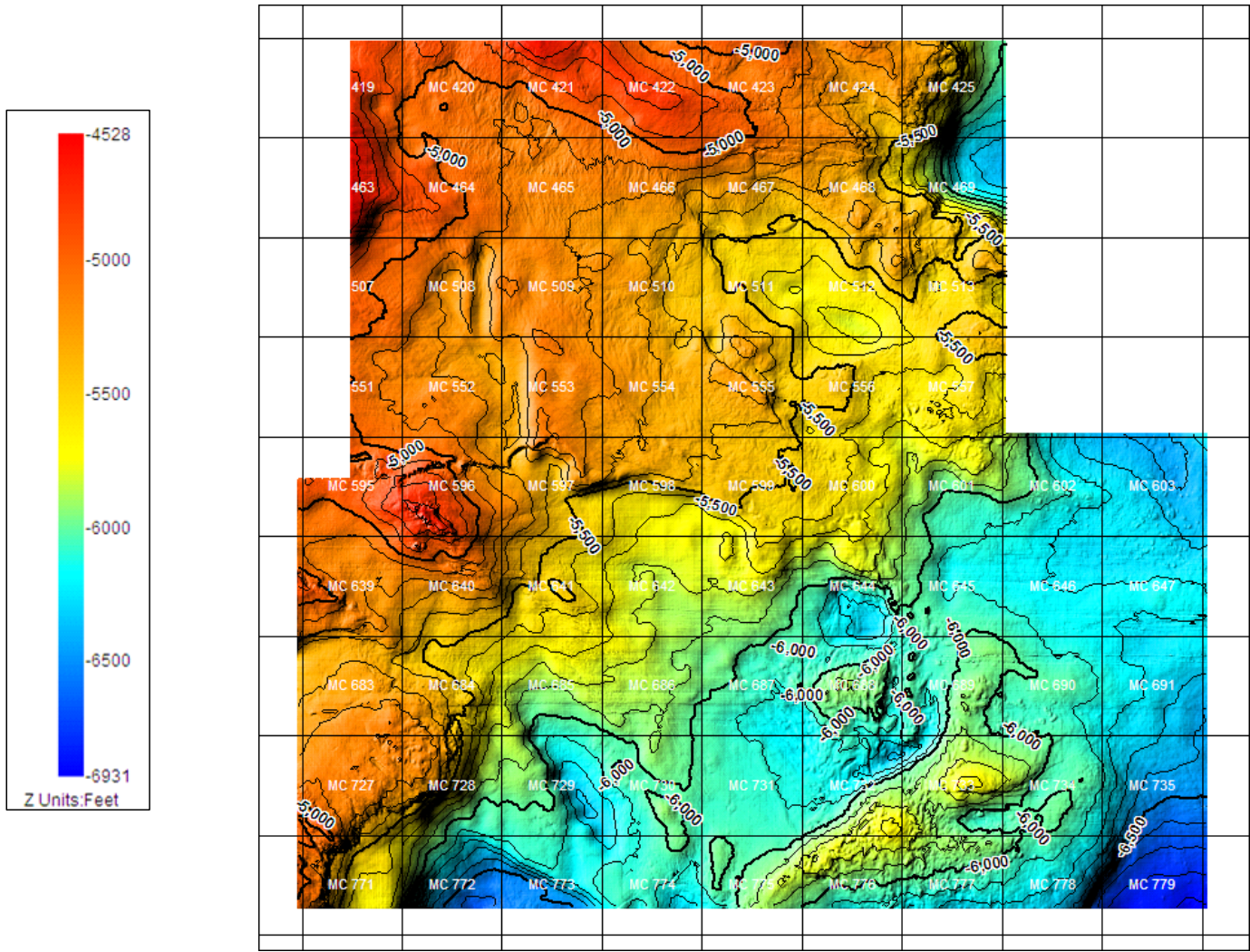


Figure 85. Structure map, Sequence IV. Surface defined as depth from sea-surface to the top of sequence IV (Horizon B). Contour interval = 100ft. Index Contour every 500ft.

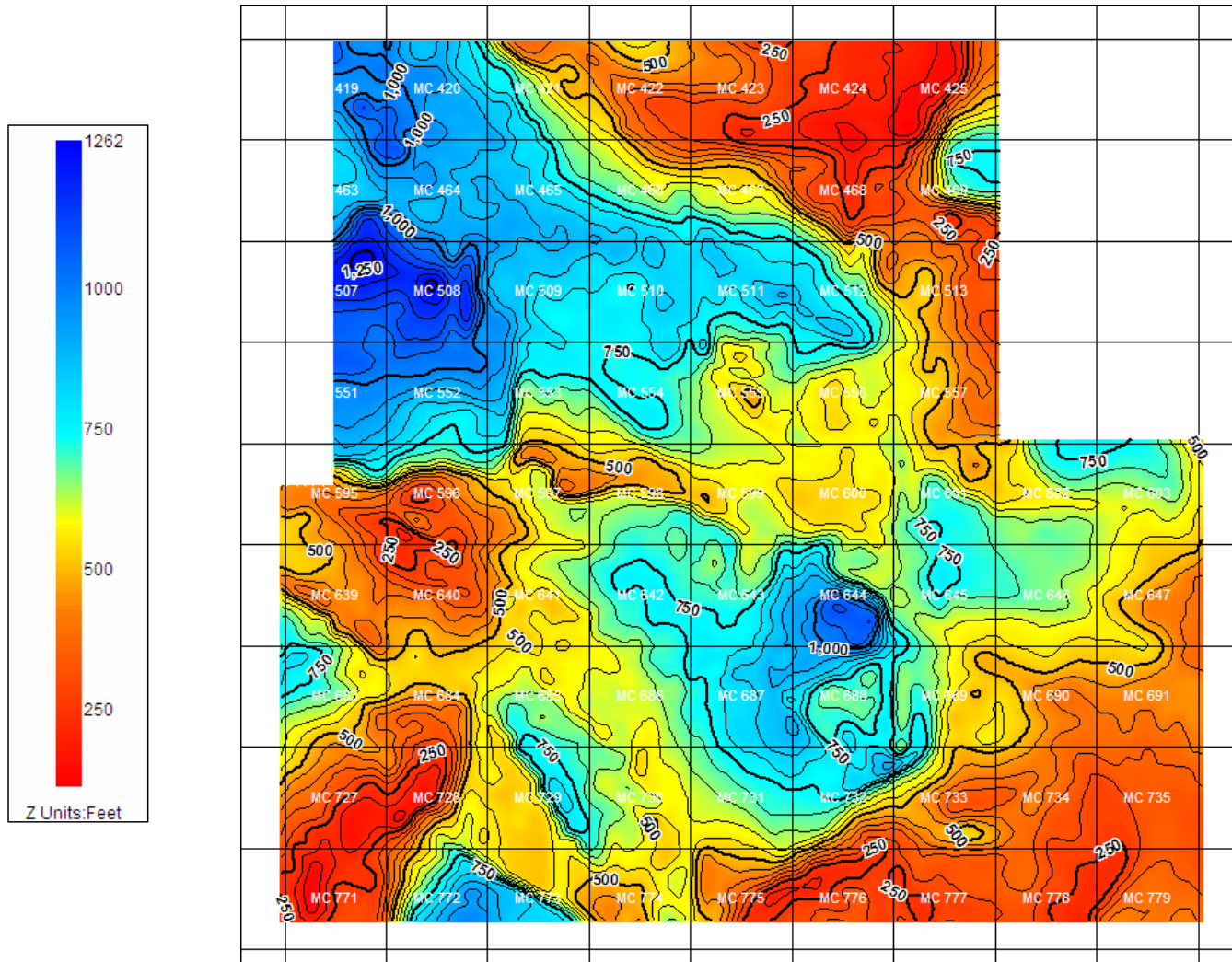


Figure 86. Isopach map, Sequence IV. Image depicts thickness of sediment from seafloor to the top of sequence IV (Horizon B). Contour interval = 50ft. Index Contour every 250ft.

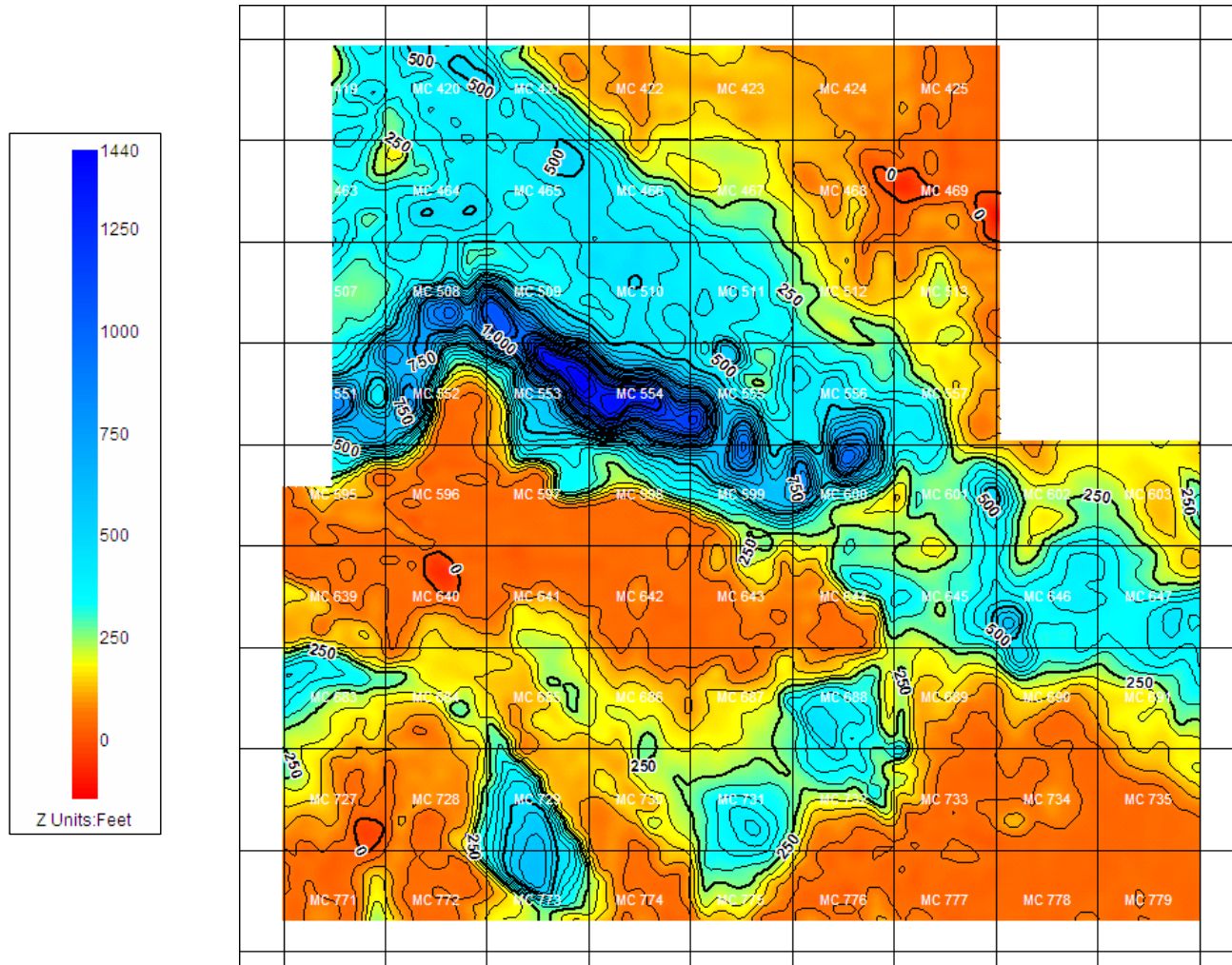
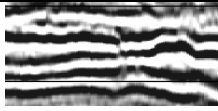




Figure 87. Thickness map, Sequence IV. Image depicts thickness of Sequence IV (Horizon B to Horizon B'). Contour interval = 50ft. Index Contour every 250ft. Note the focused increase in thickness corresponding to position of the channel where it significantly incised into underlying Sequence II as well as the localized accumulation in the basin constricted by SBII and SB III.

Table 6. Sequence IV seismic facies.

Sequence IV Facies Designation	Seismic Character	Seismic Interpretation	Geologic Interpretation
Facies 1		High-amplitude, sub parallel reflectors.	High-energy, ponded turbidite deposits.
Facies 2		Moderate to High-Amplitude, chaotic reflectors.	Debris slide, slump, or mudflow deposits.
Facies 3		High-amplitude, chaotic reflectors.	Channeled mass transport deposits.

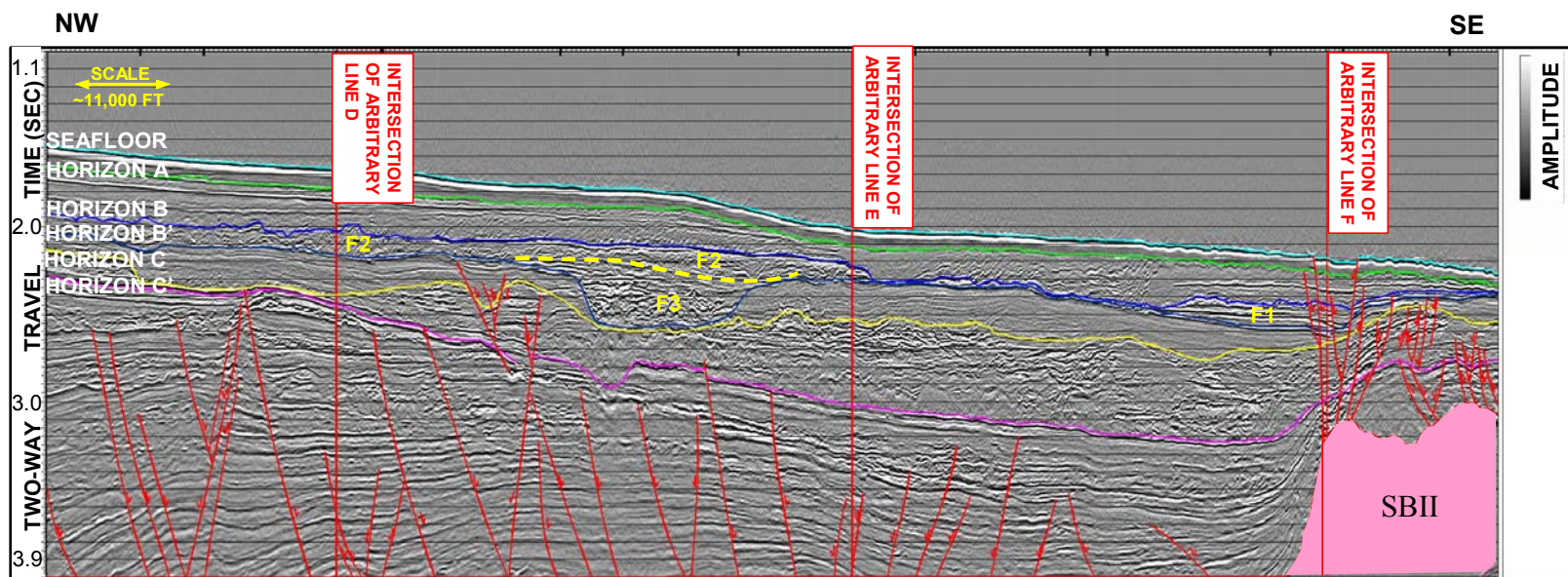


Figure 88. Arbitrary Seismic Line B showing Sequence IV facies. F1-F3 are Facies 1 through Facies 3 as defined in Table 6. Pink shaded area denotes salt. Colored lines denote mapped horizons. Red lines denote faults.

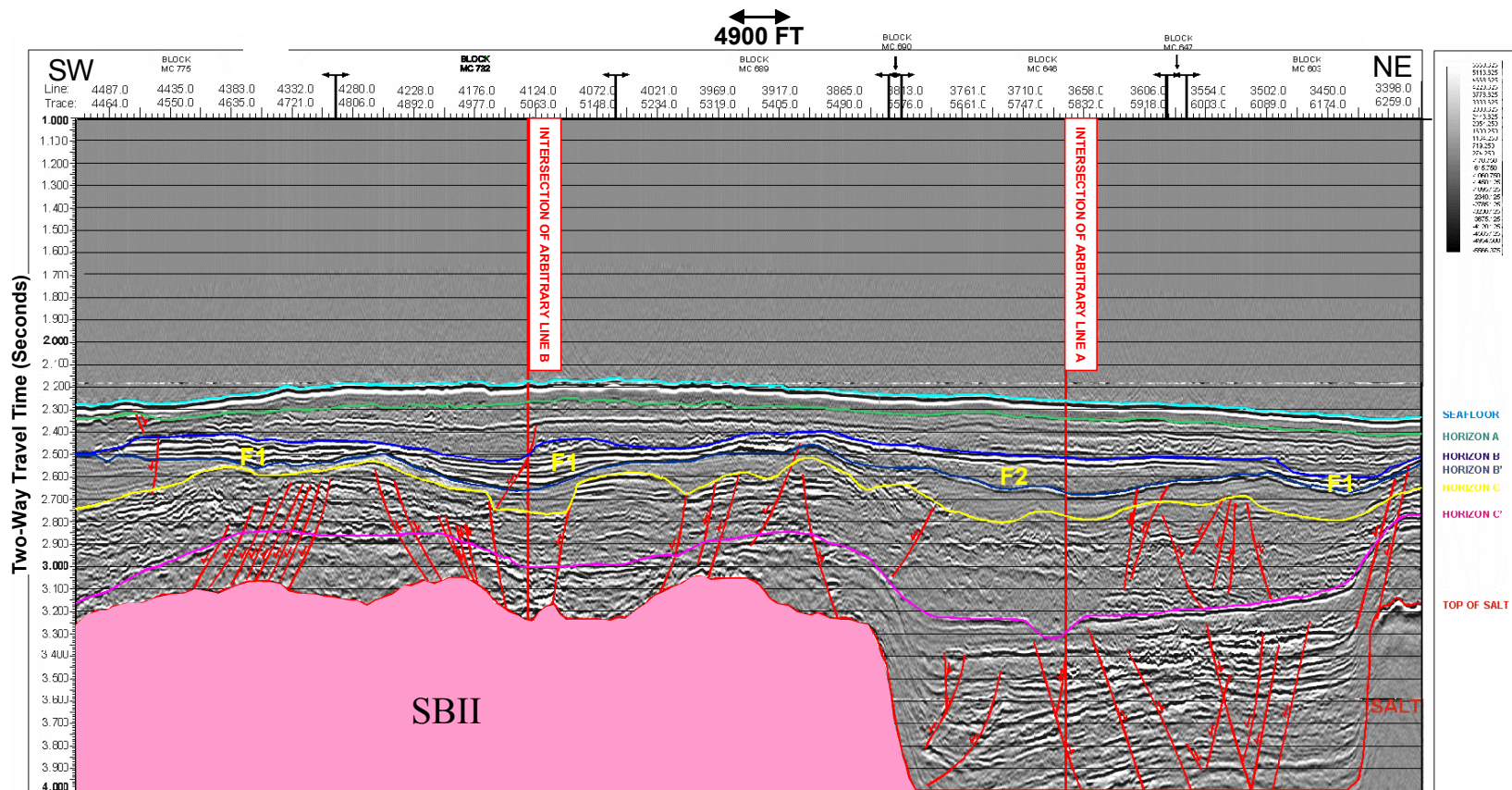


Figure 89. Arbitrary Seismic Line F showing Sequence IV facies. F1 and F2 are Facies 1 and Facies 2 as defined in Table 6. Pink shaded area denotes salt. Colored lines denote mapped horizons. Red lines denote faults.

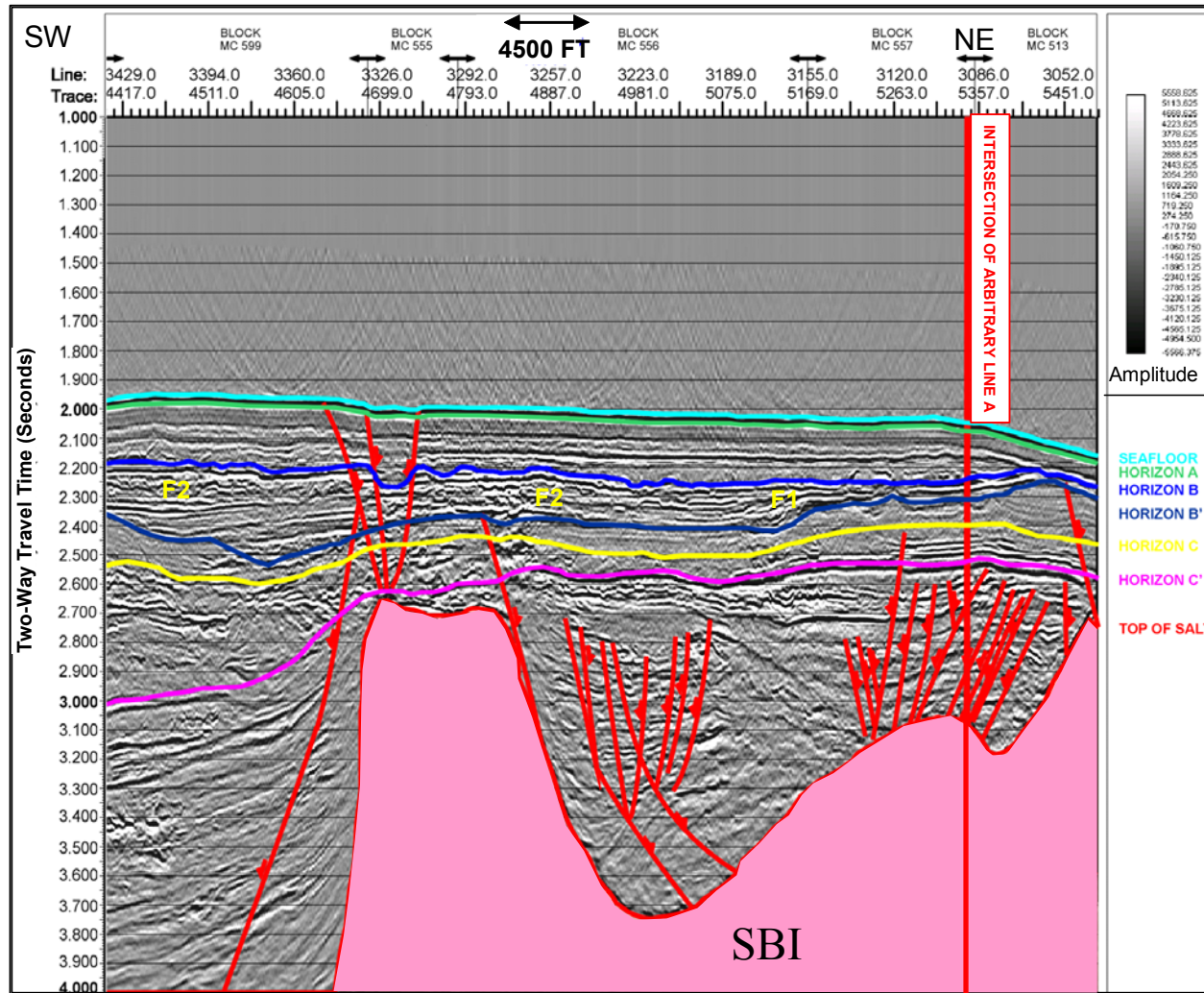


Figure 90. Arbitrary Seismic Line E line showing Sequence IV facies. F1 and F2 are Facies 1 and Facies 2 as defined in Table 6. Pink shaded area denotes salt. Colored lines denote mapped horizons. Red lines denote faults.

of sediments via mass wasting events by diverting them toward the basin. The basin provided a suitable topographic low for the deposition of these high-energy turbidites as they ran downslope.

Facies 2 is composed of moderate to high-amplitude, chaotic reflectors, and is interpreted to be debris slide or slump deposits of variable grain size and composition. Figure 91 illustrates the RMS amplitude of the sequence and illustrates the active depositional nature of the sequence. Facies 2 is distributed throughout the entire study area. Of note is the difference in the geologic facies associated with Gulfport and Chandeleur Valley (Figure 91). Gulfport valley trends southeast from the northwest corner of the study area. Here the facies is lower in amplitude and represent multiple episodes of fine-grained debris slide, slump, or mudflow deposits with mudflow deposits being the most dominant. In Chandeleur Valley, the amplitude is slightly higher and is interpreted to represent more active, higher-energy, coarser grained debris slide, slump, or turbidite deposits. Of note is the very large, well-defined slump feature in the center of the survey area. This slump actually occurs in Sequence V but has eroded the top of Sequence IV during failure and rotation.

Facies 3 is composed of high-amplitude, chaotic reflectors interpreted to be channeled, mass-transport deposits. This extent of Facies 3 is limited to the feature interpreted to be a channel that runs through the center of the survey. This channel, and associated facies, has deeply cut into underlying sequence III and, in some places, has possibly removed the sequence entirely. The edges of the channel also have appeared to have undergone incipient slumping possibly indicating that the channel was incised

rather quickly and then backfilled by smaller mass-transport events and slumps resulting from failure of the oversteepened channel banks. Some overbank deposits from this channel have been interpreted and are shown in Figures 88, 89, and 90. A possible scenario is that the channel was incised by the multiple, high-energy turbidites that were deposited in the basin to the south and form Facies 1. Subsequent mass-transport events such as debris slides and slumps subsequently filled the channel.

The full distribution of these seismic and geologic facies within the sequence is previously illustrated in Figure 91.

E. Sequence V: Horizon A to Horizon B

Sequence V is present throughout the study area (Figure 92 and 93). The top of the sequence, Horizon A, lies between 3800 and 6800 ft below the sea surface (structure map, Figure 92) and between 29 ft and 466 ft below the seafloor (isopach map, Figure 93). The base of the sequence, Horizon B, lies between 114 ft and 1262 ft below the seafloor (Figure 86). The sequence ranges between 0 ft to 986 ft thick (Figure 94). Sediments of the sequence thicken in areas associated with basin features and structural lows surrounding the uplifted salt bodies in the study area. Sediments are thinner in areas associated with these salt uplifts.

Sequence V contains two seismic and geologic facies. These facies are shown in Table 7. Seismic examples illustrating this facies are presented in Figures 95, 96, and 97. Facies 1 is composed of variable amplitude, inclined and chaotic reflectors and is

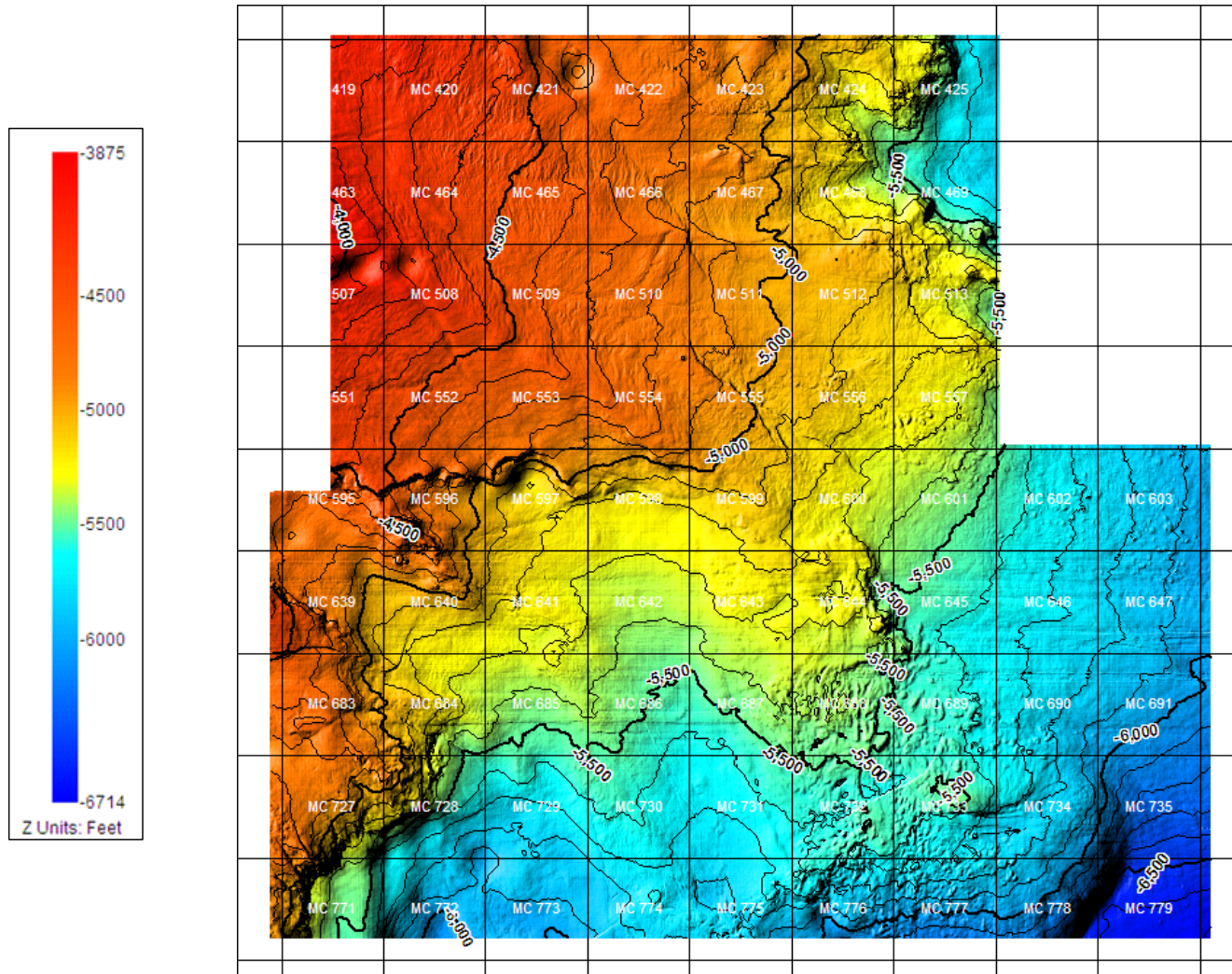


Figure 92. Structure map, Sequence V. Surface defined as depth from sea-surface to the top of sequence V (Horizon A). Contour interval = 100ft. Index Contour every 500ft.

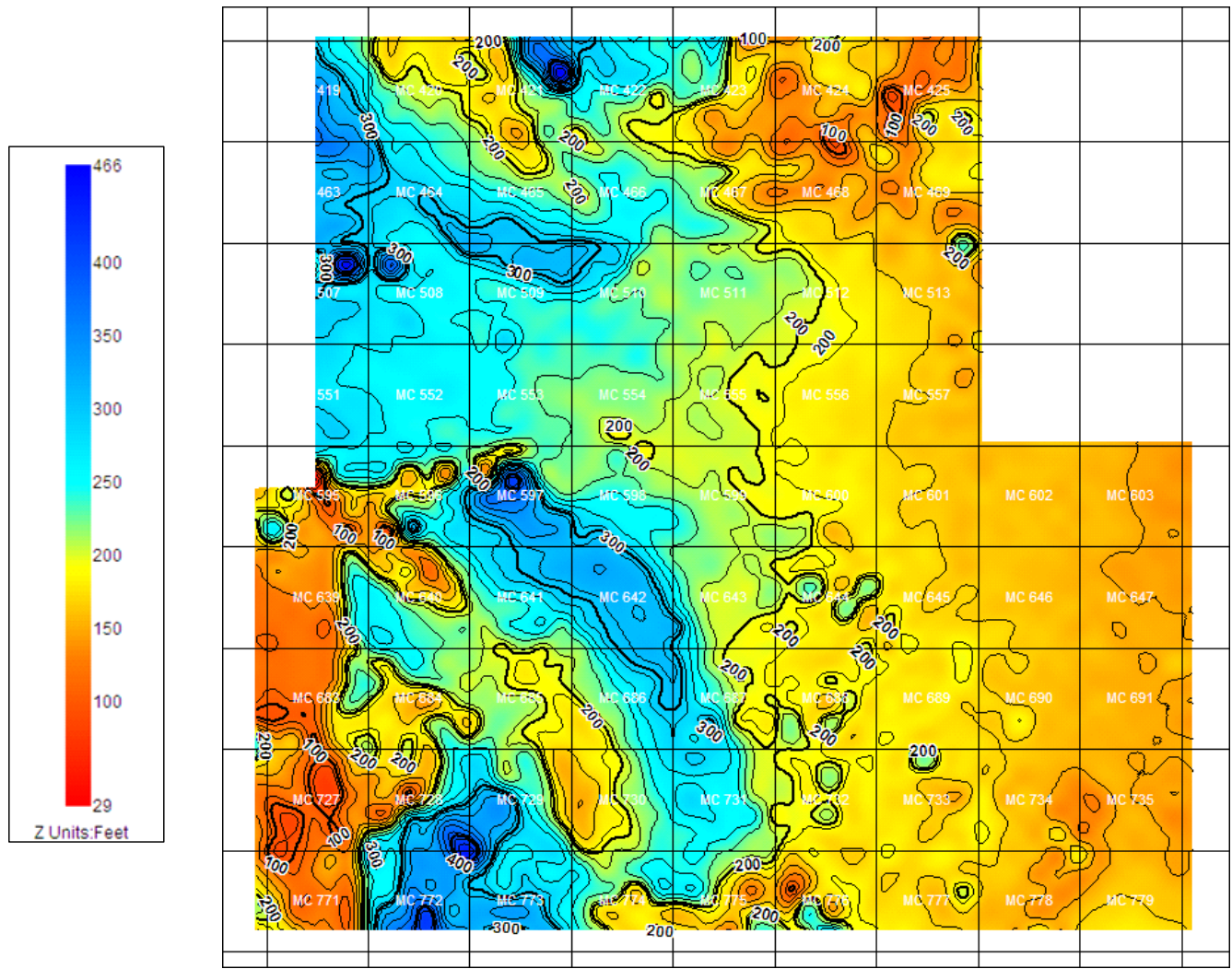


Figure 93. Isopach map, Sequence V. Image depicts thickness of sediment from seafloor to the top of sequence V (Horizon A). Contour interval = 20ft. Index Contour every 100ft.

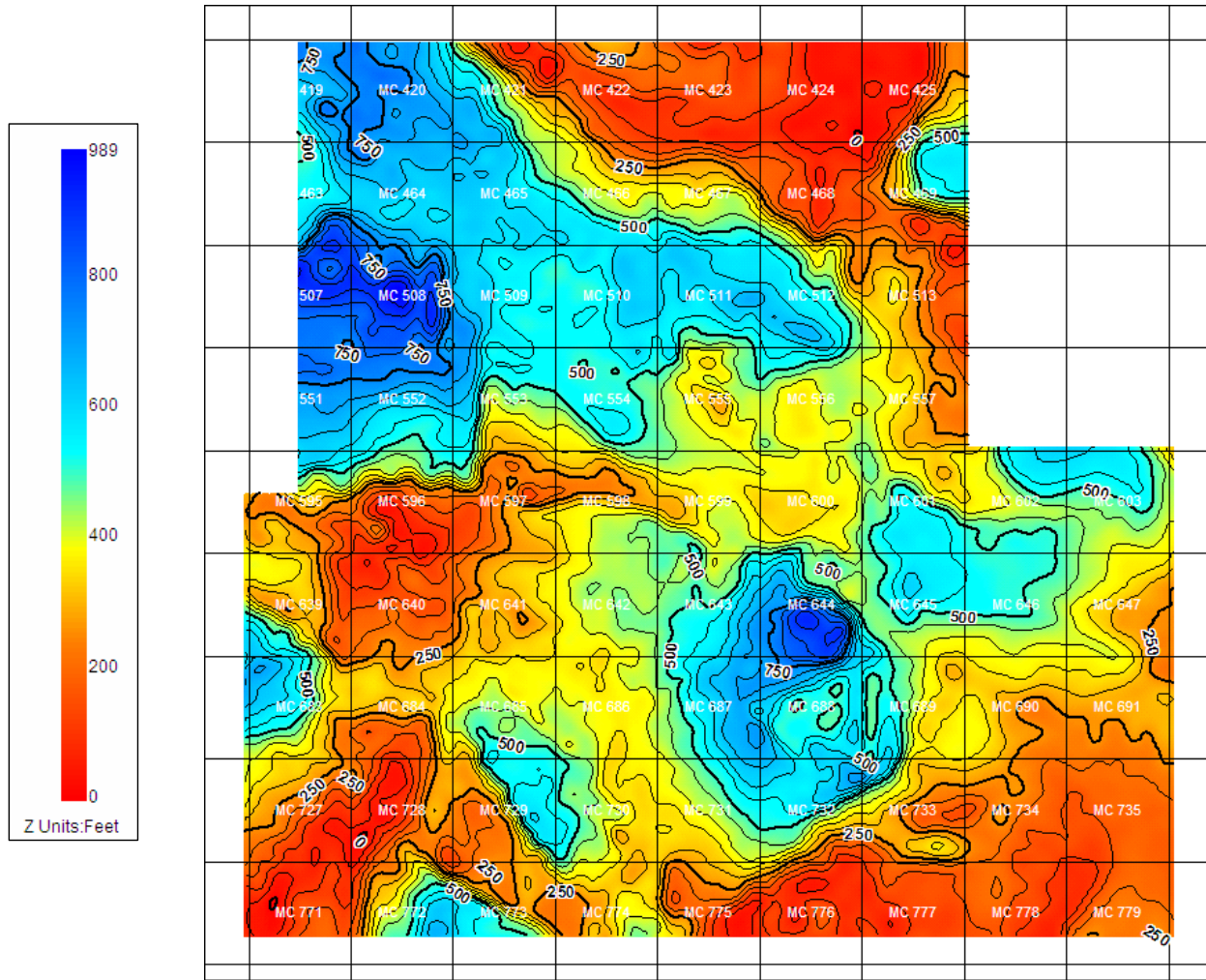
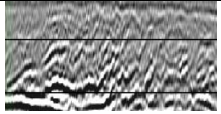
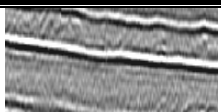


Figure 94. Thickness map, Sequence V. Image depicts thickness of Sequence V (Horizon A to Horizon B). Contour interval = 50ft. Index Contour every 250ft. Note increase in thickness in the lower central portion of the study area associated with thickening of sediments at the toe of the slump feature.

Table 7. Sequence V seismic facies.

Sequence V Facies Designation	Seismic Character	Seismic Interpretation	Geologic Interpretation
Facies 1		Variable-amplitude, inclined and chaotic reflectors.	Precontemporaneous deformed slump deposits.
Facies 2		Low-amplitude, chaotic reflectors separated by single, high-amplitude reflector..	Fine-grained debris slide and mudflow deposits separated by thin, condensed sections..

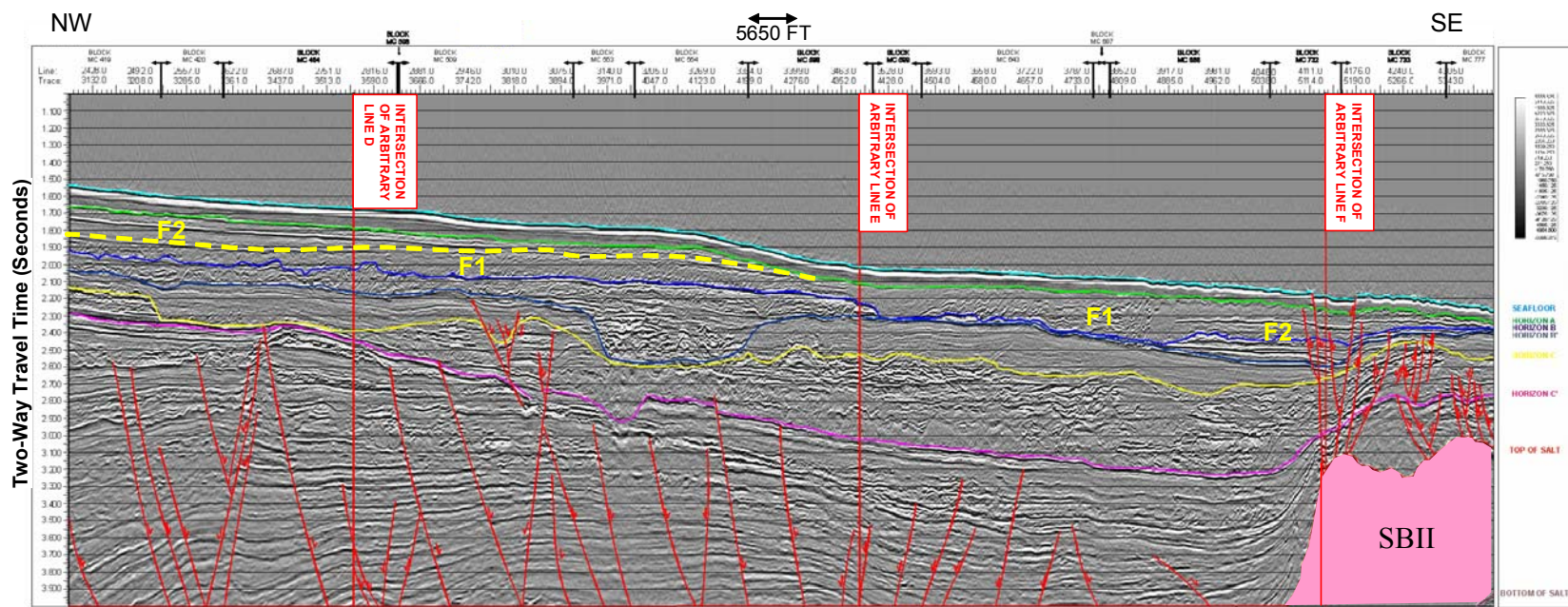


Figure 95. Arbitrary Seismic Line B showing Sequence V facies. F1 and F2 are Facies 1 and Facies 2 as defined in Table 7. Pink shaded area denotes salt. Colored lines denote mapped horizons. Red lines denote faults.

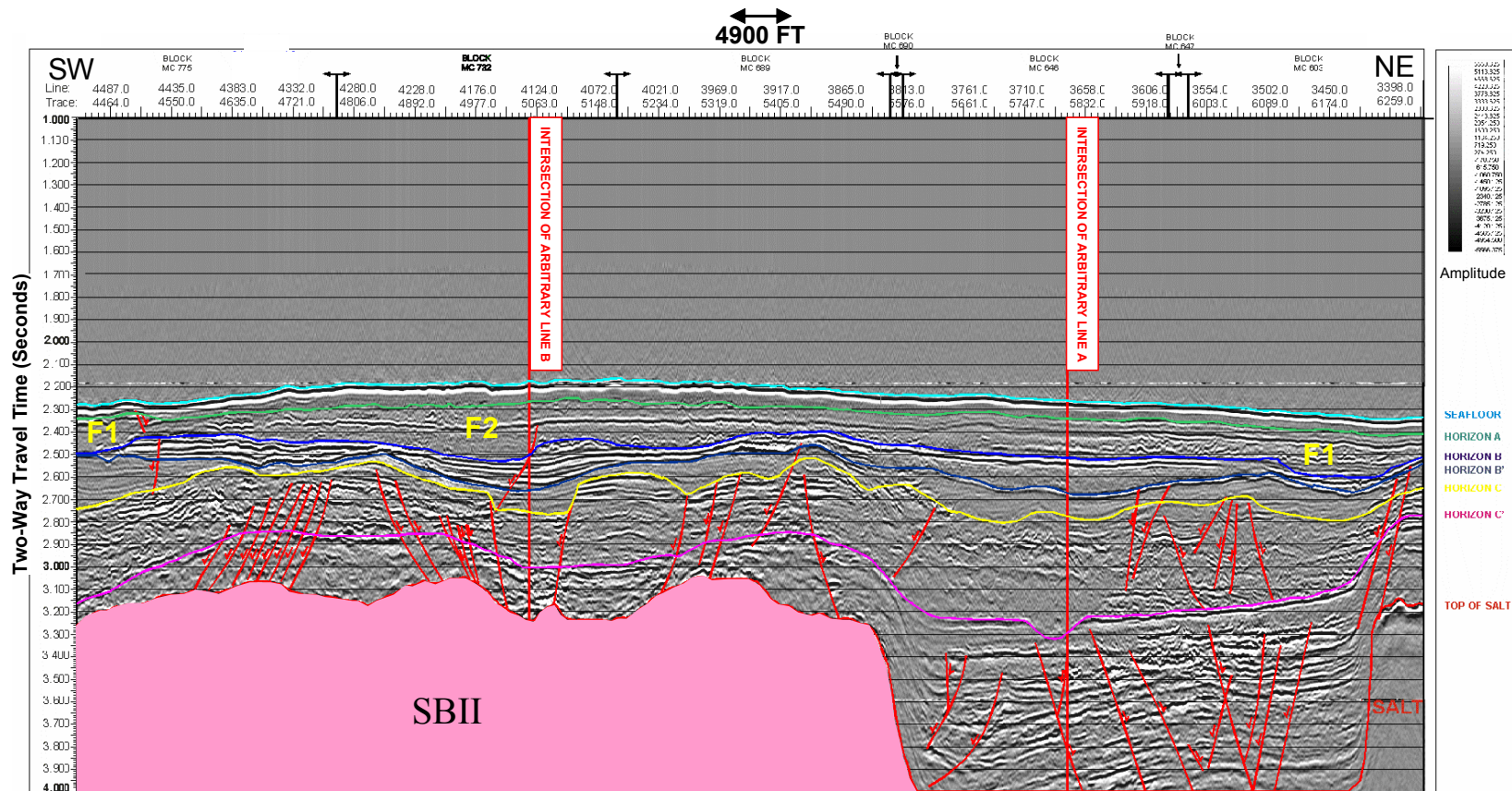


Figure 96. Arbitrary Seismic Line F showing Sequence V facies. F1 and F2 are Facies 1 and Facies 2 as defined in Table 7. Pink shaded area denotes salt. Colored lines denote mapped horizons. Red lines denote faults.

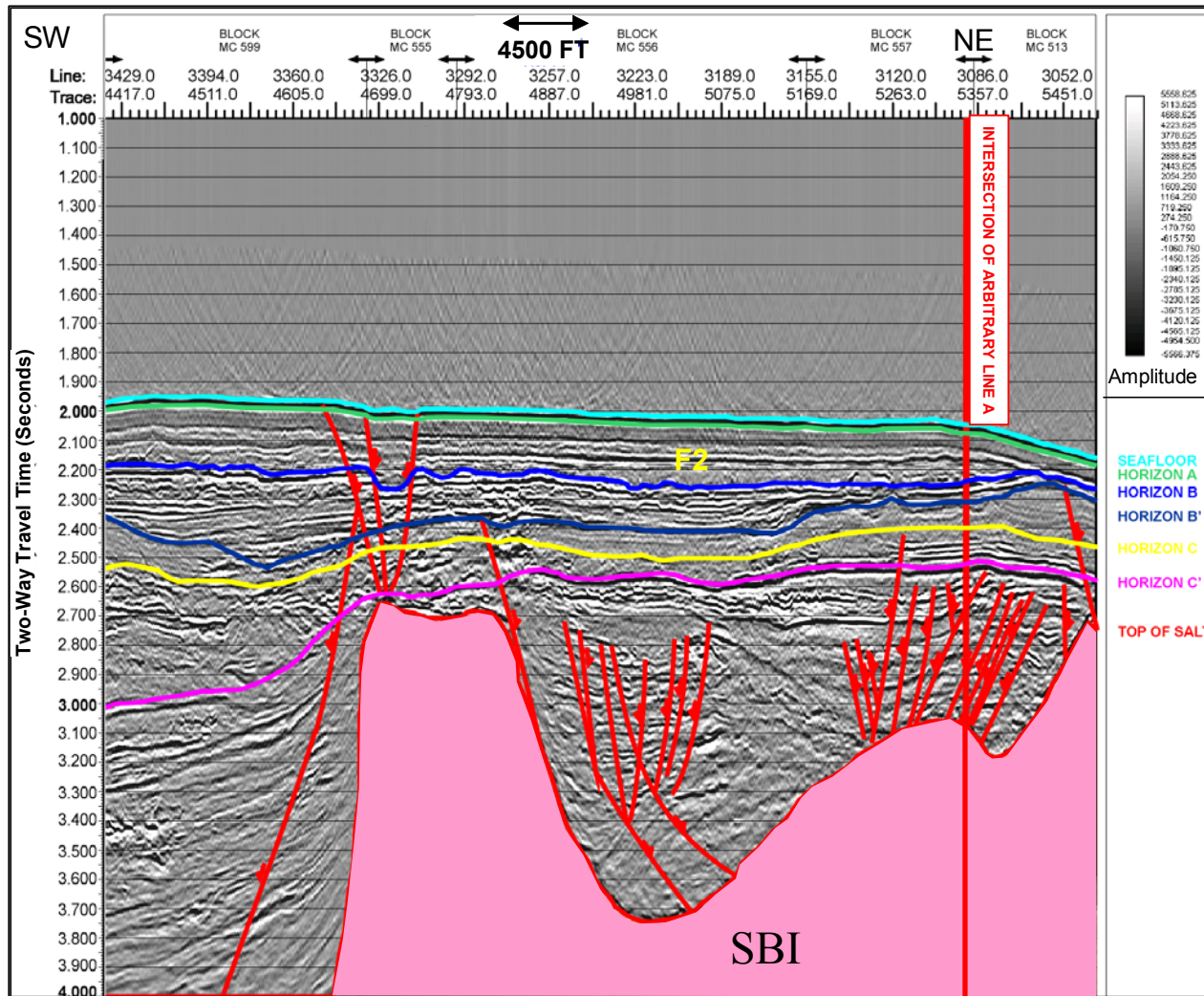


Figure 97. Arbitrary Seismic Line E showing Sequence V facies. F2 is Facies 2 as defined in Table 7. Pink shaded area denotes salt. Colored lines denote mapped horizons. Red lines denote faults.

interpreted to be deformed slump deposits. The facies is confined to one large slump event in the center of the study area. The entire sequence is deformed suggesting the slump must have occurred either near the end or shortly after the formation of Sequence V. The overlying sequence is not disturbed by the slump. The slump also has eroded and reworked sediments from the underlying Sequence IV evident from originally high-amplitude parallel continuous to discontinuous facies in the sequence now rotated and deformed into high-angled, imbricately thrust reflectors within the slump.

Facies 2 is present throughout the study area. It is composed of low-amplitude, chaotic reflectors each separated by a single high-amplitude reflector. The facies is interpreted to be predominantly fine-grained debris slide and mudflow deposits separated by thin condensed sections. Figure 98 illustrates the RMS amplitude of the sequence and illustrates the higher-energy depositional nature of both facies. Of note are the pronounced debris slide deposits at the mouth of Chandeleur Valley where intact blocks of debris can be identified. There are also potential levees and overbank deposits along the southern edge of the valley.

F. Sequence VI: Seafloor to Horizon A

Sequence VI is present throughout the study area (structure map, Figure 92). The sequence ranges between 40 ft to 466 ft thick (isopach map, Figure 93). Sediment thickness is relatively constant over the study area with only local variations in thickness (Figures 99, 100, and 101). Facies 1 is composed of low-amplitude to seismically

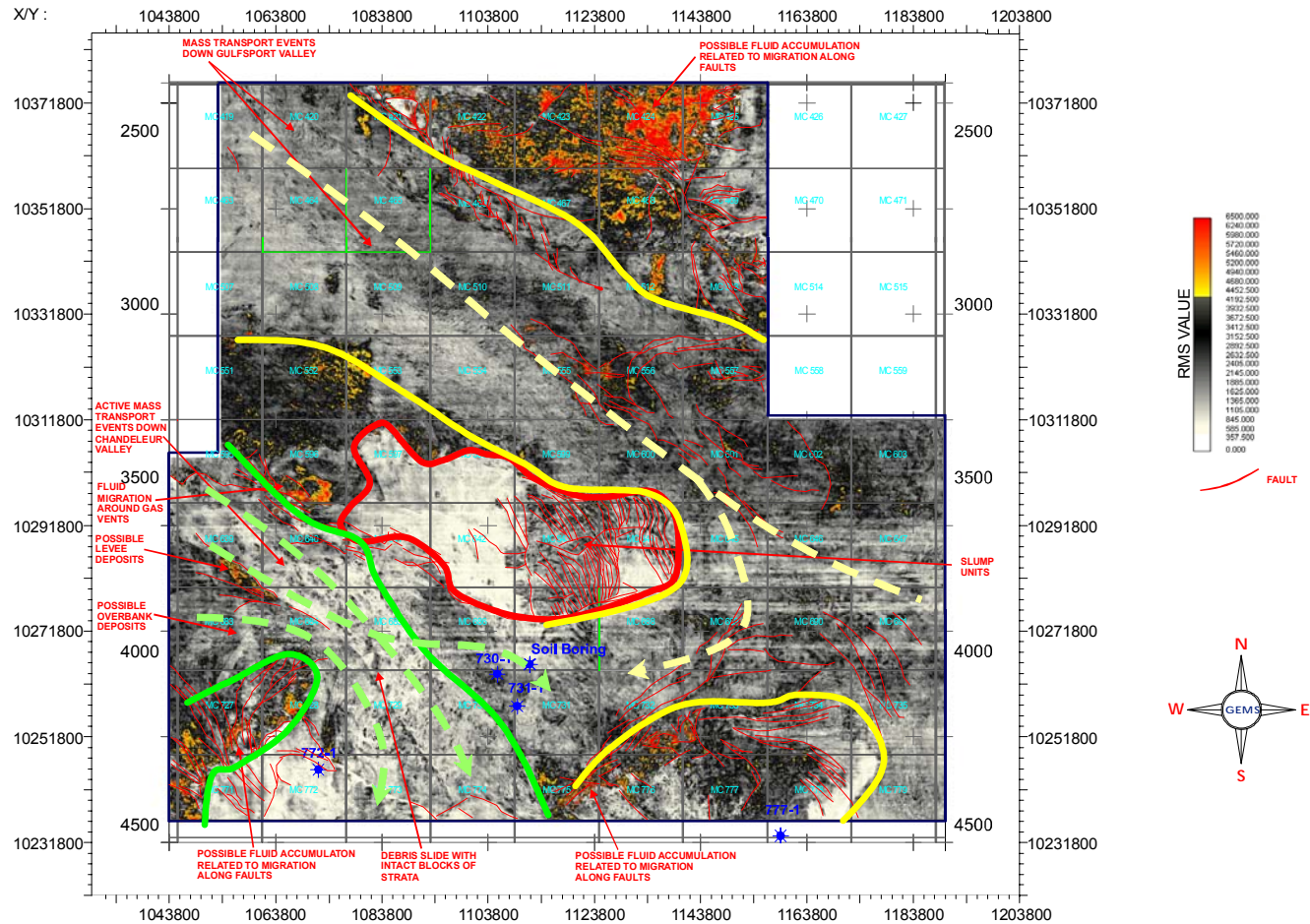


Figure 98. Sequence V RMS amplitude display. High RMS values (yellow to orange) are concentrated above the salt where fluids can migrate up faults (red lines), predominantly above SBI. Sequence morphology is evident on the RMS (white to black) as mass transport deposits down both Gulfport and Chandeleur valley are visible (bounded by yellow lines, proposed sediment pathways in dashed yellow). Activity down Chandeleur Valley appears greater with numerous, overlapping events inferred from the display (bounded by green solid lines, proposed pathways for individual events are dashed green). The large rotational slump near the middle of the study area is also evident on the RMS display (encircled by the thick red solid line). X/Y coordinates are NAD 27, UTM 16, USFT.

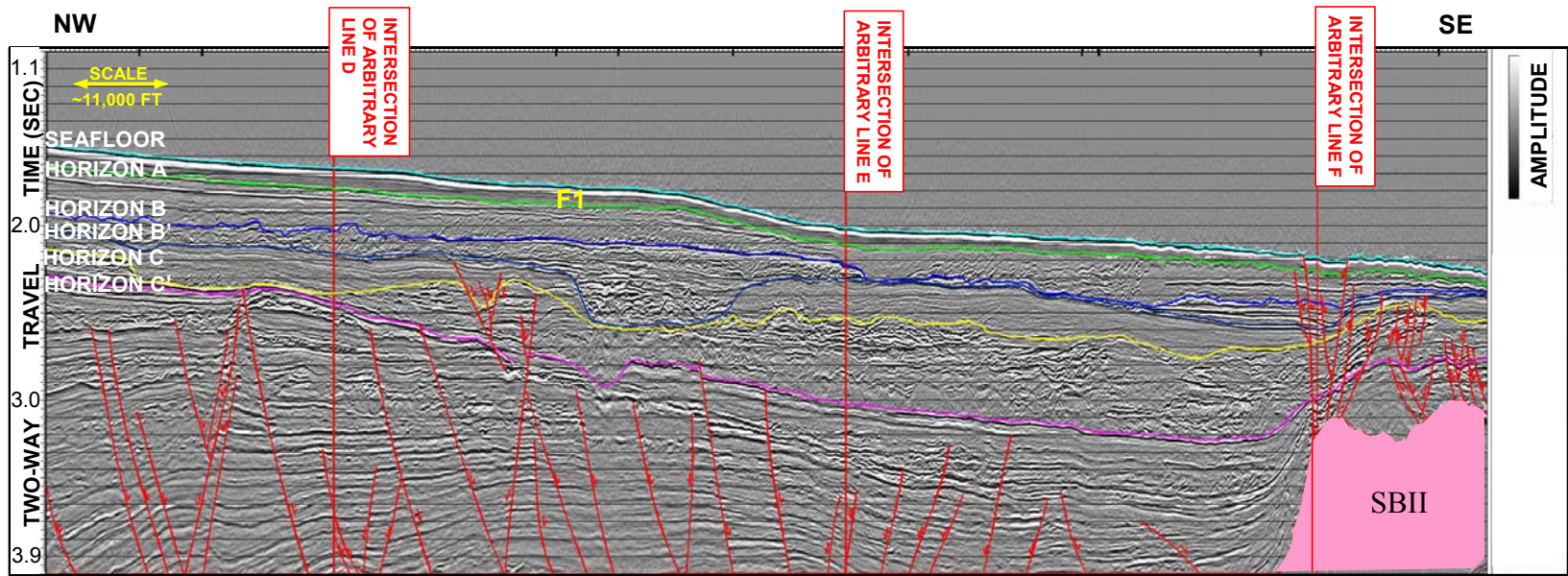


Figure 99. Arbitrary Seismic Line B showing Sequence VI facies. F1 is Facies 1 as defined in Table 8. Pink shaded area denotes salt. Colored lines denote mapped horizons. Red lines denote faults.

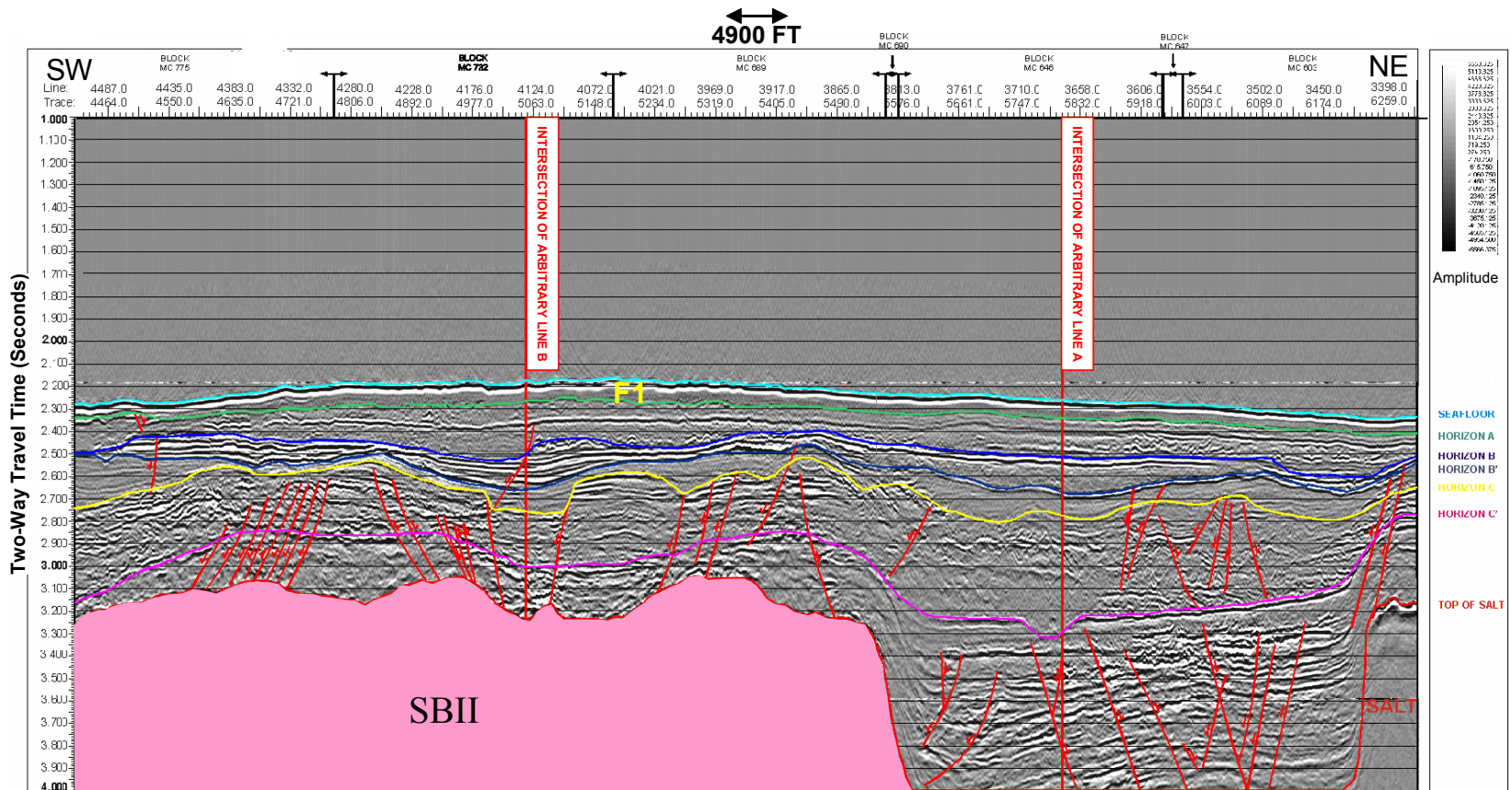


Figure 100. Arbitrary Seismic Line F showing Sequence VI facies. F1 is Facies 1 as defined in Table 8. Pink shaded area denotes salt. Colored lines denote mapped horizons. Red lines denote faults.

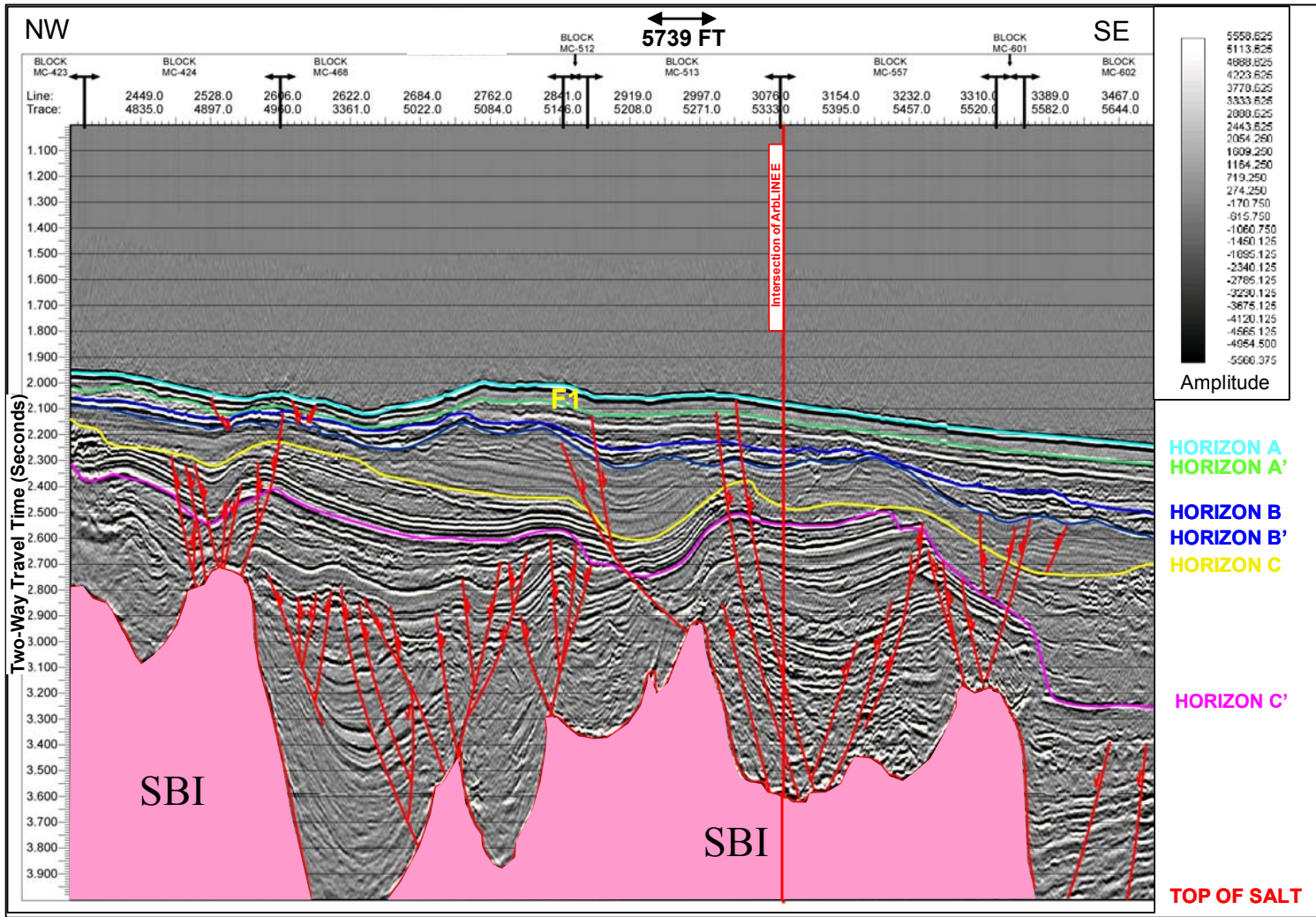
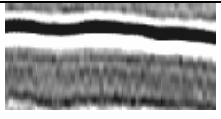


Figure 101. Arbitrary Seismic Line A showing Sequence VI facies. F1 is Facies 1 as defined in Table 8. Pink shaded area denotes salt. Colored lines denote mapped horizons. Red lines denote faults.

amorphous, parallel and continuous reflectors. Table 8 illustrates the seismic facies of the sequence. Facies 1 represents a condensed section composed of hemipelagic clays. This hemipelagic drape comprises the final and youngest sequence in the study area.

Table 8. Sequence VI seismic facies.

Sequence VI Facies Designation	Seismic Character	Seismic Interpretation	Geologic Interpretation
Facies 1		Low-amplitude to amorphous, parallel reflectors.	Hemipelagic sheet drape.

CHAPTER VI

STRATIGRAPHIC SEQUENCE CORRELATION

The study area lies to the north of the Eastern Mississippi Fan as defined by Dixon and Weimer (1998), Figure 27. This fan consists of sedimentary sequences whose primary source was from the Appalachian drainage area, whereas the ancestral Mississippi River provided sediments to the Western Mississippi Fan. Weimer (1989) identified 17 seismic packages of late Pliocene to Pleistocene (About 3 million yrs to 15,000 yrs B.P., before present) in the deeper stratigraphic sequence across the Mississippi Fan. The ages of the stratigraphic sequences were derived by work done by Walters (1985) who took age information derived from wellbores and was able to tie them to seismic reflectors and trace them seaward down the continental slope. Nine of the 17 sequences in the Western Fan are considered coeval with those of the Eastern Fan (Dixon and Weimer, 1994). These coeval sequences are 8-11 and 13-17 (Figures 33 and 34). Dixon and Weimer (1994) have interpreted these sequences to be fed by canyons located immediately east of the modern Mississippi birdfoot delta. These sequences are interpreted to be present in the study area making it possible to extend the interpretation of the Eastern Fan northward. This section describes the correlation between the stratigraphic sequences mapped by Dixon and Weimer and the stratigraphic sequences (Sequences I through VI) identified in this study.

Dixon and Weimer (1994) provided age constraints for the nine primary sequences in the Eastern Mississippi Fan. Table 9 illustrates the sequence number and the age of these sequences starting from youngest and proceeding to oldest.

Sequence 12 is not included by Dixon and Weimer (1994) in the correlation of Western Fan sequences and Eastern Fan Sequences. This is a result of active deposition occurring in the Western Fan but a depositional hiatus occurring in the Eastern Fan (resulting in a diastem). Thus, the sequence is not coeval (both sequence stratigraphically and chronostratigraphically) across both fans. Of note is the major expanse of time associated with Sequence 13. Sequence 13 is interpreted to have a series of stacked condensed sections at its top (Dixon and Weimer 1994). This thick series of condensed sections is interpreted to have occurred during a major westward shift in the Pleistocene depocenter (Figures 12, 24, and 33). This resulted in a condition of terrigenous sediment starvation to the Eastern Fan between 400,000 years BP to 71,000 years BP. This regionally extensive condensed section at the top of Sequence 13 has been identified as Sequence III in this study and is characterized by a thick, very low amplitude sequence bounded by high-amplitude sequences both above and below, conformable to Sequences 15/16 and the lower part of Sequence 13, respectively. This condensed section is the key to extrapolating Dixon and Weimer's sequences for the Eastern Fan to the study area. It is the common reference point from which the relative ages of Dixon and Weimer's sequences can be correlated with the sequences mapped in the study area. Once established, a comparison of the facies within the shallower and

Table 9. Sequence number and age of stratigraphic sequences defined by Dixon and Weimer (1994).

Sequence Number (Dixon and Weimer 1994)	Interpreted Sequence Age (Dixon and Weimer 1994)
17	23,000 years BP to Present
16	40,000 years to 23,000 years BP
15	55,000 years to 40,000 years BP
14	71,000 years to 55,000 years BP
13	450,000 years to 71,000 years BP
12	500,000 years to 450,000 years BP
11	600,000 years to 500,000 years BP
10	700,000 years to 600,000 years BP
9	800,000 years to 700,000 years BP
8	1,100,000 years to 800,000 years BP

deeper stratigraphic sequences with those defined by Dixon and Weimer found good correlations between the two, down to Sequence I.

The correlation between sequences extends the area mapped as the Eastern Mississippi Fan approximately 50 miles northward. Table 10 illustrates the interpreted correlation between the Eastern Fan sequences, and respective ages, mapped by Dixon and Weimer and those mapped during this study. The following is a discussion of the correlation of facies and depositional processes between those sequences mapped by Dixon and Weimer and those mapped during this study. These sequences will be correlated starting with a discussion of the oldest sequence in the study area, Sequence I, and moving to the youngest sequence in the study area, Sequence VI.

Sequence I is the most difficult sequence to correlate as the seismic record in the study area extends to only 4.00 seconds below the sea-surface and the base of this sequence is interpreted to extend beyond the limit of the seismic data. Thus the bottom of the sequence(s) cannot be determined or correlated. Sequence I may be Sequences 8-12 as defined by the works of Dixon and Weimer (1994, 1998). However, there is another possibility as to the age of the sequence.

The palipinastic model reconstructions by both Wu et al. (1990a) in Figure 29 and Schuster (1995) Figure 55 both show the stratigraphic section to be deformed until the Pleistocene, with overlying strata on top of the salt structures being purely Pleistocene. These two independent constructions place the boundary or the Pliocene and the Pleistocene to be at the level of Horizon C', the top of Sequence I. It is therefore plausible that Sequence I may consist of Pliocene-aged strata with Horizon A being the

Table 10. Sequence correlation and inferred ages of sequences between those defined by Dixon and Weimer (1994) and this study.

Sequence Number (This study)	Sequence Number (Dixon and Weimer, 1994)	Interpreted Sequence Age
VI	17	23,000 years BP to Present
V	16,15	55,000 years to 23,000 years BP
IV	14	71,000 years to 55,000 years BP
III	Top of 13	400,000 years to 71,000 years BP
II	Bottom of 13	450,000 years to 400,000 years BP
I	8,9,10,11,12(?) OR Pliocene/Pleistocene Boundary (?)	1,100,000 years to 450,000 years BP

Pliocene/Pleistocene boundary. This would imply a significant depositional hiatus or unconformity at the Pliocene/Pleistocene boundary in the study area. The remaining interpretations and correlations of the sequences of the Eastern Fan to the study area are still considered valid as both reconstructions have the remaining section defined as Pleistocene and there are excellent correlations between the remaining sequences when hung on the condensed sections of both Sequence III (Top of Sequence 13 for Dixon and Weimer) and Sequence VI (Sequence 17 for Dixon and Weimer). Sequence II has been interpreted to be contain facies associated with at least two, massive submarine slide events. Sequence II is interpreted to be representative of the bottom part of Weimer sequence 13. Dixon and Weimer (1994, 1998) describe the lower half of Sequence 13 of the Eastern Fan to be composed entirely of massive submarine slide deposits. The largest slide is described as being greater than 5000 sq. km in area, similar to slides present on the lower continental slope northwest of Dixon and Weimer's study area. The study area for this research lies immediately northwest of their study area and would have been impacted by the same submarine slide events. This is evident in the facies of Sequence II being entirely composed of submarine slide deposits and are quite similar to those described for Sequence 13. No other massive submarine slide sequences are found in the upper sequences of the Eastern Mississippi Fan which further substantiates the correlation between Sequence III of this study and the bottom of Sequence 13 by Dixon and Weimer.

Dixon and Weimer also discuss the association of condensed sections as suitable decollement surfaces for the initiation of submarine slides that could have facilitated the

large submarine slides. It has already been acknowledged that there may be one or more interpretations for the age of Sequence I, being either Sequences 8-12 of the Eastern Fan, or, the Pliocene/Pleistocene boundary. Sequence 12 was previously defined as not being coeval between the Western Fan and the Eastern Fan (Dixon and Weimer, 1998) as there was a lack of deposition during its formation in the Eastern Fan. The results would have been a nonconformity or condensed section. The condensed section of Weimer's Sequence 12 (at the top of Sequence I) may have been present and subsequently eroded/reworked by the submarine slides of Sequence II. If the top of Sequence I is the Plio/Pleistocene boundary then there is a significant unconformity between Sequence I and Sequence II that has occurred either via significant erosion or a prolonged period of no deposition resulting in a diastem.

Sequence III is interpreted to be representative of the top part of Weimer Sequence 13. Dixon and Weimer (1994, 1998) describe a series of stacked condensed sections that occurred during an extended period of sediment starvation to the Eastern Fan from approximately 400,000 years to 71,000 years BP. This time of depositional quiescence signifies a major westward shift in the Pleistocene depocenter of the Mississippi Delta from its location from the eastern Green Canyon area to the Mid-Louisiana shelf. The ages of this shift is confirmed by (Berryhill et al., 1986). This would infer that the sediment supply to the Eastern Fan was, in some part, had the Mississippi River as its source and, and not an entirely separate depositional source as Dixon and Weimer have inferred. Sequence III is interpreted to be a stacked series of condensed sections; similar to those described by Dixon and Weimer. Sequence III

exhibits very low amplitude, almost seismically amorphous character resulting from very little change in the soil properties (and thus depositional environment and rate) for the section. Generally, condensed sections are seen as single high-amplitude reflectors, however, given the amount of time (~330 ky) within the sequence, a thicker, low-amplitude to amorphous character is reasonable. It should be noted that the thickness or properties of a section do not define a condensed section. Condensed sections are called such because time is condensed in the section. In other words, the section is not as thick as one would expect for a given period of time using average depositional rates for the Gulf of Mexico. So, for Sequence III, the “thick” condensed section is not an oxymoron, rather, it signifies a very large amount of time where sedimentation rates were quite low. The correlation between Sequence III and the top of Sequence 13 is the common reference point, via the condensed section, for the correlation of the sequences mapped in the study area with those already mapped for the Eastern Mississippi Fan.

Sequence IV is interpreted to be representative of Weimer Sequence 14. Weimer (1989) described this sequence as being composed of a number of channel, levee-overbank, fine-grained turbidite, and mass-transport complex deposits. Sequence IV has been interpreted to be comprised of coarse-grained turbidites, debris slide and slump facies, and channeled mass-transport deposits. A well defined, west to east trending channel is present in the center of the study area (Figures 82 and 102). Figure 102 is a perspective view of the base of the channel in the study area. The work of Dixon and Weimer noted an eastward shift in the depositional system that formed Sequence 14 (Sequence IV). This in turn led to the formation of a new canyon system to

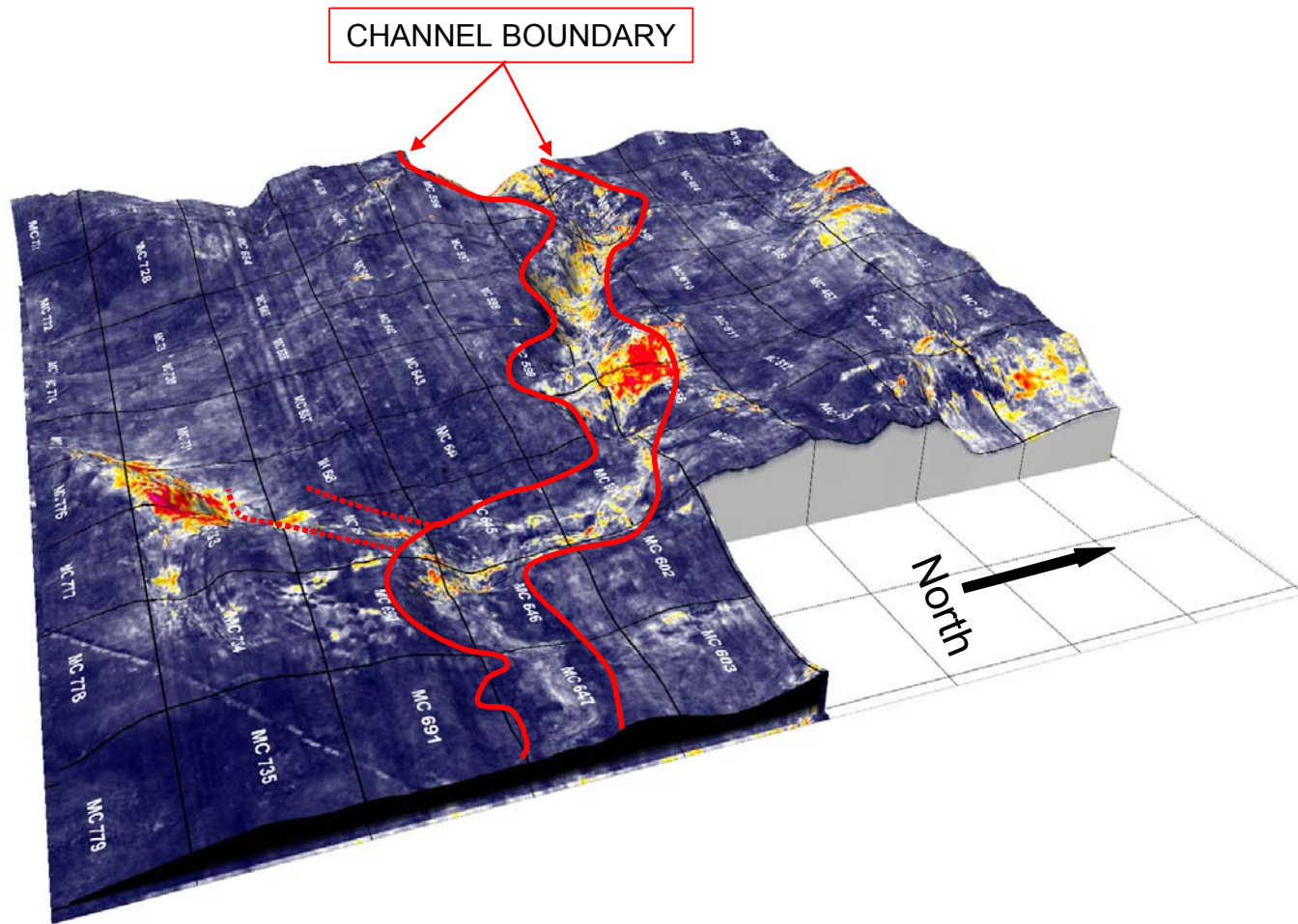


Figure 102. Perspective view of Sequence IV channel structure with RMS overlay. Surface is structure map from sea surface to base of Sequence IV (Horizon B'). RMS display is of Sequence III. Location of the channel is more prominent in the RMS for Sequence III due to the overall low-amplitude of the condensed sequence (Blue to gray colors). High amplitudes associated with the Sequence IV channel (Yellow to Red) that incised into Sequence III are therefore better expressed and result in the base of the channel's course being more evident.

accommodate the transmission of sediments from the shelf to the slope. Weimer identified three channels within this sequence. Of note is Channel 14a (Figure 103), which developed with this shift in depocenter and has been identified within Sequence IV. The channel in the study area correlates with channel 14a mapped by Dixon and Weimer (1998) in the Eastern Mississippi Fan. This channel trends west to east and has been interpreted to be the eastern extension of the channel identified in this area (Figure 103). The channel in Sequence IV is presumed to be Channel 14a because the two channels are present in the same sequence and line up and connect to each other perfectly at the eastern edge of the study area (Figure 103). Extending Channel 14a westward through the study area implies that the source of this channel was the newly formed depocenter associated with the Mississippi River and not the canyon system located in the Mobile Bay area, supposedly sourced from the separate Appalachian drainage area.

Sequence IV also contains a thick unit of coarse-grained, high-energy turbidite deposits. These deposits are composed of high-amplitude, subparallel seismic facies. Weimer described the nature of these facies as being sediments that were transported through a channel (interpreted to be Channel 14a from this study) and deposited beyond. The location of these deposits is confined to a topographic low between two salt bodies in the study area. This study concurs with the interpretation of Weimer as it is likely these coarse-grained turbidites passed through the channel and were deposited into the salt-constricted basin south of the channel (Figure 104). These deposits are also significant in that they may represent a basin floor fan complex and are interpreted to be

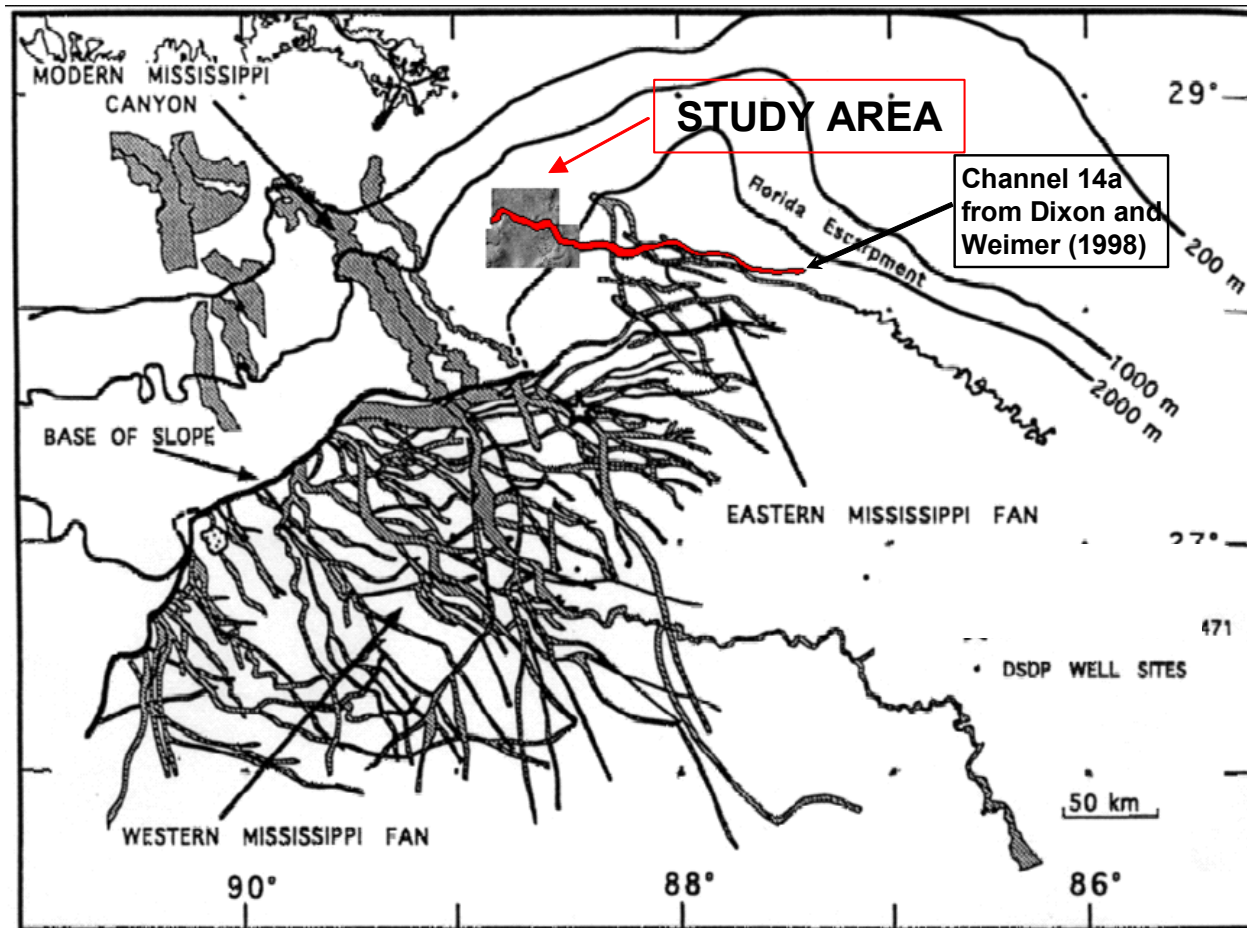


Figure 103. Location of channel (this study) in relation to previously mapped fan channels. Channel is in Sequence IV of this study which correlates to Channel 14a of Sequence 14 from Dixon and Weimer (1998). Gray image of study area is structure map to base of Sequence IV. Red channel is a composite of the course of Channel 14a previously mapped by Dixon and Weimer (1998) and further extended westward through the study area by this study. Previous channels from Dixon and Weimer (1998). Gray areas in the Eastern Fan and below Base of Slope in the Western Fan are defined channels. Gray areas above Base of Slope in the Western Fan, in the upper left of the image, are known shelf/slope canyon systems.

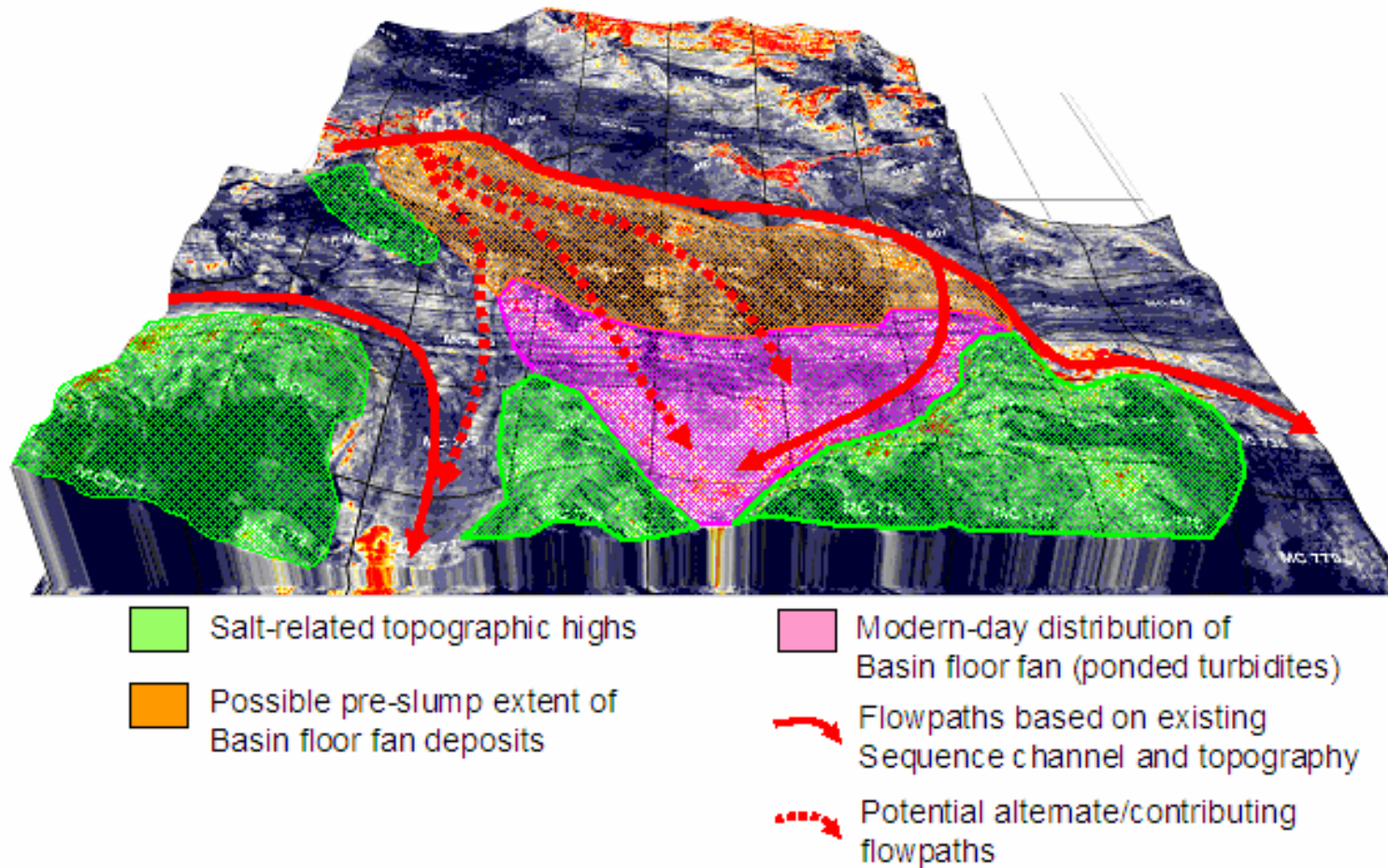


Figure 104. Deposition of ponded turbidites in salt-constricted basin in this study. The salt related topographic highs (green) divert mass-transport deposits (i.e. turbidities) into the interspersed salt-constricted basins. Ponded turbidites in Sequence IV traveled downslope in the channel in the sequence and accumulating, via a number of potential pathways, in the topographic low between salt highs. Background image is perspective view of structure map to the base of Sequence IV overlain with the RMS display for the same sequence.

such. Dixon and Weimer (1998) were only able to identify one basin-floor fan in the Eastern Fan for their study area. This fan was identified in Sequence 9. The fan deposits were identified by their limited areal extent, mounded cross section with bi-directional downlap, proximity to salt highs, and characterization by high-amplitude, laterally continuous reflections. Table 6 and Figure 105 illustrate the nature of the interpreted basin floor fan facies in Sequence IV. The basin floor fan in Sequence IV (Sequence 14) is now the second fan sequence to be identified in the Eastern Mississippi Fan and not only has geohazard implications, but also provides a geologically recent analogue to older, sand-rich, topographically-constricted, basin floor fan systems in this portion of the Mississippi Canyon area that may be of interest for hydrocarbon exploration.

Sequence V is interpreted to be representative of Weimer's Sequences 15 and 16. Weimer describes these sequences to be composed of numerous small slides. These slides were interpreted to have formed on very low slope gradient ($<0.5^\circ$) fan surfaces. These gradients are very much like those of the modern seabed slope in the study area of this research (Figure 106, slope figure). Weimer describes the slides of these sequences within the center of his study area to be composed of stacked facies indicating that older slides may have influenced the location of younger slides. These slides are separated by prominent condensed sections representative of periods of time between slide events. The detachment surfaces of these slides are found to occur on top of these condensed sections (Dixon and Weimer, 1998). Condensed sections have been noted to be failure surfaces on the continental slope of the Gulf of Mexico

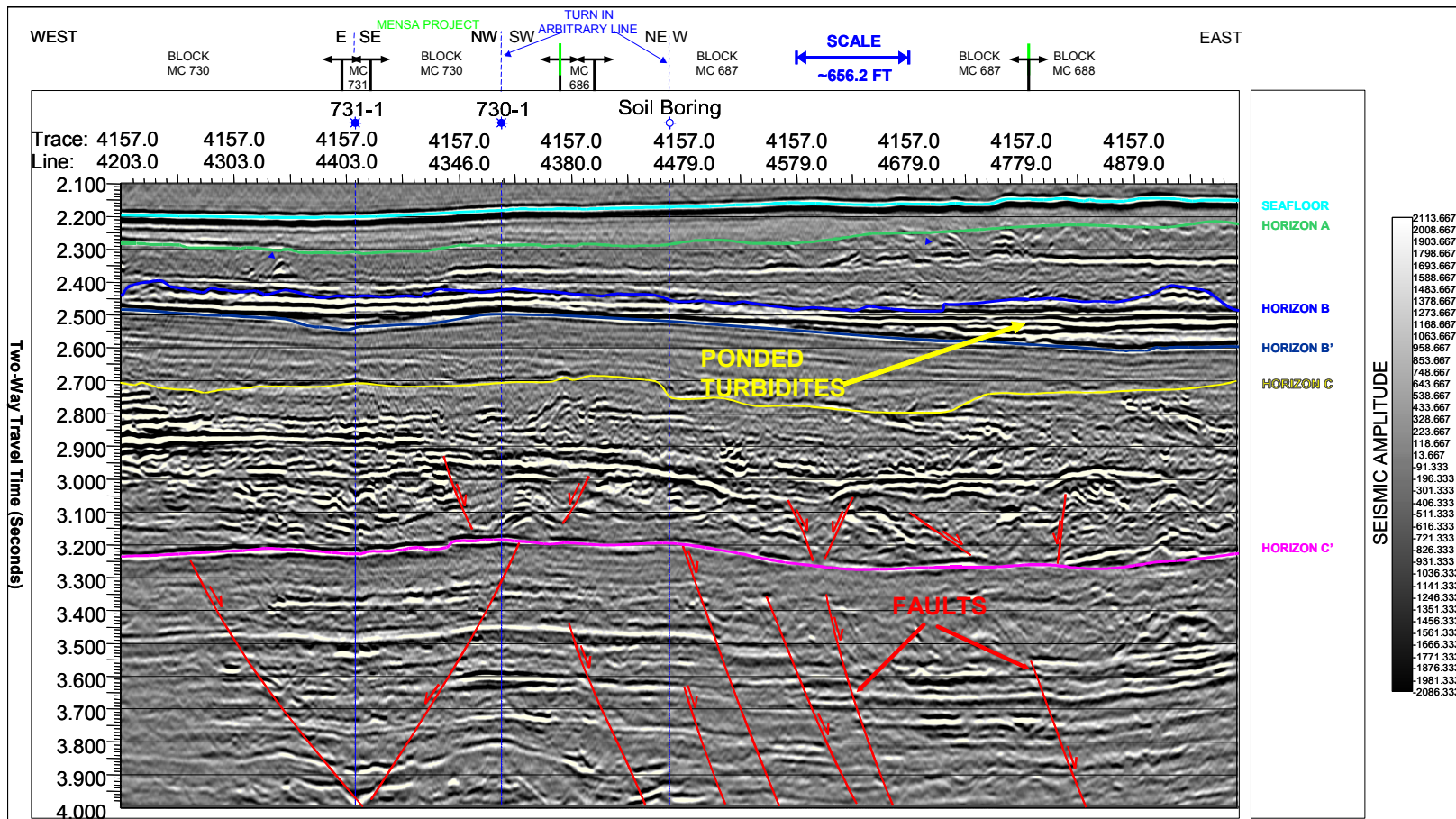


Figure 105- Ponded turbidite facies in Sequence IV.

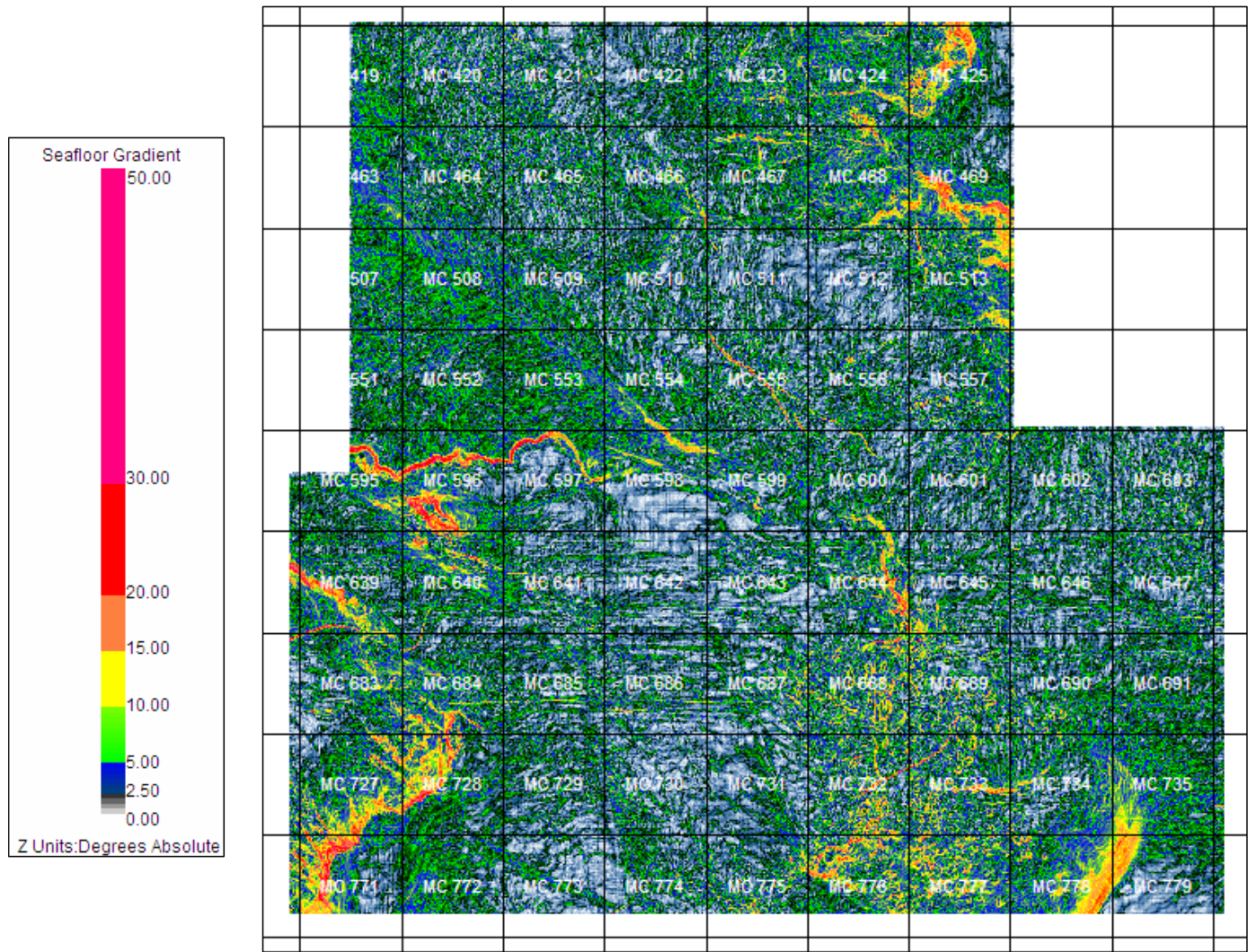


Figure 106- Seafloor gradient map.

(Doyle et al., 1996; Roberts, 1993). The condensed sections appear to be a relatively weak geotechnical unit along which failure can occur. Weimer also posited that the location of these smaller slides is proximal to shallow salt bodies, the movement of which is identified as a possible catalyst for slide initiation. Sequence V contains stacked chaotic facies interbedded with single-wavelet high-amplitude reflectors. The seismic character and geometry of facies in the sequence has been interpreted to be debris slide and slump facies separated by thin, seismically prominent, condensed sections and correlates to the facies description of Weimer's Sequences 15 and 16. Of note is the large rotational slide in the center of the study area and its proximity to the shallow salt body immediately west of the headscarp of the slide. This small slide is likely analogous to the process of slope failure where a portion of the slope, oversteepened from salt uplift, fails along an underlying condensed section resulting in the deposition of slump deposits. Evidence of numerous slides is illustrated in Figure 91. Also of note is the apparent increase in depositional activity in Chandeleur Valley (Figure 91) and a decrease in depositional activity in Gulfport Valley (Figure 91). This may possibly be representative of a westward shift in depocenter causing more sediment to travel down Chandeleur Valley than Gulfport Valley. It may also represent an increase in salt movement in the region northeast of the study area, spurring the debris slides that have traveled down Chandeleur Valley.

Sequence VI is interpreted to be representative of Weimer's Sequence 17 where both sequences are condensed sections. Figure 32 illustrates the shallow sequences for both the Western and Eastern Mississippi Fan. Sequence 17 of the Eastern Fan is not

depositionally coeval with that of the Western Fan. During active deposition of Sequence 17 in the Western Fan, there was very low or deposition in the Eastern Fan. The non-deposition in the Eastern Fan has resulted in a condensed section that continues to the present day with correlation between Sequence 17 for the Eastern fan and Sequence VI of this study.

CHAPTER VII

GEOLOGIC MODEL

Introduction

The stratigraphic section in the study area is a result of the interaction of salt tectonics and upper continental slope depositional processes associated with changes in eustatic sea level. Models describing the effects of eustatic fluctuations on deposition within the Mississippi Fan Complex (western and eastern fans) have been discussed by in numerous previous studies (Bouma et al., 1986; Bouma et al., 1989; Bouma et al., 1992; Bouma and Coleman, 1985; Feeley, 1984; Feeley et al., 1985; Feeley et al., 1990). The timing and distribution of sequences within the eastern fan has been controlled by both salt tectonics and Pleistocene eustatic cycles. Correlated condensed sections between active transport sequences in the two fans suggest that eustatic levels control the rate and type of deposition in both fans. During highstands, there was relatively low deposition composed of primarily hemipelagic sediments and some small-scale mudflows. High influxes of sediments occurred during lowstands and early transgression to highstand (Kolla and Perlmutter, 1993). The general depositional model for the eastern fan can be described as follows: relative sea level began to fall during the early Pleistocene, deltas prograded to the pre-existing shelf margin and incised valleys began to form on the shelf. With continued fall in sea level, the valleys either formed

submarine canyons or became connected to pre-existing submarine canyons providing conduits for the rapid delivery of sediments to the deep slope. While sea level remained low, well-defined channel/levee systems were defined in the overall coarse-grained sediments delivered to the mud-dominated eastern fan. As sea level rose, gradually finer sediments, eventually filled in the valleys and channels. At highstand, sedimentation was significantly reduced with formation of a condensed section. Slides and slope failures occurred at any given time during the eustatic cycle and may be caused by the interaction of rapid deposition on slopes and oversteepening of the seafloor slope by tectonic movement of salt. Continued salt movement beyond lowstand, in response to low stand loading of sediments, may be the cause of slides occurring at any point in the eustatic cycle.

Due to the lack of available data, the ages of sequences within the eastern Mississippi Fan are difficult to accurately determine. Several studies have described the stratigraphy within the Western Mississippi Fan (Dixon and Weimer, 1994; Feeley et al., 1990; Weimer, 1989; 1990, 1991). The chronostratigraphic work by Dixon and Weimer for the western fan has been transferred to the coeval sequences of the Eastern Fan. The age of the Eastern Fan is estimated to be 1.1Ma to 0.023 Ma (Pleistocene). The correlation between sequences 8-11 is straightforward with coeval condensed sections. The large series of condensed sections at the top of sequence 13 also represents a large period of non-deposition that can be traced between both fans. These correlations can be further applied to Sequences I through VI in the study area, which correspond to sequences 11 through 17 and are all interpreted to be Pleistocene in age.

The formation of the shallow stratigraphy in the study exemplifies the interaction of salt-tectonics and slope depositional processes through varying phases of the sea-level cycle. Figure 107 illustrates the general depositional patterns for the northern Gulf of Mexico (inclusive of study area) relative to sea level. Figure 108 illustrates a recent modification to depositional systems and systems tracts with respect to sea level; relevant to the study area. Figure 109 illustrates a general model of interaction of sedimentation and salt movement in slope depositional systems. Figure 110 presents a nearby Gulf of Mexico Miocene shelf-slope depositional system that illustrates the interaction of salt tectonics related topography and slope depositional processes. This deposystem can be used as an analogue to the Plio-Pleistocene/Holocene deposystem within the study area.

Consideration must also be given to not only eustatic sea-level change but also to the shift in Pliocene/Pleistocene depocenters of the terrigenous river systems feeding this portion of the Eastern Mississippi fan that is the study area. It is the interaction of these three factors that provide the basis for the following proposed geologic model for the formation of the shallow stratigraphy in the study area which revises the aforementioned documented work in this area.

The geologic model and depositional history of the study area is presented by identifying the dominant geologic process that determined the seismic and stratigraphic character of each sequence. Each sequence (I through VI) has formed its present day

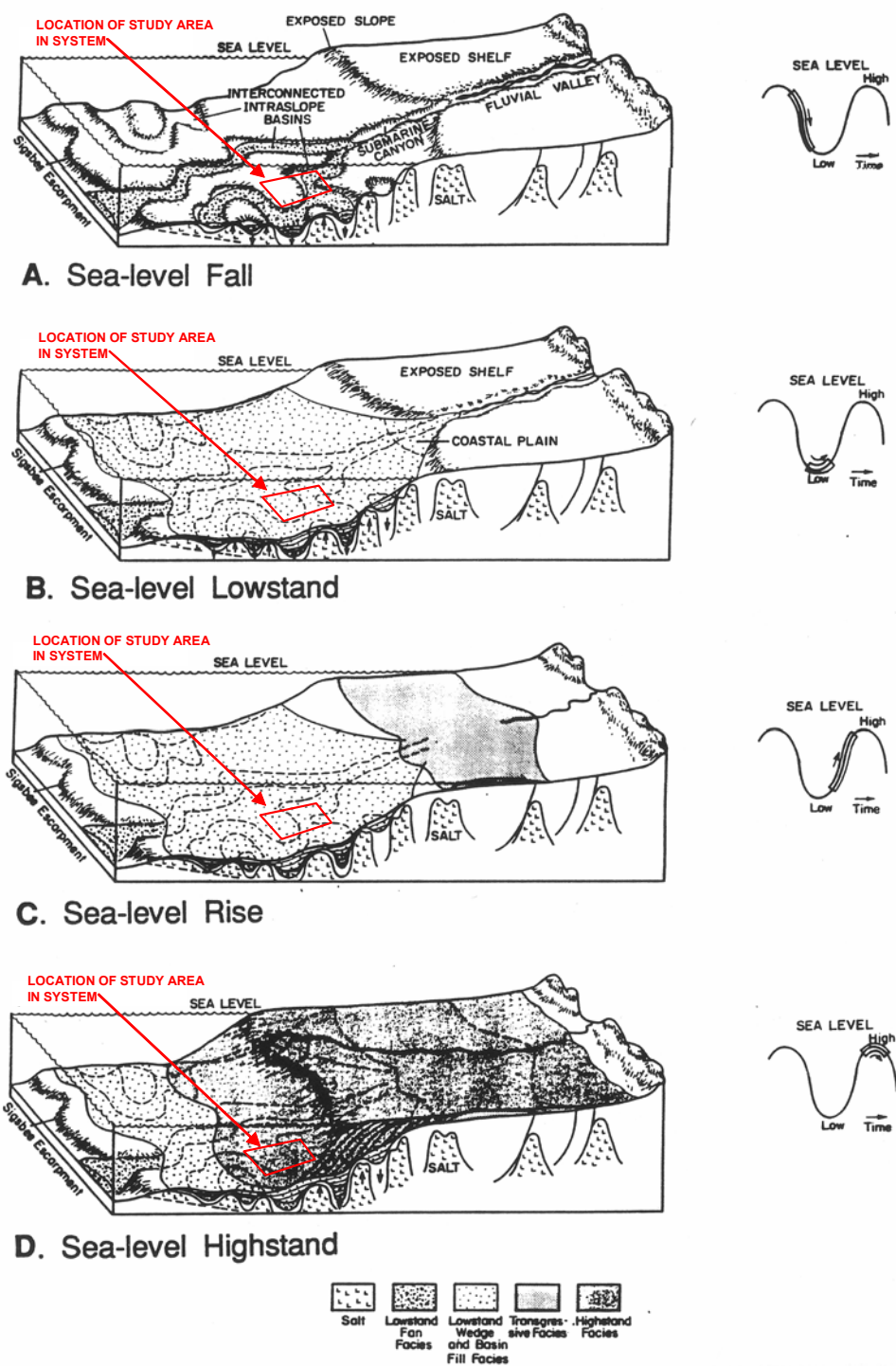


Figure 107. General depositional patterns for the Gulf of Mexico (Lee, 1990).

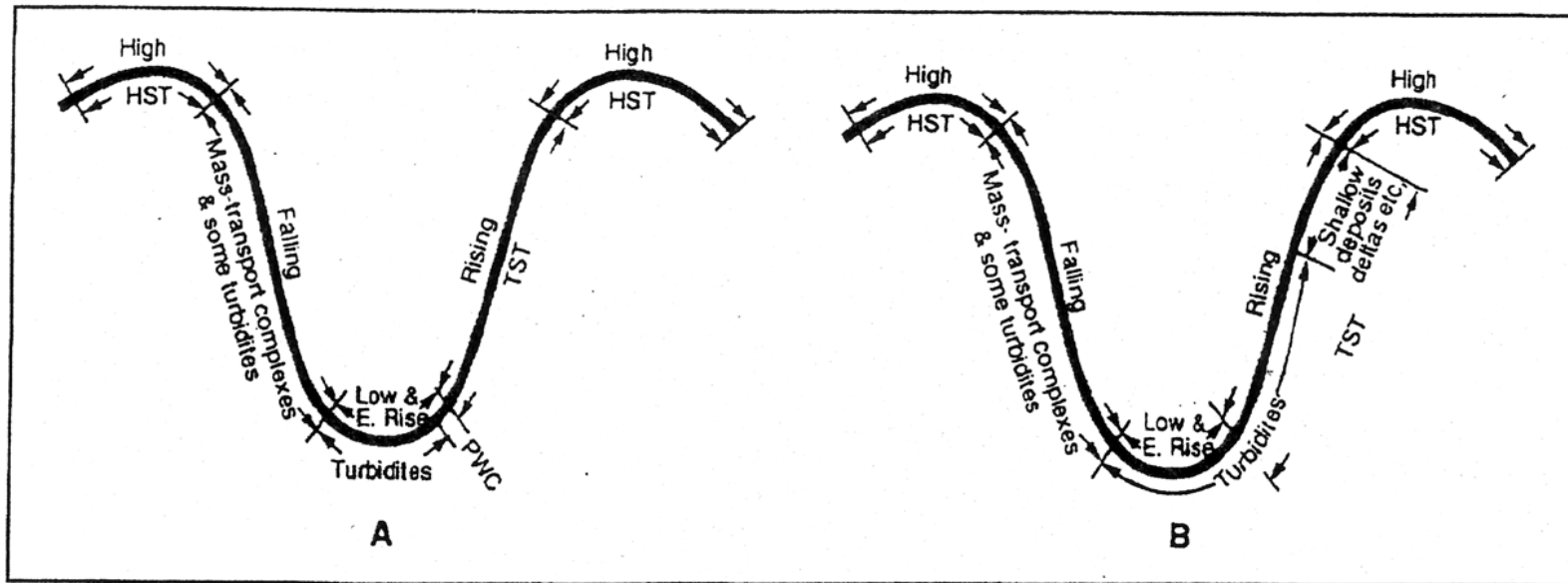


Figure 108. Recent modification to depositional systems and systems tracts with respect to sea level (Kolla and Perlmutter, 1993) modified from (Posamentier and Vail, 1988) and Weimer (1990). A represents conventional model for timing of turbidite delivery with respect to sea-level. B represents suggested modification proposed Kolla and Perlmutter (1993) from observations of the Mississippi Canyon/Fan system. The conventional model has turbidites delivered only near and at absolute lowstand whereas the revised model has turbidite delivery occurring well into transgression of sea level to high stand.

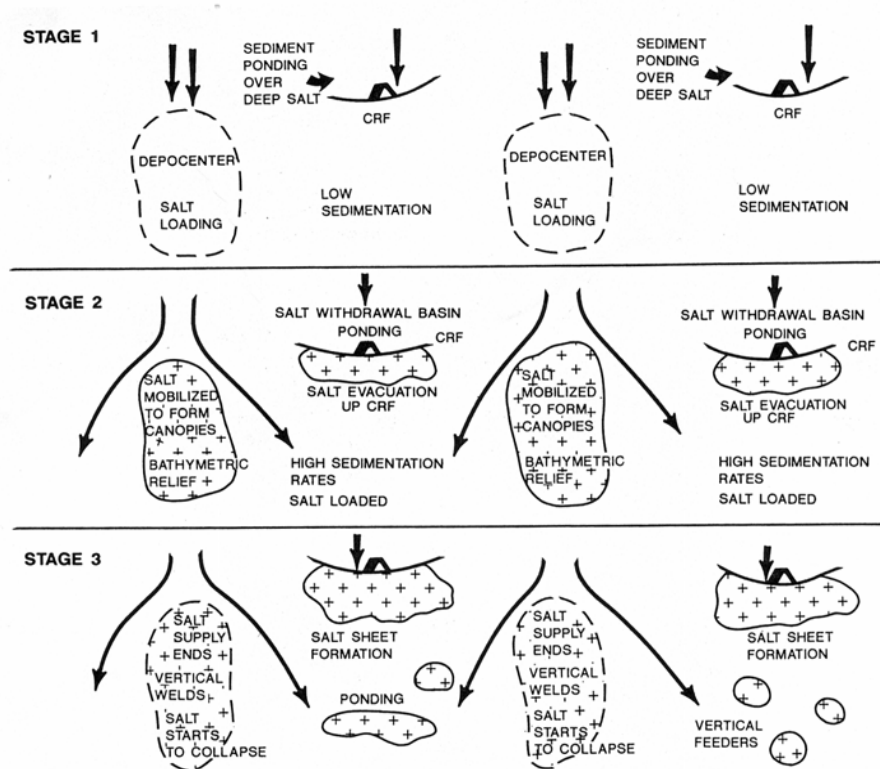


Figure 109. Basic model for interaction of sedimentation and salt movement in slope depositional systems (Jamieson, 1996). Stage 1 has sediments delivered to a local slope depocenters resulting in loading of the salt. Areas in between local slope depocenters undergo low sedimentation or “virtual highstands” with sediments ponding over deep salt underneath the upper slope/shelf resulting in the formation of a counter-regional fault (CRF). Stage 2 has salt underlying the local slope depocenters mobilized to form shallow canopies resulting in bathymetric relief. The relief diverts and concentrates sediment deposition into areas of the slope previously experiencing low sedimentation rates (virtual highstands) resulting in loading of underlying. Salt withdrawal under the upper slope/shelf causes bathymetric lows that result in ponding of sediments and salt evacuation up the CRF. Stage 3 has depletion of salt supply and associated collapse of salt canopies and reduction of bathymetric relief. Sediments remain diverted toward new depocenters and pond in topographic lows between highs formed by emerging salt bodies. Salt migrated up the CRF now undergoes gravity sliding forming salt sheets. Thus, the interaction of sedimentation and salt movement results in progressively complex distributions of salt structures and depocenters on the slope.

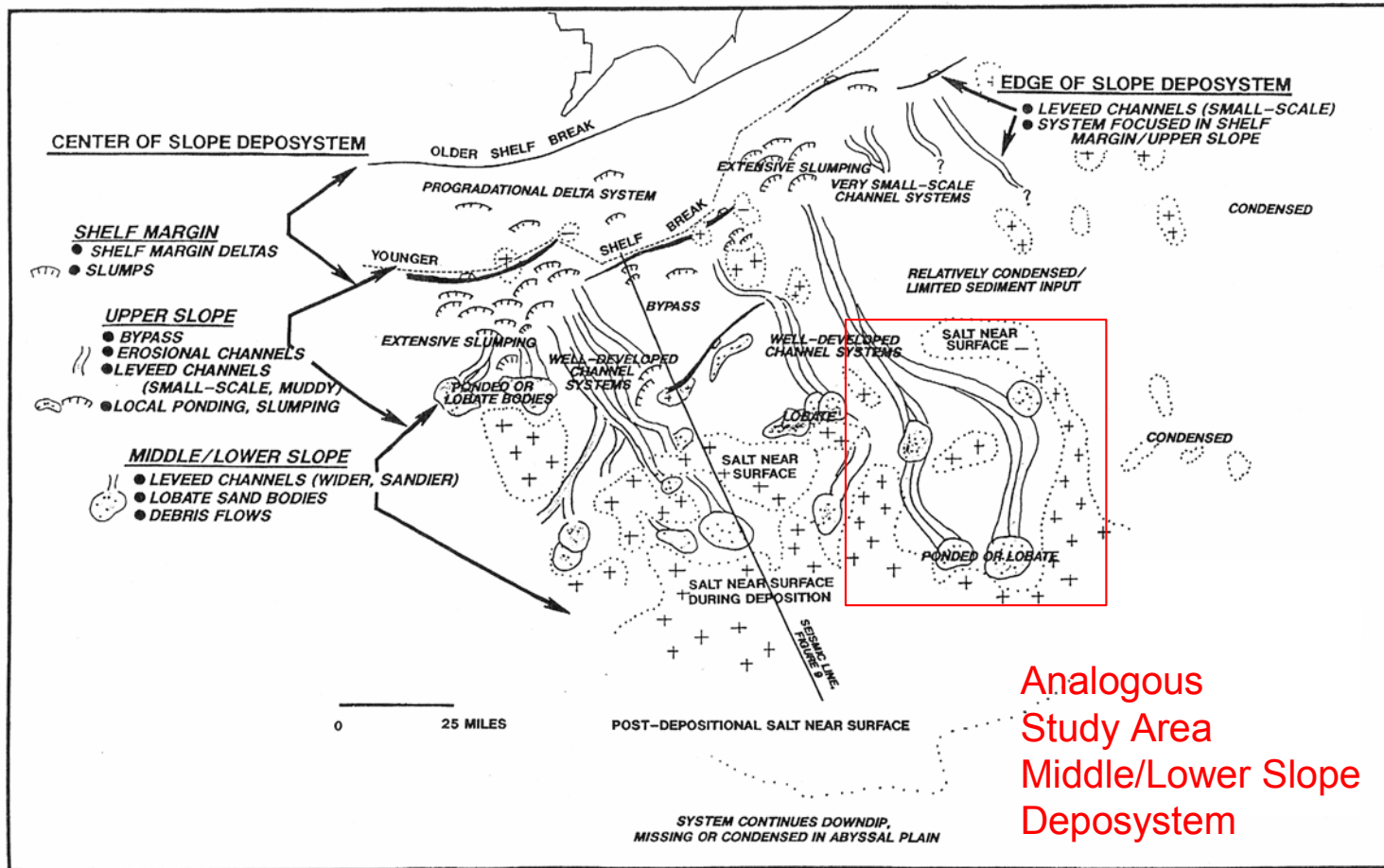


Figure 110. Miocene middle-lower slope deposystem analogous to the Plio/Pleistocene in the study area (Yielding and Apps, 1994). Location of image is on the Louisiana Continental Slope south of the Mississippi River delta. Note how location of a given portion of the slope with respect to the location of the depocenter is critical in determining deposition and resulting morphology. Areas of slope to the east of the study area undergo little deposition resulting in formation of a condensed section. Areas of slope to the west of the study area undergo significantly higher rates of deposition. Features present in the study area are similar to those in the figure for a portion of the slope that lies on the edge of the depocenter.

systems for salt in the study area and will be described based on their relative impact on deposition of a given sequence.

Sequence I (1.1Ma to 0.45Ma, BP)

Sequence I is most influenced by salt movement and is highly faulted. The majority of these faults are extensional in nature and extend below the limit of the seismic data, possibly all the way to the top of the salt or the salt weld located at some depth below. The majority of the faults truncate at the top of Sequence I indicating that salt movement that caused the extensional stresses within the sequence ceased either very close to or at the end of the deposition of Sequence I, certainly before the deposition of Sequence II. The number of faults in unison with near exact offsets would seem to indicate a constant, perhaps rapid, lateral movement during which extensional stresses affected much of the overlying stratigraphy in the section within the TI basins above the salt. This movement was also contemporaneous with local uplift of the section occurring downdip of the TI basins, where the salt has intruded higher into the vertical section resulting in the greatest amount of deformation of Sequence I. This uplift appears to have displaced whatever remaining section of Sequence I was above it. The seismic line, Figure 72, shows a thick section of Sequence I above the salt. Wu et al (1990b) posited that the latest episode of salt intrusion began in the Miocene and continued into the Plio-Pleistocene. However, there is a distinct transition from a regional, extensional, horizontal component of salt to a local, more vertical component

of salt, the latter of which is evidenced by the more local deformation of Sequence I around the present day salt bodies as well as deformation of the younger and shallower sequences (all considered to be Pleistocene) above the sequence. The transition from horizontal to vertical movement is linked to the evolution of the originally placed allochthonous salt sheets to their end-member components. The rendering of the structure at the top of Sequence I (Figure 69) shows the extreme structural deformation of the sequence by salt. Figure 73 is an RMS display of the sequence which highlights the extent of faulting (mapped from the RMS) affecting the sequence as well as illustrating the intrasalt basins that were present during formation of the sequence. No other sequence is as highly faulted as Sequence I.

It is also understood that some of the deformation of the sequence has probably been ongoing as salt movement continued during deposition of later sequences, however, Sequence I still remains most dominated by structural deformation by salt movement and intrusion in the study area.

Sequence II (0.45Ma to 0.40Ma, BP)

Sequence II was deposited, and in many places, incised into and eroded Sequence I. Sequence II is composed of thick mass transport deposits that thicken in the basins around the salt and thin on top of the salt. The fact that many of the faults in Sequence I do not extend above the erosional conformity at the boundary between Sequence I and II suggest that the overall horizontal regional movement of salt had

ceased before deposition of Sequence II. If regional salt movement had still been active, the faults present in Sequence I would have offset the sediments within Sequence II as well.

During deposition of Sequence II, salt movement became locally concentrated in the vertical/horizontal motions associated with the shallow spires, sills, and ridges in the study area as end-member components of the salt structure became established. This transition from what is considered to be regional salt motion to more local motion signals the establishment of the end-member systems. Some faults from the regional extension do extend into sequence II. These faults may represent some residual movement of the either fully, or nearly, depleted salt in the TI basins resulting in continued minor motion along these faults. Figure 78 is a RMS display of the sequence showing the concentration of faults on top of the topographic highs while becoming less numerous in the TI basins. The faults were mapped from the RMS value of the sequence and subsequently plotted with red lines to designate their location. Sequence II is thick in the existing suprasalt basins into which it was deposited. The rendering of the structure at the top of Sequence II (Figure 74) illustrates how the massive slides of this sequence filled in much of the existing topographic lows, drowning the salt and reducing its structural expression. The thickness of the unit, as shown in Figure 76, also illustrates the amount of infill in this sequence. The sequence thins rapidly along the rims of these basins, indicating that there was significant vertical relief on the seafloor at the time of deposition, the salt had already been vertically emplaced. Not only did the slides, for the most part, fill these basins; they also overspilled on top of the salt

structures as the basins became increasingly filled. This gives credence to the observed thick concentrations in the basins as well as the presence of the sequence on top of the salt structures in the study area.

Sequence II represents large, regional slides that occurred upslope due to the interactions of regional oversteepening of stratigraphy resulting from the vertical, shallow emplacement of salt. The geologic conditions upslope have been much like those observed to have started during deposition of Sequence I and continued through deposition of Sequence II.

Sequence III (0.40Ma to 0.071Ma, BP)

Sequence III is a thick sequence of stacked condensed sections composed almost entirely of hemipelagic clays interbedded with some periodic clay-rich mudflow deposits. The sequence drapes the irregular surface of Sequence II and in many places is deformed, probably due to the irregular surface below.

This sequence represents a major avulsion in the terrigenous depocenter that fed this portion of the Gulf of Mexico between ~400ky and 70ky, B.P. Figure 12 shows the proposed locations of major Pleistocene depocenters for the Gulf of Mexico. It is quite possible that the depocenter shifted westward onto the Texas/Louisiana shelf and slope, thus starving the study area of terrigenous sediment input. The mudflow events probably represent numerous, minor slope failures related to continued oversteepening of the seafloor by the underlying salt. Figure 79 is a structure rendering of the top of

Sequence III. The sequence is relatively flat, as the condensed sections became thick enough to mask the irregular surface of Sequence II. The top of Sequence III, however, has been altered by erosion from the active deposition of Sequence IV. This is most evident across the middle of the study area where a large channel has incised into Sequence III. The top of Sequence III is considered an erosional unconformity between III and IV.

The entire sequence was formed through primarily hemipelagic deposition and low-energy slope processes with salt tectonic effects localized in the area of the end-member salt structures. Figure 84 is a RMS display of the seismic volume of the sequence. The channel that has incised into the sequence during the formation of overlying Sequence IV is very evident. Faulting is less prevalent and concentrated primarily on top of the salt bodies in the study area. Faults are also seen along the sides of the channel and may indicate incipient faulting following initial channel incision. Of note are the relatively low RMS values for the sequence, indicative of low amplitude, fine-grained hemipelagic, and mudflows. Several of these mudflows are evident in the southwest corner of the study area. These mudflows traveled down Chandeleur Valley. The walls at the lower end of the valley are formed by the seafloor expression of SB III and SB IV. This is the first appearance of activity within Chandeleur Valley in the study area. It is possible that this activity is related to the establishment of a more eastern depocenter whose source was the Mississippi River. This statement is further supported by the incision of this sequence by the channel in Sequence IV, which has been correlated with channel systems coeval in both the eastern and western Mississippi Fan.

Sequence IV (0.071Ma to 0.055Ma ,BP)

Sequence IV is an active transport sequence composed of debris slides and a turbidite rich basin floor fan. Figure 104 shows how these fan deposits were deposited into the back basin created by the salt sill of SB II. The turbidites filled the back basin and, in some cases, overspilled it. Minor continued uplift and movement by the salt has faulted this sequence in places but overall, it is a "cut" (eroding into Sequence III) and "fill" (ponding and filling topographic lows) sequence. This term is normally reserved for channel descriptions but is appropriate in its use here. Figure 91 is a RMS display of the seismic volume for the sequence. This display shows a number of features related to active depositional processes. The most important features are those associated with the Chandeleur and Gulfport Valley and the channel/basin floor fan complex present through the middle and lower half of the study area.

Chandeleur Valley, mentioned above, is marked by a number of debris slides and mass-transport events. The facies of these features are interpreted to be composed of mixed sediments, intact blocks of debris, and potential turbidite flows. The overall nature of the facies indicates a much higher energy regime than the mudflows in the valley in Sequence III. This is probably a result of a continued eastward shift in the Mississippi Depocenter coupled with an increase in sediment influx onto the continental shelf northwest of the study area.

Gulfport Valley also became active during deposition of this sequence. Gulfport Valley is rimmed mainly by SB I to the northeast. It is partially constrained

by topography associated with SB IV and SB II along its southern limit. A number of individual episodes of fine-grained mass-transport deposition are identified in Figure 91. The seismic facies in Figures 88 and 89, and Table 6, coupled with the low RMS values in Figure 91, confirm the fine-grained nature of these deposits.

The large channel incised through the middle of the study area is interpreted to be Channel 14a from Dixon and Weimer (1998). They postulated that the channels present in the Eastern Fan were sourced in from the Mobile River. However, they also documented an eastward shift in the higher energy, more sand-rich Mississippi River depocenter during this time. The amount and relative energy of debris slide and potential turbidite deposits down Chandeleur Valley indicates a source with great sediment influx, the Mississippi River. Channel 14a would have to be higher energy to have incised into Sequence III as deep as it has. In addition, channel 14a flows from west to east across the study area. The interpreted high-energy nature is evident in the turbidite, sand-rich, basin floor fan that has ponded in the southern half of the study area (Figure 88 and 89). Drilling reports through this unit at Shell's Mensa prospect (Burman, 1998) indicate thick, almost pure sands interbedded with thin clays and shales. The thickness and "clean" sands in this basin floor fan support very high-energy transport and deposition (good sorting) from a sand rich source upslope to the west, northwest of the study area. These sands are likely to have been sourced from the Mississippi River, not the Mobil River. However, finer-grained mass-transport deposits overlie the northern half of the study area. Given the geometry and relief of the shelf and upper continental slope northwest of the study area (Figure 2 and Figure 25) these

finer-grained mass-transport deposits were not likely sourced from the Mobile River, but rather from the Mississippi River. These deposits could have a shelf-slope delivery system along the periphery of the Mississippi depocenter where fine-grained sediments would likely be more abundant and subsequent failures composed almost entirely of fine-grained sediments. Sequence IV likely represents a lower slope depositional system from which a bifurcated channel/valley system extends shelfward to the west linking with Mississippi river depocenters of the Western Fan.

Sequence V (0.055Ma to 0.023Ma, BP)

The sequence is composed entirely of slumps and debris slides interbedded with condensed sections. This sequence may represent subtle oscillations in sea level with each condensed section representing a small highstand high-stand, or, the sequence could be a reflection of slope adjustments to changes in slope topography due to salt tectonics that can continue beyond lowstands of sea level. Dixon and Weimer (1994, 1998) have repeatedly documented that slumps can occur at anytime.

Active deposition within Sequence V appears more active around Chandeleur Valley. A number of debris slides are evident on the RMS display for this sequence (Figure 98). Individual blocks of strata are identified both in Figure 98 and on the seismic data (Figure 111). Of note is the large slump occurring in the middle of the study area (Figure 95 and 98). This slump created a large scarp at its headwall and

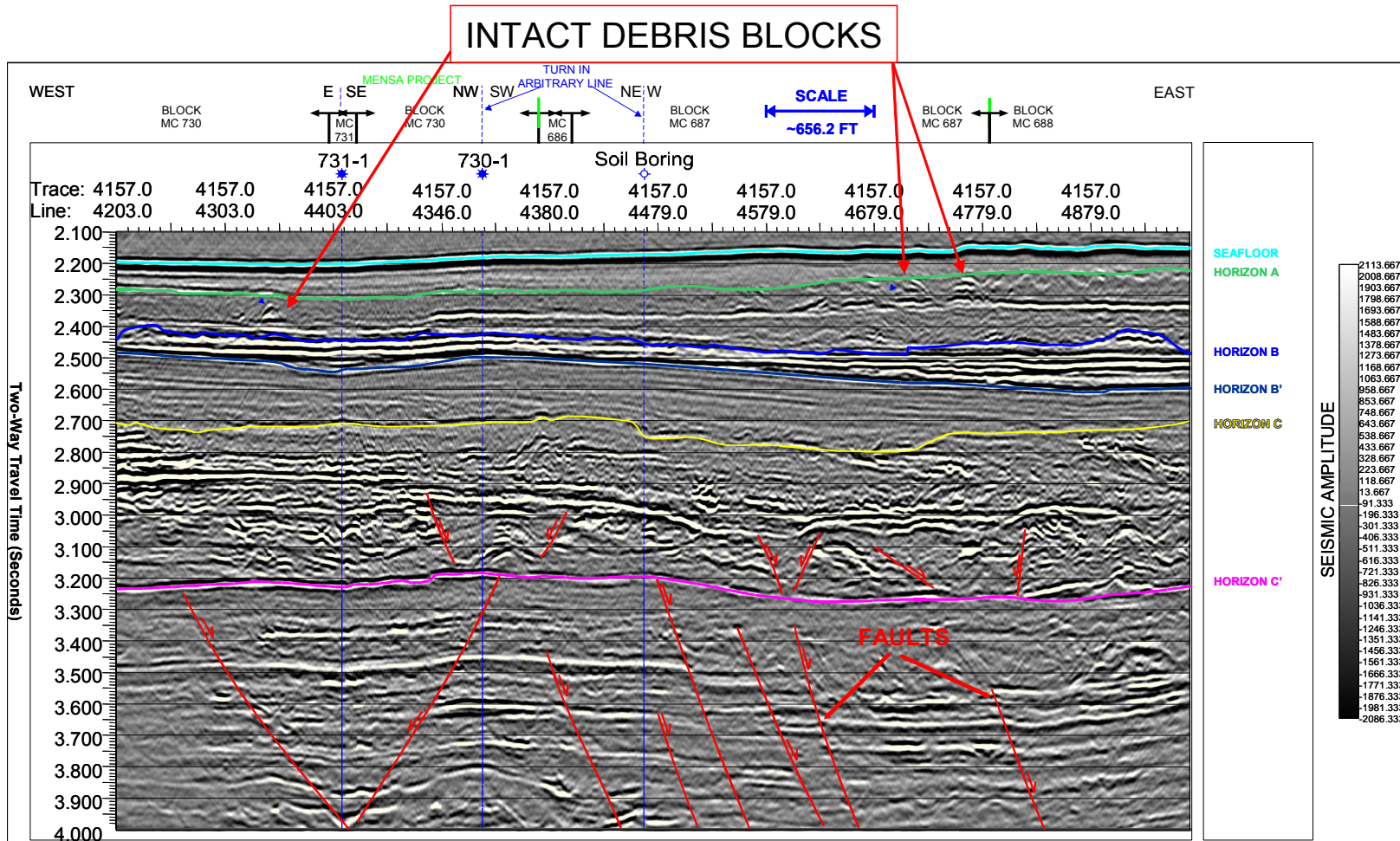


Figure 111. Seismic line illustrating intact debris blocks in Sequence V. Interpretation is substantiated by examining the lateral continuity of the reflectors within the slide deposits via the RMS display for this sequence (Figure 98). Colored lines are mapped horizons. Red lines are faults.

depositional lobe in its runout. This event established the local seafloor topography in the study area and has dictated the geometry of the seafloor in this part of the study area to the present. This slump may have occurred as a result of undercutting by the debris slides and other mass-transport episodes that traversed down Chandeleur Valley. This undercutting coupled with uplift and faults associated with SBIV probably resulted in an unstable, oversteepened condition that caused the slope to fail. The activity of deposition in the study area associated with Gulfport Valley was also present during this sequence as a number of well-defined slumps are identified in the seismic record (Figure 95).

Sequence VI (0.023Ma, BP to Present)

Sequence VI is a condensed section that represents the reduction in sediment supply to the study area due in part to shifting depocenters and high-stand of sea-level to the present day (Figure 99 and Table 8). The sequence is composed of a hemipelagic clay drape that has covered Sequence V. The sequence is relatively thin, allowing for most of the features and topography established during the formation of Sequence V to be identifiable at the seafloor. The seafloor rendering shows the scarp left by the large slump in the center of the study area, as well as a number of other features. In geologic terms, the current depositional environment is conducive to formation of a condensed section. Neither active slope depositional processes nor salt tectonic movement is

dominant. Normal, slow, pelagic/hemipelagic deposition is the dominant processes at this time.

CHAPTER VIII

GEOLOGIC HAZARDS

Introduction

The following sections describe the geologic hazards in the study area resulting from the analysis of the digital seismic data. The hazards are presented starting with the seafloor and working downward in the stratigraphic section through Sequences VI to Sequence I.

A. Seafloor Morphology

The Enhanced Seafloor Rendering (Figure 4) shows an illuminated two-dimensional perspective of the seafloor morphology based upon the water bottom pick extracted from the 3-D seismic data. This illustration highlights the topographic features in more detail than the contour bathymetric map is able to achieve (Figure 3). 3-dimensional isometric views (Figure 112) help to illustrate the overall geomorphology of the study area.

Chandeleur Valley is the most prominent seafloor feature in the southwest quadrant of the study area. The northern wall of the valley consists of east to west trending, steep scarps (Figure 112). These scarps formed during past slump events. The

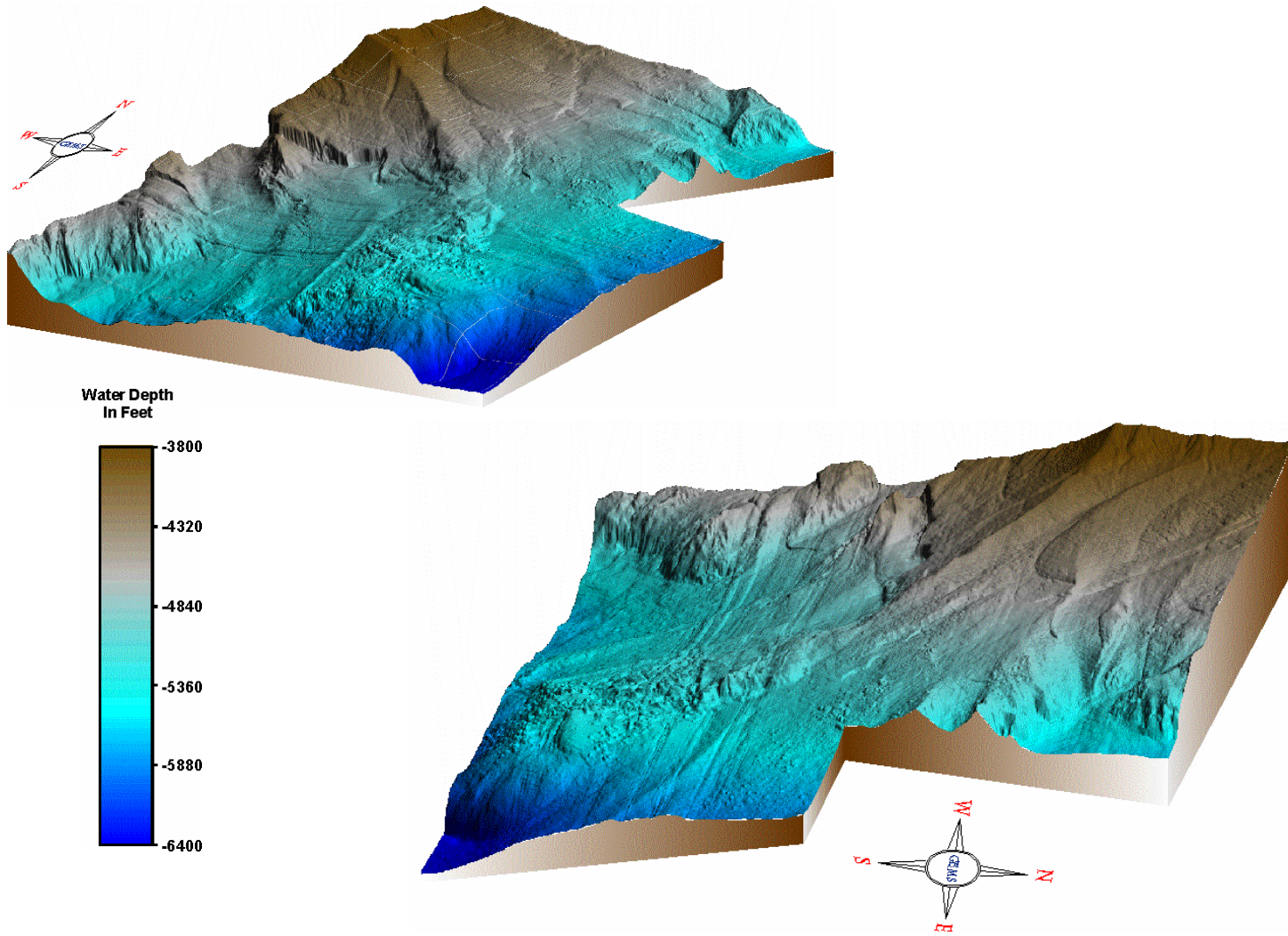


Figure 112. Seafloor perspective views.

southern wall of the valley is the seafloor expression of salt at depth. Numerous northwest to southeast trending seafloor faults are present, roughly perpendicular to the strike of the valley wall. A curvilinear seafloor fault is present in portions of MC 639, MC 683, MC 684, and MC 640. Numerous smaller faults are present at the seafloor as the valley opens into the basin. These faults have the same trend as the valley axis and are the surface expression of shallow faults, possibly related to the differential compaction of sediments below.

Two northwest to southeast trending, linear seafloor features are present in the basin in the southwest quadrant of the study area. These lineations are the surface expression of the boundaries of shallow buried debris slide deposits (Figure 112). A semi-isolated topographic high, or “island”, is present in MC 596 and part of MC 660. This feature is an isolated block of intact strata bounded by slump scarps to the east of the remnant channel of Chandeleur Valley to the west. Two well-defined seafloor mounds are present just south of this “island” in MC 640. They have abnormally high-amplitude seafloor returns suggesting probable fluid expulsion and/or hardground conditions at the seafloor. Seismic data through these features confirms the presence of anomalous high-amplitude events associated with faulting. Fluids are likely to have migrated from depth along these faults, accumulated in the shallow subsurface, and have been expelled at the seafloor.

Gulfport Valley crosses the northwest quadrant of the study area (Figure 112). This area shows north-northeast to south-southwest trending ripple-like bedforms. These features are likely the surface expression of buried relict sediment creep. Within

the valley is a number of northeast to southwest trending troughs. These troughs are probably the surface expression of buried pathways for past debris slides or turbidites. These pathways are no longer active as they are covered by a uniform sediment drape. The troughs may be related to faulting and displacement of overlying sediments during differential compaction.

A number of well pronounced seafloor ridges are also present in the northwest quadrant of the area. Most of these ridges are related to seafloor or near seafloor faulting. However, in MC 510 and MC 556, the seafloor geometry not only reflects faulting, but also shallow sediment deformation from underlying stresses.

The dominant seafloor feature in the northeast quadrant of the study area is a small basin. The basin itself is the result of salt withdrawal and the subsidence of overlying sediments. The salt that once floored the basin has migrated out and upward into the surrounding sediments. This process has resulted in a highly faulted basin rim. Redfish Valley enters the basin from the north-northwest. An irregular seafloor, consisting of a number of isolated mounds in MC 423, MC 512, and MC 513, may indicate a past buried slump or debris flow event that moved down the valley before basin formation.

A topographic high resulting from the presence of a shallow salt sill at depth is the dominant feature in the southeast quadrant of the study area (Figure 112). The seafloor on top of the salt sill is very irregular. This irregular character is the surface expression of shallow slump related deposits in the subsurface. A large southwest to northeast trending seafloor fault is present in MC 732, MC 733, and MC 689 (Figure

112). Evidence of a near surface slide is present in MC 733 and MC 734 (Figure 112). The irregular seafloor on top of the sill contrasts with the smooth seafloor in the deep basin located in the southeast corner of the study area.

B. Bathymetry and Seafloor Gradient

The water depth over the study area varies from -3620 ft to -6520 ft (Figure 3). The shallowest water depths are located in the northwest quadrant of the study area and are associated with normal slope progradation conditions. The seafloor in this area generally dips to the southeast with local variations in water depth attributed to a number of seafloor troughs located within the greater Gulfport Valley (Figure 112). Seafloor gradients in the northwest quadrant average between 1.0° (1.7%) and 2.0° (3.4%) (Figure 106). Locally, gradients in this area can reach up to 8.0° (14.05%) along these seafloor troughs.

Water depths deepen to the east into a small basin in the northeast quadrant (Figure 112) of the study area. Water depths range from approximately -5000 ft to -5600 ft below sea surface (Figure 3). The maximum water depth occurs on the floor of a basin in the extreme northeast corner of the study area. Seafloor gradients around the perimeter of this basin average 1.0° (1.7%) to 4.0° (3.4%), Figure 106. Local gradients up to 12.0° (21.0%) occur along the flanks of the basin and in areas affected by seafloor faults.

Water depths increase in the southwest quadrant and range from approximately –5000 ft to –6400 ft (Figures 3 and 112). The water depth generally increases to the southeast and the topography is irregular. The irregular topography is the surface expression of buried slump deposits. The seafloor topography is affected by the surface expression of faults.

The seafloor grade is variable in the southeast quadrant, but generally range from 1.0° (1.7%) and 4.0° (3.4%). Seafloor gradients in areas of slumping or faulting can, however, be as high as 12.0° (21%), Figure 106. Along the southeast limit of an underlying salt sill, the seafloor gradients range between 4.0° (6.9%) and 10.0° (17.6%).

Water depths in the southwest quadrant of the study area range from –4700 ft to –5700 ft and increase to the south and southeast (Figures 3 and 112). Local variations in water depth occur along the northern wall of Chandeleur Valley where previous slump events have left prominent seafloor scarps. The southwest wall of Chandeleur Valley is a topographic high resulting from salt diapirism. Seafloor grades corresponding to this feature range from 4.0° (6.9%) to 15.0° (26.0%) and can reach as high as 32.0° (62.0%) along the northern valley wall (Figure 106). Chandeleur Valley empties into a basin in the southern half of the quadrant. Seafloor gradients in the basin average between 1.0° (1.7%) and 3.0° (5.2%), but can be as much as 9.0° (15.8%) in areas of shallow subsurface debris flows and faulting.

C. Seafloor Amplitude

High, positive amplitude responses reflect relative consolidation of the seabed and highlight vent-related hard bottom structures or carbonate accumulations (Roberts et al., 1992; and Doyle et al., 1996). High negative-amplitude responses may serve to identify fluid expulsion or fluid saturated mass-movement events.

The following list highlights lease blocks within the study area that may contain hydrocarbon seeps and related structures:

- MC 595, 596, and 640;
- MC 727 and 771;
- MC 775;
- MC 732, 733, 776, and 777;
- MC 424 and 428; and
- MC 555.

High-amplitude events on the seafloor in the study area are generally associated with areas of high seafloor gradients (compare Figures 106 to Figure 113) and faulting. High-amplitude events seen in MC 595, MC 596, and MC 640 are related to possible gas or fluid expulsion vents. Seismic sections through this area (Figure 114) show high-amplitude returns at the seafloor and wipeout zone below the event. The seismic sections also show faults extending from a salt body that may provide possible conduits for the migration of fluids. Carbonate hardground may also be likely at this location.

High-amplitude seafloor events are also present in MC 727 and MC 771 (Figure 113). These events are associated with faults. The seafloor is not necessarily offset by the faults but may reflect accumulations of fluids just below the seafloor. No structures

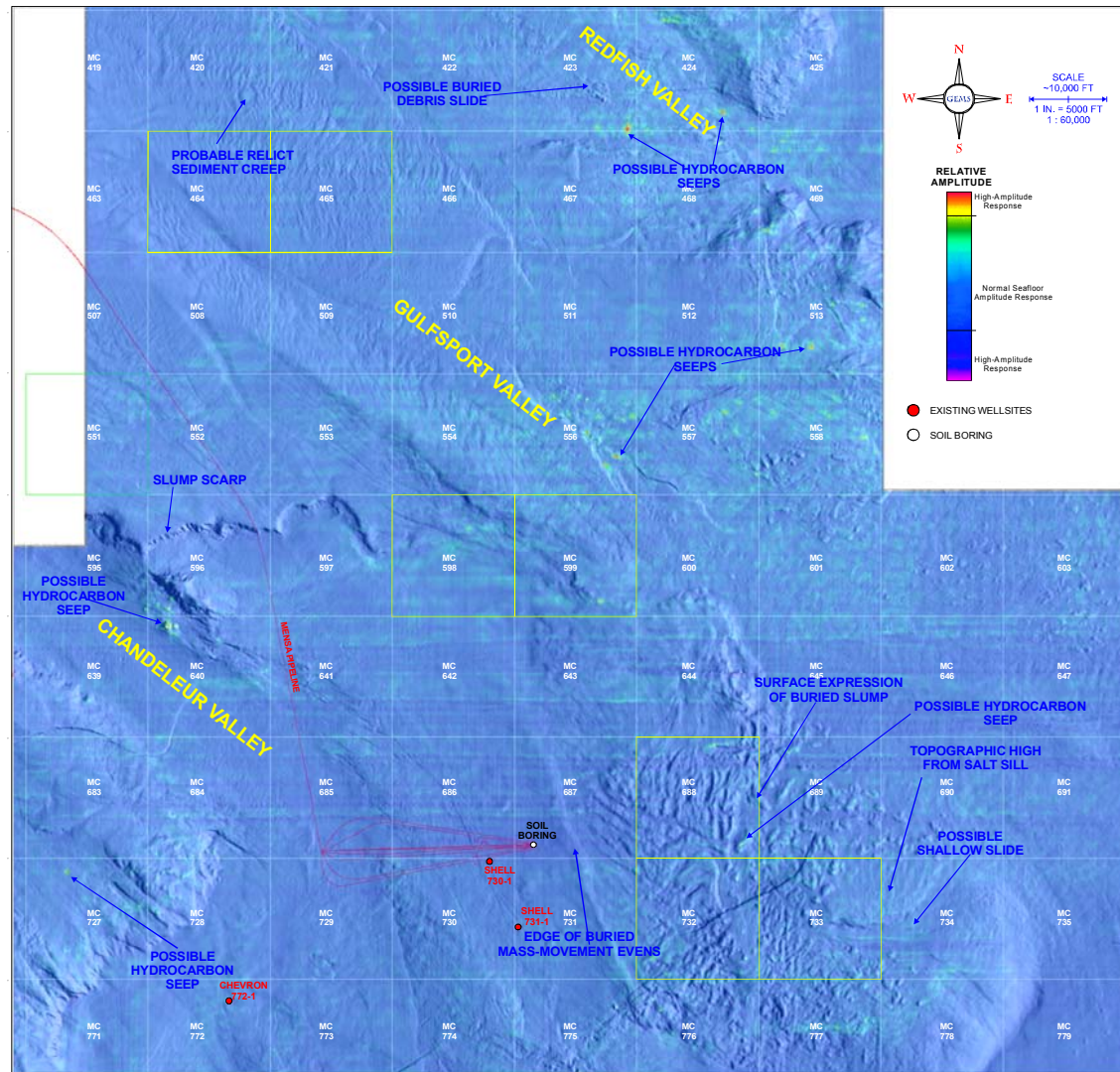


Figure 113. Seafloor amplitude map. Higher amplitudes are focused around seafloor expressions of underlying end-member salt.

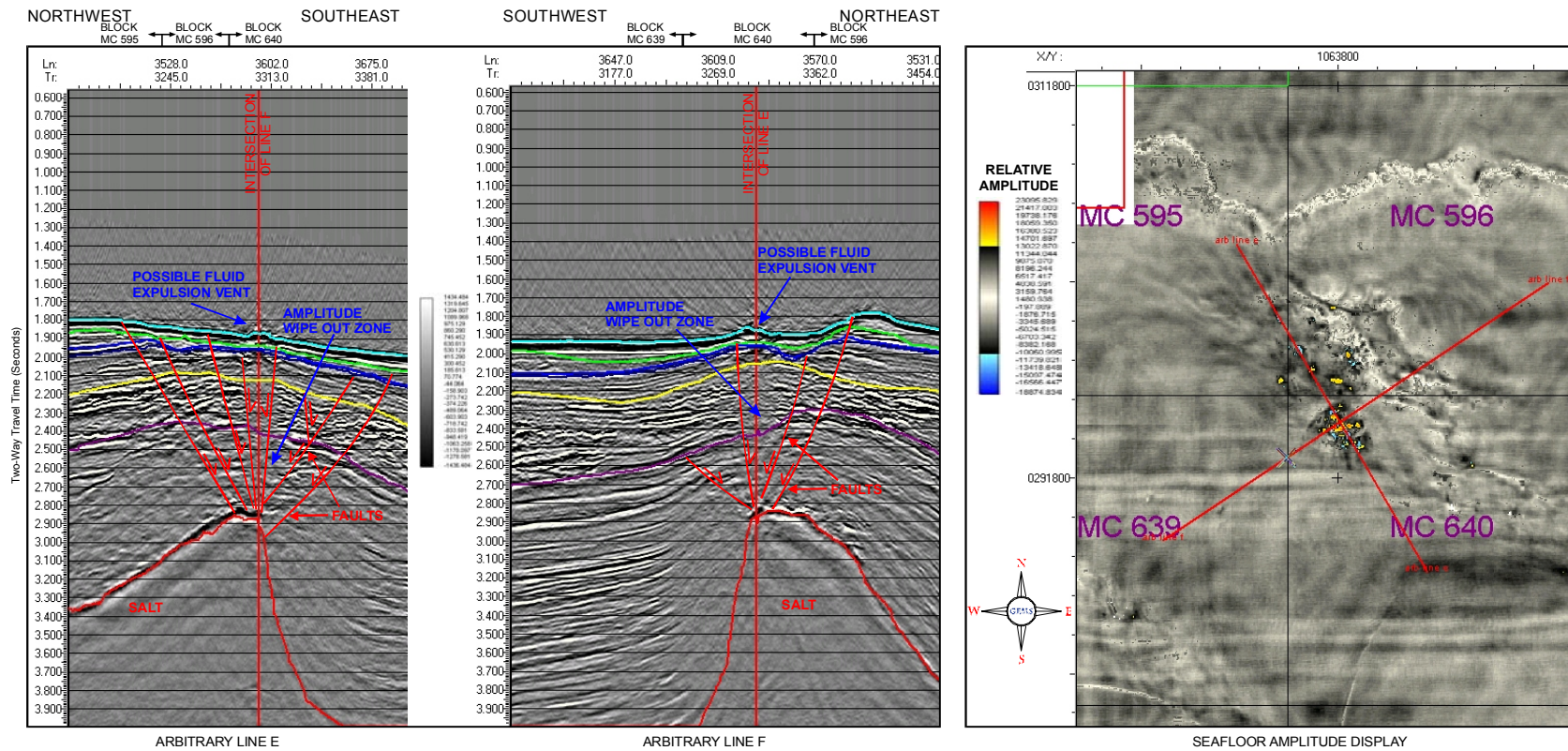


Figure 114. Potential location of hydrocarbon seeps and chemosynthetic communities. Note possible expulsion vent and associated amplitude wipeout. Note the concentration of high seafloor amplitude values around corresponding to the location of the vent and wipeout zone above SBIV (salt in figure). These conditions are conducive to hydrocarbon seeping at the seafloor and potential habitation by chemosynthetic organisms.

such as vents, mounds, craters, chimneys, or amplitude wipeout zones could, however, be identified with these features. This does not preclude the possibility that fluids have at one time migrated to the seafloor in these areas.

High-amplitude events on the seafloor in MC 775 may be related to hydrocarbon vents. These small zones overlie faults in the shallow subsurface. A small crater, possibly associated with expulsion of hydrocarbons at the seafloor, is present near the middle of MC 775 (Figure 113). The seafloor amplitude response in this area shows a number of circular features that fall just outside of the amplitude cutoff chosen to depict anomalous seafloor amplitudes. These features trend southwest to northeast and line up with the anomalies located in MC 775. Seismic sections examined through this area show a number of small, isolated high-amplitude events underlain by faults extending from the top of salt. These features are present in MC 732, MC 733, MC 776, and MC 777 and may be related to the slow migration of fluids up these fault planes.

High-amplitude anomalies are also evident in MC 423 to MC 425, and MC 467 to MC 469 (Figure 113). Most of these anomalies do not show any structure or conditions indicative of hydrocarbon venting and are likely a result of over-consolidated seafloor sediments related to steep slopes. Two areas occur on the boundary between MC 424 and MC 428 and in MC 424. These events may be related to hydrocarbon expulsion at the seafloor as they are underlain by subtle faults with possible accumulations of fluids in the deeper subsurface.

A number of small high-amplitude seafloor anomalies are present in MC 555 (Figure 113). They are near a northwest to southeast trending fault that runs through the lease block.

D. Sequence VI: Seafloor to Horizon A

Sequence VI is composed of an amorphous sediment drape (Table 8). Horizon A is the base of this unit. This sequence is generally thicker in the western portion of the study area (Isopach map, Seafloor to Horizon A, Figure 93). The increase in thickness is attributed to the presence of mass transport features just above Horizon A. These mass transport deposits thicken toward the centers of Gulfspout and Redfish valleys. This unit also thickens in areas where buried slumps occur below Horizon A. The drape unit thins within the Chandeleur Valley and may indicate recent (Late Pleistocene) sediment transport activity. The section is uniform over the eastern half of the study area, thinning in areas of irregular seafloor topography (Isopach Map, Seafloor to Horizon A, Figure 93).

Figure 115 is the RMS display for the seismic volume of this sequence. The sequence between the seafloor and Horizon A is composed of very soft to soft, hemipelagic clays. The drape unit locally contains high-amplitude events. These events are probably associated with the upward migration of fluids from depth or in situ generation of biogenic gas. The presence of these features within this sequence may indicate the vent is potentially active.

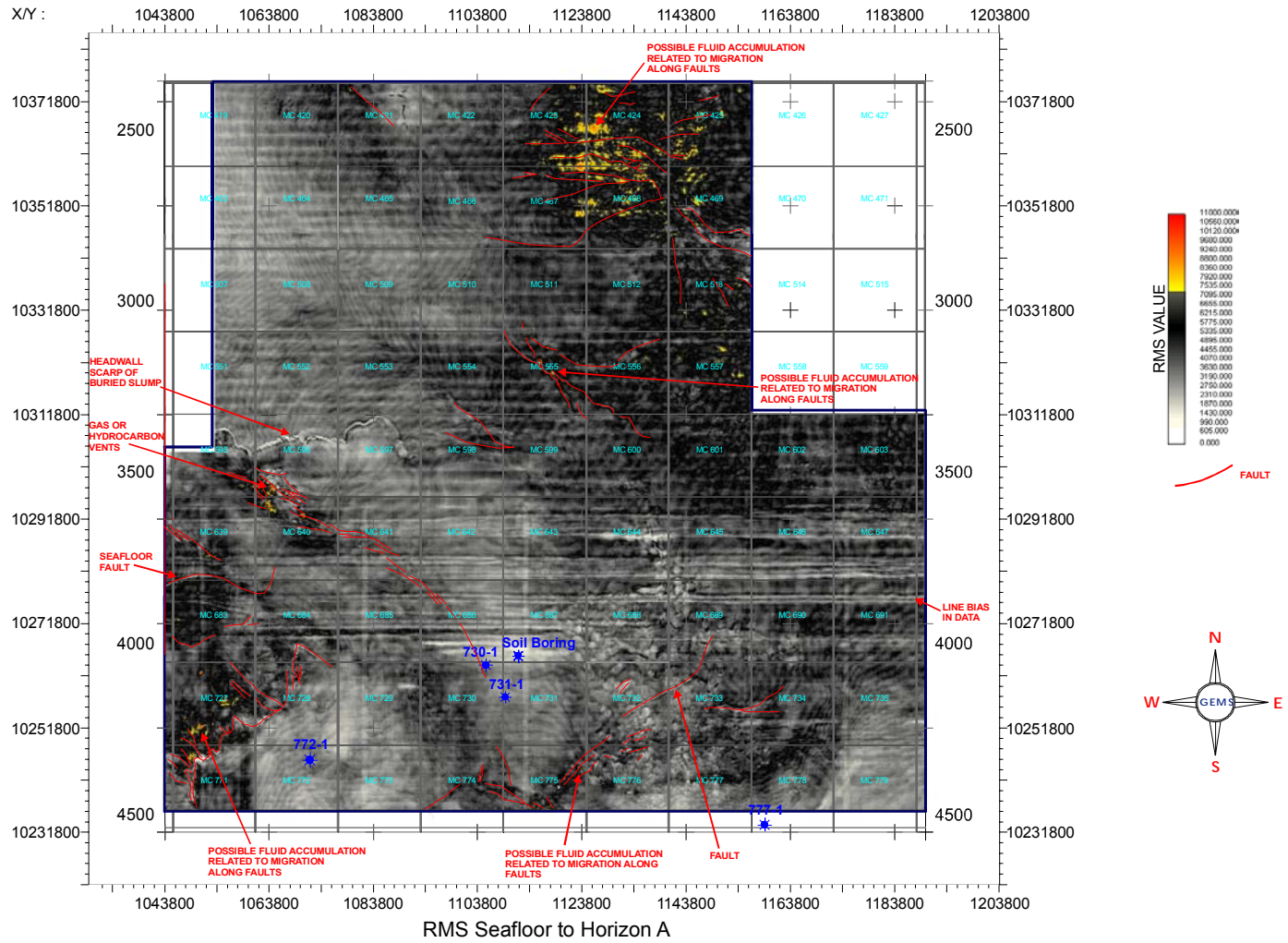


Figure 115. Sequence I RMS amplitude display.

E. Sequence V: Horizon A to Horizon B

The stratigraphic unit between Horizons A and B is comprised of alternating sequences of parallel and chaotic reflectors that contrast with the overlying drape sediments above Horizon A (Table 7). Sediments overlying Horizon B thicken in the valleys and in basin surrounding salt uplift. Seafloor topographic highs have probably served to direct and focus the downslope movement of sediments into these areas.

This sequence is interpreted to be fine-grained pelagic separating numerous debris slide deposits. Debris slides are identified in this RMS display for this sequence (Figure 98) and correlated on the seismic examples (Figures 95, 96, and 97). Possible levee and overbank deposits from these events have been identified are evident (Figure 95). The lower event is slightly more chaotic than the shallower event and has higher-amplitude character. The high-amplitude character suggests lenses of sand that are possibly fluid bearing within a mixed clay and silt matrix. Small zones of parallel, high-amplitude reflectors present within these mass movement deposits suggest blocks of intact strata that have been transported downslope during the mass movement events (Figure 111). The sequence is highly faulted above the salt bodies in the area and has corresponding high RMS values indicating the possible presence of hydrocarbon migration and trapping in the sequence.

F. Sequence IV: Horizon B to Horizon B'

The stratigraphic unit between Horizon B and B' represents an active sediment transport sequence characterized by a combination of moderate to high-amplitude reflectors. This unit correlates to the Blue Unit discussed by Burman and Norton (1998) in the discussion of the Mensa prospect. The Blue Unit was penetrated during drilling operations for Shell's Mensa prospect in MC 687, MC 730, and MC 731. The unit has been mapped over the entire study area, but is distinctly more chaotic in the northern half where there is no major structural control (Figure 88). The unit shows a similar parallel and continuous seismic character as seen at the Shell Mensa prospect in MC 685-689, MC 729-732, and MC 775 (Figure 105). The Sequence IV isopach map (Figure 86) shows a thickening of the Blue Unit in a structural low formed by salt uplift of SBII and SB III.

This seismic character (Figure 105 and Table 6) is probably representative of individual, sand-rich turbidite units interbedded with sandy silts, thin shales, and clays. Downslope movement of sediment during these events was impeded by structural uplift related to salt diapirism in the southern half of the study area. The uplifting also resulted in surrounding structural lows where these sediments could accumulate. Faulting and diapirism east of the Mensa wells has disturbed the Blue Unit. This faulting may have relieved the pressure regime in this sand unit. However, this does not exclude the possibility that abnormally high pore pressures may still exist locally.

The RMS display for this sequence (Figure 91) shows Chandeleur Valley was also active during deposition of this sequence. Sediment ponding behind salt structures is evident in the southern half of the study area, possibly contributing the sands that have formed this sequence. Intact blocks of strata are present in a debris slide event in Chandeleur Valley (Figures 91).

Gas vents are present through this sequence in MC 596 and MC 640 (Figure 114). Small circular areas are evident associated with the possible vent areas (Figure 114) that may indicate the accumulation of fluids in the subsurface strata.

The sequence is highly faulted on top of salt bodies in the study area. Figure 91 shows very high values in the sequence and may indicate fluid migration and accumulation of hydrocarbons (either gas or oil) in this sand-prone sequence.

G. Sequence III: Horizon B' to Horizon C

The stratigraphic unit between Horizon B' and Horizon C is composed of mostly low-amplitude, parallel reflectors (Table 5). This sequence was penetrated during the soil boring operations at the Shell Mensa prospect in MC 687 and showed hard clay from 801 ft to 1199 ft (bml).

The base of this sequence, Horizon C, marks the transition from the passive sequence described above to a chaotic active depositional unit below in sequence II. This transition is not readily evident by a specific seismic reflector but rather a reflector

character change on the seismic data (Figures 82 and 83). Horizon C was manually picked to differentiate between this seismic character. Horizon C ranges from about 400 to 2100 ft below the seafloor (Figure 80). Sediments overlying Horizon C thicken in areas associated with valley features and structural lows surrounding salt uplift. Paleotopography along Horizon C probably served to direct and focus the downslope movement of sediments into these areas. The sediment unit over Horizon C thins over salt structures. Horizon C is the shallowest horizon to accurately depict the location of the underlying salt bodies. Faulting of Horizon C and associated high-amplitude anomalies (Figure 84) are most prevalent on top of the salt bodies and represent hydrocarbon and local fluid trapping along fault planes that pierce this sequence.

H. Sequence II: Horizon C to Horizon C'

The stratigraphic unit between Horizon C and Horizon C' is composed of moderate to high-amplitude, chaotic reflectors (Table 4). This sequence correlates with the "Chaotic Sands" unit cored at the Mensa prospect. Scout tickets from the exploration wells in MC 730 and MC 731 indicated water flow from this sequence at 1855 ft and 2072 ft (bml), respectively. The well in MC 731 also produced gas below 2072 ft (bml), Burman and Norton (1998).

This sequence is very chaotic with a high-amplitude seismic character (Figure 77). This unit is a heterogeneous mix of sand, silt, and clay. Many faults intersect this

sequence due to its relative nearness to salt. High-amplitude seismic anomalies near these faults suggest fluid migration from depth through this sequence. Vertical fluid migration appears to be trapped by the sediments overlying this unit possibly sealing overpressured fluids, particularly near faults. The presence of thick, hard clays above Horizon C may form a seal against which overpressured fluids could accumulate.

The base of this sequence, Horizon C' (Figures 77) defines the bounds the high-amplitude, chaotic unit above from parallel continuous stratigraphy below. Horizon C' ranges from about 200 to 1400 ft below the seafloor (Figure 70). Sediments overlying Horizon C' thicken in areas associated with valley features and structural lows and thin over salt structures. Seafloor topographic highs have probably served to direct and focus the downslope movement of sediments into these areas.

I. Sequence I: Horizon C' to Top of Salt/4.00 Seconds

The sediments between Horizon C' and the Top of Salt vary in seismic character (Table 3). In areas where salt is not present, the seismic data shows alternating units of parallel and chaotic reflectors. The parallel strata are likely to be composed of clays and silts. The chaotic reflectors are probably mass movement events (Figures 71 and 72). These alternating sequences are a common occurrence in inter-salt basins on the continental slope. The debris slides or turbidites that comprise the mass-movement episodes originate from upslope failures or may be caused by more local instability along the flanks of the salt bodies in the area.

High-amplitude events between Horizon C' and the Top of Salt (Figure 73) likely indicate accumulations of fluids that have migrated along faults. Numerous lineations over and around salt uplifts represent faults (Figure 73). The boundaries of the salt are evident as a white "halo" on the RMS display.

The Isopach Map, Seafloor to Top of Salt (Figure 46) shows the sediment thickness from the seafloor to the top of salt. The map illustrates where salt could be mapped from the seismic data. In areas not mapped as salt (Figure 46), the salt was either not present, not mappable, or was deeper than 4.00 seconds (the time/depth cutoff for the data). Salt bodies are present in the northeast, southeast, and southwest quadrants of the study area, and along the west central perimeter of the study area.

Fluid migration may be occurring along faults that pierce this sequence. This sequence is highly faulted with numerous associated amplitude anomalies (Figure 73). Fluids may become trapped in the more granular soils associated with the mass-transport events in this sequence. Local overpressured fluids may be present where clays have sealed isolated sand lenses or strata within the mass-transport events in this sequence.

CHAPTER IX

OBSERVATIONS

The analysis of the seismic data within the study area with respect to salt tectonics, slope depositional processes, sequence stratigraphy, and the geologic model has yielded the following twenty-one observations:

1. The study lies at the convergence of three tectonostratigraphic provinces. Four salt bodies (SBI-SBIV) are present in the study area and mapping of these bodies relative to these tectonostratigraphic provinces has been refined from past regional studies.
2. SBI may lie along a thin-skinned, strike-slip boundary defined by Peel et al. (1995). Formation of SBI may have resulted from the formation of dip elongate shallow salt bodies along the strike-slip transfer zone described by Peel et al. (1995). This boundary has been proposed by Diegel (1995) as the transition between a Plio-Pleistocene Detachment and Salt Dome/Minibasin Province. SBI is the southern extent of a regional Roho system as defined by Schuster (1995). SBI should be considered entirely part of the Mississippi Canyon Plio-Pleistocene Detachment province.

3. SBII has undergone salt emplacement and subsequent gravity sliding like that proposed by Wu et al. (1990a). SBII is part of a Tabular Salt Minibasin Province proposed by Diegel (1995). SBII is interpreted to be in the middle stage of allochthonous salt body formation and early stages of tabular salt formation. The overlying deformation of the stratigraphy above SBII suggests the salt is not in equilibrium with lateral extension from gravity sliding still occurring at present.
4. SBIII is a small allochthonous salt body that is part of a large salt canopy covering most of the southwestern Mississippi Canyon area. SBIII is part of the same Tabular Salt Minibasin Province as SBII. It is also part of the Canopy I salt complex proposed by Peel et al. (1995). SBIII is a secondary or isolated salt stock originally part of Canopy I and subsequently segmented by Cenozoic sedimentation along the eastern periphery of the canopy.
5. SBIV is a very small allochthonous salt body that is also part of Canopy I complex and Tabular Salt Minibasin Province. Minimal uplift and offlap of overlying sediments implies geologically recent, rapid, vertical emplacement. SBIV is the youngest salt body in the study area.
6. Two types of sedimentary basins were identified in the study area (TI and TII). TI basins are deep, intrasalt basins located between salt bodies. TII basins are suprasalt (on top of salt) basins formed by the differential loading and

remobilization of the surface of salt bodies in the study area. SBI has the most and deepest TII basin and I propose that SBI is the oldest salt body in the study area.

7. Seven prominent horizons (A, B, B', C, C', and Top of Salt) were mapped to define the shallow stratigraphy in this study. These horizons were used to separate six stratigraphic sequences (SI-SVI) for further analysis. These six sequences are analogous to Dixon and Weimer's Sequences 8 through 17 identified in the Eastern Mississippi Fan and extend their work approximately 45 miles to the north-northwest.

8. Sequence I was mapped from Horizon C' to the Top of Salt and is estimated to have been deposited between 1.1 Ma and 0.450 Ma, BP. It is composed of six seismic facies representing deposition of both fine-grained hemipelagic and coarser grained mass-transport events. The sequence is present in both TI and TII basins. The sequence in TI basins is composed of alternating condensed and expanded sections related to changes in eustatic sea level and individual mass-transport events. The sequence in TII basins sediments that have either all, or partially, undergone some form of deformation by the remobilization of salt. This sequence is analogous to Dixon and Weimer's sequences 8-12.

9. Sequence II was mapped from Horizon C to C' and is estimated to have been deposited between 0.450 Ma and 0.400 Ma, BP. It is composed of two seismic facies. These facies represent thick, low and high-energy mass transport deposits resulting in a thick slide sequence. This sequence has almost completely filled in the TI basins in the study area and thins significantly on top of SB I-IV. The sequence is not present in TII basins. This sequence is analogous to the lower part of Dixon and Weimer's sequence 13.

10. Sequence III was mapped from Horizon C to Horizon B' and is estimated to have been deposited between 0.400 Ma and 0.070 Ma, BP. It is composed of one seismic facies representing a series of thick, condensed sections interbedded with thin mudflows. This sequence represents a major avulsion to the west in the depocenter feeding this part of the Eastern Mississippi Fan. Sequence III is analogous to the thick condensed sections at the top of Dixon and Weimer's sequence 13.

11. Sequence IV was mapped from Horizon B' to Horizon B and is estimated to have been deposited between 0.070 Ma and 0.055 Ma, BP. It is composed of three active depositional facies representing sand-rich turbidite deposits, debris slides, and channeled mass-transport deposits. This sequence marks the eastward shift in the Mississippi River depocenter noted by Weimer and is analogous to sequence 14.

12. Sequence IV contains a large channel that incised into Sequence III and was subsequently infilled mass-transport deposits and incipient slumping. This channel is identified as Dixon and Weimer's Channel 14a and extends this channel some 27 miles further west.

13. Sequence IV contains the Blue Unit which is composed of thick deposits of almost pure sand turbidites interbedded with thin clays and shales. These ponded sediments comprise a basin floor fan whose source high-energy turbidites that traveled down Channel 14c and ponded in a salt minibasin bounded by SB II and SBIII. The facies and geometry of these deposits satisfy those Dixon and Weimer used to identify a basin floor fan in Sequence 9 in their work in the Eastern Fan. The fan identified in Sequence IV becomes the second basin floor fan identified in the Eastern Mississippi Fan complex.

14. Sequence V was mapped from Horizon A to Horizon B and is estimated to have been deposited between 0.055 Ma and 0.23 Ma, BP. One facies represents deformed slump deposits. The other facies represents repeated debris slide deposits separated by condensed sections. The number of slides, punctuated by condensed sections may represent a number of minor oscillations in sea level. They may also reflect the interaction of salt tectonics and deposition upslope of the study area during deposition of Sequence IV/V. The numerous slides in the

area may have undercut the slope in the lower half of the study area at the same time as minor uplift was occurring from SBIV, predicating the large rotational slump located in the middle of the study area. Sequence V is analogous to sequences 15 and 16 identified in studies by Dixon and Weimer.

15. Sequence VI was mapped from the Seafloor to Horizon A and is estimated to have been deposited from 0.023Ma to Present. It is composed of one seismic facies representing a thick condensed section. This condensed section represents sediment starvation of the study area by the establishment of the modern Mississippi River depocenter as well as the last high-stand of sea level, which continues to the present.
16. The shallow stratigraphy has formed due to the interaction of salt tectonics and slope depositional processes. A transition in salt motion has been identified. The salt has been mobilized from original allochthonous salt sheets via secondary mobilization to defined Roho end-members.
17. Sequence I is most dominated by the movement of salt. Salt movement has resulted in extensive faulting and uplift of Sequence I. The distribution of thickness of the massive slides in Sequence II was dictated by the pre-existing seafloor topography initiated by the salt.

18. The remaining Sequences (II-VI) are more influenced by slope depositional processes with the affect of regional salt tectonics playing a minimal role in their formation.
19. Sequences IV and V represent mass-transport and deposition in a high-energy regime.
20. Sequence VI is a clay drape sequence whose thickness and distribution is entirely dominated by sediment starvation (a quintessential slope process) and hemipelagic deposition under high stand conditions.
21. The interaction of salt tectonics and slope depositional processes has formed the present day shallow stratigraphy in the study area. These processes have dictated the rate, aerial distribution, and relative thickness of sequences in the shallow section. Therefore, they have dictated the number, kind, distribution, and magnitude of hazards and/or constraints to exploration or production drilling for this newly analyzed part of the Eastern Mississippi Fan.

These observations form the literal basis for the discussion of the more significant, broader-impact geological processes and concepts that resulted from this study in the following DISCUSSION chapter.

CHAPTER X

DISCUSSION

Introduction

The analysis of the data for this study has yielded six significant results about the geology and geological processes for this portion of the Louisiana Continental Slope as well as the northern Gulf of Mexico. They are as follows:

- Despite different histories, salt structures in the study area are mature end-members and exhibit a shift in mobilization history from regional to very local deformation of the suprasalt section.
- The shift from regional salt tectonics as the dominant process to depositional no later than ~450 ky before present.
- Stratigraphic sequences in the study area correlate to those of Dixon and Weimer and expand interpretations for Eastern Mississippi Fan westward.
- Eastern Mississippi Fan likely sourced from an avulsing Pleistocene Mississippi River depocenter, NOT from Mobile River and Lagniappe Delta.
- Although sequence stratigraphy ties to oxygen isotope stages, it is more dependent upon location of Pleistocene depocenter than on sea-level change.

These points are discussed in the following sections.

Salt End-Members and Shift in Mobilization History

The four salt bodies in the study area SBI-SBIV (Figures 44 and 45) are considered to be individual allochthonous salt bodies each with its own source and emplacement history. Figure 37 illustrates the position of tectonostratigraphic provinces with respect to the study area. Figure 43 show the position of the salt in the study area relative to regional distribution of salt. Despite different sources and deformational histories, there is compelling evidence to show that presently the salt bodies in the study area have evolved to mature allochthonous structural end-members (specifically Roho end-members) and in doing so, exhibit a shift in mobilization history from regional to very local deformation of the stratigraphic section. The evidence is found by synthesizing previous work such as that by Schuster (1995) and Wu et al (1990a), with observations from the seismic data of the location of the salt bodies, the geometry of the salt surface, and the corresponding deformation of the surrounding stratigraphic section, specifically with respect to SBI and SBII.

SBI has been identified as the seaward expression of a Roho end-member system. Schuster discussed two different end-member system models toward which shallow, horizontally emplaced salt sheets have been found to mobilize toward based on observations of seismic data in the Gulf of Mexico. The models are designated Roho and Stepped Counter-Regional end-members and are illustrated in Figure 52. In both cases horizontally emplaced allochthonous salt sheets are remobilized due to sediment loading and result in the end-member geometries.

The key point in discussing end-members systems is that they are just that, the end results of allochthonous salt mobilization. For both cases, the original volume of the allochthonous salt is mobilized basinward resulting in subsidence and faulting of the overlying stratigraphic section. The result is a basin under which most or all of the salt has been mobilized proximal to a shallow salt body on the seaward end of the system. As the salt transitions from a regional allochthonous salt sheet to a more locally focused end-member so too the deformation of the surrounding stratigraphic section will become focused around the end-member salt. Once the salt underneath the basin is fully isolated, or depleted, the system shuts down with only secondary mobilization of the now shallow seaward end-member salt body occurring.

This is such the case for SBI. Figure 53 illustrates the position of SBI with respect to the Roho end-member salt body identified by Schuster (1995). A deep seismic line (Schuster, 1995) shows the position of SBI in the overall Roho end-member system. The seismic line shows a deep, normal-faulted stratigraphic basin overlying very thin and depleted salt flanked on the seaward end by a shallow salt body (SBI). Of note on Figure 53 is the depth in the stratigraphic section above which most of the extensive normal faulting of the stratigraphic section appears to cease with only more regional adjustments with apparent minor offsets affecting the section. This same feature can be seen on Figure 116. Note on the figure how the extensive faulting in the bottom half of the figure does not extend beyond the top of Sequence I (Horizon C') Only minor displacements occur above the horizon or are locally focused above SBII (implied to be analogous to the stratigraphic section north of SBI outside of the study

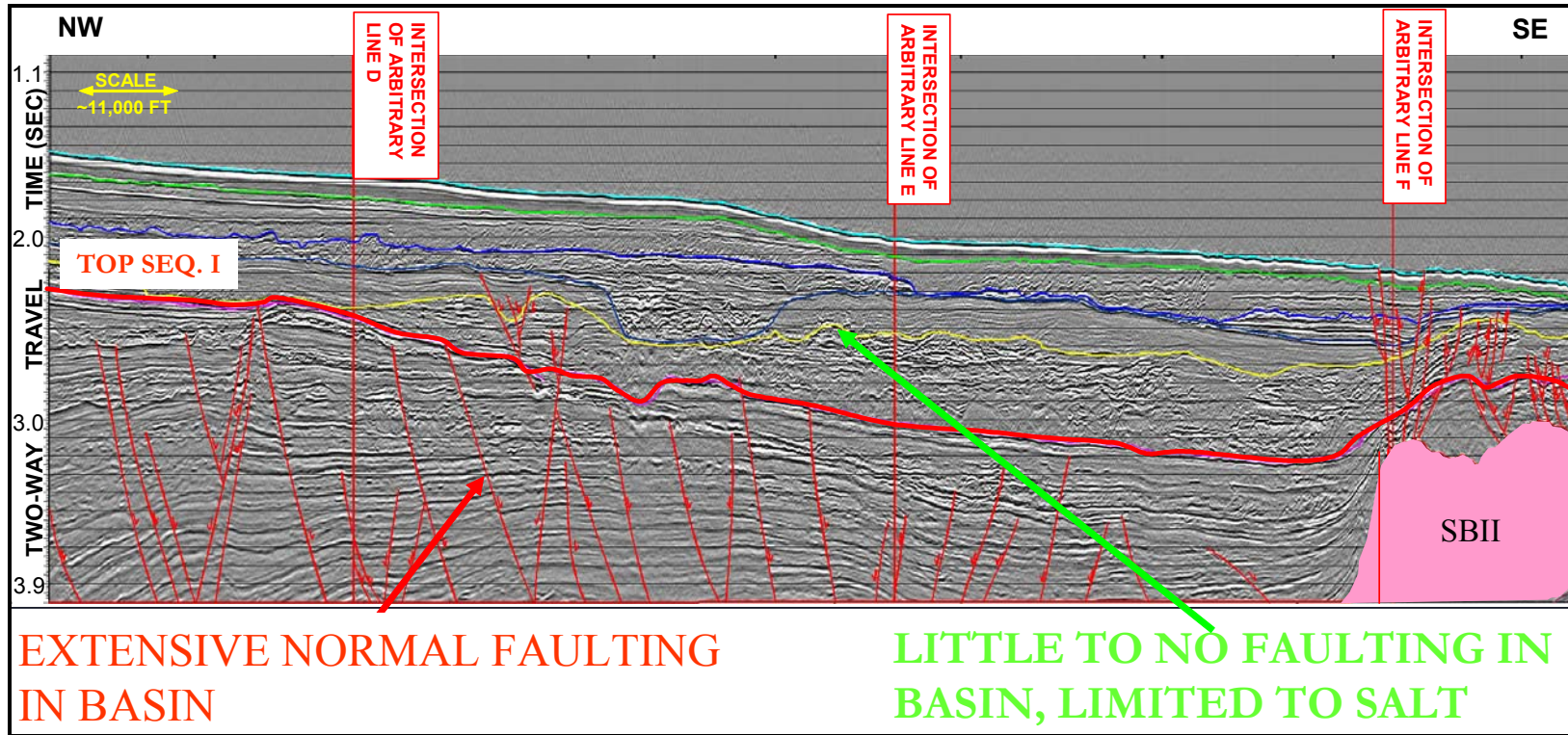


Figure 116. Arbitrary Seismic Line B illustrating extent of normal faulting. Note little to no faulting above top of Sequence I. Note also lack salt tectonic affect on stratigraphy above the top of Sequence I as well as concentration of faults above end-member SBII. Thin red lines are faults. Thick red line is top of Sequence I. Colored lines are horizons separating stratigraphic sequences.

area). The upper limit of displacements in both Figure 53 and Figure 116 signify the end of significant extension associated with salt withdrawal and full establishment of the end-member geometry. As the salt volume under the basin nears full depletion, regional subsidence and associated extension of the overlying stratigraphic would cease with only minor motions occurring along the larger, more established normal faults within the system. This would also signify a shift of the affect of salt mobilization from regional to local focus around the established end-member salt

There are further similarities between the regional seismic example of the Roho end-member system on Figure 53 and Figure 116. The shallow stratigraphy above the limit of prevalent faulting in Figure 53 shows little structural expression of the deep basin below. Figure 53 exhibits the same geometry as sequences above Sequence I (Horizon C') do not exhibit any structural deformation indicative of subsidence toward the basin. The only location where structural deformation of the stratigraphic section above Sequence I occurs locally over the salt of SBII (again, deemed analogous to the section north of SBI). Again, features such as this signify the establishment of the end-member salt as well as provide evidence for a shift from regional salt mobilization and deformation to a more local extent focused on the established end-member salt bodies such as SBI.

Note also the irregular surface of SBI in the deep seismic line in Figure 53 and the similarities on seismic data from this study on Figure 48 and Figure 49 as well as the perspective view of the salt surface on Figure 45. The rugose salt surface of SBI is suggestive of secondary mobilization (Nelson and Fairchild, 1989). Secondary

mobilization is expected to occur over allochthonous salt sheets where the feeder stock has either been significantly reduced or depleted (Nelson and Fairchild, 1989). The source of end-member salt bodies is either nearly or fully depleted, making the end-member salt vulnerable to remobilization by the local sediment load atop the salt body. A rugose, irregular salt surface with numerous TII suprasalt basins illustrates the salt is undergoing secondary mobilization expected from an end-member such as SBI.

SBII exhibits many of the traits of SBI and an end-member system. The correlations between Figure 53 and Figure 116 for SBII are applicable. The main difference between SBI and SBII is the expression of the end-member salt. SBII is a shallow; allochthonous end member is a salt sill that is undergoing gravity sliding (Wu et al., 1990a). A palipinastic model for the formation of SBII is shown in Figure 29. SBII is in the Cessation and Burial stage of end-member development. The back of the salt in Figure 116 shows an overlying graben and concave inflection of the salt surface. Wu et al. (1990) describe this geometry occurs when the rate of salt supply from the feeder is reduced, or cutoff, and the salt body begins to undergo collapse and secondary mobilization.

End-member salt systems in the area are exemplified in the discussion of SBI and SBII. It important to understand that the models for end-member formation are simplistic and each salt will have an individual expression in its respective end-member system. However, seismic sections in the area show the limit of regional deformation associated with the mobilization of the salt bodies to their respective end-member systems and illustrate the transition from regional deformation (faulting) to more local

deformation (focus faulting above salt, stratal uplift and folding, suprasalt basin formation through secondary mobilization) as the end-member is established.

Shift in Dominance from Salt Tectonics to Slope Depositional Processes

The previous section discussed the process of formation and geometry of end-members systems in the study area using SBI and SBII as examples. The establishment of salt end-members in the study area signifies a transition from a regional salt tectonic influence to local salt tectonic influence focused around the established end-member salt bodies (local faulting and affect of secondary mobilization such as TII basin formation). This shift is quite significant as it also marks the transition from salt tectonics as the dominant geologic process to slope depositional processes. Based on the observations of this study, this shift is defined to have occurred no later than ~450ky ago.

Evidence for this is tied to the extent of significant regional faulting within the stratigraphic section and the assigned ages of those stratigraphic sequences affected and not affected by regional salt tectonics as well as those affected and not affected by local salt tectonics. In the previous section, Figure 116 illustrated the extent of regional salt tectonics, in the form of pervasive faulting, ceased at the top of Sequence I with deformation occurring in the form of minor adjustments along pre-established faults or localized around end-member salt bodies thereafter. Regional structural deformation ceased after the deposition of Sequence I, therefore, the age of Sequence I and overlying Sequence II are critical in establishing the transition between regional salt tectonics to

local salt tectonics related to establishment of the end-member salt bodies. This in turn marks the end of active regional salt tectonic processes and a transition in dominance from those regional tectonic processes to slope depositional processes in formation of the stratigraphic section.

The ages of the stratigraphic sequences have been established through correlation of the sequences in the study area with those sequences identified by Dixon and Weimer (1994, 1998) and their work on the Western and Eastern Mississippi Fan (Weimer 1989, 1990, Dixon and Weimer 1994, 1998) for which the ages were established. Extensive discussion of the correlation occurs in the previous chapters. The correlation in sequence identification between this study and previous work by Dixon and Weimer is found in Table 10. The age of Sequence I was difficult to correlate to the previously established sequences because the seismic data for this study was not deep enough to see the base of Sequence I. There are two hypotheses for the age of Sequence I. The first is that it correlates to ~Sequence 8-12 of Dixon and Weimer (1994) which would put the top of the sequence at ~450ky before present. The second hypothesis is that the sequence is much older than that of Sequences 8-12 and may in fact be the top of the Pliocene. Evidence for this is derived from the two independent palipinastic reconstructions of salt evolution in the study area by Schuster (1995, Figure 55) and Wu et al. (1990, Figure 29). The reconstruction on Figure 55 shows a transition in basin formation and implied salt motion occurring at the boundary marked "Plio" which designates the top of the Pliocene. Figure 29 also suggests the same in the 10th panel in the evolution of what is SBII where there is a relatively thin, near flat-lying Pleistocene

section. Thus it is possible that the age of Sequence I could range from top of Pliocene to ~450ky before present.

The age of Sequence I is not as critical as the boundary between Sequence I and Sequence II. Sequence II has been correlated with confidence (due to its position relative to the condensed section in Sequence III and descriptions of underlying stratigraphy under that condensed section by Dixon and Weimer (1994, 1998) matching those of Sequence II) and assigned an age of ~450ky to ~400ky before present. There is an unconformity at the boundary between Sequence I and Sequence II (Figure 116). The significance of the unconformity is that it shows either erosion or non-deposition representative of missing time in the section. Thus, the exact end of regional faulting and associated establishment of salt end-members cannot be determined. However, Figure 116 illustrates that regional tectonics, signified by faulting, truncates at the top of Sequence I/base of Sequence II. With confident correlation in the identification of Sequence II, the base of the sequence is ~450ky before present. Truncation of the faults at the base of Sequence II shows that regional salt tectonics and its affect on the stratigraphic section had ceased no later than ~450ky. This marks the transition from regional salt tectonics to local salt tectonics associated with the end-member salt systems. It also signifies the punctuated shift in dominance from salt tectonics to slope depositional processes in the study area. This is further substantiated by the structure map of the top of Sequence II (Figure 74) when compared to the structure map of the top of Sequence I (Figure 69). In Figure 69, the salt structure is dominantly expressed. Note the well defined and steep edges of the salt and the depth of the TI basin in between.

Compare that to the Figure 74 where the expression of the salt structure is denuded and the TI basin begins to fill. With slope depositional processes becoming dominant and salt in its end-member state, the salt structure obvious in Figure 69 starts “drowning” under the deposits from Sequence II and will continue to do so with subsequent deposition of Sequences III-VI.

Correlation With and Extending the Eastern Mississippi Fan Westward

Previous work done in identifying the Eastern Mississippi Fan by Dixon and Weimer (1994, 1998) are landmark papers on Gulf of Mexico sequence stratigraphy. An objective of this study was to attempt to correlate sequences of the Eastern Fan into the study area. The location of the study area is west of the northern limit of the Eastern Fan interpretations evident of Figure 27.

Six stratigraphic sequences were identified in the study area independent of the previous interpretations of sequence stratigraphy by Dixon and Weimer (1994, 1998). Correlation of the sequences between the study area and those previously identified for the Eastern Fan (Dixon and Weimer, 1994, 1998) used methods established by Dixon and Weimer for extrapolating sequences from the Western Mississippi Fan to the Eastern Mississippi Fan. Due to the cycles of deposition, erosion, and redeposit, they found it was difficult to correlate higher-energy, active depositional sequences between the two fans. However, the key to correlation was in the condensed sections that were found in the two fans. Correlating the condensed sections between the Eastern and

Western Fan allowed for correlation of sequences both above and below the condensed sections. The same method was applied to the sequences in the study area with condensed sections being vital to correlation to condensed sections in the previously defined sequences of the Eastern Fan.

There are two condensed sections in the study area, one being Sequence III and the other being Sequence VI. The thick, stacked series of condensed sections in Sequence III was the common reference point correlating for the remaining stratigraphic sequences. Sequence III represents a significant condensed section that affected at least the whole Eastern Fan as the Pleistocene shelf-edge depocenter shifted west to the middle of the Gulf of Mexico continental shelf (Berryhill et al., 1986). Thus, the sequence could be correlated seismically between the Eastern Fan (based on sequence description and interpreted seismic expression in the study area) to the study area. The sequence was also correlated by descriptions by Dixon and Weimer (1994, 1998) for the sequences immediately above and below the condensed section. The same methodology was applied to Sequence IV which is the last (youngest) sequence in the Eastern Fan.

Once correlation of the condensed sections were established the remaining stratigraphic sequences in the study area (Sequences I–IV) were correlated to previously established sequences for the Eastern Fan (Dixon and Weimer, 1994, 1998) based on their seismic facies descriptions and implied depositional processes. Table 10 represents the correlation and ages of sequences between those of this study and those previously established for the Eastern Fan. The previous section identified the problems with confidently assessing the correlation of Sequence I of this study to Sequences 8-12 of the

Eastern Fan. However, the remaining sequences of this study (II-VI) are extended into the study area with good confidence resulting from correlation of the condensed sections and matching facies descriptions of sequences both above and below the condensed sections.

Correlation of a significant channel defined by Dixon and Weimer (1994, 1998) also provided further confidence in the correlation. They described a channel, 14a, present within their Sequence 14. This sequence in the study area was defined as Sequence IV and directly overlies the major condensed section in Sequence III (top of Sequence 13 for Dixon and Weimer). The presence of the channel was confirmed in the study area (Figure 103). This is significant because well-defined channels are only present in Sequence 14 (Sequence IV this study) in this portion of the Eastern Fan (Dixon and Weimer 1994, 1998).

Correlation of the Eastern Fan sequences defined by Dixon and Weimer (1994, 1998) to the study area extends the interpretations of the Eastern Mississippi Fan ~28 miles west (Figure 27), increases the aerial extent of the interpreted Eastern Fan by ~720 square miles, and extends the only well-defined channel in this portion of the Fan west. These are not trivial as extending the Eastern Fan westward has implications for understanding the source of the Eastern Fan.

Mississippi River is Source of the Eastern Mississippi Fan

The previous section established the correlation of the sequence stratigraphy in the study area to study area thereby extending interpretations ~28 miles westward and expanding the aerial extend of Eastern Fan interpretations by ~720 square miles. This is significant in that is has extended the fan west toward the Mississippi River. Dixon and Weimer (1994, 1998) established that based on the relative small size and clay-dominant composition of the Eastern Fan that it must have been sourced not from the Mississippi River but from the Mobile River via the shelf-edge Lagniappe delta.

No studies have been conducted to refute this interpretation; however, extending the Eastern Fan interpretations west suggests an alternate source of the Eastern Fan. Nowhere is this more evident than in the trend of the previously described channel within Sequence IV (Dixon and Weimer Sequence 14), channel 14a. Identifying channels and their location are critical to establishing conduits for the delivery of sediment from shelf-edge depocenters to the continental slope. The location of established Eastern Fan channels relative to the study area is found in Figure 27. Figure 117 shows the location of the channel within Sequence IV on a seismic line through the study area. The channel is easily recognizable as it has incised and completely removed underlying Sequence III (condensed section) deposited beneath it. The facies for Sequence IV are presented in Table 6. Figure 80 shows the structure map to the base of Sequence IV (top of Sequence III) showing the increase in depth associated with the channel cut. Figure 81 illustrates the Isopach thickness of the stratigraphic section above

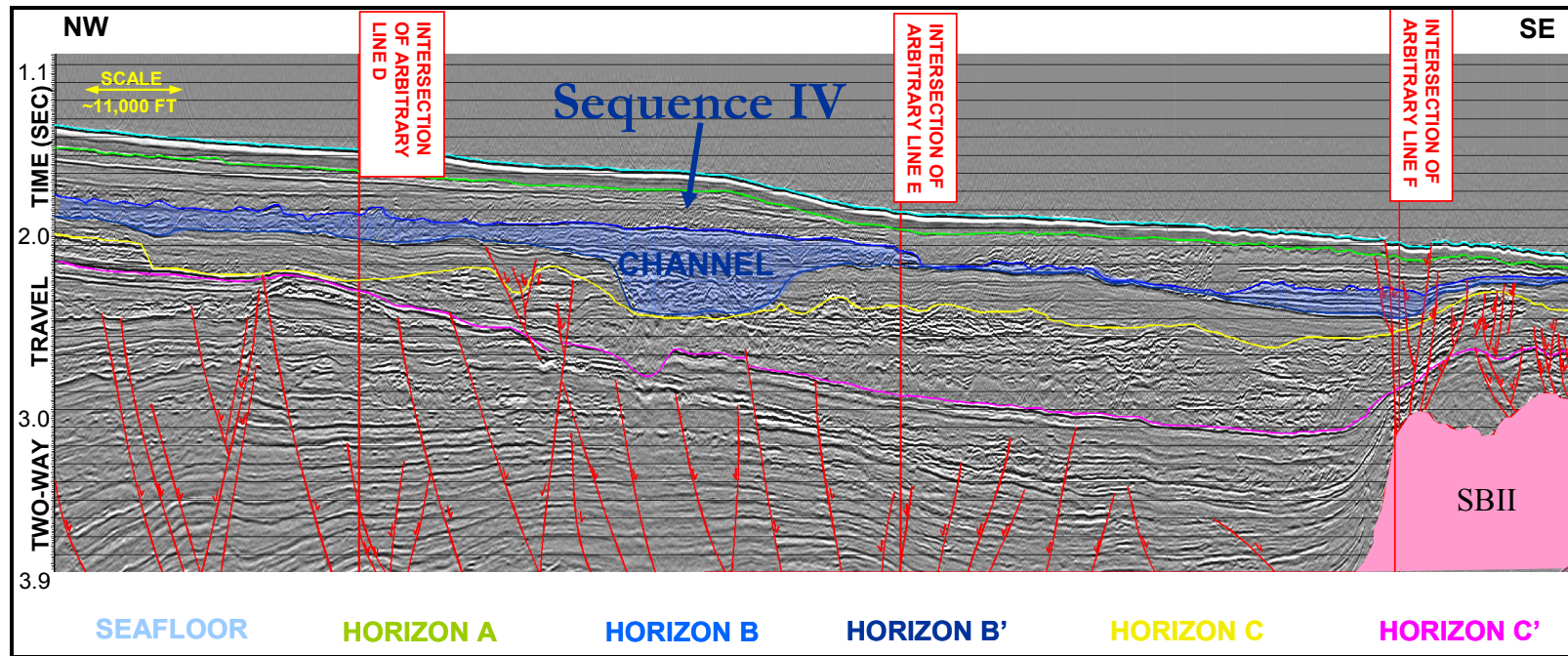


Figure 117. Location of channel in Sequence IV. Shaded area is Sequence IV. Red lines are faults. Colored lines are horizons separating stratigraphic sequences. Pink shaded area is salt.

the base of Sequence IV (top of Sequence III) showing the deepest sediment thickness (fill) above the channel cut. Figure 84 is an RMS display of the underlying Sequence III showing the location of the base of the channel incision. Being a condensed section, the overall low amplitude of Sequence III expressed the position of the channel cut into the sequence better than the overlying higher-amplitude sequence in which the channel is contained. The position of the channel is marked on the RMS display in Figure 84. Figure 102 is a perspective of the structure to the base of Sequence IV (top of Sequence III) overlain with the RMS from Sequence III (also seen on Figure 84). From the image you can see the position of the structural low (channel cut) and associated high-amplitudes associated with the base of the channel concentrated in the channel.

The significance of thoroughly identifying the extent of this channel lies in extending it west approximately another 28 miles west (Figure 103). Based on the shelf slope geometry (Figure 2), location of the Lagniappe Delta on the shelf east of the modern Mississippi River delta (Figure 2), and azimuth of the channel, it is not possible that the Lagniappe Delta was the source of sediment that scoured or filled the channel. The channel must have an origin that lies on the shelf somewhere south of the modern Mississippi birdfoot delta and been sourced from a Mississippi River depocenter.

Further evidence to support this theory is found in recent work on Mississippi River Pleistocene deposystems (Winker and Booth, 2000). Figure 118 shows the location of the study area and extension of channel 14a in Sequence IV on a composite of their work on the Pleistocene Mississippi River deposystem. There are three things to note: 1) The close proximity of the study area and channel to established Mississippi

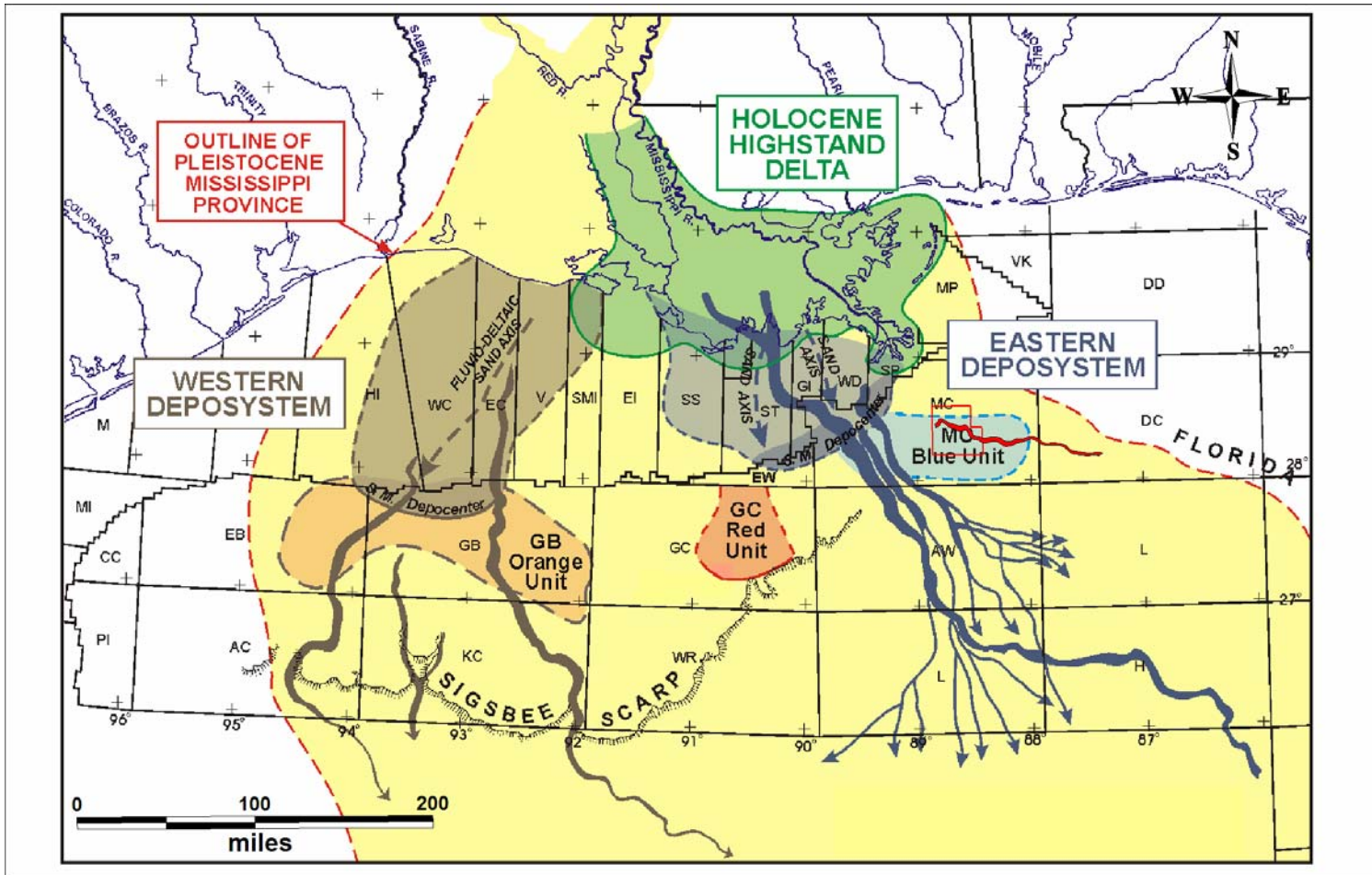


Figure 118. Composite Mississippi River Pleistocene deposystem (Winker and Booth, 2000). Regions are annotated on the image. Dark blue arrows are Eastern Deposystem sediment pathways. Dark brown arrows are Western Deposystem sediment pathways. Study area outline in thin red. Channel 14a is the red channel feature. Note the location of study area with respect to the S.M. (Sea level minima depocenter) and the MC Blue Unit (Sequence IV turbidites) with respect to the location of the study area. Note also the trend of channel 14a to the west northwest toward the eastern edge of the depocenter.

River Pleistocene sediment pathways, 2) The azimuth of the channel trending west toward these pathways, and 3) The location of what Winker and Booth (2000) call the Blue Unit. The Blue Unit (Winker and Booth 2000) is the same Blue Unit identified as turbidite sands in the study area by Burman and Norton (1998), also located in Sequence IV (same as channel 14a). The Blue Unit has been determined to be a turbidite sheet sand deposit sourced from a Pleistocene Mississippi River depocenter. The presence of channel 14a provides compelling evidence for its source being the same depocenter. The remaining sequences are also likely to be sourced from a Pleistocene Mississippi River depocenter. The variation in size and composition of the Eastern Fan and the Western fan, which lead to the original hypothesis for the Eastern Fan's origin being the Mobile River by Dixon and Weimer (1994, 1998), may actually be related to the location of the Eastern Fan relative to the avulsing Pleistocene Mississippi River depocenter through time.

Eastern Fan Sensitivity to Depocenter Location and Sea-Level Change

The previous section suggested an explanation for the size and composition of stratigraphy in the Eastern Fan is that the Fan is that the fan is not sourced from the Mobile River, but rather the Mississippi River, and may be sensitive to the location of the shifting Mississippi River depocenter through time. There is evidence to support this theory and requires a novel look at the relationship of the sequence stratigraphy in the Eastern Fan relative to its proximity to the shifting Pleistocene Mississippi River

depocenter and changes in eustatic sea-level. The observations from this study suggest that although the sequence stratigraphy ties to oxygen isotope stages, it is more dependent upon location of Pleistocene depocenter rather than on sea-level change. In other words, for the Eastern Fan, the location of the Pleistocene depocenter dictates the formation of the sequence stratigraphy while sea-level change plays only a minor role.

Evidence for this is found when plotting the ages of the sequences for this study, correlated to those by Dixon and Weimer (1994, 1998) of the Eastern Fan, on a plot of oxygen isotope stage and sea-level change (Morton and Suter, 1996) for the last 200ky (Figure 119). The age of the oxygen isotope/sea-level curve covers Sequence III-VI. Note how the age boundaries of the sequences correspond well with the boundaries for individual oxygen isotope stages. The top of Sequence III corresponds to the transition between Stage 5 and Stage 4. The top of Sequence IV is close to the transition between Stage 4 and Stage 3. The top of Sequence V is very close to the transition between Stage 3 and Stage 2 with Sequence VI occupying Stages 2 and 1. The bottom of the figure shows the facies associated with each Sequence identified in this study.

Sequence III represents the condensed section associated with the westward avulsion of the Mississippi depocenter onto the middle continental shelf (Berryhill et al., 1986). However, note the sea-level curve during the formation of Sequence III. The sea level minima at the end of Stage 6 (Illinoian) is the most significant minima outside of the late Wisconsinian minima during Stage 2 yet the sequence stratigraphy in the study area is a condensed section and does not reflect this significant lowstand (or regression/transgression). During this time, this portion of the continental slope is in a “pseudo”-

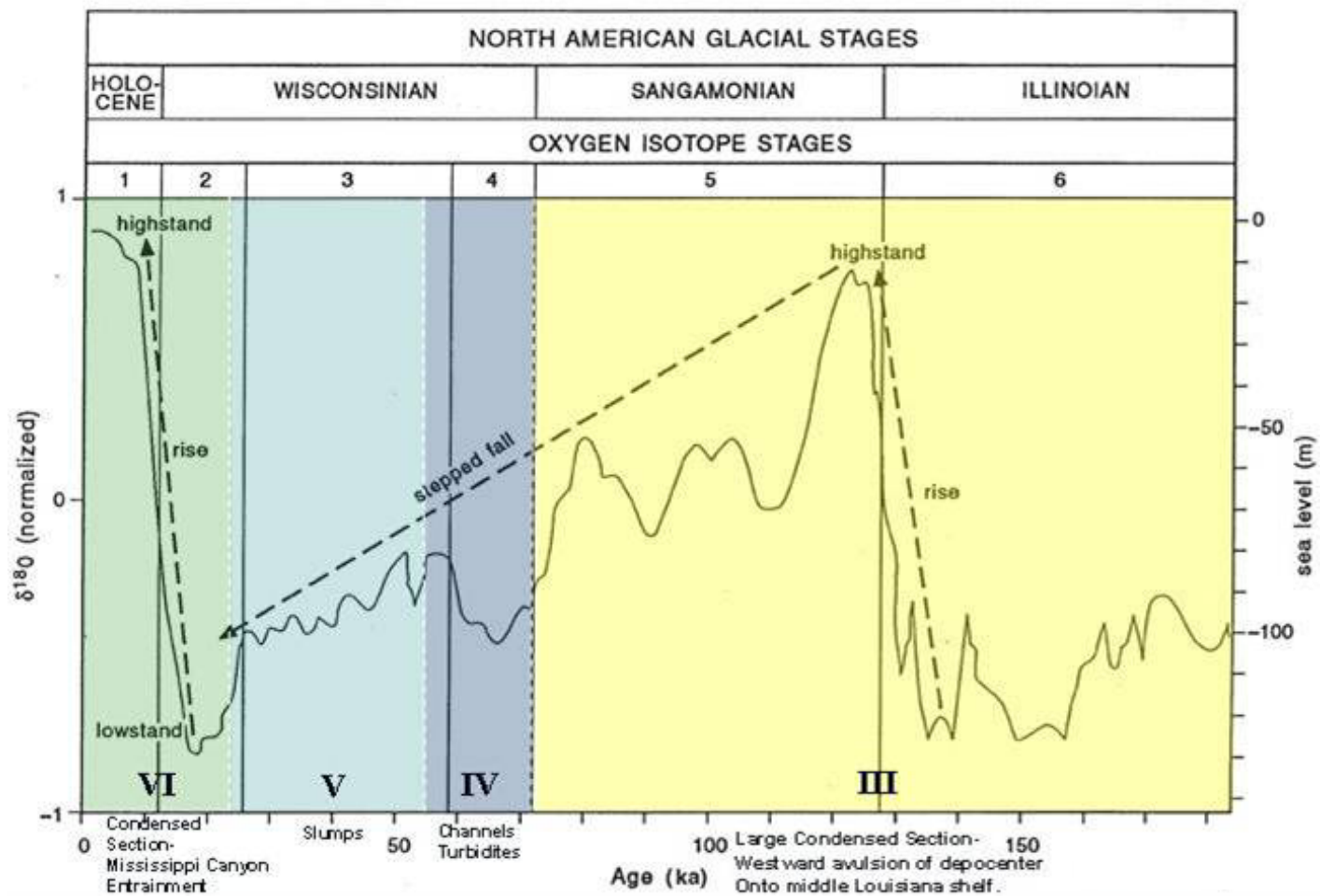


Figure 119. Comparison of oxygen isotope stages and sea level curve (from Morton and Suter, 1996) to ages of stratigraphic sequences III-VI (shaded colored regions) in the study area. Note the correlation of sequence ages with oxygen isotope ages. Note also the lack of correlation between stratigraphic sequence and sea level change. The disparity in the correlation between sequence facies and sea level is likely a result of shifting location of the Pleistocene Mississippi River depocenter playing a greater role in determining formation of the stratigraphic sequence in the study area.

highstand and is insensitive to sea level change because the source depocenter is a significant distance west of the study area. This is significant because condensed sections are generally thought to form during highstand, not lowstand, and the sequence stratigraphy for the Mississippi Fan is thought to be primarily controlled by changes in eustatic sea level. In this case however, it appears that the location of the depocenter relative to the study area is more critical in determining sequence formation than sea level change.

Sequence IV is a high-energy sequence composed of turbidites and channels. The Pleistocene Mississippi depocenter is purported to have shifted back east in closer proximity to the study Eastern Fan (Dixon and Weimer, 1994). With this shift there was increased sediment supply to the shelf edge depocenter and subsequent delivery to the continental slope. The sequence corresponds to Stage 4 (early Wisconsinian) where there was a moderate drop and then rise in sea level over the duration of the age of Sequence IV. This is interesting in that Kolla and Perlmutter (1993) proposed a modified model for turbidite delivery from the Mississippi Fan to the continental slope in which turbidites occur not only at lowstand but far into transgression to highstand. The fact that ponded turbidites occur in the sequence and appear to be at the top or above the channel fill suggests the channel was incised the minima during the “hanging” lowstand and the turbidites above it possible during the transgression to the “hanging” highstand near the end of Stage 4/top of Sequence IV. In a case where the depocenter has relocated in close proximity to the study area, conventional models for sediment delivery and sequence formation appear to apply. This is not contradictory to the

opening statement of this section. Rather, it shows how sensitive the sequence formation is to the location of the depocenter. When the depocenter is near the study area, it is sensitive to sequence formation dictated by sea-level change. When the depocenter is away from the study area, the sequence evolution is decoupled from sea-level change.

Sequence V corresponds to Stage 3 (middle Wisconsinian) and is comprised of numerous slumps interbedded with thin condensed sections. The slumps represent slides that likely propagated downslope from the west and northwest of the study area (Dixon and Weimer, 1998). The condensed sections represent periods of very low deposition rates. Dixon and Weimer postulated that a sequence such as this could be related to subtle fluctuations in sea level and that is what is evident in the sea-level curve in Figure 119. The sea level curve shows minor fluctuations in sea level in an overall drop during regression toward the late Wisconsinian lowstand (Stage 2). However, there are plausible alternate explanations for the periodicity of these slumps. That is that the condensed sections represent another “pseudo”-lowstand in the study area that is periodically interrupted by slope failures generated upslope due to salt tectonic processes coupled with heavy sedimentation during the previous “hanging” lowstand. This would imply that the depocenter has shifted slightly to the west outside of the direct influence on sequence formation in the study area. Another possibility is that evolving salt topography upslope has constricted the downslope movement of sediments that only overcome by mass wasting processes such as slumps.

Sequence VI is the youngest sequence in the study area and is a condensed section occurring in the study area during Stages 2 and 1 (late Wisconsinian). Note the

sea level curve on Figure 119. The late Wisconsinian sea level minima is the most significant in the last 200ky and yet there is no impact on the formation of the sequence stratigraphy. This is likely associated with the establishment of the late Pleistocene (late Wisconsinian) Mississippi Canyon that entrained the Mississippi depocenter during this time allowing for direct bypass of the shelf edge down the canyon. The shelf/upper slope area west and northwest of the study area probably received very little sedimentation. Sequence VI is another “pseudo”-highstand and represents another period of time where depocenter location and dynamics dictate the sequence formation that is essentially decoupled in the study area from sea-level.

The location of the Pleistocene Mississippi depocenter has a critical impact on the formation of the sequence stratigraphy, more so than changes in sea level, in the study area and likely for the whole Eastern Mississippi Fan. This is due to the unique location of the study area along the eastern fringe of the Pleistocene depocenter. A Miocene analogue of the depositional processes along the fringe of the Miocene Mississippi depocenter (Figure 110) illustrates the sensitivity of the study area with respect to the shifting depocenter. The figure shows depositional systems and features seen in the study area with salt near the surface, extensive slumping at the shelf-edge north of the study area (see Sequences II and V), and defined channels and ponded, lobate sand bodies (see Sequence IV). Note that to the west, closer to the center of the slope deposystem in the figure, there is an increased scale to the occurring depositional processes. However, the key is to look east of the study area in Figure 110, where a condensed section is forming. Thus, the magnitude and scale of depositional processes

and resultant sequence stratigraphy is gradational across the slope deposystem. Given the location of the study area on the eastern fringe of the Miocene depocenter analogue, it is easy to envision a subtle shift of the depocenter to the west resulting in the formation of a condensed section in the study area while the processes to the west of the study area would remain active.

A Pleistocene deposystem analogue for the Pleistocene is presented in Figure 120. The study area lies along the eastern fringe of the most recent Pleistocene depocenter defined by Winker and Booth (2000). Sand axes connect the center of the depocenter to the upper slope facilitating delivery of the Blue Unit turbidites to the study area. Proposed upslope sediment pathways connect the eastern edge of the depocenter to channel 14a in the study and provide potential conduits for the delivery of sediments from the shelf edge into the study area. The entire Pleistocene depocenter is represented and illustrates the broad coverage of the Mississippi River depocenter during the Pleistocene. As with the Miocene depocenter analogue, it is easy to envision how a subtle westward shift of the depocenter at any time during the Pleistocene would have a significant affect on the formation of the stratigraphic sequence in the study area.

The Eastern Mississippi Fan lies downslope along the eastern fringe of the Pleistocene deposystem. The size and sequences of the Eastern Fan likely are dictated more by the changes in the position of the ever-shifting deposystem than changes in eustatic sea level.

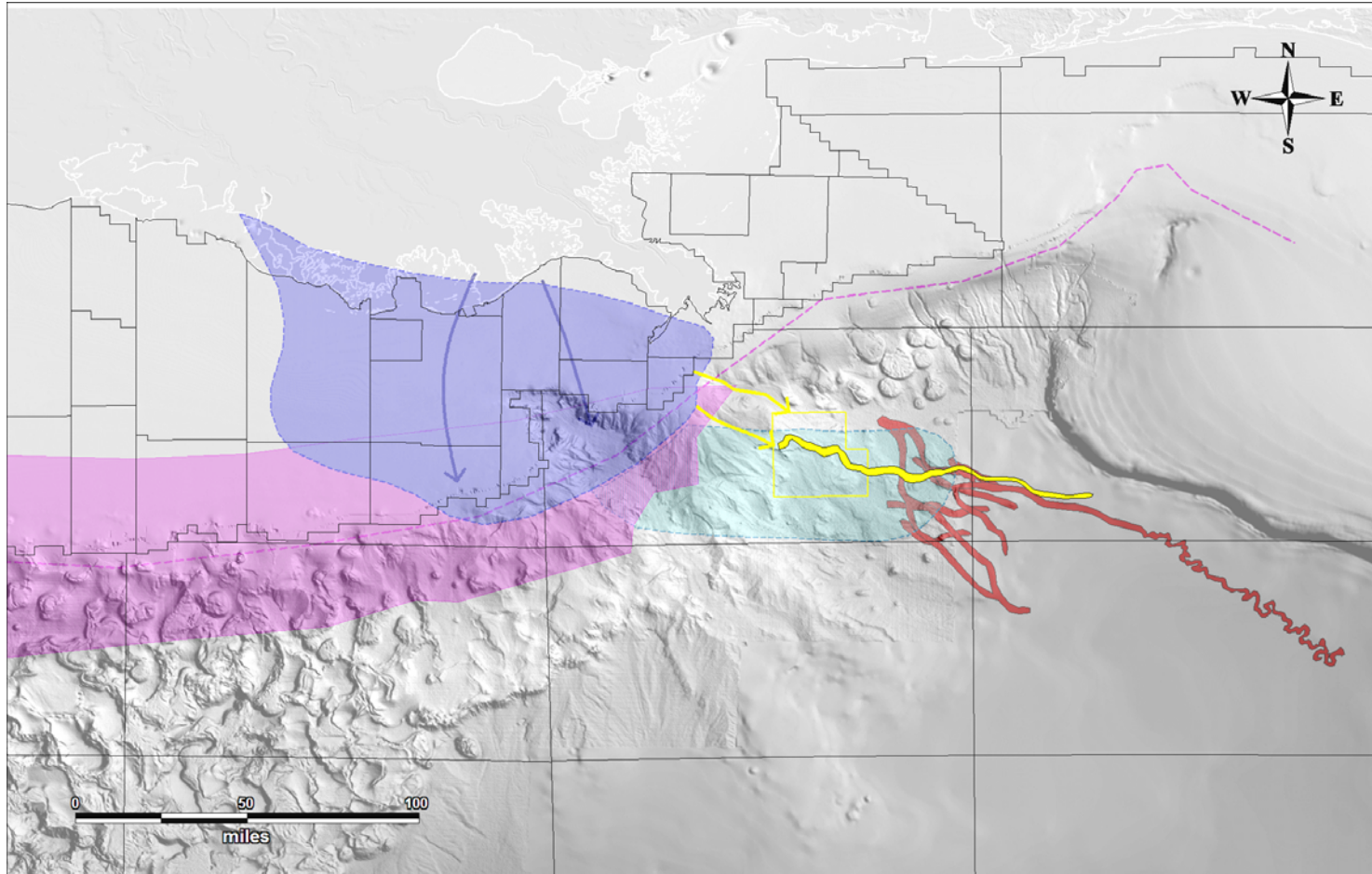


Figure 120. Proposed Pleistocene deposystem analogue composite (this study). Dark blue shaded area is most recent Pleistocene depocenter from Winker and Booth (2000). Study area outlined in thin yellow line. Channel 14a is yellow region through study area. Red regions are other channels of the Eastern Mississippi Fan (Dixon and Weimer, 1994). Yellow arrows are proposed shelf edge/upper slope sediment delivery pathways to Channel 14a and the remaining study area. Light blue region is MC Blue Unit turbidite sheet sand from Winker and Booth (2000). Purple region is extent of Pleistocene depocenter from Berryhill et al. (1986). Seafloor rendering image courtesy of Geoscience Earth and Marine Services, Inc.

CHAPTER XI

CONCLUSION

Primary salt mobilization to Roho-style structural end-members occurred up to approximately 450 ky, BP where salt tectonics, as the dominant process, gave way to slope depositional processes. These processes are responsible for the formation of the shallow sequence stratigraphy and thus geologic hazards. The sequence stratigraphy for the study area correlates with those defined by Dixon and Weimer for the Eastern Mississippi Fan, extending the Fan westward, and providing evidence for the Mississippi River as the source of the Eastern Fan, specifically Channel 14a. The stratigraphic sequences for the Eastern Fan are punctuated by condensed sections that allow for correlation of stratigraphic sequences across the fan and indicate periods of significantly reduced sedimentation. These periods correlate with the timing of oxygen isotope stages, however, they do not directly correlate with changes in sea-level. This portion of the slope lies at the edge of the Pleistocene depocenter and is therefore more sensitive to the location of the depocenter, through time, in the formation of the sequence stratigraphy than Gulf of Mexico changes in sea level. Findings from this study suggest conventional application of sequence stratigraphic interpretation with respect to eustatic sea level change may not be directly applicable with further consideration given to the sensitivity to the position of the shifting Mississippi River Pleistocene depocenter on the formation of the sequence stratigraphy in the Eastern Mississippi Fan.

REFERENCES CITED

- Alberty, M. W., M. E. Hafle, J. C. Minge, and T. M. Byrd, 1997, Mechanisms of shallow waterflows and drilling practices intervention: Proceedings of the Offshore Technology Conference, paper 8301.
- Amery, G. B., 1969, Structure of Sigsbee scarp, Gulf of Mexico: AAPG Bulletin, v. 53, p. 2480-2482.
- Apps, G. M., F. J. Peel, C. J. Travis, and C. A. Yielding, 1994, Structural controls on Tertiary deep water depositional systems in the US Gulf of Mexico: Transactions of the Gulf Coast Society of Economic Paleontologists and Mineralogists Foundation 8th Annual Research Conference, p. 6-14.
- Bailey, E. B., 1931, Salt plugs: Geological Magazine, v. 68, p. 335-336.
- Barton, D. C., 1933, Mechanics of formation of salt domes with special reference to Gulf Coast salt domes of Texas and Louisiana: AAPG Bulletin, v. 17, p. 1025-1083.
- Beard, J. H., J. B. Sangree, and L. A. Smith, 1982, Quaternary chronology, paleoclimate, depositional sequences, and eustatic cycles: AAPG Bulletin, v. 66, p. 158-169.
- Behrens, E. W., 1985, Unifite muds in intraslope basins, northwest Gulf of Mexico: Geo-Marine Letters, v. 4, p. 227-233.
- Berryhill, H. L., J. R. Suter, and N. S. Hardin, 1986, Late Quaternary facies and structure, northern Gulf of Mexico: interpretations from seismic data: AAPG Studies in Geology 23, p. 131-189.
- Bishop, R. S., 1978, Mechanism for emplacement of diapirs: AAPG Bulletin, v. 62, p. 1561-1583.
- Bouma, A. H., 1981, Depositional sequences in clastic continental slope deposits, Gulf of Mexico: Geo-Marine Letters, v. 1, p. 115-121.
- Bouma, A. H., and C. E. Stelting, 1984, Mississippi Fan: internal structure and depositional processes: Geo-Marine Letters, v. 3, p. 147-153.
- Bouma, A. H., and J. M. Coleman, 1985, Mississippi Fan: Leg 96 program and principal results, *in* A. H. Bouma, W. R. Normark, and N. E. Barnes eds., Submarine fans and related turbidite systems: New York, Springer-Verlag, p. 247-252.

- Bouma, A. H., J. M. Coleman, and A. W. Meyer, 1986, Initial reports of the Deep Sea Drilling Project, Leg 96: Washington, D. C., U.S. Govt. Printing Office, 824 p.
- Bouma, A. H., J. M. Coleman, and C. E. Stelting, 1989, Influence of relative sea level changes on the construction of the Mississippi Fan: *Geo-Marine Letters*, v. 9, p. 161-170.
- Bouma, A. H., H. H. Roberts, and J. M. Coleman, 1992, Late Neogene Louisiana continental margin construction timed by sea-level fluctuations, *in* J. S. Watkins, F. Zhuqiang, and K. J. McMillen eds., *American Association of Petroleum Geologists Memoir 53*, p. 333-341.
- Brooks, J. M., M. C. Kennicutt, C. R. Fisher, S. A. Macko, K. Cole, J. J. Childress, R. R. Bidigare, and R. D. Vetter, 1987, Deep-sea hydrocarbon seep communities: Evidence for energy and nutritional carbon sources: *Science*, v. 238, p. 1134-1142.
- Buffler, R. T., and D. S. Sawyer, 1985, Distribution of crust and early history, Gulf of Mexico basin: *Gulf Coast Association of Geological Societies Transactions*, v. 35, p. 333-344.
- Buffler, R. T., 1989, Distribution of crust, distribution of salt, and the early evolution of the Gulf of Mexico basin: *SEPM Gulf Coast Section Tenth Annual Research Foundation Conference*, p. 25-27.
- Burman, S. S., and S. J. Norton, 1998, Mensa project: well drilling and completion: *Proceedings of the Offshore Technology Conference*, paper 8578.
- Byrd, T. M., J. M. Schneider, D. J. Reynolds, M. W. Albery, and M. E. Hafle, 1996, Identification of flowing water sand drilling hazards in the deepwater Gulf of Mexico: *Proceedings of the Offshore Technology Conference*, paper 7971, p. 137-142.
- Cobbold, P. R., and P. Szatmari, 1991, Radial gravitational gliding on passive margins: *Tectonophysics*, v. 188, p. 249-289.
- Coleman, J. M., D. B. Prior, and J. F. Lindsay, 1983, Deltaic influences on shelf edge stability processes: *SEPM Special Publication 33*, p. 121-137.
- Coleman, J. M., D. B. Prior, and H. H. Roberts, 1986, Geologic development and characteristics of continental margins, Gulf of Mexico: *Gulf Coast Association of Geological Societies Transactions*, v. 36, p. 61-64.

- Coleman, J. M., 1990, Depositional systems and tectonic/eustatic history of the Oligocene Vicksburg episode of the northern Gulf coast, Ph.D. Dissertation, The University of Texas at Austin, Austin, TX, 538 p.
- Crans, W., G. Mandl, and J. Haremboure, 1980, On the theory of growth faulting: a geomechanical delta model based on gravity sliding: *Journal of Petroleum Geology*, v. 2, p. 265-307.
- Diegel, F. A., J. F. Karlo, D. C. Shuster, R. C. Shoup, and P. R. Tauvers, 1995, Cenozoic structural evolution and tectonostratigraphic framework of the northern Gulf Coast continental margin, *in* M. P. A. Jackson, D. G. Roberts, and S. Snelson eds., *Salt Tectonics: a global perspective*: AAPG Memoir 65, p. 153-175.
- Dixon, B. T., and P. Weimer, 1994, Regional sequence stratigraphic setting of the Mississippi Fan complex, northern deep Gulf of Mexico: implications for evolution of the northern Gulf basin margin, *Gulf of Mexico Salt Tectonics, Associated Processes and Exploration Potential*: GCSSEPM Foundation Fifteenth Annual Research Conference Programs and Abstracts, p. 373-381.
- Dixon, B. T., and P. Weimer, 1998, Sequence stratigraphy and depositional history of the eastern Mississippi Fan (Pleistocene), northeastern deep Gulf of Mexico: *AAPG Bulletin*, v. 82, p. 1207-1232.
- Dobrin, M. B., 1941, Some quantitative experiments on a fluid salt-dome model, and their geological implications: *American Geophysical Union Transactions*, v. 22, p. 528-542.
- Doyle, E. H., J. S. Jr. Smith, P. R. Tauvers, J. R. Booth, M. C. Jacobi, A. C. Nunez, F. A. Diegel, and M. J. Kaluza, 1996, The usefulness of enhanced surface renderings from 3-D seismic data for high-resolution geohazards studies: *Proceedings of the Offshore Technology Conference*, paper 7967.
- Feeley, M. H., 1984, Seismic stratigraphic analysis of the Mississippi Fan, Ph.D. Dissertation, Texas A&M University, College Station, TX, 209 p.
- Feeley, M. H., R. T. Buffler, and W. R. Bryant, 1985, Depositional units and growth of the Mississippi Fan, *in* A. H. Bouma, W. R. Normark, and N. E. Barnes eds., *Submarine fans and related turbidite systems*: New York, Springer-Verlage, p. 253-257.
- Feeley, M. H., T. C. Jr. Moore, T. S. Loutit, and W. R. Bryant, 1990, Sequence stratigraphy of Mississippi Fan related to oxygen isotope sea level index: *AAPG Bulletin*, v. 74, p. 407-474.

- Feng, J., 1995, Post mid-Cretaceous seismic stratigraphy and depositional history, deep Gulf of Mexico, Ph. D. Dissertation, The University of Texas at Austin, Austin, TX, 253 p.
- Feng, J., and R. T. Buffler, 1996, Post Mid-Cretaceous depositional history, Gulf of Mexico basin, *in* J. O. James and R. L. Freed eds., GCAGS Special Publication-Structural Framework of the northern Gulf of Mexico, p. 9-25.
- Fletcher, R. C., 1995, Salt glacier and composite sediment-salt glacier models for the emplacement and early burial of allochthonous salt sheets, *in* M. P. A. Jackson, D. G. Roberts, and S. Snelson eds., Salt tectonics: a global perspective: AAPG Memoir 65.
- Galloway, W. E., 1989a, Genetic stratigraphic sequences in the basin analysis I: Architecture and genesis of flooding-surface bounded depositional units: AAPG Bulletin, v. 73, p. 125-142.
- Galloway, W. E., 1989b, Genetic stratigraphic sequences in the basin analysis II: Application to northwest Gulf of Mexico Cenozoic basin: AAPG Bulletin, v. 73, p. 143-154.
- Galloway, W. E., and R. T. Buffler, 2004, Gulf Basin Depositional Synthesis Project, <<http://www.ig.utexas.edu/research/projects/gbds/gbds.htm>>, Accessed February 22, 2004.
- Harrison, T. S., 1927, Colorado-Utah salt domes: AAPG Bulletin, v. 11, no. 2, p. 111-133.
- Hubbert, M. K., 1937, Theory of scale models as applied to the study of geologic structures: GSA Bulletin, v. 48, p. 1459-1520.
- Hudec, M. R., R. A. Fletcher, and I. A. Watson, 1995, The composite salt glacier: extension of the salt glacier model to post-burial conditions (abs.): AAPG Annual Convention Official Program, p. 45a.
- Humphris, C. C. Jr., 1978, Salt movement on continental slope, northern Gulf of Mexico, *in* A. H. Bouma, G. T. Moore, and J. M. Coleman eds., Framework, facies, and oil-trapping characteristics of the upper continental margin: AAPG Studies in Geology, v. 7, p. 69-85.
- Jackson, M. P. A., and W. E. Galloway, 1984, Structural and Depositional Styles of Gulf Coast Tertiary Continental Margins: Application to Hydrocarbon Exploration: AAPG Continuing Education Course Note Series 25, 225 p.

- Jackson, M. P. A., and C. J. Talbot, 1986, External shapes, strain rates, and dynamics of salt structures: *GSA Bulletin*, v. 97, p. 305-323.
- Jackson, M. P. A., C. J. Talbot, and R. R. Cornelius, 1988, Centrifuge modeling of the effects of aggradation and progradation on syndepositional salt structures: Report of Investigations no. 173, -93 p.
- Jackson, M. P. A., and C. J. Talbot, 1989, Salt canopies: SEPM Gulf Coast Section Tenth Annual Research Foundation Conference Program and Abstracts, p. 72-78.
- Jackson, M. P. A., 1995, Retrospective salt tectonics: Salt tectonics: a global perspective: *AAPG Memoir* 65, p. 1-28.
- Jamieson, G. A., 1996, Salt distribution in the Louisiana South Additions Area from 3D seismic data: Proceedings of the 1996 Offshore Technology Conference, paper 8014, p. 515-525.
- Jenyon, M. K., 1986, Salt tectonics: London, Elsevier, 191 p.
- Kennicutt, M. C., J. M. Brooks, R. R. Bidigare, R. R. Fay, T. L. Wade, and T. J. McDonald, 1985, Vent-type taxa in hydrocarbon seep region on the Louisiana Slope: *Nature*, v. 317, p. 351-353.
- Koen, A. D., 1995, Economics and technology spark gulf deepwater projects: *Oil and Gas Journal*, p. 25-31.
- Kohl, B., and H. H. Roberts, 1994, Fossil foraminifera for four active mud volcanoes in the Gulf of Mexico: *Geo-Marine Letters*, v. 14, p. 126-134.
- Kolla, V., and M. A. Perlmutter, 1993, Timing of turbidite sedimentation on the Mississippi Fan: *AAPG Bulletin*, v. 77, no. 7, p. 1129-1141.
- Kornacki, A. S., J. W. Kendrick, and J. L. Berry, 1994, The impact of oil and gas vents and slicks on petroleum exploration in deepwater Gulf of Mexico: *Geo-Marine Letters*, v. 14, p. 160-169.
- Kvenvolden, K. A., and L. C. Barnard, 1983, Hydrates of natural gas in continental margins: *AAPG Memoir* 34.
- Lachmann, R., 1910, Uber autoplaste (nichttektonische) formelemente im bau der salzgesteine norddeutschlands: *Deutschen Geologischen Gesellschaft Monatsbericht*, v. 62, p. 113-116.

- Lee, G. H., 1990, Salt tectonics and seismic stratigraphy of the Keathley Canyon area and vicinity, northwestern Gulf of Mexico, Ph.D. Dissertation, Texas A&M University, College Station, TX, 182 p.
- Lehner, P., 1969, Salt tectonics and Pleistocene stratigraphy on continental slope of northern Gulf of Mexico: AAPG Bulletin, v. 53, p. 2431-2479.
- Letouzey, J., B. Colletta, R. Vially, and J. C. Chermette, 1995, Evolution of salt-related structures in compressional settings: Salt Tectonics: A Global Perspective: AAPG Memoir 65.
- Liro, L. M., 1989, Seismic investigation of salt deformational styles, lower slope of the northwestern Gulf of Mexico, Gulf of Mexico Salt Tectonics, Associated Processes and Exploration Potential: GCSSEPM Foundation Tenth Annual Research Conference Programs and Abstracts, p. 94-100.
- Lopez, J. A., 1989, Distribution of structural styles in the northern Gulf of Mexico and Gulf Coast, Gulf of Mexico Salt Tectonics, Associated Processes and Exploration Potential: GCSSEPM Foundation Tenth Annual Research Conference Programs and Abstracts, p. 101-108.
- Martin, R. G., 1978, northern and eastern Gulf of Mexico continental margin: stratigraphic and structural framework, *in* A. H. Bouma, G. T. Moore, and J. M. Coleman eds., Framework, facies and oil-trapping characteristics of the upper continental margin: AAPG Studies in Geology, v. 7, p. 21-48.
- Martin, R. G., and A. H. Bouma, 1978, Physiography of Gulf of Mexico, *in* A. H. Bouma, G. T. Moore, and J. M. Coleman eds., Framework, facies, and oil-trapping characteristics of the upper continental margin: AAPG Studies in Geology, v. 7, p. 3-19.
- McGuinness, D. B., and J. R. Hossack, 1993, The development of allochthonous salt sheets as controlled by rates of extension, sedimentation, and salt supply: GCSSEPM Foundation 14th Annual Reserach Conference-Rates of Geological Processes.
- Minerals Management Service, 2000, Free ASCII Data Files,
<<http://www.gomr.mms.gov/homepage/pubinfo/freeascii/freedesc.html>>,
Accessed August 21, 2000.
- Mitchum, R. M. Jr., and P. R. Vail, 1977, Seismic stratigraphy and global changes of sea level, part 7: Seismic stratigraphic interpretation procedure: AAPG Memoir 26, p. 135-144.

- Morton, R. A., and W. E. Galloway, 1991, Depositional, tectonic, and eustatic controls on hydrocarbon distribution in divergent margin basins: Cenozoic Gulf of Mexico case history: *Marine Geology*, v. 102, p. 239-263.
- Morton, R. A., and J. R. Suter, 1996, Sequence stratigraphy and composition of late Quaternary shelf-margin deltas, northern Gulf of Mexico: *AAPG Bulletin*, v. 80, no. 4, p. 505-530.
- Nelson, T. H., and L. Fairchild, 1989, Emplacement and evolution of salt sills in the northern Gulf of Mexico: *Houston Geological Society Bulletin*, v. 31, p. 6-7.
- Nelson, T. H., 1991, Salt tectonics and listric-normal faulting, *in* A. Salvador ed., *The geology of North America; the Gulf of Mexico basin: GSA Decade of North American Geology*, v. J, p. 73-89.
- Nettleton, L. L., 1934, Fluid mechanics of salt domes: *AAPG Bulletin*, v. 27, p. 1175-1204.
- Nettleton, L. L., 1955, History of concepts of Gulf Coast salt-dome formation: *AAPG Bulletin*, v. 39, p. 2373-2383.
- Neurauter, T. W., and W. R. Bryant, 1990, Seismic expression of sedimentary volcanism on the Continental Slope, northern Gulf of Mexico: *Geo-Marine Letters*, v. 10, no. 699, p. 702.
- Neurauter, T. W., and H. H. Roberts, 1994, Three generations of Mud Volcanoes on the Louisiana Continental Slope: *Geo-Marine Letters*, v. 14, no. 120, p. 125.
- Peel, F. J., J. R. Hossack, and C. J. Travis, 1995, Genetic structural provinces and salt tectonics of the cenozoic offshore U.S. Gulf of Mexico: A preliminary analysis, *in* M. P. A. Jackson, D. G. Roberts, and S. Snelson eds., *Salt tectonics: A global perspective: AAPG Memoir 65*, p. 153-175.
- Pilger, R. H., 1981, The opening of the Gulf of Mexico: implications for the tectonic evolution of the northern Gulf: *Geological Societies Transactions*, v. 31, p. 377-381.
- Posamentier, H. W., and P. R. Vail, 1988, Eustatic controls on clastic deposition II—sequence and systems tract models: *SEPM Special Publication 42*, p. 125-154.
- Prior, D. B., and B. D. Bornhold, 1989, Submarine sedimentation on a developing Holocene fan delta: *Sedimentology*, v. 36, p. 1053-1070.
- Rainwater, E. H., 1964, Transgressions and regressions in the Gulf Coast Tertiary: *Gulf Coast Association of Geological Societies Transactions*, v. 14, p. 217-230.

- Ramberg, H., 1980, Diapirism and gravity collapse in the Scandinavian Caledonides: *Journal of Geological Society of London*, v. 137, p. 261-270.
- Ramberg, H., 1981, *Gravity, deformation and the earth's crust*: London, Academic Press, 452 p.
- Ramsayer, G. R., 1979, Seismic stratigraphy, a fundamental exploration tool: *Proceedings of the Offshore Technology Conference*, paper 3568, p. 1859-1867.
- Rettger, R. E., 1935, Experiments on soft rock deformation: *AAPG Bulletin*, v. 19, p. 271-292.
- Roberts, H. H., and J. M. Coleman, 1988, Sedimentary development of the Louisiana continental shelf related to sea level cycles, part 2: seismic response: *Geo-Marine Letters*, v. 8, p. 109-119.
- Roberts, H. H., P. Aharon, J. Carney, J. Larkin, and R. Sassen, 1990, Sea floor responses to hydrocarbon seeps, Louisiana continental slope: *Geo-Marine Letters*, v. 10, p. 232-243.
- Roberts, H. H., D. J. Cook, and M. K. Sheedlo, 1992, Hydrocarbon seeps of the Louisiana continental slope: seismic amplitude signature and seafloor response: *Gulf Coast Association of Geological Societies Transactions*, v. 42, p. 349-362.
- Roberts, H. H., 1993, Geologic features of the northern Gulf of Mexico continental slope: a high resolution view (abs.): *American Association of Petroleum Geologists Annual Convention Program*, p. 192.
- Salvador, A., 1987, Late Triassic-Jurassic paleogeography and origin of Gulf of Mexico basin: *AAPG Bulletin*, v. 71, p. 419-451.
- Salvador, A., 1991, Origin and development of the Gulf of Mexico, *in* A. Salvador ed., *The Geology of North America*, v. J, p. 389-444.
- Sangree, J. B., P. R. Vail, and R. M. Sneider, 1988, Evolution of facies interpretation of the shelf-slope: application of the new eustatic framework to the Gulf of Mexico: *Proceedings of the 1988 Offshore Technology Conference*, v. 2, p. 133-144.
- Sangree, J. B., and J. M. Widmier, 1977, Seismic stratigraphy and global changes of sea level, part 9: seismic interpretation of clastic depositional facies: *Seismic stratigraphy-applications of hydrocarbon exploration: AAPG Memoir 26*, p. 165-184.
- Schuchert, C., 1909, Paleogeography of North America: *Geological Society of America Bulletin*, v. 20, p. 427-606.

- Schuchert, C., 1935, Historical geology of the Antillean-Caribbean region: New York, John Wiley & Sons, 811 p.
- Schuster, D. C., 1995, Deformation of allochthonous salt and evolution of related salt-structural systems, eastern Louisiana Gulf Coast, *in* M. P. A. Jackson, D. G. Roberts, and S. Snelson eds., Salt tectonics: a global perspective: AAPG Memoir 65.
- Seni, S. J., 1994, Salt tectonics on the continental slope, northeast Gulf of Mexico: Evolution of Stocks and Massifs from reactivation of salt sheets: Report of Investigations no. 212, 102 p.
- Spindler, W. M., 1977, Structure and stratigraphy of a small Plio-Pleistocene depocenter, Louisiana continental shelf: Gulf Coast Association of Geological Societies Transactions, v. 27, p. 180-196.
- Stuart, C. J., and C. A. Caughey, 1977, Seismic facies and sedimentology of terrigenous Pliocene-Pleistocene depocenters, outer continental shelf, Louisiana and Texas: AAPG Memoir 26, p. 249-275.
- Swiercz, A. M., 1992, Seismic stratigraphy and salt tectonics along the Sigsbee Escarpment, southeastern Green Canyon region, *in* R. A. Geyer ed., CRC Handbook of Geophysical Exploration at Sea: 2nd ed., p. 227-294.
- Talbot, C. J., 1978, Halokinesis and thermal convection: *Nature*, v. 273, p. 739-741.
- Talbot, C. J., 1994, Spreading of salt structures in the Gulf of Mexico: *Tectonophysics*, v. 228, p. 151-166.
- Vail, P. R., and R. M. Jr. Mitchum, 1977, Seismic stratigraphy and global changes in sea level, part 1: overview, *in* C. E. Payton ed., AAPG Memoir 26, p. 1-10.
- Vail, P. R., 1987, Seismic stratigraphy interpretation using sequence stratigraphy, part I: seismic stratigraphy interpretation procedure, *in* A. W. Bally ed., Atlas of seismic stratigraphy: AAPG Studies in Geology 7, v. 1, p. 1-10.
- Vail, P. R., and W. W. Wornhardt, 1990, Well-log seismic sequence stratigraphy: an integrated tool for the 90s: Eleventh Annual Research Conference Program and Abstracts of the GCSSEPM Eleventh Annual Research Conference, p. 379-388.
- Vail, P. R., and W. W. Wornhardt, 1991, An integrated approach to exploration and development in the 90s: well-log seismic sequence stratigraphy analysis: Transactions of the Gulf Coast Association of Geological Societies, v. 41, p. 630-650.

- Van Wagoner, J. C., R. M. Jr. Mitchum, H. W. Posamentier, and P. R. Vail, 1987, Part 2: Key definitions of sequence stratigraphy: AAPG Studies in Geology 27, p. 11-14.
- Walters, R. D., 1985, Seismic stratigraphy and salt tectonics of Plio-Pleistocene deposits, continental slope and upper Mississippi Fan, northern Gulf of Mexico, Master's Thesis, The University of Texas at Austin, Austin, TX 204 p.
- Watkins, J. S., and R. T. Buffler, 1996, Gulf of Mexico: Deepwater frontier exploration potential, *in* J. O. Jones and R. L. Freed eds., Structural Framework of the northern Gulf of Mexico: Gulf Coast Association of Geological Societies Special Publication, p. 79-92.
- Weimer, P., 1989, Sequence stratigraphy of the Mississippi Fan (Plio-Pleistocene), Gulf of Mexico: Geo-Marine Letters, v. 9, p. 185-272.
- Weimer, P., 1990, Sequence stratigraphy, facies geometries, and depositional history of the Mississippi Fan, Gulf of Mexico: AAPG Bulletin, v. 74, p. 425-453.
- Weimer, P., 1991, Seismic facies, characteristics and variations in channel evolution, Mississippi Fan (Plio-Pleistocene), northern Gulf of Mexico, *in* P. Weimer and M. H. Link eds., Seismic facies and sedimentary processes of submarine fans and turbidite systems: New York, Springer-Verlag, p. 323-347.
- Willis, B., 1909, Paleogeographic maps of North America: Journal of Geology, v. 17, p. 203-208.
- Winker, C. D., 1982, Cenozoic shelf margins, northwestern Gulf of Mexico Basin: Gulf Coast Association of Geological Societies Transactions, v. 32, p. 427-448.
- Winker, C. D., and R. T. Buffler, 1988, Paleogeographic evolution of deep-water Gulf of Mexico and margins, Jurassic to Middle Cretaceous (Comanchean): American Association of Petroleum Geologists Bulletin, v. 72, p. 318-346.
- Winker, C. D., and J. R. Booth, 2000, Sedimentary dynamics of the salt-dominated continental slope, Gulf of Mexico: Integration of observations from the seafloor, near-surface, and deep sub-surface: GCSSEPM Foundation Annual Research Conference, Deepwater Reservoirs of the World, p. 1059-1086.
- Woodbury, H. O., I. B. Murray, P. J. Pickford, and W. H. Akers, 1973, Pliocene and Pleistocene depocenters, outer continental shelf, Louisiana and Texas: AAPG Bulletin, v. 57, p. 2428-2439.

- Woodbury, H. O., J. H. Spotts, and W. H. Akers, 1978, Gulf of Mexico Continental-slope sediments and sedimentation, *in* A. H. Bouma, G. T. Moore, and J. M. Coleman eds., *Framework, facies and oil-trapping characteristics of the upper continental margin: AAPG Studies in Geology 7*, p. 117-137.
- Worall, D. M., and S. Snelson, 1989, Evolution of the northern Gulf of Mexico, with emphasis on Cenozoic growth faulting and the role of salt, *in* A. W. Bally and A. R. Palmer eds., *The geology of north America-an overview: The Geology of North America: Boulder, CO, v. A*, p. 97-138.
- Wornhardt, W. W., and P. R. Vail, 1990, Revision of the Plio-Pleistocene cycles and their application to sequence stratigraphy of shelf and slope sediments in the Gulf of Mexico: Foundation Eleventh Annual Research Conference Program and Abstracts of the Gulf Coast Section, Society of Economic Paleontologists and Mineralogists, p. 391-397.
- Wu, S., A. W. Bally, and C. Cramez, 1990a, Allochthonous salt, structure, and stratigraphy of the northeastern Gulf of Mexico; part I, stratigraphy: *Marine and Petroleum Geology*, v. 7, p. 318-333.
- Wu, S., A. W. Bally, and C. Cramez, 1990b, Allochthonous salt, structure, and stratigraphy of the northeastern Gulf of Mexico; part II, structure: *Marine and Petroleum Geology*, v. 7, p. 334-370.
- Yielding, C. A., and G. M. Apps, 1994, Spatial and temporal variations in the facies associations of depositional sequences on the slope: Examples from the Miocene-Pleistocene of the Gulf of Mexico: GCSSEPM Foundation 15th Annual Research Conference, *Submarine Fans and Turbidite Systems*, p. 425-437.
- Yorston, H. J., and J. F. Fox, 1985, Practical application of subsurface and seismic methods to prospecting in salt provinces with emphasis on the Gulf Coast Tertiary: an exploration workshop: *Houston Geological Society Continuing Education Series*, 33 p.

VITA

John Richard Brand

Date of Birth: November 30, 1971

Mailing Address Geoscience Earth and Marine Services, Inc.
10615 Shadow Wood Drive
Suite 200
Houston, Texas 77043

Telephone 713-468-1410 (Work)

E-mail jrbrand@gemsinc.com

Education B.S., West Virginia University (Geology)
Ph.D., Texas A&M University (Oceanography)
December, 2004.

Doctoral Dissertation: Structural and Stratigraphic Evolution of the Central
Mississippi Canyon area: Interaction of Slope Processes
and Salt Tectonics in the Formation of Engineering and
Geologic Hazards.

Experience: May 2001 to Present- Senior Geologist, Project Manager
June 1998 to May 2001- Marine Geologist, Geoscience
Earth and Marine Services, Inc.
Houston, Texas
August 1995 to June 1998- Graduate Teaching Assistant
Department of Oceanography, Texas A&M University
College Station, Texas